Loughborough University, March 2016

Electrospinning of poly (lactic) acid for biomedical applications: analysis of solution properties and process parameters, drug encapsulation and release

---

by

Raffaella Casasola

A doctoral thesis submitted in partial fulfilment of the requirements for the award of the degree of Doctor of Philosophy of Loughborough University

March 2016

ABSTRACT

Electrospinning or electrostatic fibre spinning employs electrostatic force to draw fibres from a liquid, either a polymeric solution or a polymer melt in the form of a charged jet. The jet solidifies and is deposited on a collector in the form of a non-woven fibrous mat. Electrospun fibres have diameters between several nanometres to a few microns, which is one of the main advantages of the process, as materials at the nanoscale have shown great potential in a wide range of healthcare and energy applications. The initial selection of solvents to dissolve the polymer for production of electrospun defect-free nanofibres has generally been based on experience from similar polymer-solvent systems. The selection of a solvent is important to control the fibre surface morphology that would eventually determine the field of application for the electrospun nanofibrous structures. However, little attempt has been made to study the correlation between the solubility behaviour of the polymer in different solvents and the electrospinnability of the polymer solutions. From this perspective, the first part of this thesis focused on the selection of different solvents for the production of poly (lactic acid) (PLA) nanofibres. Solution properties were measured and the electrospun nanofibrous structures were analysed in terms of morphology and nanofibre diameter. Understanding the molecular interactions between polymer and solvents enables the correct solvent selection to ensure the desired nanofibrous structure.

Solubility is not the only criterion for nanofibre formation from a polymer solution. Polymer concentration is one of the main factors affecting electrospinning. For this reason, a relationship between PLA concentration and nanofibre morphology was determined by solution property measurements. A three step systematic methodology has been proposed in this thesis in order to select appropriate solvent and polymer concentration for the production of homogeneous electrospun mats made of defect-free nanofibres. This methodology was validated for PLA nanofibres, but it can be used for a wide range of polymers. It simplifies the solvent selection process and can significantly improve the trial and error approaches used at present.

Despite several models for electrospinning having been proposed to predict the behaviour of the electrospun jet, there are no simple methods for a priori prediction of the final morphology of the electrospun mat from the knowledge of solution properties and electrospinning process parameters. Moreover the prediction of nanofibre diameter is still a

difficulty and little research has been done on this. For these reasons, the second part of this thesis is dedicated to understanding the effect of some process parameters on the jet electric current and hence on the morphology of PLA nanofibres. The values of current measured were used to verify an equation proposed in the literature for the prediction of the final diameter. The experimental diameter of the PLA nanofibres was compared with the predicted value.

In the last chapter coaxial electrospinning was employed to produce PLA nanofibres with a core shell structure for the incorporation of a model hydrophilic drug in the nanofibre core. The large surface area to volume ratio of nanofibres offers the great advantage of higher efficiency of encapsulation and better control of the release profile compared with other drug delivery systems. Even though successful encapsulation of drug and proteins have been reported, it is not clear how to verify the continuous drug distribution in the core throughout the whole length of the fibre. The solution properties of both core and shell strongly affect the outcome of the electrospinning process. For this reason, several techniques have been used to verify the formation of a core shell structure and proper encapsulation of the drug. In addition, the efficiency of drug encapsulation was evaluated and drug release studies were performed.

Keywords: electrospinning, poly (lactic acid), nanofibres, viscoelasticity, electric current, core-shell nanofibres, drug delivery.

ACKNOWLEDGEMENTS

This thesis would feel incomplete without the acknowledgements section.

When I first move to Loughborough, I was very excited about the opportunity I was given! But at the same time I was a bit scared, because I was alone in a new country and away from family and friends. It was difficult at the beginning, and probably it would have been even harder without the support of my parents and friends from Italy. Per il supporto e la pazienza in questi anni, GRAZIE!

I would like to express my gratitude to my supervisor Dr Stella Georgiadou, for giving me the opportunity to do a PhD in the UK. I appreciated her advices and the possibility to attend conferences and training schools. I have grown up professionally and personally.

A special thank you goes to my second supervisor Dr Noreen Thomas for her guidance, the financial support and for helping me with my English mistakes. Thank you very much!

Thanks a lot to my colleagues and friends in the chemical engineering department, for listening and being supportive in both good and difficult moments.

Thank you very much to all technicians from the chemical engineering department and the materials department, for all trainings and technical advices.

I would like also to thank the Cost Action MP1206 organizing committee, and in particular Dr Yang Fang and all friends in the Netherlands, who made my visit at Radboud University enjoyable!

I have learnt something from all of you in these four years! Thank you!

Table of contents

ABSTRACT ..... **ii**

ACKNOWLEDGEMENTS ..... **iv**

Table of contents ..... **v**

List of figures ..... **x**

List of tables ..... **xviii**

List of abbreviations and symbols ..... **xxi**

1 INTRODUCTION **1**

1.1 Background 1

1.2 Aims and objectives 2

1.3 Research questions 4

1.4 Publications and Conference papers 4

2 LITERATURE REVIEW **6**

2.1 Electrospinning 6

2.1.1 Mechanisms of jet motion in electrospinning 11

2.1.1.1 Prediction of the final nanofibre diameter 16

2.1.2 Electrospinning parameters 19

2.1.2.1 Solution parameters 20

2.1.2.1.1 Concentration, viscosity, molecular weight 20

2.1.2.1.2 Surface tension 23

2.1.2.1.3 Electric conductivity 24

2.1.2.2 Process parameters 25

2.1.2.2.1 Voltage 25

2.1.2.2.2 Distance between needle and collector 26

2.1.2.2.3 Flow rate 27

2.1.2.3 Ambient parameters 28

2.1.2.3.1 Temperature 28

2.1.2.3.2 Relative humidity 29

2.1.3 Solvents used for electrospinning 32
2.1.4 Electrospinning applications 34
2.1.4.1 Tissue engineered scaffolds 34
2.1.4.2 Dressings for wound healing 37
2.1.4.3 Drug delivery systems 38
2.2 Poly (lactic acid) (PLA) 39
2.2.1 Production 39
2.2.2 Structure and properties 41
2.2.3 Applications of PLAs 43
2.2.3.1 Food packaging products 43
2.2.3.2 Biomedical applications 44
2.2.4 Degradation of PLAs 45
2.3 Electrospun nanofibres as drug delivery systems 47
2.3.1 Methods of drug incorporation into nanofibres 49
2.3.1.1 Blend electrospinning 49
2.3.1.2 Coaxial electrospinning 51
2.3.1.3 Emulsion electrospinning 57
2.3.2 Drug release mechanisms 57
3 GENERAL MATERIALS AND METHODS 61
3.1 Materials 61
3.2 Electrospinning process 63
3.2.1 Electrospun PLA nanofibres 63
3.2.2 Electrospun core-shell nanofibres 65
3.3 Characterisation of solution properties 67
3.4 Characterisation of electrospun nanofibres 68
3.4.1 Scanning electron microscopy (SEM) 68
3.4.2 Transmission electron microscopy (TEM) 68
3.4.3 Confocal laser scanning microscopy (CLSM) 68

3.4.4 Focus ion beam-scanning electron microscopy (FIB-SEM) 69
3.4.5 Water contact angle measurements 69
3.4.6 Differential scanning calorimetry (DSC) 70
3.4.7 Fourier transform infrared spectroscopy (FTIR) 70
3.4.8 X-ray photoelectron spectroscopy (XPS) 70
3.4.9 High performance liquid chromatography (HPLC) 71
3.4.9.1 Efficiency of drug encapsulation 72
3.4.9.2 Drug release studies 72
4 EFFECT OF DIFFERENT SOLVENT SYSTEMS ON PLA NANOFIBRE MORPHOLOGY AND DIAMETER 74
4.1 Introduction 74
4.2 Aims and objectives 76
4.3 Results and discussion 77
4.3.1 Effect of single solvents on nanofibre morphology and diameter 77
4.3.2 Effect of binary solvent systems on nanofibre morphology and diameter 84
4.3.3 Effect of solvent ratio AC/DMF on nanofibre morphology and diameter 93
4.3.4 Effect of polymer concentration on nanofibre morphology and diameter 99
4.4 Conclusion 106
5 THREE STEP METHODOLOGY TO ENSURE SOLUTION ELECTROSPINNABILITY AND SUCCESSFUL PRODUCTION OF DEFECT-FREE PLA NANOFIBRES 108
5.1 Introduction 108
5.2 Aims and objectives 110
5.3 Results and discussion 110
5.3.1 Thermodynamic criterion: solubility parameters 110
5.3.2 Electrical criterion: solvent dielectric constant 113
5.3.3 Rheological criterion: critical entanglement concentration (C_e) determination 116

5.3.4 Validation of the methodology 125

5.4 Conclusion 130

6 ANALYSIS OF THE EFFECT OF ELECTROSPINNING PROCESS PARAMETERS ON THE JET ELECTRIC CURRENT AND ON NANOFIBRE MORPHOLOGY AND MEAN DIAMETER 133

6.1 Introduction 133

6.2 Aims and objectives 136

6.3 Results and discussion 136

6.3.1 Effect of process parameters on the nanofibre morphology and mean diameter 136

6.3.1.1 Effect of applied voltage (V) 147

6.3.1.2 Effect of collection distance (d) 150

6.3.1.3 Effect of flow rate (Q) 153

6.3.2 Measurements of electric current I 155

6.3.2.1 Current-voltage (I-V) relationship 159

6.3.2.2 Current-distance (I-d) relationship 163

6.3.2.3 Current-flow rate (I-Q) relationship 165

6.3.2.4 Predicted vs experimental nanofibre diameter 168

6.4 Conclusion 173

7 PRODUCTION OF CORE-SHELL NANOFIBRES BY COAXIAL ELECTROSPINNING FOR ENCAPSULATION OF HYDROPHILIC DRUG 175

7.1 Introduction 175

7.2 Aims and objectives 177

7.3 Results and discussion 178

7.3.1 Characterization of solution properties 179

7.3.2 Physical characterisation of nanofibres 180

7.3.2.1 Scanning electron microscopy (SEM) analysis 180

7.3.2.2 Transmission electron microscopy (TEM) analysis 187

7.3.2.3 Confocal laser scanning microscopy (CLSM) analysis 191

7.3.2.4 Focus ion beam-scanning electron microscopy (FIB-SEM) 197
7.3.2.5 Water contact angle (WCA) measurements 199
7.3.2.6 Differential scanning calorimetry (DSC) analysis 201
7.3.2.7 Fourier transform infrared spectroscopy (FTIR) analysis 205
7.3.2.8 X-ray photoelectron spectroscopy (XPS) analysis 210
7.3.2.9 Drug encapsulation efficiency and drug release 215
7.3.2.9.1 Efficiency of drug encapsulation 215
7.3.2.9.2 Drug release studies 216
7.4 Conclusion 223
8 CONCLUSION AND FUTURE WORK 225
8.1 Conclusions 225
8.2 Framework for Testing and Designing Electrospun Nanofibres 228
8.3 Future work 230
REFERENCES 232
APPENDIX 258

List of figures

Figure 2.1 - Schematic diagram of an electrospinning setup. 6
Figure 2.2 - Increase in the number of publications on electrospinning (including journal and conference papers, reviews, and books) over a fifteen year period (Source: Scopus, 18/06/2014, search using keyword 'electrospinning'). 8
Figure 2.3 – Schematic diagram of the polymeric jet path from the needle to the collector. .. 11
Figure 2.4 – Schematic illustration of the Taylor cone and jet formation: (A) the applied electric field creates surface charges in the polymeric solution; (B) increasing the voltage the drop is elongated; (C) when the voltage is higher than V_C, the polymeric jet is formed and travels towards the collector due to the charge repulsion. 12
Figure 2.5 – Diagram showing onset and development of bending instabilities (K. Garg & G.L. Bowlin 2011) 14
Figure 2.6 - Viscoelastic dumbbell representing a segment of the rectilinear part of the jet (Reproduced from (D.H. Reneker et al. 2000) 14
Figure 2.7 - (a) Axisymmetric and (b) non-axisymmetric instabilities in a fluid jet in an external electric field 15
Figure 2.8 – The concentration of PAMPS in the PAMPS/ethanol/water solutions versus electric current during electrospinning (S. J. Kim et al. 2004). 18
Figure 2.9 – Physical representation of the three solution regimes (a) dilute, (b) semidilute unentangled and (c) semidilute entangled. 22
Figure 2.10 – Cross-section morphology of PS fibres electrospun from PS solution in (a) DMF and (b) THF (J. Zheng et al. 2012). 30
Figure 2.11 – Representation of the plasma drug concentration over time in conventional drug delivery systems (Tsung & Burgess 2012). 38
Figure 2.12 – Synthesis methods for obtaining high molecular weight PLA polymers (L. T. Lim et al. 2008). 40
Figure 2.13 – Stereoisomers of lactide. 41
Figure 2.14 – Metastable states of high molecular weight crystalline PLAs (Rafael Auras et al. 2004). 42
Figure 2.15 – Metastable states of high molecular weight amorphous PLAs (Rafael Auras et al. 2004). 42

Figure 2.16 – Schematic illustration of the changes a polymer matrix undergoes during surface erosion and bulk erosion (Friederike von Burkersroda, Luise Schedl 2002). 46
Figure 2.17 – (B) Mefoxin release profile from PDLA nanofibres and (C) Mefoxin release profile in the logarithmic form to evaluate the nature of diffusion (Zong et al. 2002).....48
Figure 2.18 – Schematic coaxial electrospinning setup (Moghe & B. S. Gupta 2008). 52
Figure 2.19 – In vitro release of drug from electrospun PLA nanofibrous membranes when incubated in the buffer solution (pH 7.35, 37°C) with different PLLA shell concentrations (C. He et al. 2006). 53
Figure 2.20 – Comparison from core-shell nanofibres and blending electrospinning (G. Jin et al. 2013) 54
Figure 2.21 – Coaxial electrospinning of PCL shell material and PEO/water/EtOH core material a) optical microscopy, (b, c, d) SEM images at different magnifications PLC (Dror et al. 2007). 56
Figure 3.1 – Molecular weight distribution of PLA 4060D.....61
Figure 3.2 – Chemical structure of lidocaine hydrochloride. 62
Figure 3.3 – Electrospinning setup (A), syringe pump (B), high voltage source (C) (Loughborough University). 64
Figure 3.4 – Electrospinning setup (A), syringe pumps (B), high voltage source (C), (Radboud University, Biomaterials Department, Nijmegen, NL). 66
Figure 4.1 – Scanning electron micrographs of PLA nanofibres from solutions of 10% (w/v) of PLA in acetone: (a) 10,000X (b) 5,000X (c) 2,000X (d) nanofibre diameter distribution..79
Figure 4.2 – Scanning electron micrographs of PLA nanofibres from PLA solutions at a PLA concentration of 10% (w/v) in: (a, b) 1,4-dioxane (2,000X and 5,000X); (c, d) tetrahydrofuran (2,000 X). 81
Figure 4.3 – Scanning electron micrographs of PLA nanofibres from PLA solutions at a PLA concentration of 10% (w/v) in: (a, b) dichloromethane (3,000X and 5,000X), (c, d) chloroform (3,000 X and 5,000 X). 82
Figure 4.4 – Scanning electron micrographs of PLA nanofibres from PLA solutions at a PLA concentration of 10% (w/v) in: (a, b) dimethylformamide (5,000 X and 10,000 X); (c, d) dimethylacetamide (5,000 X and 10,000 X). 83
Figure 4.5 – Scanning electron micrographs of PLA nanofibres from solutions of 10% (w/v) of PLA in AC/1,4-DX at magnification of (a) 2,000 X (b) 5,000 X (c) 7,000 X (d) nanofibre diameter distribution. 85

Figure 4.6 – Scanning electron micrographs of PLA nanofibres from solutions of 10% (w/v) of PLA in AC/THF at magnification of (a) 2,000 X (b) 5,000 X (c) 10,000 X (d) nanofibre diameter distribution. 87
Figure 4.7 – Scanning electron micrographs of PLA nanofibres from solutions of 10% (w/v) of PLA in AC/DCM at magnification of (a, b) 5,000 X (c) 10,000 X (d) nanofibre diameter distribution. 88
Figure 4.8 – Scanning electron micrographs of PLA nanofibres from solutions of 10% (w/v) of PLA in AC/CHL at magnification of (a) 5,000 X (b, c) 10,000 X (d) nanofibre diameter distribution. 89
Figure 4.9 – Scanning electron micrographs of PLA nanofibres from solutions of 10% (w/v) of PLA in AC/DMF at magnification of (a) 4,000 X (b) 10,000 X (c) 20,000 X (d) nanofibre diameter distribution. 90
Figure 4.10 – Scanning electron micrographs of PLA nanofibres from solutions of 10% (w/v) of PLA in AC/DMAc at magnification of (a) 2,000 X (b) 5,000 X (c) 20,000 X (d) nanofibre diameter distribution. 91
Figure 4.11 – Effect of (a) surface tension, (b) viscosity and (c) conductivity of PLA solution in binary solvent system on mean nanofibre diameter....92
Figure 4.12 – Effect of the boiling point of the second solvent in binary solvent systems on mean nanofibre diameter....93
Figure 4.13 – Effect of solvent ratio (AC/DMF) on nanofibre morphology: scanning electron micrographs of PLA nanofibres from solutions of 10% (w/v) of PLA in AC/DMF at a ratio of 20/80 (v/v) (a) 3,000 X (a) 10,000 X; 40/60 (c) 5,000 X (d) 15,000X. 94
Figure 4.14. Effect of solvent ratio (AC/DMF) on nanofibre morphology: scanning electron micrographs of PLA nanofibres from solutions of 10% (w/v) of PLA in AC/DMF at a ratio of (a-b) 50/50 v/v (4,000 X - 10,000 X); (c-d) 60/40 v/v (5,000 X - 10,000 X); (e-f) 80/20 v/v (3,000 X - 10,000 X). 95
Figure 4.15 – (A) Effect of solvent ratio (AC/DMF) on surface tension of PLA solutions, (B) effect of surface tension on nanofibre diameter. 97
Figure 4.16. (A) Effect of solvent ratio (AC/DMF) on conductivity of PLA solutions, (B) effect of conductivity on nanofibre diameter. 98
Figure 4.17 – Effect of polymer concentration on nanofibre morphology: scanning electron micrographs of PLA nanofibres from solutions of PLA in AC/DMF at a ratio of 50/50 v/v at

concentration of (a, b) 3% w/v (5,000 X - 10,000 X); (c, d) 4% w/v (5,000 X - 10,000 X); (e, f) 5% w/v (5,000 X - 10,000 X).....100
Figure 4.18. Effect of polymer concentration on nanofibre morphology: scanning electron micrographs of PLA nanofibres from solutions of PLA in AC/DMF at a ratio of 50/50 v/v at concentration of (a, b) 6% w/v (5,000 X - 15,000 X); (c, d) 7.5% w/v (5,000 X - 10,000 X); (e, f) 10% w/v (5,000 X - 10,000X).....101
Figure 4.19. Effect of polymer concentration on nanofibre morphology: scanning electron micrographs of PLA nanofibres from solutions of PLA in AC/DMF at a ratio of 50/50 v/v at concentration of (a, b) 12.5% w/v (1,000 X - 10,000 X); (c, d) 15% w/v (5,000 X - 10,000 X). 102
Figure 4.20. Effect of PLA concentration on mean nanofibre diameter (a) 7.5% w/v (b) 10.0% w/v (c) 12.5% w/v (d) 15% w/v.....103
Figure 4.21. Effect of PLA concentration on viscosity of PLA solution in AC/DMF (50/50 v/v). 105
Figure 4.22. Effect of PLA concentration in acetone/dimethylformamide (50/50 v/v) on the elastic (G') and plastic (G'') modulus at 1 Hz.....106
Figure 5.1 – Representation of solvents and PLA in the Hansen tridimensional space. 112
Figure 5.2 – Solution conductivity (K) of PLA solutions in AC, DMF, and AC/DMF at several polymer concentrations.....115
Figure 5.3 – Effect of polymer concentration on nanofibre morphology - scanning electron micrographs of PLA nanofibres from solutions of PLA in AC at concentration (A, B) 3% w/v (5,000 and 10,000 X), (B, C) 4% w/v (5,000 and 10,000 X), (E, F) 5% w/v (5,000 and 10,000 X). 117
Figure 5.4 – Effect of polymer concentration on nanofibre morphology - scanning electron micrographs of PLA nanofibres from solutions of PLA in AC at concentration (A, B) 6% w/v (5,000 and 10,000 X), (C, D) 7.5% w/v (5,000 and 10,000 X), (E, F) 10 % w/v (5,000 and 10,000 X). 118
Figure 5.5 – Effect of polymer concentration on nanofibre morphology - scanning electron micrographs of PLA nanofibres from solutions of PLA in AC at concentration (A, B) 12.5% w/v (10,000 and 15,000 X), (C, D) 15.0% w/v (5,000 and 15,000 X). 119
Figure 5.6 – Effect of PLA concentration in AC solution on nanofibre diameter (A) 10% (B) 12.5% (C) 15%.....120

Figure 5.7 – Effect of polymer concentration on nanofibre morphology - scanning electron micrographs of PLA nanofibres from solutions of PLA in DMF at concentration (A) 7.5% w/v (15,000 X), (B) 10% w/v (15,000 X), (C) 12.5% w/v (5,000), (D) 15% w/v (5,000), (E) 17.5% w/v (5,000), (F) 20% w/v (10,000).....122
Figure 5.8. Effect of the polymer concentration on the shear viscosity of PLA solution in (A) AC and (B) DMF. 123
Figure 5.9. Effect of PLA concentration on elastic (G') and plastic (G") modulus of PLA solution in DMF.....125
Figure 5.10 – Scanning electron micrographs of PLA nanofibres from solutions of PLA in DX at a concentration of (A) 10% w/v and (B) 15% w/v.....126
Figure 5.11. Scanning electron micrographs of PLA nanofibres from solutions of PLA in CHL at a concentration of (A) 10% w/v and (B) 15% w/v. 127
Figure 5.12. Scanning electron micrographs of PLA nanofibres from solutions of PLA in DX/DMF (50/50 v/v) at concentration of 10% w/v 5000x (A) and 20000x (B), and concentration of 15% w/v 5000x (C) and 20000x (D). 128
Figure 5.13. Scanning electron micrographs of PLA nanofibres from solutions of PLA in CHL/DMF (50/50 v/v) at concentration of (A, B) 10% w/v (5000x and 25000x), (C, D) 15% w/v (5000x and 10000x).....129
Figure 5.14. Diameter distribution of nanofibres collected from PLA solution in DX/DMF at concentration of (A) 10% and (B) 15%, and PLA solution in CHL/DMF at concentration of (C) 10% and (D) 15%. 130
Figure 6.1 – Scanning electron micrographs of PLA nanofibres from solutions of 12.5 % (w/v) of PLA in acetone/dimethylformamide (AC/DMF) (50/50 v/v) at voltage of 7.5 kV (A, B) 0.5 ml/h, 10 cm, (C, D) 0.5 ml/h, 15 cm, (E, F) 1.0 ml/h, 15 cm, (G, H) 1.0 ml/h, 10 cm.....140
Figure 6.2 – Scanning electron micrographs of PLA nanofibres from solutions of 12.5 % (w/v) of PLA in acetone/dimethylformamide (AC/DMF) (50/50 v/v) at voltage of 10 kV and (A, B) 0.5 ml/h, 10 cm, (C, D) 0.5 ml/h, 15 cm, (E, F) 1.0 ml/h, 10 cm, (G, H) 1.0 ml/h, 15 cm....141
Figure 6.3 – Scanning electron micrographs of PLA nanofibres from solutions of 12.5 % (w/v) of PLA in acetone/dimethylformamide (AC/DMF) (50/50 v/v) at voltage of 15 kV and (A, B) 0.5 ml/h, 10 cm, (C, D) 0.5 ml/h, 15 cm, (E, F) 1.0 ml/h, 10 cm, (G, H) 1.0 ml/h, 15 cm....142
Figure 6.4 – Scanning electron micrographs of PLA nanofibres from solutions of 12.5 % (w/v) of PLA in acetone/dimethylformamide (AC/DMF) (50/50 v/v) at voltage of 20 kV and (A, B) 1 ml/h, 15 cm, (C, D) 1 ml/h, 10 cm, (E, F) 0.5 ml/h, 15 cm, (G, H) 0.5 ml/h, 10 cm.....143

Figure 6.5 – Scanning electron micrographs of PLA nanofibres from solutions of 12.5 % (w/v) of PLA in acetone/dimethylformamide (AC/DMF) (50/50 v/v) at 2 ml/h (A, B) 7.5 kV, 10 cm, (C, D) 7.5 kV, 15 cm (E, F) 10 kV, 10 cm (G, H) 10 kV, 15 cm. 144
Figure 6.6 – Scanning electron micrographs of PLA nanofibres from solutions of 12.5 % (w/v) of PLA in acetone/dimethylformamide (AC/DMF) (50/50 v/v) at 2 ml/h (A, B) 15 kV, 10 cm, (C, D) 15 kV, 15 cm (E, F) 20 kV, 10 cm (G, H) 20 kV, 15 cm. 145
Figure 6.7 – Effect of voltage on mean nanofibre diameter at flow rate of (a) 0.5 ml/h, (b) 1 ml/h, (c) 2 ml/h. 148
Figure 6.8 – Effect of collection distance on mean nanofibre diameter at voltages of (a) 7.5 kV (b) 10 kV (c) 15 kV (d) 20 kV. 151
Figure 6.9 – Effect of flow rate on mean nanofibre diameter at voltages of (a) 7.5 kV (b) 10 kV (c) 15 kV (d) 20 kV.....154
Figure 6.10 – Current measured as a function of the electrospinning process time at collection distance of 10 cm and voltage of (A) 7.5 kV, (B) 10 kV (C) 15 kV (D) 20 kV. 158
Figure 6.11 – Effect of (A) applied voltage and (B) electric field strength on the electric current (C) effect of applied voltage on volume charge density.....160
Figure 6.12 – Effect of the applied voltage on the nanofibre diameter. 162
Figure 6.13 – Effect of collection distance on current (A, B) and volume charge density (C, D) for applied voltage of 7.5, 10, 15 and 20 kV. 164
Figure 6.14 – Effect of the collection distance on the predicted diameter. 165
Figure 6.16 – Effect of flow rate on current (A, B) and volume charge density (C, D) for applied voltage of 7.5, 10, 15 and 20 kV. 166
Figure 6.17 – Effect of flow rate on the predicted nanofibre diameter.....167
Figure 6.18 – Experimental versus predicted nanofibre diameter for PLA solution in AC/DMF using a value of χ of 100.....169
Figure 6.19 – A comparison of the experimental and predicted fibre diameters (Sergey V Fridrikh et al. 2003). 170
Figure 6.20 – The terminal jet diameter h_t as a function (Q/I) compared to the theory. 171
Figure 6.21 – The log of fibre diameter versus the log of (Q/I) for several PCL concentrations (Sergey V Fridrikh et al. 2003). 171
Figure 7.1 – Scanning electron micrographs of core-shell nanofibres with no drug at different core flow rates (A, B) 0.3 ml/h, (C, D) 0.5 ml/h, (E, F) 0.7 m/h. 182

Figure 7.2 – Scanning electron micrographs of core-shell nanofibres with drug loaded in the core at different core flow rates (A, B) 0.3 ml/h, (C, D) 0.5 ml/h, (E, F) 0.7 m/h.....183
Figure 7.3 – Core shell nanofibres (no drug) presented (A, B) 2.1-0.3 ml/h, (C) 2.1-0.5 ml/h, (D) 2.1-0.7 ml/h. 184
Figure 7.4 – Core-shell nanofibres loaded with drug (A, B) 2.1-0.3 ml/h, (C) 2.1-0.5 ml/h, (D) 2.1-0.7 ml/h. 185
Figure 7.5 – Mean diameter for core-shell nanofibres. 186
Figure 7.6 – Core-shell nanofibres produced at core-shell flow rate ratio 0.3/2.1 ml/h. 188
Figure 7.7 – Core-shell nanofibres produced at core-shell flow rate ratio 0.5/2.1 ml/h. 189
Figure 7.8 – Core-shell nanofibres produced at core-shell flow rate ratio 0.7/2.1 ml/h. 190
Figure 7.9 – CLSM images of nanofibres (**no drug)** collected using a core-shell flow rate of 0.3-2.1 ml/h (A-D) 10 μm, (E-L) 50 μm. 193
Figure 7.10 – CLSM images of nanofibres (**no drug**) collected using core-shell flow rate of (A-D) 0.5-2.1 ml/h, (E-F) 0.7-2.1 ml/h. 194
Figure 7.11 – CLSM images of nanofibres **loaded with drug** collected using core-shell flow rate of (A-D) 0.3-2.1 (E-H) 0.5-2.1 (I-L) 0.7-2.1 ml/h. 196
Figure 7.12 – FIB-SEM images of nanofibres collected using core solution flow rate of 0.5 ml/h. 198
Figure 7.13 – Water contact angle values of PLA and PVA nanofibres and core shell nanofibres, with and without drug. 201
Figure 7.14 – DSC thermogram of core shell PVA/PLA nanofibres with and without LidHCl. 204
Figure 7.15 – FTIR spectra of bulk materials (PVA, PLA and LidHCl) and all electrospun nanofibrous samples, with and without drug. 206
Figure 7.16 – FTIR spectra of bulk materials and core shell nanofibres without drug (A) 2,000 to 1,400 cm^{-1} (B) 1,400 to 1,000 cm^{-1}. 208
Figure 7.17 – FTIR spectra of bulk materials and core shell nanofibres with drug (A) 2,000 to 1,400 cm^{-1} (B) 1,400 to 1,000 cm^{-1}. 209
Figure 7.18 – Survey of neat materials (A) PLA pellet, (B) PVA powder, (C) LidHCl. 211
Figure 7.19 – High resolution XPS scan of PLA pellets (A) C 1s (B) O 1s. 211
Figure 7.20 – High resolution XPS scan of PVA powder (A) C 1s (B) O 1s. 212
Figure 7.21 – High resolution XPS scan of LidHCl (A) C 1s (B) O 1s (C) Cl 2p. 212

Figure 7.22 – Calibration curve of LidHCl in PBS solution at pH 7.4 and acetate buffer solution at pH 5.5. 215
Figure 7.23 – LidHCl cumulative release from nanofibrous samples to the release medium at pH 7.4. 218
Figure 7.24. LidHCl cumulative release from nanofibrous samples to the release medium at pH 5.5. 220
Figure 7.25 – Plot of ln(Mt/M∞) versus ln(t) for LidHCl release from core/shell nanofibres fabricated at a core feed rate of 0.3, 0.5 and 0.7 ml/h. 221
Figure 7.26 – SEM images of core shell nanofibrous discs after the drug release from the sample 2.1-0.3 (A, B) release medium at pH 7.4, (C, D) release medium at pH 5.5. 222
Figure 8.1 – Flow diagram for the production of defect free electrospun nanofibres. 229
Figure A.1 – Differential scanning calorimetry thermogram of bulk PLA (green curve) and PLA nanofibres (red curve)…… 258
Figure A.2 – Differential scanning calorimetry curve of neat PVA (green curve) and PVA nanofibres (red curve)……..... 259

List of tables

Table 2.1 - List of electrospinning companies. 9
Table 2.2 – Upstream electrospun nanofibre products. 10
Table 2.3 – Downstream products in which nanofibres are incorporated. 10
Table 2.4 – Lists of the most common solvents used in the electrospinning process with their physical and chemical characteristics (BP is the boiling point, η is the viscosity, γ is the surface tension and ε is the dielectric constant). 32
Table 2.5 – PLA-based products of NatureWorks® adapted from (Jamshidian et al. 2010; Dow 2004). 44
Table 2.6 – Exponent n of the power law and drug release mechanism from polymeric controlled drug delivery system of different geometry. 59
Table 3.1 – Average molecular weights of PLA 4060D: M_n is the number average molecular weight, M_w is the weight average molecular weight, M_z is the higher average molecular weight, M_v is the viscosity average molecular weight, PD is the polydispersity index (M_w/M_n). 62
Table 3.2 – List of solvents used to dissolve PLA (chapter 4, chapter 5, chapter 6). 62
Table 3.3 – List of chemicals used in chapter 7. 63
Table 3.4 – Emission and excitation λ_{max} of the fluorescent dyes incorporated in the solutions. 69
Table 3.5 – Characteristics chromatographic column HPLC system. 71
Table 4.1 – Physical and chemical properties of the solvents used (BP is the boiling point, η is the viscosity (at 25°C), γ is the surface tension (at 20°C), K is the electrical conductivity, ε is the dielectric constant (at 20°C, δ is the solubility parameter) (Smallwood 1996). 78
Table 4.2 – Viscosity, surface tension and conductivity of PLA solution at concentration of 10% w/v in single solvents. 80
Table 4.3 – Viscosity, surface tension and conductivity of PLA solution at concentration of 10% w/v in binary solvent systems. 86
Table 4.4 – Solution viscosity, surface tension and conductivity of PLA solution at concentration of 10% w/v in AC/DMF at different ratios. 96
Table 4.5 – Surface tension and electrical conductivity of PLA solution in AC/DMF at several polymer concentrations 104

Table 5.1 – List of solvent properties: Hildebrand solubility parameter (δ), density (ρ_s), molecular weight (M_w) and Flory-Huggins parameter (χ). 111
Table 5.2. Hansen solubility parameters of PLA and all solvents (Hansen 2007). 112
Table 5.3. R_A and RED value for solvents used in this work. 113
Table 5.4 – Value of overlap (C*) and entanglement (C_e) concentration for all solvent systems. 124
Table 5.5 – Viscosity, surface tension and conductivity of PLA solution in DX and CHL. . 126
Table 5.6. Viscosity, surface tension and conductivity of PLA solution in DX/DMF and CHL/DMF. 128
Table 6.1 – List of scientific publications investigating the effect of applied voltage on the nanofibre morphology and diameter. 134
Table 6.2 – List of experiments performed. 137
Table 6.3 – Mean nanofibre diameter and standard deviation for all experiments 147
Table 6.4 – P-value of the ANOVA analysis for the voltage effect on the mean diameter. .. 149
Table 6.5 – P-value from the ANOVA analysis for the collection distance effect on the mean diameter 152
Table 6.6 – P-value from the ANOVA analysis for the flow rate effect on the mean diameter. 154
Table 6.7 – Mean value of electric current (I) recorded during all experiments with correspondent volume charge density. 156
Table 6.8 – Exponent value of the power law relationship between voltage (or electric field strength) and current. 160
Table 7.1 – List of scientific publications regarding the production of core/shell nanofibres loaded with hydrophilic molecule. 176
Table 7.2 – Solution properties of core and shell solutions. 179
Table 7.3. Glass transition temperature (T_g), melting point (T_m) and heat of fusion (ΔH_m) of core shell nanofibres with and without drug. 204
Table 7.4 – Atomic percent of each element and amount (%) of each bonding in bulk materials. 213
Table 7.5 – Binding energy for C1s and O1s for bulk materials and nanofibres. 213
Table 7.6. Atomic percent of each element (C, O, N, Cl) and amount (%) of each bonding in core shell nanofibre samples with and without drug. 214

Table 7.7 – Apparent efficiency of LidHCl encapsulation in the core shell nanofibrous samples.....216
Table 7.8 – Data fit parameters of LidHCl release profiles. 221
Table A.1 – Glass transition temperature of PLAs…….....258
Table A.2 – Melting point (T_m), heat of fusion (ΔH_m), crystallization temperature (T_c) and heat of crystallization (ΔH_c) of PVAs…….259

List of abbreviations and symbols

Abbreviations

2D	Two dimensional
3D	Three dimensional
AC	Acetone
BSA	Bovine serum albumin
BTEAC	Benzyl triethylammonium chloride
CA	Cellulose acetate
CHL	Chloroform
CLSM	Confocal laser scanning microscopy
DCM	Dichloromethane
DMAc	Dimethylacetamide
DMF	Dimethylformamide
DSC	Differential scanning calorimetry
DTAB	Dodecyltrimethylammonium bromide
DX	1,4-dioxane
ECM	Extra cellular matrix
EtOH	Ethanol
FA	Formic acid
FTIR	Fourier transform infrared spectroscopy
KH_2PO_4	Monopotassium phosphate
LiCl	Lithium chloride
LidHCl	Lidocaine hydrochloride
MeOH	Methanol
NaCl	Sodium chloride
NaH_2PO_4	Monosodium phosphate
PA6	Nylon 6
PAN	Poly (acrylonitrile)
PBS	Poly (butylene succinate)
PCL	Poly (caprolactone)
PCU	Poly (carbonate urethane)
PEG	Poly (ethylene glycol)

PELA	Poly (l,d-lactide-co-ethylene glycol)
PEO	Poly (ethylene oxide)
PEVA	Poly (ethylene-vinyl acetate)
PGA	Poly (glycolic acid)
PHBV	Poly (hydroxybutyrate-co-valerate)
PLA	Poly (lactic acid)
PLGA	Poly (lactic-co-glycolic acid)
PS	Poly (styrene)
PVA	Poly (vinyl alcohol)
PVDF	Poly (vinylidene fluoride)
PVP	Poly (vinyl pyrrolidone)
SEM	Scanning electron microscopy
TBAC	Tetrabutylammonium chloride
TEM	Transmission electron microscopy
TFE	Trifluoroethanol
THF	Tetrahydrofuran
XPS	X-ray photoelectron spectroscopy

Symbols

C	Polymer concentration	g/ml
C*	Critical overlap concentration	g/ml
C_e	Entanglement concentration	g/ml
E	Electric field strength	V/m
H (d)	Distance between needle and collector	cm
I	Electric current	A
L	Length of the needle	cm
M_w	Weight average molecular weight	g/mol
Q	Volumetric flow rate	m^3/s
R	Radius of the needle	cm

T	Temperature	°C
T_c	Crystallization temperature	°C
T_g	Glass transition temperature	°C
T_m	Melting temperature	°C
V	Voltage	V
V_C	Critical voltage	V
K	Conductivity	μS/cm

Greek letters

[χ]	Flory–Huggins chi parameter	
η	Dynamic viscosity	Pa·s
μ	Kinematic viscosity	m^2/s
γ	Surface tension	mN/m
δ	Solubility parameter	$MPa^{1/2}$
ρ	Density	kg/m^3
ε	Dielectric permittivity	
χ	Dimensionless whipping instability	
σ	Surface charge density	C/l

1 INTRODUCTION

1.1 Background

In the last twenty years nanometre scale fibres have gained the attention of scientists and engineers in fields such as filtration system, energy storage, composite production and biomedical engineering. This is due to their unique and outstanding chemical, physical and mechanical properties (Bhardwaj & Kundu 2010; K. Garg & G.L. Bowlin 2011; Z. M. Huang et al. 2003). Drawing, phase separation, template synthesis, self-assembly and electrospinning, are the techniques that could be used to produce nanofibres (Nayak et al. 2012). However, each production methods has its advantages and limitations (Barnes et al. 2007). Highly porous nanofibrous structures can be produced with the phase separation method, but several steps are required and a limited number of polymers can be processed (P. X. Ma & R. Zhang 1999; van de Witte et al. 1996). Self-assembly is a bottom up process which uses small molecules to build up blocks and give nanofibres (Whitesides & Grzybowski 2002). Morphology and properties of these nanofibres depend on the type of molecules and intermolecular forces that bring the molecules together. Therefore the scaling up of this process would be highly complex. While one-by-one single fibres are produced with drawing of solutions made of short molecules instead of long polymer chains (Ondarcuhu & Joachim 1998), long continuous nanofibres can be collected using electrospinning. Of all the techniques, electrospinning is the most promising process mainly due to its simplicity and the potential for increasing mass production. It is a relatively simple one-step, top-down process to produce nanofibres with different morphologies and geometries by changing solution and spinning parameters (Subbiah et al. 2005; Thompson et al. 2007). Furthermore, while mechanical forces are used in the conventional spinning methods, an electric field is created in the electrospinning process and this leads to the production of much thinner fibres.

Hundreds of polymers have been used to fabricate nanofibrous structures, including cellulose acetate (CA) (P Taepaiboon et al. 2006), chitosan (Peesan et al. 2006), silk fibroin (K. H. Kim et al. 2005), poly(caprolactone) (PCL) (Van der Schueren et al. 2011; D.H. Reneker et al. 2002), poly(lactic acid) (PLA) (Ishii et al. 2009), nylon 6 (PA 6) (P. Supaphol et al. 2005) and poly(ethylene oxide) (PEO) (Y.Q. Wan et al. 2007). Multi-composition nanofibres have

also been prepared by electrospinning of polymeric solutions made up of two polymers (generally one natural polymer with a synthetic polymer), a polymer blended with nanoparticles (Jamnongkan et al. 2013; E. S. Kim et al. 2010), carbon nanotubes (S. Shao et al. 2011; Y. H. Meng et al. 2008; Yeo & Friend 2006) or ceramics (Jose et al. 2009). Furthermore developments of the technique have been reported, such as multilayer electrospinning (Pham, U. Sharma & A. G. Mikos 2006) and coaxial electrospinning (Ji et al. 2010; H. Jiang et al. 2006; T. T. T. Nguyen et al. 2011). Small diameter, high pore density and large surface area to volume ratio are the main advantages that electrospun nanofibres can offer to several types of applications, such as filtration (Heidei et al. 2004), chemical and optical sensors (Ding et al. 2009; Scampicchio et al. 2012), biological scaffolds (Dahlin et al. 2011; Soliman et al. 2010; Pham, U. Sharma & A.G. Mikos 2006), wound dressings (M. Khil et al. 2003; Nawalakhe et al. 2013) and drug delivery systems (Sill & Von Recum 2008; E. R. Kenawy et al. 2002).

1.2 Aims and objectives

Nanofibres of poly (lactic acid) (PLA) have shown great potentials especially in biomedical applications (F Yang et al. 2004; Molamma P Prabhakaran et al. 2009; E. S. Kim et al. 2010). The selection of the solvent to dissolve PLA in the literature is based on experience from similar polymer-solvent systems. Most of these solvents are chlorinated, fluorinated and toxic solvents and the selection of greener solvents is still a major challenge in solution electrospinning. A better understanding of the interactions between the polymer and solvent would be very useful because different solvents lead to the production of nanofibres with different morphologies.

Considering the electrospinning process parameters, there have been discrepancies with regards to observations of the effects of the applied voltage. Some studies reported that on increasing applied voltage the fibre diameter decreased for some polymer-solvent systems, while it increased for others. The reasons for this difference in behaviour are not fully explained and no mechanism has been proposed that could justify these observations. Moreover, due to the fact that some variables are also closely correlated, such as M_w, viscosity and concentration, systematic studies should be carried out to define the concentration required for the production of defect-free electrospun nanofibres. In fact the

role of viscoelasticity on the electrospinning process and its effect of final nanofibre morphology, mean diameter and diameter distribution, has been not fully understood, and solvent evaporation has not been taken into account in modelling the electrospinning jet behaviour. The electrodynamics of the jet motion in electrospinning are affected by the rheological properties of the polymeric jet (J. J. Feng 2002) and in addition when the solvent evaporates, the solution viscoelasticity is affected as the jet is stretched and bent towards the collector. Recently Wu et al (X. F. Wu et al. 2011) revealed that solvent evaporation should be considered for better control of the electrospinning process and therefore to control nanofibre diameter and diameter distribution.

The first part of this thesis focused on the effect of different solvent systems and hence solution properties, including viscosity, solution conductivity and surface tension, on the morphology of electrospun PLA nanofibrous mats, mean nanofibre diameter and diameter distribution. The effects of the solution properties and of the polymer concentration were studied. For each solution both shear viscosity and viscoelasticity were measured and their relationship with the morphology of the electrospun PLA structures was determined (refer to chapter 4).

As the first step of electrospinning is the selection of a solvent to dissolve the polymer, an integrated three step methodology was proposed for the choice of solvent systems to produce electrospinnable solutions that form defect-free poly (lactic acid) nanofibres with narrow diameter distribution. The solvent systems were chosen using a thermodynamic approach, combined with electrical and rheological property criteria, which represented the second and the third step, respectively. This methodology can be applied for a wide range of polymers (refer to chapter 5).

Depending on the type of applications, different morphologies, fibre diameter and diameter distributions are required. However, the prediction of the final nanofibre diameter is still one of the major challenges of solution electrospinning. It would be very useful to have a scaling model which predicts mean diameter from solution properties and electrospinning process conditions. Chapter 6 presents the investigation of the effects of processing parameters on the size and structures of electrospun poly(lactic acid) fibres. The jet electric current is measured during the experiments in order to improve the understanding of the process parameters by using the proposed model which was derived from a force balance between surface tension

and electrical forces.

The last part of this thesis involved the production of electrospun PLA nanofibres with a core shell structure using coaxial electrospinning. A model drug was encapsulated in the core made of a hydrophilic polymer. Different techniques were employed to verify the formation of a continuous core shell structure and the encapsulation of the drug within the core of the fibres. Next, drug release studies were performed. The work reported in chapter 7 describes an attempt to improve the understanding of the important criterion of core-shell electrospinning for the encapsulation of hydrophilic molecules.

1.3 Research questions

This doctoral thesis seeks to address the following research questions.

- Is there a model procedure for researching new polymer and solvent systems with more environmentally friendly chemistry to enable the production of defect free nanofibres, with the minimum number of electrospinning experiments?
- Is there a relationship between polymer solubility and electrospinnability of the polymer solution to produce defect free nanofibres?
- Can the final diameter of electrospun PLA nanofibres be predicted by knowing solution properties and process parameters?
- Can a hydrophilic drug be incorporated in the core of electrospun nanofibres with a shell of hydrophobic material in a controllable way?

1.4 Publications and Conference papers

Papers

R. Casasola, N.L. Thomas, A. Trybala, S. Georgiadou; Electrospun poly lactic acid (PLA) fibres: Effect of different solvent systems on fibre morphology and diameter; *Polymer 55 (2014) 4728-4737*

R. Casasola, N.L. Thomas, S. Georgiadou; Electrospinning of poly (lactic acid): theoretical approach for the solvent selection to produce defect-free electrospun nanofibres; Journal of

Polymer Science Part B: Polymer Physics 54 (2016) 1483-1498

Oral presentations

NART 2015, Prague, Czech Republic, 31st August – 2nd September 2015; *Biodegradable Core/Shell (PVA/PLA) Nanofibres as Drug Delivery Carrier*

Research Day, Materials Department, Loughborough University, Loughborough, June 2014; *Effect of Polymer Chain Entanglements on Poly (lactic acid) (PLA) Electrospun Nanofibres*

Electrospinning: Principles, Possibilities and Practice, Institute of Physics, London 5th – 6th December 2013; *Effect of chain entanglements on electrospun poly lactic acid (PLA) fibres*

Istanbul Textile International Congress 2013, Istanbul, Turkey, 30th – 31st May 2013; *Effect of solvent systems on electrospun polymeric fibres: preliminary study on poly lactic acid (PLA)*

Research Day, Materials Department, Loughborough University, Loughborough, June 2012: *PLA Nanofibres by Electrospinning for Tissue Engineering*

Poster presentations

Research Day, Materials Department, Loughborough University, Loughborough, 17th July 2013; *Biodegradable Polymer for Tissue Engineering: Poly Lactic Acid (PLA) Nanofibres By Electrospinning*

Training schools

COST Action MP1206 - Training school 'Electrospinning: Exploiting electrodynamics and rheology for the control of nanofiber structural and physical properties', Udine, Italy, 1st – 5th September 2014

COST Action MP1206 - Training school on board of the Polymar conference, 3rd – 7th November 2013

2 LITERATURE REVIEW

2.1 Electrospinning

The term ‘electrospinning’ derives from ‘electrostatic spinning’ (Z. M. Huang et al. 2003; Bhardwaj & Kundu 2010). Electrospinning is a process that relies on the application of electrostatic forces to produce continuous fibres from polymeric solution or polymer melt. Hence, it is considered an electrodynamic phenomenon (Collins et al. 2012; D.H. Reneker & I. Chun 1996). The process requires a simple apparatus which mainly consists of a syringe pump, a glass or plastic syringe connected to a metallic needle, a high voltage power supply, and a conducting collector as shown in Figure 2.1. Electrospinning is often conducted within a closed chamber with a ventilation system because most of the solvents used to prepare the polymeric solution may be toxic and release harmful smells.

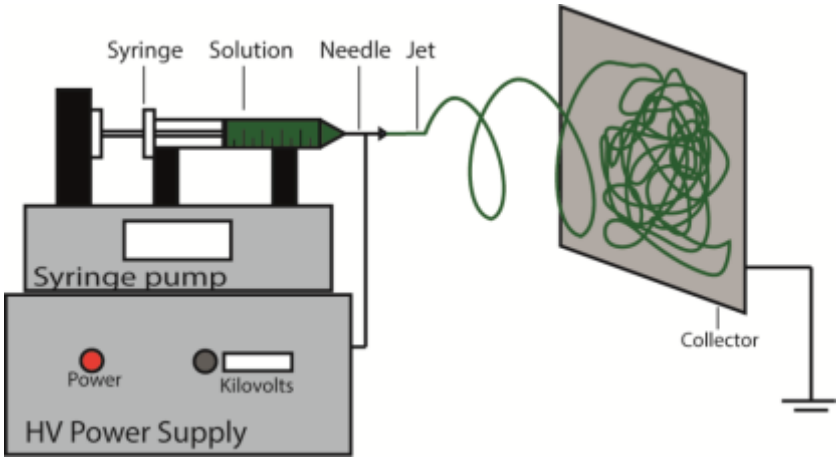

Figure 2.1 - Schematic diagram of an electrospinning setup.

The syringe pump is used to force the liquid at constant feed rate through the needle forming a pendant drop at the tip. High voltage, generally from 5 to 30 kV, is applied to the polymer solution through the metallic needle and imparts electrical charges to the polymer solution (Teo & S. Ramakrishna 2006). As the electrical forces overcome the solution surface tension force which holds the polymeric solution at the needle tip, a polymeric jet is emitted from the

needle tip and travels towards the collector. The electric field allows the evaporation of the solvent from the polymeric jet, a mass transfer process occurs and consequently nanofibres are produced (D. Liang et al. 2007; Sill & von Recum 2008). The repulsion of the electrical charges with same sign at the jet surface causes the stretching of the electrospun jet resulting therefore in the production of fibres with diameter ranging from several nanometres to few micrometres.

The interactions between a fluid in motion and an electric field were investigated by recording the process of electrospray in 1600 by William Gilbert (Tucker et al. 2012), but the process of electrospinning was first patented by John Francis Cooley (Cooley 1902) and by William James Morton (W. J. Morton 1902). The first pioneer in the Western world was Antony Formhals (Formhals 1934) who patented the electrospinning process in the 1934. Formhals produced yarns made of cellulose acetate (CA) electrospun nanofibres using an electrostatic apparatus consisted of a rotating thread collector and he owns a sequence of 22 patents from 1934 to 1944 for the fabrication of textile yarns. A list of US patents filed before 1976 is reported in the electrospinning review of Teo and Ramakrishna (Teo & S. Ramakrishna 2006). In the late 1960s Taylor (Taylor 1964) published a work related to the behaviour of a fluid droplet initially formed at the needle tip when an electric field is created. It was shown that the droplet at the needle tip forms a cone with angle of 49.3 degrees when the surface tension force is balanced by electrostatic forces. In 1971 Baumgarten and his co-workers (Baumgarten 1971) electrospun solutions of a modified poly (acrylonitrile) (PAN) in dimethylformamide (DMF) and studied the effect of solution viscosity and process parameters on jet length and nanofibre diameter. The results have shown that an increase of polymer concentration led to higher solution viscosity and therefore bigger nanofibres were produced. After a decade nanofibres of poly (ethylene) (PE) and poly (propylene) (PP) were produced from the polymer melt (Larrondo & Manley 1981a; Larrondo & Manley 1981b; Larrondo & Manley 1981c). Thinner nanofibres were produced with an increase of electric field strength, by increasing applied voltage, and also on increasing the melting temperature at fixed applied voltage. Moreover the authors verified and confirmed the value of 49.3° for the Taylor cone (Larrondo & Manley 1981a). Few years later Doshi and Reneker (Doshi & D.H. Reneker 1995) electrospun poly(ethylene oxide) (PEO) aqueous solution at several polymer concentrations to investigate the effect on the nanofibre morphology. Continuous nanofibres were produced within a certain range of viscosity (η). Only beads were collected

for either too dilute PEO solutions (η < 800 centipoise (cP)), or too concentrated PEO solutions (η < 4000 cP). In addition a value of voltage called V_{start} when the jet is initiated, and a value of voltage (V_{stop}) when the jet ceased, were recorded. The results have shown that the value of both V_{start} and V_{stop} increased as the solution concentration increased. This indicates that more electric force is required to form the jet from polymer solution with higher viscosity.

The interest of researchers on the electrospinning process substantially increased with the global rise of nanotechnology. Several reviews on the electrospinning process and its possible applications have been published (Z. M. Huang et al. 2003; K. Garg & G.L. Bowlin 2011; Teo & S. Ramakrishna 2006; Sill & von Recum 2008; Bhardwaj & Kundu 2010). Figure 2.2 shows the exponential increase of the number of scientific publications on electrospinning from 1998 to 2013. Currently more than thirty companies are selling laboratory and industrial level electrospinning setup (Table 2.1) and several companies patented upstream and downstream products made of electrospun nanofibres (Table 2.2, Table 2.3). The current commercial electrospun nanofibre products are mostly used for water adsorption and air filtration. Nanofibrous structures possess small pore size, which leads to high filtration efficiency with simultaneously high permeability due to open fibre structure.

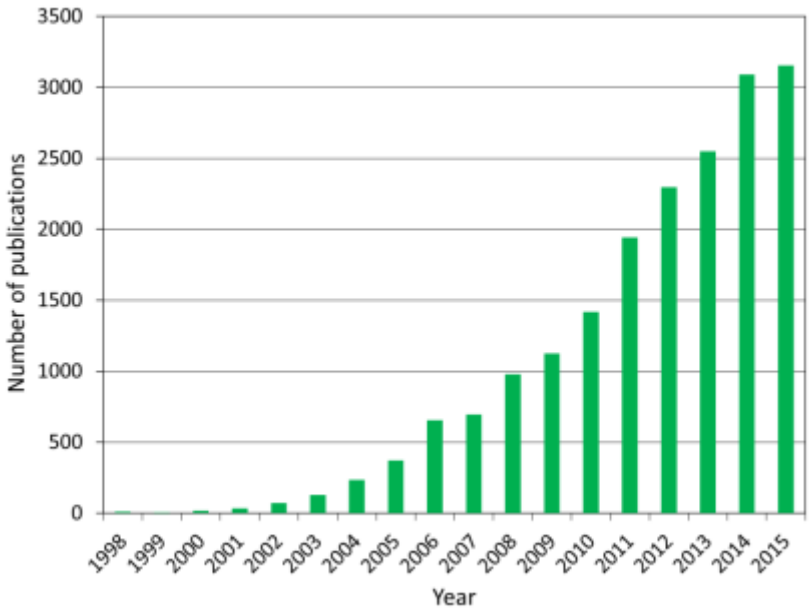

Figure 2.2 - Increase in the number of publications on electrospinning (including journal and conference papers, reviews, and books) over a fifteen year period (Source: Scopus, 18/06/2014, search using keyword ‘electrospinning’).

Table 2.1 - List of electrospinning companies.

Country	Name of the company	Type of service
Czech Republic	4SPIN	Laboratory setup and accessories
	Elmarco	Supplier of industrial level and lab scale electrospinning machine
	SPUR	Supplier of industrial level setup
Germany	Erich Huber GmbH	Laboratory setup and accessories
Hong Kong	NaBond	Lab scale electrospinning setup
India	Elixir Technologies	Supplier of lab base electrospinning machine and accessories
	E-Spin NanoTech Pvt. Ltd.	Lab scale electrospinnng setup
	HOLMARC Opto-Mechatronics	Supplier of lab scale electrospinning machine and accessories
	Nanomate Electrospinning	Supplier of lab base electrospinning machine and accessories
	Physics Equipment	Supplier of lab base electrospinning machine and accessories
	ANSTCO	Supplier of industrial level and lab scale electrospinning machine
Iran	Fnm Co. (Fanavaran Nano-Meghyas)	Supplier of industrial level and lab scale electrospinning machine and accessories
Ireland	Spraybase	Laboratory Setup and accessories
Italy	Linari Engineering s.r.l	Laboratory setup and accessories
	Nano-Cat	Laboratory setup and accessories
	SKE S.r.l.	Laboratory setup and accessories
	SPINBOW	Laboratory setup and accessories
Japan	Fuence	Lab scale electrospinnng setup
	KatoTech Co. Ltd	Lab scale electrospinning setup
	MECC Co. Ltd	Supplier of lab scale and semi-industrial level electrospinning machine
Korea	NanoNC	Supplier of lab scale electrospinning machine and accessories
Singapore	Electrospunra	Custom design for electrospinning machine; production of nanofiber for industry and lab
	Nanoflux	Supplier of lab base electrospinning machine and accessories
Spain	Bioinicia	Laboratory and industrial level setup, and accessories
	Nadetech Innovations	Laboratory setup and accessories
	Yflow	Supplier of lab scale and industrial level electrospinning machine
The Netherlands	IME Technologies	Laboratory setup and accessories
Turkey	Grafen Inc.	Supplier of lab base electrospinning machine
	Inovenso	Supplier of industrial level and lab scale electrospinning machine

Table 2.2 – Upstream electrospun nanofibre products.

Product	Company	Application
Nanosan®	SNS Nanofiber Technology LLC	Liquid absorption
Xantu.Layr	RevolutionFibres	Composite reinforcement
Phonix	RevolutionFibres	Sound barrier
ULTRA-WEB®	Donaldson	Air filtration
Fineweb™	Nano109 'The invisibile revolution'	Industrial dust collection, air filtration
NnF MBRANE®	Pardam Nanotechnology	Polymer nanofibrous membrane
SpurTex FM, material	SPUR Nanotechnologies	Liquid filtration
Petryanov's filtering cloth	Sorbent	Air, gas filtration
Filtriq™, mat	Zeus	Filtration of air, liquid, gas

Table 2.3 – Downstream products in which nanofibres are incorporated.

Product	Company	Application
Return Focus Pod	IQ Commercial (New Zealand)	Office furniture
Kilwell NZ Xantu	Kilwell (New Zealand)	Advance fishing rod
SETA™	HRV (New Zealand)	Air filter
Exceed™	eSpin Technologies (USA)	Residential/commercial buildings air Filter
MICROGRADE NF filter	MANN-HUMMEL (USA)	Air Cleaners for commercial vehicles
ProTura®	United Air Specialists (USA)	Air filter cartridge
HealSmart™	PolyRemedy (USA)	Antimicrobial wound dressing
Nanofiber plates, and dishes with random/aligned nanofibers	Nanofiber solutions (USA)	Lab Tissue Culture
Cell culture inserts	3D Biotek (USA)	Lab Tissue Culture
Silk fibroin tubular scaffolds, flat sheet scaffolds	Ske Advanced Therapies (Italy)	Lab Tissue Culture
6/12/96-well plates with random nanofibers	Electrospinning Company (UK)	Lab Tissue Culture

2.1.1 Mechanisms of jet motion in electrospinning

This section presents an overview of the mechanisms involved in the electrospinning process and some of the models that have been developed to gain a better understanding of electrospinning.

The behaviour of the polymeric jet under the electric field has been divided in three stages: the formation of a cone at the needle tip, the ejection of a straight jet, and an unstable whipping jet region, as shown in Figure 2.3 (Angammana & Jayaram 2011a; Subbiah et al. 2005; K. Garg & G.L. Bowlin 2011). A variety of forces are involved during the electrospinning process: Coulomb repulsive forces between the charged particles on the jet surface, electrostatic force due to the external electric field, viscoelasticity and surface tension of the polymeric solution, gravity and air drag forces (Angammana & Jayaram 2011b; D.H. Reneker et al. 2000).

Initially at low voltage a droplet of the polymeric solution is held at the needle tip by surface tension forces. As the voltage is increased, the solution droplet at the tip elongates and a conical shape is formed. When the applied voltage reaches a critical value V_c, the electrostatic forces overcomes the surface tension and consequently a thin electrically charged jet is stretched from the apex of the cone (Figure 2.4).

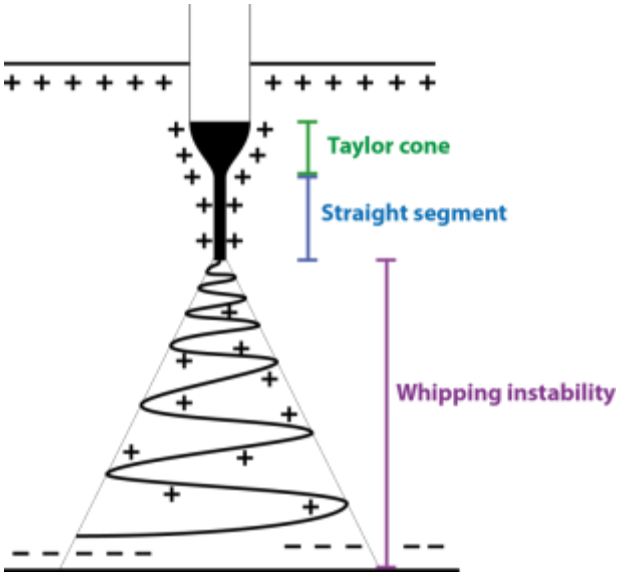

Figure 2.3 – Schematic diagram of the polymeric jet path from the needle to the collector.

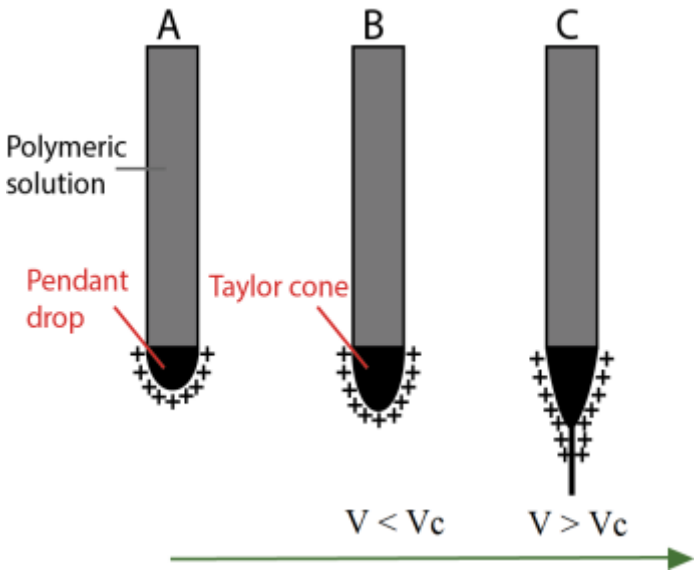

Figure 2.4 – Schematic illustration of the Taylor cone and jet formation: (A) the applied electric field creates surface charges in the polymeric solution; (B) increasing the voltage the drop is elongated; (C) when the voltage is higher than V_C, the polymeric jet is formed and travels towards the collector due to the charge repulsion.

The value of V_c can be calculated using Equation 1 (Taylor 1969), where H (cm) is the distance between the needle tip and the collector, L (cm) and R (cm) are respectively the length and the radius of the needle, and γ (dyne/cm) is the surface tension of the solution.

$$V_C{}^2 = 4\frac{H^2}{L^2}\left(\ln\frac{2L}{R} - \frac{3}{2}\right)(0.117\pi\gamma R)$$

Equation 1

The higher the surface tension of the solution is, the higher V_c is required to initiate the electrospinning process. Far away from the nozzle the electrospun jet undergoes an instability and elongation process, which allows the jet to become very long and thin. Meanwhile, the solvent evaporates and eventually nanofibres may be collected.

Regarding the formation of the Taylor cone, Yarin and his collaborators (A.L. Yarin et al. 2001b) have shown, theoretically and experimentally, that the configuration of the polymer

droplet assumes more the shape of a cone with a half angle of 33.5° rather than a Taylor cone of 49.3°. A PEO aqueous solution at concentration of 6% w/w (PEO M_w 400 000 g/mol) was used for the experiments and the solution drop at the needle tip was photographed using a camera at rate of 30 frames per second. The voltage was slowly increased in steps of about 200 V until the formation of a jet from the needle tip was observed. Hence, the angle of the cone was determined. Yarin and his group stated that the main reason of the higher value of the angle recorded by Taylor is related to the lower M_w liquid (water), which is more susceptible to atomization and perturbations.

The straight part of the jet was studied by Spivak and Dzenis (Spivak 1998) and a steady state electrospinning model was developed. The model of a weakly conductive viscous jet accelerated by an external electric field is formulated taking into account inertial, hydrostatic, viscous, electrostatic and surface tension forces. A nonlinear rheological equation applicable for polymer fluids (Oswald–deWaele law) is applied and a differential equation for the variation of jet radius with axial coordinate is derived. The power-law asymptote for the jet radius with the exponent 1/4 is obtained for non-Newtonian pseudoplastic fluids and it coincides with that for Newtonian fluids. Another group of researchers developed a slender body theory for electrospinning that couples electric field, charge transport and jet stretching (Hohman et al. 2001a). However, the model encounters difficulties, with the boundary condition at the nozzle. Steady solutions may be obtained only if the surface charge density at the nozzle is set to zero or a very low value, although no steady solution was possible for fluids with higher conductivities (Hohman et al. 2001b) due to the higher amount of instabilities at the nozzle.

The region of instability was extensively investigated by Reneker and Yarin (D.H. Reneker et al. 2000; D.H. Reneker & A.L. Yarin 2008; A.L. Yarin et al. 2001a). Using a halogen lamp, a Fresnel condenser lens and a high speed electronic camera, Reneker and his co-workers observed that after a straight section of 2-3 cm, the jet of a PEO aqueous solution undergoes a process of instability, which leads to its thinning (D.H. Reneker et al. 2000). The jet starts to bend and stretch inside a conical envelope with a series of spiralling loops as shown in Figure 2.5. On increasing loop diameter, the jet becomes thinner and as it reaches the collector, fibres with small diameter are eventually produced. The dynamics of the electrospinning process were analysed using a discrete three dimensional model. The three-dimensional paths of continuous jets were calculated, both in the nearly straight region where

the instability grew slowly and in the region where the bending dominated the path of the jet (A.L. Yarin et al. 2001a; D.H. Reneker et al. 2000). The bending instabilities in electrospun jets were modelled by a system of connected viscoelastic dumbbells as shown in Figure 2.6 (D.H. Reneker et al. 2000).

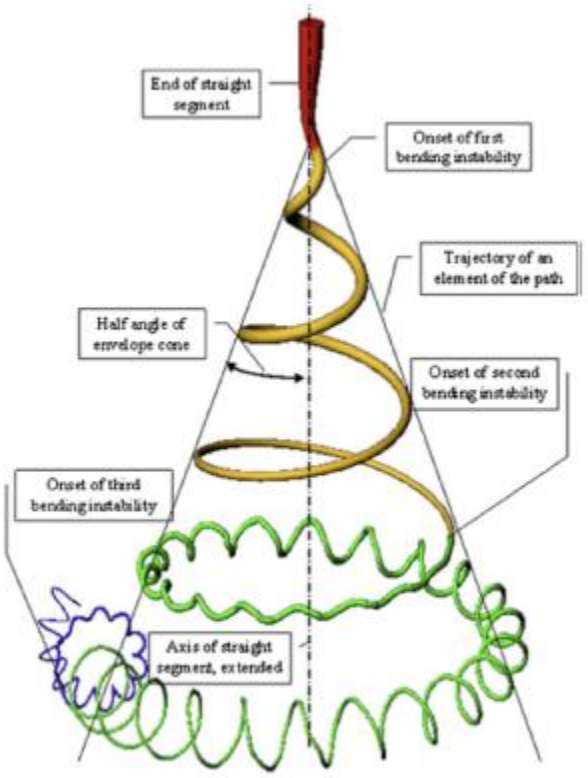

Figure 2.5 – Diagram showing onset and development of bending instabilities (K. Garg & G.L. Bowlin 2011)

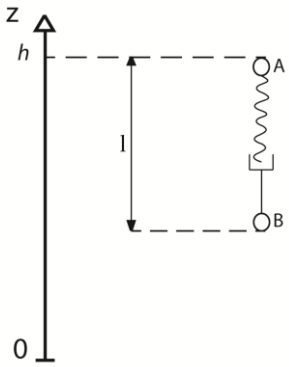

Figure 2.6 - Viscoelastic dumbbell representing a segment of the rectilinear part of the jet (Reproduced from (D.H. Reneker et al. 2000).

The beads A and B of Figure 2.6 have a certain mass and charge and they are connected by a spring and a dashpot. Springs and dashpots represent the elastic and the viscous component of the viscoelastic polymeric jet, respectively. In the electric field the beads are charged and therefore Coulombic repulsion forces are also considered. A PEO solution (6% w/w) in a mixture of water/ethanol was electrospun at electric field strength of 100 kV/m. It was demonstrated that the prediction of the jet trajectory was in good agreement with the experimental results, when the solvent evaporation rate was introduced in the model. In fact as the electrospinning process proceeds, the electrospun jet become more viscous due to the solvent evaporation (A.L. Yarin et al. 2001a). Similar observations were reported by another group of researchers using a PEO solution (2% w/w) in water (Y. M. Shin et al. 2001). Three types of instability were introduced by Hohman and his collaborators (Hohman et al. 2001a): the Rayleigh axisymmetric mode, the axisymmetric conducting mode and the whipping conductive mode. The Rayleigh instability takes place when the solution viscosity is very low and the electrostatic forces cannot overcome the surface tension. This instability causes the breaking-up of the electrified jet into droplets due to surface tension force which tends to reduce the surface area of the solution drop at the needle tip. On increasing electric field strength (E), this instability is inhibited. The governing conductive mode, axisymmetric and non-axisymmetric, depends strongly on the charge density of the electrospun polymeric jet and on the solution viscosity (Figure 2.7 a). It was observed that axisymmetric conductive mode controls the jet instability at lower charge density and it consists of variation of the jet diameter. On the other hand, the whipping mode (non-axisymmetric) governs the jet motion at higher charge density (Hohman et al. 2001b). The whipping involves the curvature of the jet from its centreline (Figure 2.7 b). The charge density could be increased on either increasing electric field strength or solution conductivity.

Figure 2.7 - (a) Axisymmetric and (b) non-axisymmetric instabilities in a fluid jet in an external electric field.

2.1.1.1 Prediction of the final nanofibre diameter

Most of the models proposed to understand the mechanism and the behaviour of the electrically charge jet during the electrospinning process, are quite complex for numerical solutions. So far, one correlation has been introduced to predict a relationship between the final nanofibre diameter and solution and process parameters (Sergey V Fridrikh et al. 2003). One of the biggest challenges is the production of nanofibres of uniform diameters, so that high level of process reproducibility may be reached for both industrial applications and scientific modelling. Nevertheless, several factors affect the final fibre morphology, mean diameter and diameter distribution.

Fridrikh et al (Sergey V Fridrikh et al. 2003) proposed a force balance between the solution surface tension and the electrostatic charge repulsion to obtain the diameter of the jet close to the collector. Hence Equation 2 was developed.

$$h_t = \left(\gamma \bar{\varepsilon} \frac{Q^2}{I^2} \frac{2}{\pi(2ln\chi - 3)}\right)^{1/3}$$

Equation 2

A dimensionless whipping instability value is introduced, $\chi \sim R/h$, with R being the radius of curvature of whipping jet and h is the jet diameter. The terminal diameter of the whipping jet (h_t) is a function of flow rate Q, electric current I, surface tension γ and $\bar{\varepsilon}$ dielectric permittivity of the outside medium (usually air). The final diameter of the nanofibres collected was related to the terminal jet diameter (h_t) by correcting the value for the polymer concentration (c).

$$d_t = h_t * c^{1/2}$$

Equation 3

The model was verified with the electrospinning of three polymeric solutions: poly (acrylonitrile) (PAN) in dimethylformamide (DMF), poly (ethylene oxide) (PEO) in water and poly (caprolactone) (PCL) in a solvent mixture of chloroform (CHL) and methanol (MeOH). While the experimental diameter of PAN and PEO nanofibres was in good

agreement with the predicted values, the stretching of PCL was over predicted. Smaller predicted diameters were determined compared to the experimental values for PCL nanofibres at several polymer concentrations. The authors stated that these observations may be explained with the mechanism of charge transport. PCL was dissolved in high volatile solvents, chloroform and methanol. In this case some charges may leave with the solvent molecules and contribute to the measured current, although they are not taken into account for the force balance. Therefore this would lead to disagreement between the predicted and the experimental values (Sergey V Fridrikh et al. 2003). The solvent evaporation and elastic effects have been neglected in Fridrikh's model.

The electric current (I) of a jet with radius r is set by the electric resistivity of the jet and therefore it is directly proportional to the charge carried. It has been considered to be formed of two components: the Ohmic bulk conduction current (I_c) and the surface convection current (I_s) (Ji Huan He & Yu Qin Wan 2004) (Equation 4).

$$I = I_c + I_s = \pi r^2 KE + 2\pi r u \sigma$$

Equation 4

The bulk conduction current is a function of the electric field strength (E) and the solution conductivity (K) and it is dominant in the region close to the needle where most charges are distributed in the jet's volume. On the other hand, the surface convection current is dependent on velocity of the jet (u) and surface charge density (σ). Far from the needle charges reside predominantly on the jet surface and move together with the fluid mass. Therefore the part of current due to conduction (I_c) is considered small enough to be neglected and the total electric current of the jet is controlled by surface charge density and jet flow rate (Hohman et al. 2001a). Though the surface charge density is often used as a given parameter in the models proposed to describe the dynamics of the electrospinning process (A.L. Yarin et al. 2001a; Y. M. Shin et al. 2001), the calculation of its value is quite complex. The importance of electric current and surface charge density is well known by researchers, but the effects of both solution properties and process parameters on the electric current and consequently on the final morphology of the nanofibrous structures have not been studied in depth (Samatham &

K. J. Kim 2006; Fong et al. 1999; Angammana & Jayaram 2011b).

Kim et al (S. J. Kim et al. 2004) investigated the effect of polymer concentration on the electric current and morphology of the electrospun nanofibrous mats. Poly (2-acrylamido-2-methyl-1-propane sulfonic acid) (PMAPS) was dissolved in a mixture of ethanol and water at several polymer concentrations. A maximum value for the current was recorded for the middle value of polymer concentration (6% w/v) and nanofibres with narrow diameter distribution were collected (Figure 2.8). This was explained by a balance between the ion mobility and the number of charged ions. Though the low viscosity of solution at concentration below 6% w/v was responsible of the high mobility of the polymer ions, the low number of charged ions led to low value of current resulting in beaded nanofibrous structures. On the other hand, on increasing polymer concentration above 6% w/v the number of charged ions in solution increased, but the high solution viscosity led to a reduction of the ions mobility. Hence smaller values of current were recorded. The morphological analysis have shown that nanofibres with wider diameter distribution and some beads were formed from solution at polymer concentration of 2% w/v, while nanofibres with higher mean diameter but narrower diameter distribution were collected using solution at higher polymer concentration (10% w/v).

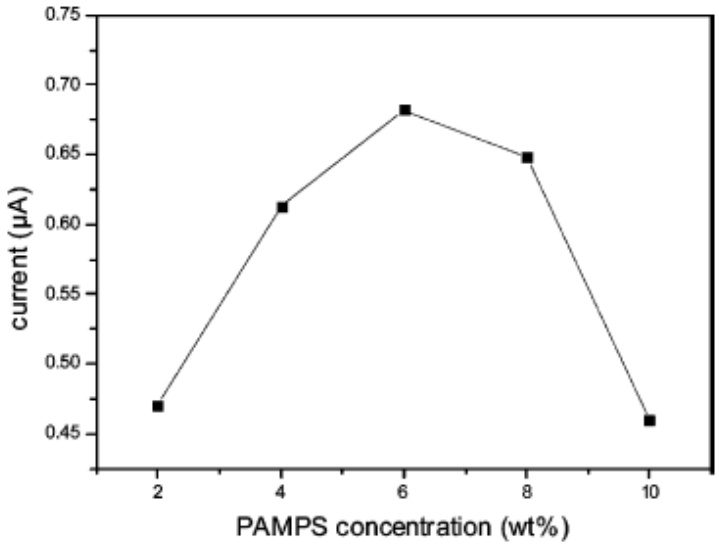

Figure 2.8 – The concentration of PAMPS in the PAMPS/ethanol/water solutions versus electric current during electrospinning (S. J. Kim et al. 2004).

The effect of applied voltage on electric current has shown a power law with exponent between 2 and 5 depending on the types of polymeric solution (S. A. Theron et al. 2004; Ji Huan He & Yu Qin Wan 2004). However, the effect of the electric current on the nanofibre morphology and mean diameter has not been explored as much as the effect of other solution parameters.

The prediction of the nanofibre diameter would be a great advantage compared to the 'trial and error' approaches commonly used. A better understanding of how charges are created and transported on the jet surface is probably required to predict the final nanofibre diameter. The types of solvents used to dissolve the polymer and the electrospinning setup are probably the most significant factors affecting the charge generation and transport within the polymeric jet.

2.1.2 Electrospinning parameters

Several variables can be manipulated to obtain nanofibres with specific morphology and definite mechanical properties. Doshi and Reneker classified these variables in the following three categories (Doshi & D.H. Reneker 1995):

- solution parameters: polymer molecular weight (M_w), polymer concentration (C), solution conductivity (K), solution surface tension (γ), type of solvent;
- process parameters: flow rate (Q), applied voltage (V), distance between needle and collector (d), needle diameter, type of collector;
- ambient parameters: temperature, relative humidity and air velocity.

A discussion of how these parameters affect the morphology of the electrospun nanofibrous samples and the nanofibre diameter is reported in the following sections.

2.1.2.1 Solution parameters

2.1.2.1.1 Concentration, viscosity, molecular weight

The effects of solution viscosity (η), polymer concentration (C) and polymer molecular weight (M_w) on solution electrospinnability and consequently on nanofibre morphology and diameter cannot be studied separately (Pham, U. Sharma & A.G. Mikos 2006; Bhardwaj & Kundu 2010; Deitzel et al. 2001). In fact, an increase of polymer concentration at fixed M_w leads to higher solution viscosity, whereas at fixed concentration on decreasing M_w the solution viscosity decreases. For every polymer-solvent system an optimal range of polymer concentration exists and it is particularly important since it defines the nanofibre formation window (Costa 2010; Hekmati et al. 2013; W. K. Son et al. 2004; Bosworth & Downes 2012; Morota et al. 2004). A minimum value of concentration is required to first produce nanofibres and as the polymer concentration is increased, nanofibres with larger diameter may be collected (Koski et al. 2004; Chowdhury & G. Stylios 2010; Chowdhury & G. K. Stylios 2012). For example Costa et al (Costa 2010) conducted a study regarding the effect of concentration of poly (vinylidene fluoride) (PVDF) in N,N-dimethylformamide (DMF), and in dimethylformamide/acetone (DMF/AC) solutions, on the transition between electrospray and electrospinning. Only small droplets were collected from PVDF solution in DMF at concentration below 7 % w/w, and from PVDF solution in DMF/AC at 5% w/v, therefore indicating the electrospray process. With increasing polymer concentration nanofibres with few defects were produced at concentration of 10 and 7% w/w in PVDF/DMF solution and PVDF/DMF/AC solution, respectively. Defect-free nanofibres were first formed at concentration of 15% w/w in PVDF/DMF solution, and 10% w/w in PVDF/DMF/AC solution. The morphological observations demonstrated that the range of polymer concentration which defines the types of nanofibre morphology is dependent on the types of polymer-solvent system. In addition the authors stated that the lower solution viscosity of AC was responsible of the production of thinner nanofibres from PVDF solution in AC/DMF compared to nanofibres collected from solution in DMF. However, there are other solvent properties that should be considered and may affect the nanofibre morphology and diameter.

Similar findings were reported by Chowdhury et al (Chowdhury & G. K. Stylios 2012) for poly (ethylene oxide) (PEO) aqueous solution at several concentrations. Beaded nanofibres were collected using a PEO aqueous solution at concentration of 10% w/w, while defect-free

nanofibrous structures were observed as the polymer concentration was increased to 14%. In addition the nanofibre diameter was measured. The results have shown an increase in the mean diameter from 386 to 452 nm on increasing the polymer concentration. However above 14% w/w, no nanofibres were produced due to the high solution viscosity. The polymer concentration is related to the entanglements between the polymer chains. If there are not enough entanglements, the viscoelastic force cannot counteract the electrostatic force resulting therefore in the production of beads instead of nanofibres.

The formation of beads has also been explained investigating the effect of the polymer molecular weight (M_w). Higher M_w indicates longer chain lengths (Bhardwaj & Kundu 2010; Koski et al. 2004). If the polymer concentration is fixed, polymer with low M_w tends to form mostly beads, while smooth nanofibres can be obtained on increasing M_w (F. Liu et al. 2009; Koski et al. 2004). While bead string morphology was observed from the electrospinning of an aqueous solution of poly (vinyl alcohol) (PVA) with molecular weight of 9,000–13,000 g/mol as a result of the low number of entanglements, defect-free fibrous structure was collected on increasing M_w to 13,000–23,000 g/mol. Moreover a change in the fibre cross-section from circular to flat was distinguished using high molecular weight of 31,000–50,000 g/mol. These observations indicate that a specific level of solution viscosity depending on the types of polymer-solvent system is necessary to counteract the electrostatic forces and produce a uniform electrospun jet during electrospinning. Hence this would lead eventually to the collection of defect-free nanofibres.

Poly [(lactic acid)-co-(glycolic acid)] (PLGA) with various molecular weights were dissolved in a mixture of THF/DMF (3/1 v/v) at a concentration of 10% w/w (F. Liu et al. 2009). At fixed process conditions, the morphology varied from a beaded structure (M_w of 15,000 g/mol) to a defect-free nanofibrous mat (M_w of 81,000 g/mol). However, if a sufficient level of viscosity is guaranteed by a sufficient level of intermolecular interactions, low M_w can also lead to the production of defect-free nanofibres.

The sufficient level of entanglements needed to first produce nanofibres can be defined by a value of concentration called entanglement concentration (C_e). Four different concentration regimes for polymer dissolved in a good solvent were identified by measuring the dependence of concentration on the solution viscosity (Figure 2.9): dilute, semi dilute unentangled, semi dilute entangled and concentrated (R.H. Colby et al. 1991; Krause et al.

2001; de Gennes 1979). In the dilute regime, polymer chains do not overlap and the specific viscosity η_{sp} is proportional to $C^{1.0}$. The specific viscosity η_{sp} is defined by $\eta_{sp} = \eta_o/\eta_s - 1$, η_o and η_s are the zero shear viscosity of polymer solution and the viscosity of pure solvent, respectively. Polymer chains start to overlap in the semi dilute unentangled regime and it was found that the specific viscosity η_{sp} is proportional to $C^{1.25}$. Then on further increasing polymer concentration more entanglements between the polymer chains are formed and the specific viscosity is proportional to $C^{4.25\text{-}4.5}$ in the semi dilute entangled regime.

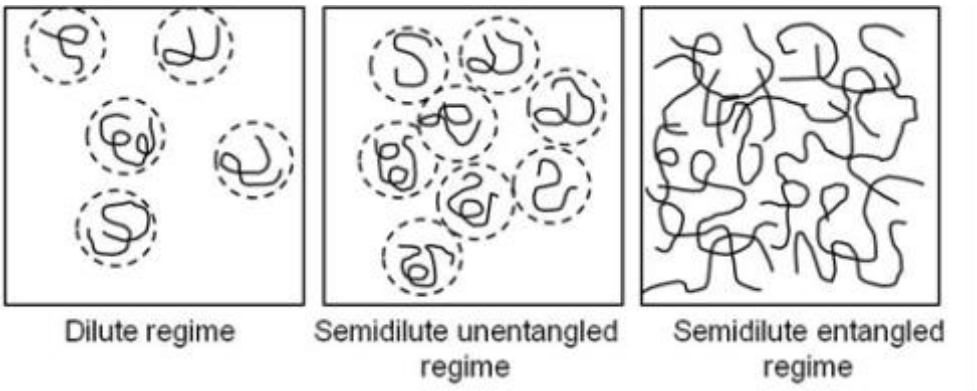

Figure 2.9 – Physical representation of the three solution regimes (a) dilute, (b) semidilute unentangled and (c) semidilute entangled.

The influence of these regimes on the electrospun nanofibre formation and morphology can be explained as followed. The polymer chains are separated by the solvent molecules in the dilute regime, and therefore only polymer droplets can be collected from the electrospinning of solution at low concentration. On increasing polymer concentration the chains start to overlap each other at the overlap concentration, C*, but there is no entanglement and therefore only droplets are still formed (Chisca et al. 2012; M.G. McKee et al. 2004). The entanglement concentration C_e represents the transition between the semi dilute unentangled and the semi dilute entangled. When the concentration is higher than C_e, fibres with beads are collected. The frequency of bead formation decreases as the polymer concentration increases and generally defect-free nanofibres have been observed when the concentration is 2-2.5 times C_e (Matthew G. McKee et al. 2004; Koski et al. 2004). However no fibres are formed with further increase of polymer concentration as a result of the high solution viscosity which obstructs the electrospinning process.

Few researchers investigated the effect of different M_w on the value of C_e (Bonino et al. 2011; S. H. Tan et al. 2005) and the results have shown that C_e is lower for polymer with higher M_w. A polymer with lower M_w occupies a smaller hydrodynamic volume in solution and therefore a higher concentration is required before the polymer chains begin to entangle (P. Gupta et al. 2005; Tanford Charles 1961).

In the last few years a few scientific publications reported that importance of the entanglements concentration C_e for the production of defect-free nanofibres and zero shear viscosity values have been reported. Nevertheless, there is still lack of viscoelasticity measurements for different polymer-solvent systems. Polymer blends and composite materials have been widely electrospun, hence it would be very useful to measure the viscoelastic properties in order to predict the final nanofibre morphology and reduce the number of trial and error experiments.

2.1.2.1.2 Surface tension

The effect of surface tension on the nanofibre morphology depends on type of solvent, polymer and the polymer-solvent molecular interactions (Fong et al. 1999). In the electrospinning process the surface tension force is the parameter in competition with the electrostatic forces and the electrospun jet is initiated when the electrical forces overcome the surface tension force (J. J. Feng 2003; D.H. Reneker et al. 2000). In fact, while the electrical forces try to increase the surface area through the jet elongation, the surface tension attempts to reduce the surface area by forming spheres (Y. M. Shin et al. 2001; D.H. Reneker et al. 2000).

PEO solutions in water and in a mixture of water and ethanol (EtOH) were prepared and electrospun by Fong et al (Fong et al. 1999). The morphological observations have shown that while beaded fibres are produced from the aqueous PEO solution, the addition of EtOH decreases the solution surface tension and therefore defect-free nanofibres with larger diameter are collected. Nevertheless, the application of a lower surface tension to get defect-free nanofibrous mats is not a general rule. The addition of EtOH to aqueous PVA solution have shown different effects on the solution properties and nanofibre morphology (C. Zhang et al. 2005). Nanofibrous mat with higher bead density was produced as a result of the

decrease of the solution surface tension accompanied by reduction of viscosity. The different findings are due to the fact that EtOH is a solvent for PEO and therefore increases the solution viscosity, while it is a non-solvent for PVA and decreases the solution viscosity. Therefore, the lower solution viscosity results to a reduced entanglements density and consequently more beads are formed within the nanofibrous structure.

2.1.2.1.3 Electric conductivity

A number of scientific publications has shown that generally nanofibres with smaller diameter can be produced with increasing solution conductivity (Zong et al. 2002; Zuo et al. 2005; Mit-uppatham et al. 2004). Solutions with higher conductivity are subjected to greater tensile force with the application of the electric field as a result of a higher number of charged ions on the jet surface (Y. Liu et al. 2008). The higher charge repulsion on the jet surface is responsible of stronger whipping instability and hence the jet is further stretched. However the value of solution conductivity mainly depends on the types of solvent used to dissolve the polymer.

The addition of salts has shown to decrease bead formation and enhance the production of thinner nanofibres (Jun et al. 2003; X.-H. Qin et al. 2007; Uyar & Besenbacher 2008; B. Kim et al. 2005). For example Jun et al (Jun et al. 2003) incorporated pyridium formiate (PF) at concentration ranging from 0.2 to 0.8% w/w to PLA/methylene chloride (MC) solutions. Smaller nanofibres with fewer beads were observed as the concentration of PF increased due to the increase of solution conductivity from 1.7 to 3.6 μS/cm. Similarly, the sharp increase of solution conductivity by adding benzyl triethylammonium chloride (BTEAC) to a PLGA solution in chloroform led to a lower entanglement concentration C_e. In addition the average nanofibre diameter was found to decrease from 760 nm to 450 nm (You et al. 2006). Nevertheless, an increase of amount of salt in solution may also result in the production of nanofibre with larger diameter. Mit-uppatham et al (Mit-uppatham et al. 2004) reported that an increase of sodium chloride (NaCl) in PA solution leads to higher solution conductivity, but also higher solution viscosity. As a result, PA nanofibres with diameter of about 98 nm are collected with the addition of salt of 1% w/v, while larger nanofibre (134 nm) are formed on increase the amount to 5% w/v. Though an increase of conductivity should result in higher jet stretching, the increased viscosity represents an increase in the viscoelastic force

counteracting the Coulombic stretching force. Hence this prevents the charged jet from being stretched by the electrostatic forces, resulting in the formation of bigger nanofibres.

An increase of solution conductivity has also been observed with the addition of surfactants (Kriegel et al. 2009; T. Lin et al. 2004; Ziani et al. 2011; Jian-yi Zheng et al. 2014). Generally the main effect of a surfactant is the reduction of the solution surface tension which would enhance the electrospinning process. Few authors also reported that the solution conductivity may be increased with anion and cationic surfactants, whereas it does not vary with the addition of non-ionic surfactant (L. Jia & Xiao-hong Qin 2012; Jian-yi Zheng et al. 2014). Less beaded and thinner nanofibres were overall produced mainly due to the reduced solution surface tension.

To summarise, it has been shown that the most significant solution parameter is the polymer concentration and hence the solution viscosity. In the next paragraphs the effect of the main process parameters will be examined.

2.1.2.2 Process parameters

2.1.2.2.1 Voltage

Of all process parameters the effect of applied voltage is quite debated and controversial. On increasing voltage different effects on the morphology of the electrospun nanofibrous webs and the mean nanofibre diameter have been observed depending on the type of polymer-solvent system, polymer concentration and distance between needle and collector. The applied voltage (V) and the distance between the needle and the collector (d) affect the electric field strength (E) which is defined as the ratio V/d.

Some researchers have shown that with the increase of the applied voltage nanofibres with smaller diameters were collected (Megelski et al. 2002; X. Y. Yuan et al. 2004; Larrondo & Manley 1981a; Ding et al. 2002; J. S. Lee et al. 2004; S.-Y. Gu & J. Ren 2005). For example Chowdhury et al (Chowdhury & G. K. Stylios 2012) prepared PEO solution in water and in a mixture of water and ethanol (60/40 v/v) to investigate the effects of both solution properties and process parameters on nanofibre morphology and mean diameter. The morphological observations have shown that thinner nanofibres were collected on increasing the applied

voltage at fixed collection distance. This may be explained by the fact that higher voltage leads to a more elongated polymeric jet due to the increased electrostatic forces. Hence fibres with smaller diameter are produced. On the other hand, other researchers observed an increase of the fibre diameter and broader diameter distribution as the voltage increases (C. Zhang et al. 2005; Morota et al. 2004; Zong et al. 2002). In addition a few groups have shown that a non-linear relationship exists between the voltage and the mean diameter (F. Liu et al. 2009; Mazoochi et al. 2012). For example PLGA solutions in THF/DMF (3/1 v/v) were electrospun by Liu et al (F. Liu et al. 2009). An increase in the mean nanofibre diameter from 412 to 751 nm is observed as the voltage is increased from 14 to 20 kV. However a further increase of the voltage to 22 kV leads again to a reduction of the mean diameter at 636 nm. The higher voltage enhances the 'whipping' instability, the jet become more unstable and therefore thinner nanofibres are collected (X. Y. Yuan et al. 2004; C. M. Hsu & S. Shivkumar 2004). Most likely the different findings depend on the type of solvent, polymer and polymer-solvent interactions, but also on the type of electrospinning setup and ambient conditions.

2.1.2.2.2 Distance between needle and collector

The collection distance affects both the time available for nanofibre deposition on the collector and the strength of the electric field (E = V/d), as reported in the previous paragraph. A number of researchers observed that a minimal distance is required to allow the complete evaporation of the solvent (Bhardwaj & Kundu 2010; Sill & von Recum 2008) and hence dry nanofibres can be collected.

The majority of researchers reported that thinner nanofibres were produced with larger distance between needle tip and collector (Doshi & D.H. Reneker 1995; D.H. Reneker et al. 2007; Chowdhury & G. K. Stylios 2012; K.H. Lee et al. 2002). Longer distance gives more time for the bending instabilities to develop, for the solvent to evaporate and therefore more time for the stretching of the polymeric jet. However Lee et al (J. S. Lee et al. 2004) have shown a non-linear relationship between the distance and the nanofibre diameter. The mean diameter of PVA nanofibre decreases from about 300 to 250 nm with an increase of distance from 4 to 7 cm, although a broader diameter distribution was determined. Further increasing distance more uniform nanofibrous structure were produced but larger diameter were measured. This may suggest that the electrostatic forces are too weak to stretch the polymeric

jet as a result of the weakness of the electric field strength (E).

Regarding the nanofibres morphology, bead formation may occur at either too low or too high collection distance (Ki et al. 2005; Megelski et al. 2002; Mazoochi et al. 2012). If the collector is too close droplets will form as a result of short time available for the collection. At higher collection distance defect-free nanofibres may be produced as the electric field strength is high enough to overcome the surface tension force and there is good balance between all forces. However if the collector is too far, nanofibres with beads may be formed due to the weakness of the electric field strength. Despite the different observations, the effect of the collection distance on the mean nanofibre diameter is less significant than the effect of applied voltage.

2.1.2.2.3 Flow rate

The solution flow rate is generally set by a syringe pump and it affects the rate of material transferred from the needle tip to the collector and the jet velocity. Only a few studies on the relationship between flow rate, fibre morphology and mean diameter have been reported (Fujuan Liu et al. 2009; Chowdhury & G. K. Stylios 2012). In general a lower flow rate is more desired to give the solvent a sufficient time to evaporate from the polymeric jet, and therefore smaller nanofibres can be collected (Wannatong et al. 2004; X. Y. Yuan et al. 2004). However if the flow rate is too low, the solution at the needle tip is fast removed from the electric forces and in turn may cause blockage of the needle (Baumgarten 1971). On the other hand, if the flow rate is too high the solvent does not have enough time to evaporate from the polymeric jet. Consequently the electrostatic forces are not able to sufficiently stretch the polymeric jet towards the collector and bead formation may occur (Zuo et al. 2005; Zargham et al. 2012). For example Liu et al (F. Liu et al. 2009) electrospun PLGA solutions and morphological observations have shown more homogeneous nanofibrous webs at the lowest flow rate of 0.5 ml/h. Moreover the mean diameter decreased from 586 nm to 465 nm as the flow rate was decreased from 2 to 0.5 ml/h.

2.1.2.3 Ambient parameters

Compared to solution and process parameters, there are not many scientific publications regarding the effect of ambient parameters on the nanofibre morphology and mean diameter, most probably due to difficulty of controlling and varying them.

2.1.2.3.1 Temperature

A small number of publications about the effect of solution temperature and ambient temperature on nanofibre morphology and mean diameter are available in the literature (De Vrieze et al. 2009; C. Wang et al. 2007; Mit-uppatham et al. 2004). A reduction in the mean diameter was determined on increasing the temperature of PA6 solution in 85% v/v formic acid from 30 to 60°C (Mit-uppatham et al. 2004), as a result of the reduced solution viscosity. As reported in the previous paragraphs, solution of lower viscosity leads to a reduction in the viscoelastic force to counteract the electrostatic force, resulting therefore in the production of thinner nanofibres. On the other hand, De Vrieze et al (De Vrieze et al. 2009) observed the production of thinner nanofibres at the lowest and the highest ambient temperature. The temperature and humidity were controlled using a fan inside the connection tubes. The different findings are probably due to the type of polymer-solvent systems, the range of temperature and the different electrospinning setup. De Vrieze and his collaborators (De Vrieze et al. 2009) selected three values of temperature (283, 293, and 303K) for the electrospinning of poly (vinyl pyrrolidone) (PVP) solution in ethanol and cellulose acetate (CA) solution in acetone/dimethylacetamide (AC/DMAc). For both polymeric solutions thinner nanofibres were collected at the lowest (283K) and the highest ambient temperature (303K). Solvent evaporation rate and solution viscosity are the two opposing effects. A decrease of temperature leads to slower evaporation of the solvent. Therefore as the solvent remains for longer time in contact with the polymer, the jet can be further stretched by the electrostatic force within the electric field and consequently thinner nanofibres are formed. On the other hand, an increase of temperature leads to lower solution viscosity. During the electrospinning process the viscoelastic force counteracts the electric force responsible of the stretching of the jet. This indicates that at higher temperature the jet stretching is enhanced due to the higher molecular chain mobility and consequently thinner nanofibres are collected.

2.1.2.3.2 Relative humidity

Different observations about the effect of relative humidity on the morphology of nanofibrous structures have been related mainly to the chemical nature of the polymer and the solvent (Ying Yang et al. 2006; Megelski et al. 2002; Pai et al. 2009; Tripatanasuwan et al. 2007; L. Huang et al. 2011). De Vrieze et al (De Vrieze et al. 2009) collected thinner nanofibres from PVP solution in ethanol on increasing humidity, while nanofibres with bigger diameter were formed from CA solution in AC/DMAc (De Vrieze et al. 2009). The different trends are attributed to the different interactions between the polymer and the water molecules in the surrounding air. Water is a solvent for PVP, while it is a non-solvent for CA. As the humidity is increased thinner PVP nanofibres are formed. The absorption of more water molecules at higher humidity causes the fibres to solidify slower and hence there is more time for the jet stretching. Nevertheless at very high humidity (60%) a film of fused fibres was formed. On the other hand, higher amount of water molecules causes the precipitation of CA resulting in nanofibres with larger diameter. Similar findings were found by Huang et al (L. Huang et al. 2011) for the electrospinning of PSU and PAN solutions in DMF. An increase of relative humidity led to larger PAN nanofibres with relative uniform diameter distribution, whereas PSU electrospun samples presented a bimodal diameter distribution as a result of the higher instability of the electrospinning process. Furthermore morphological analysis of the fibre surface revealed different results. While smooth nanofibres were collected from PAN solution, a porous structure was observed on the surface of PSU nanofibres. This is explained by the higher hydrophobicity of PSU compared to PAN. Since the surface of PSU fibre is less wetted by water, the condensation of water molecules from the surrounding air on the fibre surface leads to precipitation of the polymer and consequently pores are formed. The reason of these observations is explained in the following paragraphs.

The effect of relative humidity on the morphology of poly(styrene) (PS) nanofibres have been widely investigated by several researchers (Casper et al. 2004; J. Zheng et al. 2012; J. Lin et al. 2010; Megelski et al. 2002). THF, DMF and a mixture of THF and DMF were used to prepare PS solutions. While smooth nanofibres with no pores are collected using 100% DMF, uniform nanopores are formed on the surface of electrospun nanofibre from 100% THF and the pore diameter increases on increasing relative humidity from 30% to 70%. These different

observations demonstrate that solvent volatility is an important factor affecting the pore formation. With the addition of DMF to the PS solution in THF, the solvent evaporation is slowed down because the boiling point (BP) of DMF (151°C) is much higher than that of THF (66°C). Therefore the polymeric jet is further stretched and less pores are formed on the surface with increasing amount of DMF (Megelski et al. 2002). However, images of cross sections of the electrospun nanofibres from a 30% PS/DMF solution have shown that some pores were formed in the fibre core (Pai et al. 2009). Similar findings were published by Zheng et al (J. Zheng et al. 2012). For example Figure 2.10 shows the cross section of PS fibres collected from electrospinning of PS solution in DMF and THF at relative humidity of 55% and 45%, respectively. The hydrophobicity of PS and the low evaporation rate of DMF from the electrospun jet led to a porous core as shown in image (a), while a porous surface is observed for the fibre from PS/THF solution (b). Moreover, as a result of the fast evaporation of THF from the electrospun jet, a polymer skin formed first and then a pressure difference between inside and outside of the fibre surface resulted in the ribbon and collapsed structure.

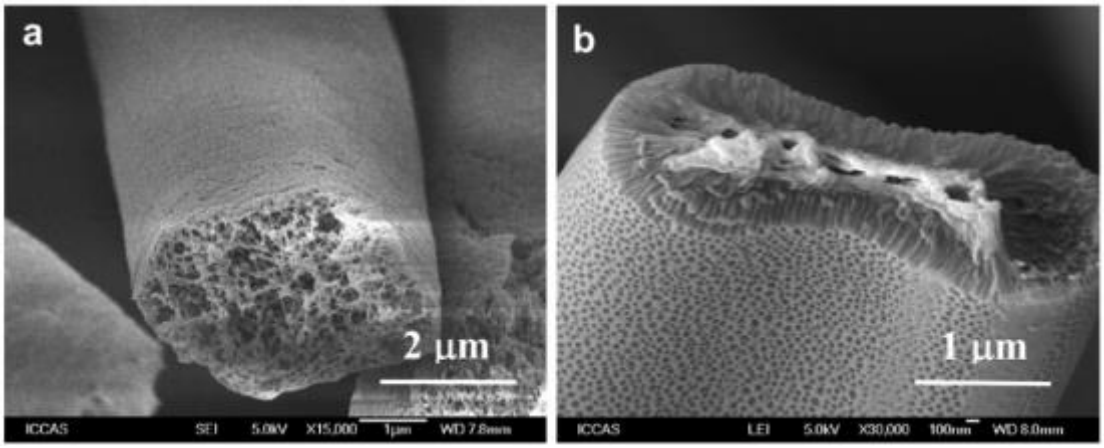

Figure 2.10 – Cross-section morphology of PS fibres electrospun from PS solution in (a) DMF and (b) THF (J. Zheng et al. 2012).

Recently Nezarati and his group (Nezarati 2013) electrospun different polymer-solvent systems in a range of relative humidity between 5% and 75%. Poly(ethylene glycol) (PEG), poly(caprolactone) (PCL), and poly(carbonate urethane) (PCU), were dissolved in chloroform (CHL), a mixture of CHL/DMF (80/20 v/v), and dimethylacetamide (DMAc), respectively. A significant difference in the nanofibre morphology between the different polymer-solvent systems was observed. The hydrophilic polymer PEG produces smooth

nanofibres with no pores at high relative humidity (50%), while the hydrophobic polymer (PCL in CHL/DMF) produces porous nanofibres as the humidity was increased due to the high volatility of the solvent mixture and hydrophobicity of the polymer. PCU, the most hydrophobic between the three polymers, was dissolved in a water miscible solvent (DMAc). No pores on the surface were observed due to the low volatility of DMAc, but a porous core was observed after fibre cross-section as a result of the polymer hydrophobicity.

To summarise, these findings highlight that the effects of relative humidity on the morphology of electrospun nanofibres are dependent on polymer hydrophobicity, solvent miscibility with water and solvent volatility. Two mechanisms have been introduced in order to explain the pore formation on the electrospun structures: phase separation and breath figures. Thermal-induced phase separation (TIPS) and vapour-induced phase separation (VIPS) are considered the most relevant phase separations that occurred during the electrospinning process. Phase separation occurs when the polymeric solution becomes thermodynamically unstable due to the solvent evaporation. In turn a polymer rich and a polymer poor region are created within the polymeric jet. In TIPS the thermodynamic instability is caused by the decrease of temperature of the electrospun jet as it travels towards the collector, while VIPS occurs instead when non-solvent (water) vapour molecules penetrate into the polymer solution causing therefore phase separation.

On the other hand, the breath figures mechanism was observed by Srinivasarao et al (Srinivasarao et al. 2001), who first described the formation of pores on a polystyrene (PS) film in a humid environment. It has been described that breath figures are formed on the surface of a cold solid or liquid surface in contact with moist air. The rapid solvent evaporation from the PS film leads to fast cooling of the surface. Hence water molecules condense and leave an imprint on the surface in the form of pores. Though the formation of pores in the fibre core can be explained with VIPS (J. Zheng et al. 2012), both breath figures and TIPS may explain the formation of pores on the surface of nanofibres collected from solution in high volatile solvents, such as PS solution in THF (Casper et al. 2004).

A greater understanding of the pore formation mechanisms depending on the type of polymer-solvent systems would provide better control of the nanofibre morphology, because different types of nanofibrous structures may be required depending on the application.

2.1.3 Solvents used for electrospinning

The first step of the electrospinning process is the dissolution of the polymer in a good solvent. The most common solvents used to prepare solution for the production of electrospun nanofibres are reported in Table 2.4. Few groups of researchers investigated the effect of different solvents and solvent mixtures on nanofibre morphology and mean diameter (K.H. Lee et al. 2003; H. Liu & Y. L. Hsieh 2002; Y. Liu et al. 2008; Mit-uppatham et al. 2004; Choktaweesap et al. 2007).

Table 2.4 – Lists of the most common solvents used in the electrospinning process with their physical and chemical characteristics (BP is the boiling point, η is the viscosity, γ is the surface tension and ε is the dielectric constant).

Solvent	***BP*** ***°C***	**η** ***cP (at 25°C)***	**γ** ***mN/m***	***ε*** ***(at 20°C)***
Acetic acid	118	1.13	26.9	6.2
Acetone	56	0.33	25.2	21.0
Chloroform	62	0.57	26.5	4.8
Dichloromethane	40	0.44	27.2	9.1
Dimethylformamide	153	1.43	37.1	38.3
Ethanol	78	1.08	21.9	24.0
Formic acid	101	1.78	37.0	58.0
Methanol	65	0.60	22.3	33.0
Tetrahydrofuran	66	0.55	26.4	7.5
Trifluoro acetic acid	72	0.81	13.5	8.4
Trifluoro ethanol	78	1.75	21.1	27.0
Water	100	1.00	72.8	80.0

Lee et al (K.H. Lee et al. 2003) dissolved poly(caprolactone) (PCL) in three solvents: dichloromethane (DCM), a mixture of DCM and toluene, and a mixture of DMC and DMF. Nanofibres with mean diameter of about 550 nm and narrow diameter distribution are collected using DCM, while on increasing amount of DMF in the mixture DCM/DMF thinner nanofibres are produced. Higher stretching of the polymeric jet was considered to be a result of the increased solution conductivity accompanied by the reduced viscosity and reduced surface tension. During the electrospinning process, viscoelastic and surface tension forces

counteract the electrostatic force responsible of the jet stretching. On the other hand, the addition of toluene to MC did not facilitate the electrospinning as it is a poor solvent for PCL.

The effect of several solvents on the morphology of poly(styrene) (PS) electrospun structures was also investigated (Jarusuwannapoom et al. 2005; Wannatong et al. 2004; Megelski et al. 2002). For example Wannatong et al (Wannatong et al. 2004) observed that the nanofibre diameter decreases as the boiling point of the solvent increases. Of all solvents used to dissolve PS, DMF was found to be the best solvent in terms of productivity due to its high dielectric constant, but the nanofibrous mats appeared to be wet as a result of the low evaporation rate of DMF from the electrospun jet as it travels to the collector (BP of 151°C). The addition of a solvent with high dielectric constant increases the charge density on the jet and therefore the electrospun jet may be exposed to higher stretching by the electrical force. Hence, the electrospinning process may be improved resulting in the production of thinner nanofibres with narrow diameter distribution (Gholipour Kanani & Bahrami 2011; X. Gu et al. 2014; C.-M. Hsu & Satya Shivkumar 2004).

The influence of vapour pressure was evident when PS solution with different THF/DMF combinations were electrospun (Megelski et al. 2002). Different fibre morphologies were observed. While very high density of pores was observed on the surface of the PS nanofibres electrospun from THF, the addition of DMF in solution led to larger and less uniform pores. The volatility of the mixed solvent system decreases due to the high vapour pressure of DMF, and consequently the pore formation is hindered. The boiling point and hence the vapour pressure affect both the evaporation rate of the solvent from the electrospun jet and the drying time. The authors stated that the temperature-induced phase separation (TIPS) occur using THF resulting in the production of nanofibres with porous surface.

To summarise, the morphology electrospun nanofibrous structure and the size of the nanofibres strongly depend on solution properties, but different solvents may contribute different solution surface tensions and solution viscosities. Solvent properties such as its boiling point, dielectric constant and surface tension may determine the production of nanofibres with different morphologies. However, in most scientific publications the selection of a solvent to dissolve a polymer is based on experience on similar polymer-solvent systems. Additionally the effect of different solvent systems has not been studied for electrospun blends of natural and synthetic polymer, although many researchers reported the

great advantages of composite nanofibrous structures for example in tissue engineering applications (H. W. Kim et al. 2008; Jia Xu et al. 2009; Sell et al. 2009; Pham, U. Sharma & A.G. Mikos 2006). For each polymer the solvent selection is an important factor in order to prepare electrospinnable solution and produce defect-free uniform nanofibrous webs, but it depends on several solvent characteristics which cannot be studied separately. A systematic methodology should be introduced for the selection of suitable solvent or mixture of solvents to produce electrospinnable solutions that form defect-free nanofibres with narrow diameter distribution.

2.1.4 Electrospinning applications

Nanofibrous structures made by electrospinning have shown promising potentials in an extensive range of applications, such as water and air filtration (Aluigi et al. 2012; Sundarrajan et al. 2014), in protective clothing (Dhineshbabu et al. 2014; C. Guo et al. 2013), in biomedical applications as tissue engineered scaffolds (D. Liang et al. 2007; Bianco et al. 2011; F Yang et al. 2004), dressings for wound healing (T. T. T. Nguyen et al. 2013; Tehrani et al. 2012; Hongliang Jiang et al. 2004) and as drug delivery systems (Cui et al. 2006; Zamani et al. 2013; J. Xie & C.-H. Wang 2006).

The follow paragraphs focus on the biomedical applications of electrospun nanofibrous structures.

2.1.4.1 Tissue engineered scaffolds

Tissue engineering is a field that seeks to apply the principles of biology and engineering to the development materials consisting of a mixture of cells, biomaterials and bioactive molecules in order to repair damaged tissues and organs (Langer & Vacanti 1993). The current techniques used to repair or restore organs and tissues are autografting and allografting (Ashammakhi et al. 2008). In the autografting method a tissue is transplanted from a part of the body, often the iliac crest, to the damaged part. Even if the biocompatibility is guaranteed, the main disadvantages are chronic pain and possible complications associated with conducting the surgical procedure. On the other hand, allografting involves the

transplant of the tissue or organ got from a donor, but risks of infection, rejection and donor shortage limit this method.

Therefore to overcome these problems, tissue engineering proposes three general strategies for the creation of new tissue (E. Zussman et al. 2002; Langer & Vacanti 1993):

1) healthy cells, are delivered to the damaged tissue;
2) tissue-inducing molecules, as growth factors, are delivered to the damaged tissue and their function is the stimulation of cells to re-establish the normal functionalities;
3) three-dimensional structures, called scaffolds, are produced to support cellular growth and consequently the regeneration of neo native tissue.

In the recent years the last approach has gained more attention. Different techniques can be used for the production of these scaffolds but a number of basic requirements are needed for the application in tissue engineering (Srouji et al. 2006; Kanani & Bahrami 2010). The structures of the scaffolds should mimic as much as possible the native extra cellular matrix (ECM) to allow cell adhesion, proliferation and growth and therefore to support new tissue formation. When the scaffold is implanted in the body to repair the damaged tissue, the body should recognize this scaffold as part of itself and therefore start the regeneration of the neo native tissue (G. Chen, Ushida, & Tateishi, 2002). The material selected for the production of the scaffolds must be biocompatible in order to avoid inflammations and it is preferred to be biodegradable, with a degradation rate that matches neo tissue formation rate. In addition adequate mechanical properties together with specific pore size are important for nutrient and waste product exchange and for the stability of the neo tissue structure. Different materials have been used for the production of these scaffolds: ceramics, metals, polymers. While ceramics and metals are not biodegradable and the processing is difficult, natural and synthetic polymers meet better the requirements previously mentioned.

Electrospun nanofibres have gained a lot of attention for the production of engineered scaffolds mainly due to the small diameter of nanofibres (N. Khan 2012; Armentano et al. 2010; Lannutti et al. 2007). In addition the high surface area to volume ratio allows good cell attachment and proliferation and the high pore density with variable pore size enhances nutrient and waste products exchange (C. Liu et al. 2007). The electrospun scaffolds can closely mimic morphology and size scale of the native ECM and depending on the type of

tissue that has to be regenerated a wide range of materials have been investigated. Proteins, as collagen (Rho et al. 2006; Venugopal et al. 2005), gelatine (Z. M. Huang et al. 2004), silk fibroin (B. M. Min, G. Lee, et al. 2004; B. M. Min, L. Jeong, et al. 2004) and elastin, and polysaccharides, as chitosan (Pillai & C. Sharma 2009), hyaluronic acid (X. Wang et al. 2005) and cellulose acetate (H. Liu & Y. L. Hsieh 2002), are the most common natural materials used. They have better biocompatibility than synthetic materials and they provide adequate surface for cell adhesion and proliferation. However the difficulties of processing and loss of properties after dissolution in solvent for the electrospinning process are the main disadvantages (J. A. Matthews et al. 2002) (Mengyan Li et al. 2005) (Aznar-Cervantes et al. 2012). Addional disadvantages are the weak mechanical properties of the electrospun nanofibres and disease transmission risks.

Among synthetic polymers, poly(lactic acid), (PLA) (F Yang et al. 2004; Q. Yu et al. 2011; J. Chen et al. 2006), poly(glycolic acid) (PGA) (Boland et al. 2004; Z. X. Meng et al. 2010), poly (caprolactone) (PCL) (Williamson et al. 2006; C. M. Hsu & S. Shivkumar 2004) are the most popular polymers which gained FDA (Food and Drug Administration, US) approval for biomedical applications. They are biodegradable and, after hydrolytic degradation, the by-products can be eliminated from the body by natural processes without adverse reactions. They degrade from several weeks to few months depending on the structure and morphology of the scaffolds, its crystallinity, orientation and molecular weight (D. Liang et al. 2007). Synthetic polymers are cheaper than natural polymers and also have higher mechanical properties. On the other hand, they exhibit hydrophobic surfaces that reduce cell attachment. Therefore to overcome problems of cell affinity and mechanical strength, synthetic and natural polymers are often blended together (H. S. Wang et al. 2009; Dan Kai et al. 2012). The resultant electrospun nanofibres maintain the bioactivity of the natural polymer and the mechanical strength and stability of the synthetic material.

For the work presented in this thesis, the interest was focused on PLA. More details of the structure and properties of PLA are given in section 2.2.

2.1.4.2 Dressings for wound healing

The treatment of wounds and burns of a human skin requires a dressing that can achieve the highest rate of healing without leaving scar and also protect from bacterial infections (Zahedi et al. 2009; G. H. Kim et al. 2011). The desirable properties for wound dressing materials are (Zahedi et al. 2009):

a) To maintain the most suitable environment at the interface between wound and dressing;
b) To absorb excess exudates, allow gaseous and fluid exchanges;
c) To provide thermal insulation, mechanical and bacterial protections;
d) To absorb wound odours, be no-adherent to the wound and easily removable without trauma;
e) To be non-toxic, non-allergic, sterile and no-scaring.

However depending on the type of wounds or burn, different types of dressings have been developed (Powers et al. 2013; K. Vowden & P. Vowden 2014), moist dressing such as hydrogel and hydrocolloids, or adsorbent dressings, as foam and alginate (Boateng et al. 2008).

Electrospun nanofibrous materials could be an excellent modern candidate as wound dressing materials (Leung et al. 2011; Rieger et al. 2013). Due to their high porosity they are suitable for an efficient drainage of wound exudates and the permeation of atmospheric oxygen to the wound. Hydrophilic polymers are preferable because the moist wound environment enhances the migration of epithelial cell and therefore the rate of healing (Romana Rošic et al. 2013). The most common polymers that have been so far electrospun and investigated for potential wound care applications are poly(vinyl alcohol) (PVA) (Jannesari et al. 2011; Kataria et al. 2014), chitosan (Homayoni et al. 2009; Y. O. Kang et al. 2010; Tchemtchoua et al. 2011), gelatine (S. E. Kim et al. 2009; Chong et al. 2007), collagen (Rho et al. 2006), hyaluronic acid (Uppal et al. 2011) and polyurethane (M. Khil et al. 2003). Nevertheless, synthetic polymers have been also used and the electrospun nanofibrous mats investigated as wound dressing membranes. PLA electrospun nanofibres and PLA nanofibres loaded with curcumin have shown to enhance the rate of wound closure in vivo in a mouse model (T. T. T. Nguyen et al. 2013). Moreover, in another study, the alignment was found to improve cell infiltration

into the PLA nanofibrous mats compared to randomly oriented webs (Guarino et al. 2011).

2.1.4.3 Drug delivery systems

Delivery of the drugs can be achieved using various types of dosage forms including capsules, tablets, creams, ointments, aerosols and injections (Rasool Hassan 2012). An optimal drug delivery system should release a known amount of drug in a specific period of time and maintained the drug concentration in the therapeutic range, above the minimal effective drug concentration (MEC) and below the minimal toxic concentration (MTC) as shown in Figure 2.11 (Tsung & Burgess 2012). A single dose may lead to a rapid rise and fall in drug concentration (solid curve), but generally the patient needs several doses of the drug during the day to achieve and maintain therapeutically effective plasma concentrations However this may cause significant fluctuations in plasma levels and the drug level could fall below MEC or exceed MTC (solid curve followed by dotted curve). Zero order release (dot–dash curve) leads, after an initial rise, to a constant concentration in plasma which lies between MEC and MTC.

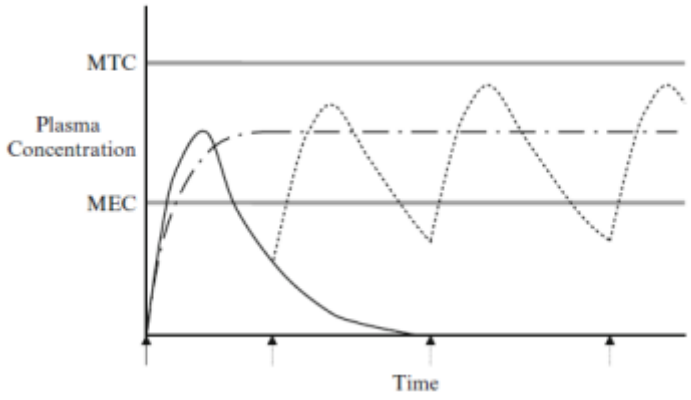

Figure 2.11 – Representation of the plasma drug concentration over time in conventional drug delivery systems (Tsung & Burgess 2012).

The main disadvantages of the conventional drug delivery systems are burst release and low efficiency of encapsulation of the therapeutic agent (Zamani et al. 2013). Electrospun nanofibres can overcome these limitations mainly due to two aspects. First, the high surface area to volume ratio and the high porosity improve the drug diffusion through the nanofibrous

membrane. The second feature is the possibility of control of the processing parameters, such as the type of polymer, biodegradable or non-biodegradable, drug concentration, voltage and flow rate of the solution and therefore tailored the drug release depending on the type of applications (Pillay et al. 2013; D.-G. Yu 2009; Y. J. Son et al. 2014). Moreover both biodegradable and non-biodegradable polymers have been used to produce drug-loaded nanofibrous membranes which have been mainly applied as topical or implanted drug delivery systems; wound-dressing and local cancer treatments have been so far the most investigated area (Zamani et al. 2013; Xiuli Hu et al. 2014). In the last decade several reviews on nanofibres as drug delivery system have been published (Xiuli Hu et al. 2014; D.-G. Yu 2009; Cui et al. 2010; Y. J. Son et al. 2014). The potential application of electrospun nanofibres as drug delivery system is discussed in more details in section 2.3.

2.2 Poly (lactic acid) (PLA)

2.2.1 Production

Poly (lactic acid) (PLA) is biodegradable aliphatic polyester, made up of monomeric units of lactic acid (2-hydroxy propionic acid). The monomer comes from renewable plant sources, mainly corn, starch and sugar beets, due to their richness in carbohydrates (glucose, sucrose, lactose). Carbohydrate fermentation using homolactic organisms (genus *Lactobacilli*) is the most common method in order to achieve a high yield of lactic acid (B. Gupta et al. 2007; Södergård & Stolt 2002).

Three different methods are generally used to produce poly lactic acid (PLA) as shown in Figure 2.12:

(a) direct condensation of lactic acid;
(b) azeotropic dehydrative condensation.
(c) ring opening polymerization (ROP) of the cyclic lactide dimer;

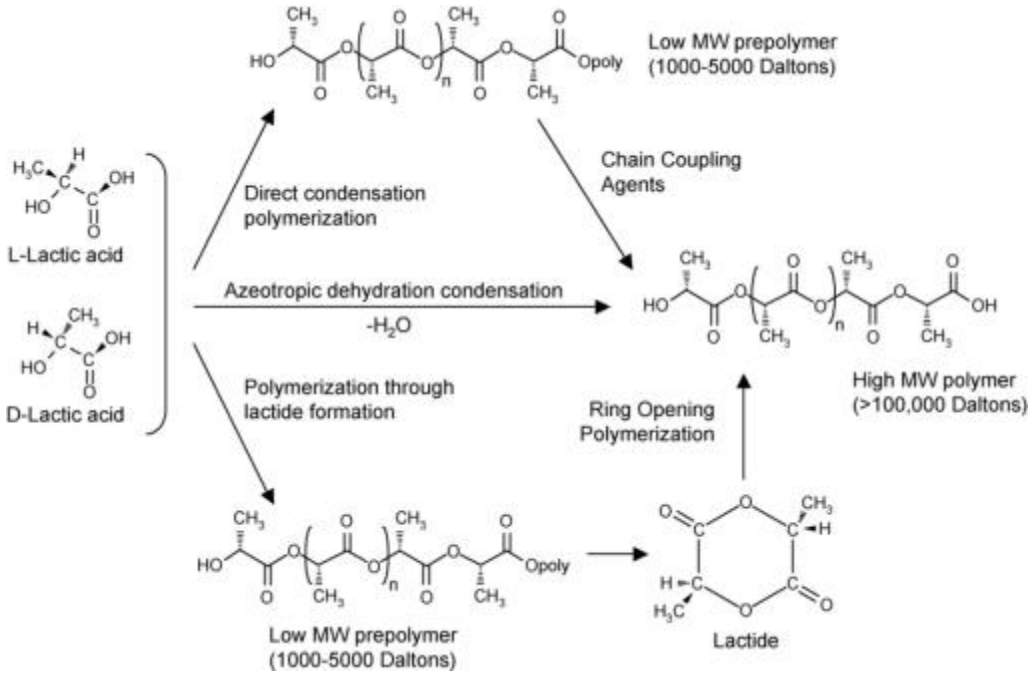

Figure 2.12 – Synthesis methods for obtaining high molecular weight PLA polymers (L. T. Lim et al. 2008).

The least expensive method is *direct condensation*, which involves the esterification of monomers using some solvents. Chain coupling agents are then required to remove impurities and produce high molecular weight PLA polymers. However these agents add complexity and cost to this route (Jamshidian et al. 2010). The production of high molecular weight PLA polymers by direct polycondensation in an azeotropic solution is more practicable. The *azeotropic distillation process* is used by Mitsui Toatsu Chemicals (Enomoto et al. 1994). The process consists in reducing the distillation pressure of an azeotropic solution for a couple of hours at 130°C. PLA is then separated from the solvent using molecular sieves.

In 1992 Cargill Dow LLC patented a novel method, *ring opening polymerization* (ROP), which is a low-cost continuous process and today is the commercial method used for the production of high molecular weight PLA polymers (M_w > 100,000 Daltons) (R. P. Gruber et al. 2001). It consists first of a pre-polymerization of the monomer, lactic acid to produce low molecular weight PLA (prepolymer), followed by depolymerisation under pressure to allow the production of a mixture of L-lactide, D-lactide or meso-lactide using tin catalysts. Next, vacuum distillation allows purification of the lactide and finally high molecular weight PLAs can be obtained using ROP (Drumright et al. 2000). A wide range of anionic and cationic

initiators can be used, but the most common used organometallic catalysts are tin octaoate and aluminium and tin alkoxides (Savioli Lopes et al. 2012).

Formed in November 1997 NatureWorks® LLC is the present leader in PLA production. It is headquartered in Minnetonka, Minnesota, and it is jointly owned by Cargill Dow LLC and PTT Global Chemical, a Thai state-owned company. In 2001, the world's first and largest PLA facility was opened in Blair, Nebraska (US), capable of producing 150,000 metric tons per year.

2.2.2 Structure and properties

Lactic acid, the monomer of poly lactic acid, contains chiral carbon. Therefore it exists in two optically active configurations: L-lactic acid and D-lactic acid. The cyclic dimer, lactide, has three optical arrangements, L-lactide, D-lactide and *meso* lactide as shown in Figure 2.13 (Jamshidian et al. 2010).

The poly (D, L-lactic acid) (PDLLA) is a racemic polymer obtained from an equimolar mixture of L- and D-lactic acid molecules. It is amorphous with weak mechanical properties, whereas pure poly (L-lactic acid) (PLLA) and poly (D-lactic acid) (PDLA) are semi crystalline with similar chemical and physical properties. Generally, PLA polymers with L-lactic acid greater than 93% are crystalline, while PLA polymers with L-lactic acid between 50% and 93% are amorphous (Rafael Auras et al. 2004).

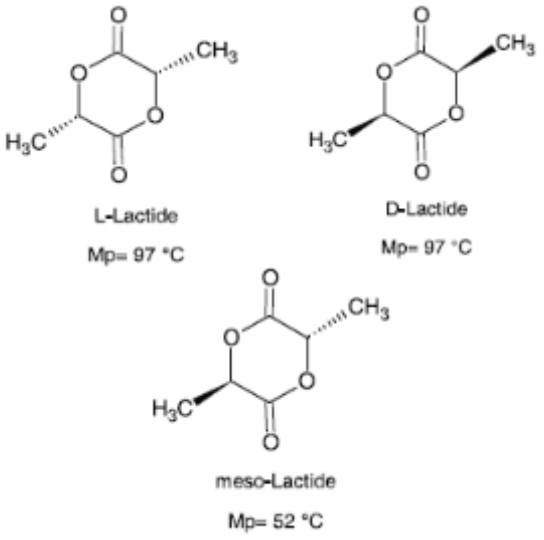

Figure 2.13 – Stereoisomers of lactide.

Pure PLA (either poly L-lactic acid or poly D-lactic acid, semicrystalline) has a glass transition temperature T_g of between 55 and 70°C and a melting point T_m of about 175°C with an enthalpy of 40-60 J/g (Figure 2.14). PLA is a glass below its T_g, while it is a rubbery above its T_g. The β-relaxation temperature, T_β, at -45°C represents the transition below which PLAs are completely brittle. The temperature of decomposition of amorphous PLA varies between 215 and 285°C. On the other hand, amorphous PLAs do not present T_m, but the material changes from rubbery to viscous between 110 and 150°C, depending on the molecular weight and the shear stress (Figure 2.15).

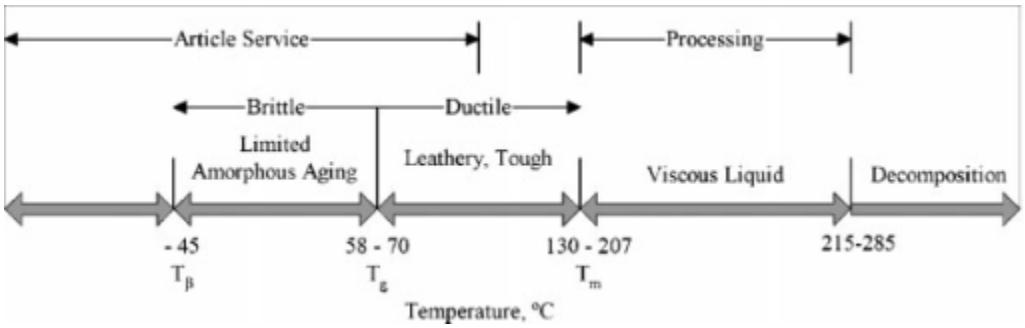

Figure 2.14 – Metastable states of high molecular weight crystalline PLAs (Rafael Auras et al. 2004).

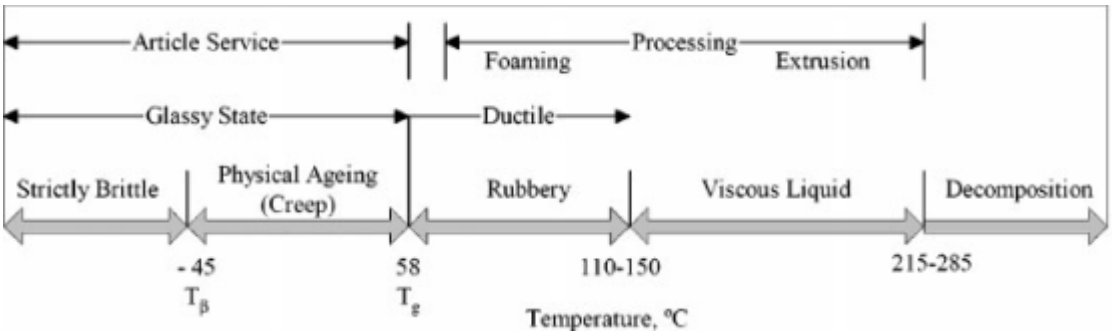

Figure 2.15 – Metastable states of high molecular weight amorphous PLAs (Rafael Auras et al. 2004).

Compared with other thermoplastic polymers such as PET and PS, PLA has a higher T_g and a lower T_m (L. T. Lim et al. 2008). A reduction of L-stereoisomer in the polymer decreases melting temperature (T_m), glass transition temperature (T_g) and crystallinity of the polymer. Melting temperature and crystallinity are also affected by the molecular weight. An increase

of M_w leads to higher T_m, whereas crystallinity decreases. The heat of melting ΔH_m for 100% crystalline PLLA or PDLA is 93.1 J/g (Rafael Auras et al. 2004).

Molecular weight, crystallinity and composition also affect the solubility of PLA. Amorphous PLAs (racemic or meso-lactide) are completely soluble in chlorinated organic solvents, as chloroform and methylene chloride, in acetonitrile, dioxane, xylene, ethyl acetate, dimethylsulfoxide, dimethylformamide. Acetone, ethyl benzene, tetrahydrofuran and toluene only partly dissolve PLAs at room temperature, but they can completely dissolve PLAs by heating the solution to the boiling temperature (Rafael Auras et al. 2004; Södergård & Stolt 2002). On the other hand, crystalline PLAs are insoluble in acetone, ethyl acetate and tetrahydrofuran. Water, some alcohols (methanol, ethanol) and alkanes do not dissolve PLAs. PLA is a pseudoplastic polymer and its rheological properties are influenced by molecular weight, temperature and shear rate. At shear rate of 10-50 s^{-1}, PLA with high molecular weight has melt viscosities in the order of 500-1000 Pa·s and behave like a pseudoplastic, non-Newtonian fluid (L. T. Lim et al. 2008).

2.2.3 Applications of PLAs

2.2.3.1 Food packaging products

Nowadays packaging is the largest end use market for PLAs. Food containers, drinking cups and wrapping films are an example (Drumright et al. 2000). PLA is considered an excellent alternative to the petrochemical based-materials, as poly styrene (PS) and poly ethylene terephthalate (PET), mainly because of the greater reduction of carbon dioxide (CO_2) emissions. It is believed that CO_2 is an important contributor to global warming. PLA is produced from corn, which can absorb CO_2 from air for its growth. Therefore use of PLA has the potential to emit fewer greenhouse gases compared to competitive hydrocarbon-based polymers (Vink et al. 2003). PLA is a more eco-friendly material, biodegradable and compostable material (Conn 1995; Rafael Auras et al. 2004).

Examples of commercially available products of NatureWorks® LLC are reported in Table 2.5. Additionally, in early 2003 the company launched Ingeo™ Fibers, which combines the qualities of natural and synthetic fibres in a new way. Fill for duvet and pillows,

and fabrics for furnishings as carpet, are some applications of the new technology.

Table 2.5 – PLA-based products of NatureWorks® adapted from (Jamshidian et al. 2010; Dow 2004).

Business segment	Commercially available applications
Biaxially-oriented films	Candy twist and flow wrap Envelope and display carton windows Lamination film Product (gift basket) overwrap Lidding stock Die cut labels Floral wrap Tapes Stand-up pouches Cake mix, cereal, and bread bags
Bottles	Shelf-life milk Edible oils Bottled water
Rigid thermoforms	Clear fresh fruit and vegetable clamshells Deli meat trays Opaque dairy (yogurt) containers Bakery, fresh herb and candy containers Consumer displays and electronics packaging Disposable articles and cold drink cups

2.2.3.2 Biomedical applications

PLA has been also widely studied as material for medical applications due to its biocompatibility and biodegradability. It has been approved by the FDA for several uses such as sutures (Lou et al. 2008), rods, plates and screw for bone (B. Gupta et al. 2007; Ahmed & Varshney 2011; Savioli Lopes et al. 2012). The term 'biocompatibility' refers to the ability of a material to interact with the human body without cause any allergic and/or toxic reactions. The term 'biodegradability' indicates the ability of material to be biologically broken down by bacteria or other living organisms. PLA degrades into no toxic products, that enter the Krebs cycle and then degrade to CO_2 and water (A.J. Domb et al. n.d.). Due to its crystallinity structure and the long degradation time, the crystalline PLA was first applied as bone fixation (Ueda & Tabata 2003). In the market, under the product name Fixsorb (Takiron Co.) and Neofix (Gunze Ltd) PLLA has been used as a bone fixator.

Several reviews on the potential application of PLA in biomedical devices are available in the

literature (Lasprilla et al. 2012; Pawar et al. 2014; B. Gupta et al. 2007). Rods, porous scaffolds, films, drug releasing micro particles and recently electrospun nanofibres have been created using different types of PLA for culturing different cell types for regeneration of bone (Kelloma et al. 2000; C. M. Agrawal et al. 1995; Elst et al. 1999), cartilage (Puppi et al. 2010) and nerve tissue (Molamma P. Prabhakaran et al. 2011; F Yang et al. 2004). Osteogenic stem cells seeded on scaffolds of this material and implanted in bone defects or subcutaneously can recapitulate both developmental processes of bone formation: endochondral ossification and intramembranous ossification (Lasprilla et al. 2012). In many cases PLA is blend or copolymerized with other polymers but also blended with other materials, such as ceramics (B. Gupta et al. 2007) depending on the type of applications.

2.2.4 Degradation of PLAs

PLA generally starts to degrade after several months by a hydrolysis mechanism which consists of two steps (Rafael Auras et al. 2004). First, random non-enzymatic chain scission of the ester group occurs as a result of the water molecules attack and leads to smaller molecules of length of the degraded chains. Eventually, the process results in short fragments of chains having carboxyl end groups (COOH) that become soluble in water. The remaining oligomers can reduce the local pH and consequently catalyse the hydrolysis of other ester bonds and speed up the degradation process (Grizzi et al. 1995). Then, oligomers soluble in the surrounding medium can diffuse out of the bulk polymer and be used by microorganisms, yielding carbon dioxide and water (B. Gupta et al. 2007).

Several factors may affect the degradation rate, such as initial molecular weight, crystallinity, temperature, moisture, water diffusion, UV light, metal impurities from the catalyst, as well as device geometry and size (Weir et al. 2004; Ulery et al. 2012). For example high temperature and humidity (50-60°C and RH > 60%) were observed to cause rapid degradation of PLA films (Rudeekit et al. 2008). The degree of degradation can be estimated from change in morphology, decrease in molecular weight and mass loss. Figure 2.16 shows two possible way of erosion which is the loss of mass from degradable polymer matrices (Friederike von Burkersroda, Luise Schedl 2002). The polymer will undergo bulk erosion if the diffusion of water into the polymer matrix is faster than the degradation of polymer bonds.

On the other hand, surface erosion will occur if the degradation of the polymer bonds is faster than the diffusion of water, indicating therefore that the material will be consumed by the hydrolysis of the chemical bonds on the surface.

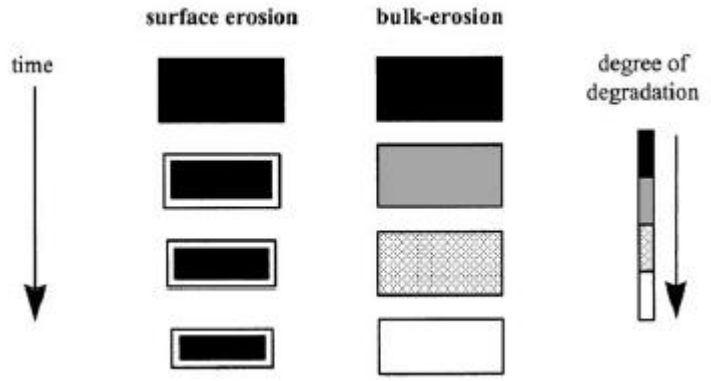

Figure 2.16 – Schematic illustration of the changes a polymer matrix undergoes during surface erosion and bulk erosion (Friederike von Burkersroda, Luise Schedl 2002).

PLA is typically considered a bulk eroding polymer (Weir et al. 2004). However, regarding the degradation of PLA nanofibres several authors reported that the possibility of autocatalysis in the electrospun scaffolds is very limited due to the small dimension of the nanofibres and the degraded oligomers can quickly escape from the surface (K. Kim et al. 2003; Sui et al. 2007). The degradation studies of PLA nanofibres have mainly used amorphous PDLLA due to the higher intake of water molecules resulting therefore in much lower degradation time (Y. Dong et al. 2009; Cui et al. 2006). The long degradation time of PLA-based scaffolds, such as films and foams, could be reduced by electrospun PLA nanofibres. The degradation of electrospun nanofibres and solvent casting films of PDLLA and PELA (poly(D,L-lactide)-poly(ethylene glycol)) was investigated by Cui et al (Cui et al. 2008) with regard to mass loss of the fibre matrix and molecular weight reduction of the polymer matrix. The degradation was performed by immersion of the sample in a phosphate buffer solution at pH 7.0 to mimic physiological condition in human body. The authors stated that surface erosion occurs in the PDLLA nanofibrous samples as a result of the higher mass loss (20.6%) compared to the M_w reduction (6.5%) after 8 weeks, while the significant reduction of M_w (40.7%) higher than the mass losses (11.6%) in the PLLA cast film indicates that bulk degradation occurs due the autocatalysis phenomena. Different degradation patterns between electrospun fibrous mats of PELA and PDLLA were also observed. The hydrophilic

group of PEG in the chemical structure of PELA led to higher molecular weight and mass reduction for both cast film and nanofibrous mats compared to those of PLLA structures.

Recently, the degradation of different type of nanofibrous meshes with or without cells has been reported by Dong et al (Y. Dong et al. 2010). Though degradation was clearly observed with PGA and PLGA nanofibres as a result of the more hydrophilic structures which enhance the hydrolysis, nanofibres made of poly(l-lactide-co-caprolactone) (P(LLA-CL)) did not show obvious change in morphology up to 100 days during degradation with or without cell culture. The cell interactions with the polymeric scaffolds are significantly dependent on the nanofibre composition, but the degradation behaviour of polymer nanofibres with cultured cells is still not well understood.

To summarise, degradation profiles and surface wettability of the electrospun nanofibres are important features to consider for biomedical applications, including tissue scaffolds, drug delivery systems and wound dressing materials. More studies should be carried out to investigate the effect of the nanofibre diameters on the degradation rate.

2.3 Electrospun nanofibres as drug delivery systems

It was in the early 2000s when nanofibres were first investigated as drug delivery system (E. R. Kenawy et al. 2002). PLA, poly(ethylene-co-vinyl acetate) (PEVA) and a blend of the two polymers (50/50 v/v) were dissolved in chloroform. The model drug, tetracycline hydrochloride, was solubilised in a small amount of methanol and then incorporated in nanofibres by dissolution in the polymer solution. Cast films were also prepared by casting of the solutions containing 5% of drug onto glass Petri dishes. An initial burst release in the first 10-12 hours was observed for all formulations due to the presence of some drug crystals on the fibre surface as shown by morphological analysis. However, the total percentage released from the cast film is much lower than the electrospun samples as a result of the lower surface area to volume ratio of cast film compared to nanofibres. The release studies have shown that PLA nanofibrous mats releases the drug immediately as a result of the weak interaction with the polymer, but only 35% of drug was released within 120 hours as a result of the polymer crystallinity. On the other hand, a smoother initial release was observed from PEVA and the blend PLA/PEVA nanofibrous structure. 65% of the incorporated drug was released from

PEVA sample within 120 hours and 50% from the PEVA/PLA nanofibres. The higher crystallinity and more hydrophobicity of PLA compared to PEVA limits the drug diffusion from the nanofibres. The higher compatibility of the drug with PEVA enhances the encapsulation efficiency and consequently slower drug release is achieved compared to PLA sample. A commercial product (Actisite) which is generally used for periodontal disease was also compared with the nanofibrous samples. This product is made of PEVA fibres and containing 25% w/w tetracycline hydrochloride. The authors observed that the amount of drug released from PEVA electrospun samples was approximately twice the amount released from Actisite after 5 days. This may be explained by the higher surface area to volume ratio of the electrospun nanofibres, which therefore makes these types of nanofibrous structures suitable as drug delivery system.

However, the immediate release of a drug may be required for certain biomedical applications, such as after surgery since infections may occur within the first few hours. Zong and his collaborators (Zong et al. 2002) reported the drug release of a common antibiotic, Mexofin, from PDLA nanofibrous membranes. The drug release data were plotted in the form of ln (M_t/M_∞) versus time. Though a burst release of the drug is observed in the first three hours, making this type of nanofibres applicable for prevention of infections, a non-linear relationship was found indicating that drug release profile is not governed by the matrix diffusion only, as shown in Figure 2.17.

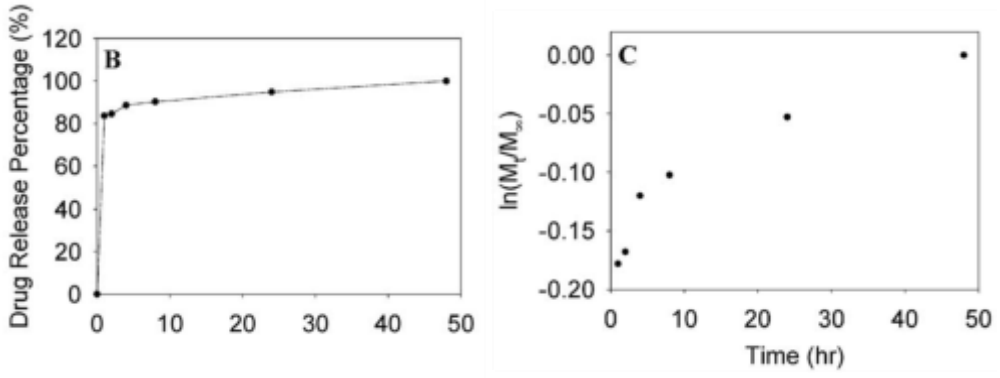

Figure 2.17 – (B) Mefoxin release profile from PDLA nanofibres and (C) Mefoxin release profile in the logarithmic form to evaluate the nature of diffusion (Zong et al. 2002).

In the last decade a wide variety of active pharmaceutical ingredients have been used as model drugs, such as proteins (Y Z Zhang et al. 2006; Ji et al. 2010), poorly water-soluble or

water soluble drug, DNA, genes, growth factors, antibiotics (Katti et al. 2004; Jannesari et al. 2011), anticancer (Ranganath & C.-H. Wang 2008; J. Xie & C.-H. Wang 2006) and anti-inflammatory agents (P Taepaiboon et al. 2006; E.-R. Kenawy et al. 2007; E. Yan et al. 2014). However, different ways have been proposed to incorporate the drug in the nanofibrous structures depending on the type of applications. These methods are described in the next paragraphs.

2.3.1 Methods of drug incorporation into nanofibres

2.3.1.1 Blend electrospinning

The simplest way of drug incorporation is the direct dissolution of the drug in the polymer solution and hence electrospinning. One of the main factors affecting the type of drug loading method is the solubility of the drug and its affinity with the polymer matrix (Buschle-Diller et al. 2007; Ranganath & C.-H. Wang 2008; Z.-M. Huang et al. 2006).

Three different type of drugs were loaded in PLLA solution by Zeng et al (J. Zeng et al. 2003): rifampin, a drug for tuberculosis, paclitaxel and doxorubicin hydrochloride, anticancer drugs. Rifampin and paclitaxel are lipophilic drugs, while doxorubicin hydrochloride is hydrophilic. Though smooth PLLA nanofibres from all formulations were observed from morphological analysis, some doxorubicin hydrochloride crystals were detected on the nanofibre surface as a result of the poor compatibility with PLLA. Later the same authors reported the release of paclitaxel, doxorubicin hydrochloride and doxorubicin base form from PLLA nanofibres within 70 hours (J. Zeng et al. 2005). While there is no paclitaxel release indicating that it is mainly released with the degradation of PLLA fibres, 70% of doxorubicin hydrochloride is released within 60 minutes. This confirms the poor compatibility between PLLA and doxorubicin hydrochloride.

Drug molecular weight and drug concentration have also shown to have an effect on the release rate (Jannesari et al. 2011; P Taepaiboon et al. 2006). Four model drugs were loaded in PVA solutions: sodium salicylate (SS), diclofenac sodium (DS), naproxen (NAP) and indomethacin (IND) (P Taepaiboon et al. 2006). Regardless of the different drug solubility in water, smooth nanofibrous membranes were produced from all formulations as shown by

morphological observations. This indicated that all drugs are perfectly incorporated. However, on increasing drug M_w the amount of drug released from the nanofibrous sample decreases. As a result of better solubility and smaller molecule size, sodium salicylate could diffuse from the polymer matrix to the release medium easier than the other drugs. Similar observations were reported by Rujiravanit et al (Rujiravanit et al. 2003) for chitosan/fibroin blend films. The amount of salicylic acid released at pH of 7.2 was 73.5%, while the amount of theophylline was 69%. This is explained by the better solubility and smaller size of salicylic acid compared to theophylline.

Controlling of the drug release may be achieved by changing the chemical structure of the polymer matrix (Jannesari et al. 2011; K. Kim et al. 2004; Nageh et al. 2014). Jannesari and his collaborators (Jannesari et al. 2011) investigated the release of ciprofloxacin hydrochloride (CipHCl) from PVA, poly(vinyl acetate) (PVAc) and PVA/PVAc (50/50) electrospun nanofibres. The drug was directly incorporated in the aqueous solution of PVA and PVAc. The hydrophobicity of PVAc which indicates its less affinity to water compared to PVA, led to reduction of the degree of swelling of the electrospun samples. Consequently this resulted in sustained drug release over 250 hours, while fast and total drug release within 100 hours was achieved from PVA electrospun samples. The effect of drug concentrations was also investigated. An increase of the drug content from 5% to 10% w/w approximately doubled the initial drug release from PVAc fibres, as a result of a greater portion of drug on the fibre surface detected by SEM analysis. Similar observations were described by Verreck and his group (Verreck et al. 2003) for poly(urethane) (PU) nanofibres loaded with 10% and 40% of the model drug itraconazole.

To summarise, the incorporation of active pharmaceutical ingredients in polymeric solution for the production of electrospun nanofibrous membranes may be achieved by either direct dissolution in a common solvent or, if polymer and drug are not soluble in the same solvent, the drug can be firstly solubilise in a suitable solvent and then slightly add to the polymeric solution (Buschle-Diller et al. 2007; E. R. Kenawy et al. 2002). Generally hydrophobic drugs should be incorporated in organic solution of hydrophobic polymers, while hydrophilic drugs in aqueous solution of hydrophilic polymer (J. Zeng et al. 2003; Cui et al. 2006). The solubility and the interactions between drug and polymer are the most significant factors affecting the drug release from electrospun nanofibrous membrane. Therefore the selection of polymer or polymer blends should be done appropriately depending on the type of drug and

the application of the electrospun nanofibrous structures. However, there is a lack of solution properties measurements, including solution viscosity, surface tension and conductivity after the incorporation of the drug. The addition of a drug may vary for example the solution conductivity as suggested by Zhang et al (C. Zhang et al. 2005) which in turn may affect the stability of the charged electrospun jet.

The main disadvantage of the simple dissolution method is the likely denaturation of drugs due to direct contact with harmful organic solvents to prepare the polymer solution and the high voltage applied for the electrospinning process. For these reasons, other techniques have recently gained the attention of researchers: co-axial electrospinning and emulsion electrospinning.

2.3.1.2 Coaxial electrospinning

This method has been introduced to reduce the initial burst release resulting from drug loaded in nanofibres with blend electrospinning. The electrospinning setup is modified by using a needle with two concentric capillaries. As first described by Sun et al (Z. Sun et al. 2003), this process consists of simultaneously pumping two solutions in two different syringes, without direct initial mixing, to produce nanofibres with a core and a shell of different compositions (Figure 2.18). The drug is dissolved in its proper solvent and introduced in the inner capillary, while the polymer solution used as shell material is delivered through the outer capillary. Using this electrospinning setup core-shell nanofibres are eventually produced. The main advantages are the controllable and sustainable release and protection of the molecule bioactivity.

The key parameters regulating the efficiency of drug encapsulation in coaxial electrospinning are the polymer concentration of the shell solution (C. He et al. 2006), drug concentration (Jannesari et al. 2011; Sohrabi et al. 2013) and core/shell flow rate ratio (Z.-M. Huang et al. 2006; D.-G. Yu, Chian, et al. 2013; W. Song et al. 2013; Katti et al. 2004).

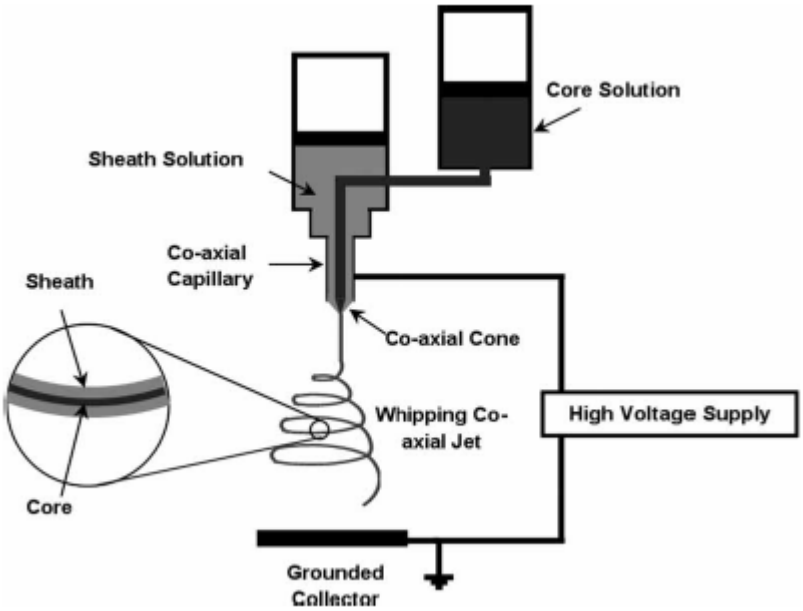

Figure 2.18 – Schematic coaxial electrospinning setup (Moghe & B. S. Gupta 2008).

Core-shell nanofibres with different PLA concentrations (5, 8 an 10%) as shell material were produced by He et al (C. He et al. 2006). The core solution consisted of a model drug, tetracycline hydrochloride (TCH) dissolved in a mixture of methanol and chloroform (2:1 w/w) with 1% of PLA. Sustained drug release was observed over 28 days for all formulations. However on decreasing the PLA concentration in the shell from 10% to 5%, faster drug release was achieved as shown in Figure 2.19. Wide shell diameter distribution were reported 150-1060 nm, 223-1840 nm, 260-3100 nm for PLA concentration of 5, 8 and 10%, respectively, and the authors stated that smaller shell diameter is responsible of faster release. The drug is released by diffusion as PLA is a crystalline hydrophobic polymer and degradation of the nanofibrous sample was not observed. In the simple electrospinning it has been shown that an increase of solution viscosity leads to larger nanofibres. However the solution properties (viscosity, conductivity) of shell and core solutions were not measured.

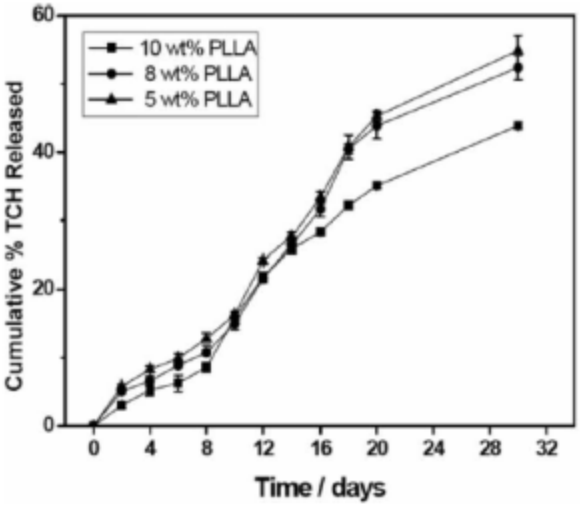

Figure 2.19 – In vitro release of drug from electrospun PLA nanofibrous membranes when incubated in the buffer solution (pH 7.35, 37°C) with different PLLA shell concentrations (C. He et al. 2006).

Several scientific publications reported the used of coaxial electrospinning for incorporation and release of other molecules including proteins and growth factors (G. Jin et al. 2013; Joung et al. 2011). Jiang et al (H. Jiang et al. 2005) used coaxial electrospinning for incorporation and controlled release of two model proteins, bovine serum albumin (BSA) and lysozyme, from biodegradable core-shell nanofibres with PEG as core material and PCL as shell material. On increasing the flow rate of the inner solution from 0.6 ml/h to 2 ml/h, an increase in the diameter of both shell and core layers was observed. A steady release of BSA and lysozyme was achieved over a period of 30 days for all formulations with a faster release from electrospun mats produced using higher core solution flow rate. SEM analysis has shown the formation of pores after 1 day of release, therefore indicating that the mechanism of release is the diffusion of the drug from the core to the fibre surface through these pores. In another study the same authors have shown that the release rate of the proteins encapsulated in the core could be tuned by altering the chemical composition of the shell (H. Jiang et al. 2006). A blend of PCL and PEG in solution DMF/CHL (3/7 v/v) was used as shell material, whereas BSA or lysozymes were added to an aqueous dextran solution and used as core material. The effects of the PEG amount on the nanofibres morphology and drug release were studied. The increase of PEG in the shell solution resulted in nanofibres with larger diameter

most likely due to increased solution viscosity, but no measurements of solution viscosity, conductivity of core and shell solutions were reported by the authors. Regarding the release profile of BSA, higher drug release was measured on increasing the amount of PEG in the shell. The authors speculated the PEG can act as pore-forming agent. Hence an increase of PEG leads to higher amount of pores on the fibre surface and this may explained the faster drug release. However the core-shell structure of the nanofibres was difficult to be visualized by TEM because of the low electronic contrast between PCL (shell material) and dextran (core material) (H. Jiang et al. 2006).

Another great advantage that could be offered by core-shell nanofibres is the possibility of encapsulation of multiple drugs (G. Jin et al. 2013; Zhiwei Xie et al. 2013; Y. Su et al. 2012). Recently multiple epidermal induction medium made of epidermal growth factor (EGF), insulin, hydrocortisone and retinoic acid was diluted into 1 ml solution with 5% BSA an used as core material, while the shell solution was a blend of gelatin (Gel) and poly(L-lactic acid)-co-poly-(e-caprolactone) (PLLCL) (G. Jin et al. 2013). A blend solution was also prepared and both blend and coaxial electrospinning were used to prepare nanofibrous membranes. The drug release profiles are shown in Figure 2.20. After 3 days a burst release of the growth factor EGF was detected from the blended nanofibres (44.9%), while a slow and steady release profile was obtained with the core-shell electrospun nanofibrous membranes.

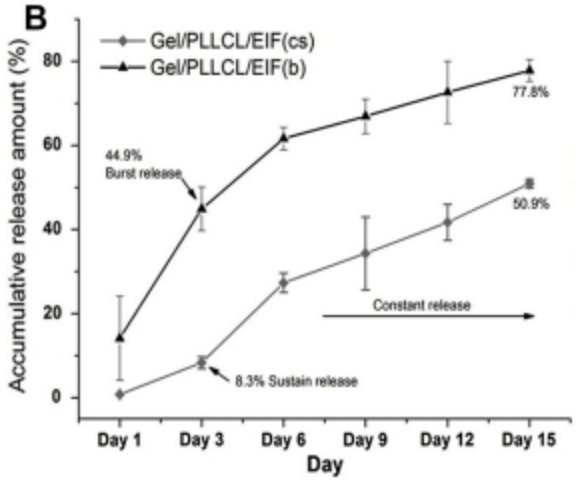

Figure 2.20 – Comparison from core-shell nanofibres and blending electrospinning (G. Jin et al. 2013)

A number of researchers compared blend and coaxial electrospinning. The overall observations are that coaxial electrospinning enhances the efficiency of drug encapsulation within the nanofibrous webs compared with blend electrospinning, as well as sustained protein release (C.-L. He et al. 2009; S. Yan et al. 2009; Maleki et al. 2013; Ji et al. 2010; D.-G. Yu, Chian, et al. 2013). Nevertheless, so far the preservation of the protein or enzyme activity has been investigated by only few researchers (H. Jiang et al. 2005; Tiwari & Venkatraman 2012). Jiang et al performed gel electrophoresis to verify the protective effect of lysozyme encapsulated in the nanofibre core on the enzymatic activity and the results suggested that the lysozyme incorporated into the nanofibers was intact. On the other hand Ji et al (Ji et al. 2010) compared the effect of blend and coaxial electrospinning on protein activity by using alkaline phosphatase (ALP) as a model protein. Both electrospinning techniques reduced the biological activity of the incorporated ALP, suggesting therefore that high voltage and contact with organic solvents are harmful to the loaded biomolecules. But the addition of PEG to ALP solution resulted in higher protein preservation regardless of electrospinning method. The author stated that PEG eliminates protein adsorption to the organic polymer phase during electrospinning. Nevertheless, solution properties such as viscosity and conductivity were not measured and reported by the authors.

The core shell structure of nanofibres produced by coaxial electrospinning is generally verified with TEM analysis, but in most scientific publications few images with only a segment of the fibre have been reported (L. Cheng et al. 2014; Merkle et al. 2013). Interesting observations have been reported by the group of Dror, Arinstein and Zussman (Dror et al. 2007; Arinstein et al. 2009). Even though core-shell nanofibres were expected from the electrospinning of a PEO solution as core and PCL solution as shell material, images of the cross section revealed that the electrospun nanofibres presented a hollow structure as shown in Figure 2.21. The authors explained that the mechanism for the formation of the electrospun microtubes is based on the different evaporation of core and shell solvents. The observations were related to the slower evaporation of the solvent mixture (water/ethanol 60/40) in the core solution through the solidified shell. A skin of PCL is quickly formed due to the fast evaporation of the solvent mixture CHL/DMF (80/20 v/v), and when the aqueous solution starts penetrating the shell, precipitation of the inner layer of the shell take place, because

water is a non-solvent for PLC (Arinstein et al. 2009; E. Zussman et al. 2006).

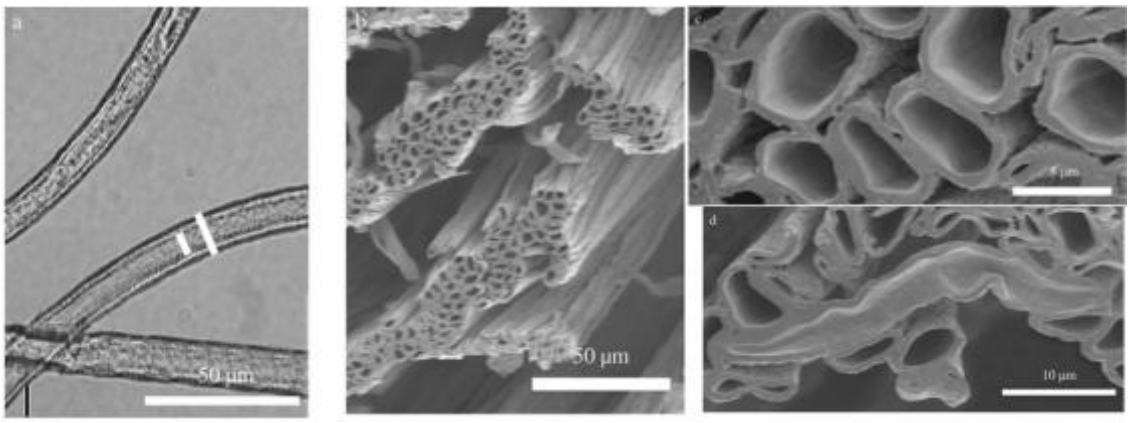

Figure 2.21 – Coaxial electrospinning of PCL shell material and PEO/water/EtOH core material a) optical microscopy, (b, c, d) SEM images at different magnifications PLC (Dror et al. 2007).

Additionally, the miscibility between core and shell solutions has shown to affect the hollow structure. Perfect cylindrical hollow nanofibres were produced using a core solution made of PVA or PEO in mixtures of ethanol and water which is immiscible with the shell solution made of PCL in CHL/DMF. On the other hand, hollow fibres with less uniform shell were collected using a PEO solution in DMF, which is miscible with the shell solution.

Miscible and immiscible core and shell solutions have been used for production of core-shell nanofibres. However this phenomenon has not been observed by other researchers, although core and shell solutions of similar compositions have been selected (S. Yan et al. 2009; Kijeńska et al. 2014; Z.-M. Huang et al. 2006). There is a lack of systematic investigation of the effect of both solution properties including viscosity, surface tension and conductivity, and process parameters on the final morphology and diameter of core-shell nanofibres. The diffusion rate of the core solvent and the interfacial tension between core and shell solutions are also significant factors for the production of core-shell nanofibres with uniform core distribution.

2.3.1.3 Emulsion electrospinning

Emulsion electrospinning has been introduced to incorporate a water-soluble drug into a hydrophobic or an amphiphilic polymer (Xiuling Xu et al. 2006; Xiuling Xu et al. 2005). An emulsion is prepared by slowly adding a drug aqueous solution to an organic polymeric solution under magnetic stirring, resulting in a water-in-oil emulsion (W/O). With emulsion electrospinning, drug and polymer are dissolved in their proper solvents, there is no need to find a common solvent and the contact of the drug with the organic solvent is minimal (Chong Wang et al. 2011; Briggs & Arinzeh 2014).

Emulsion electrospinning was first investigated by Xu and his collaborators (Xiuling Xu et al. 2005). The model drug, doxorubicin hydrochloride (Dox), was first dissolved in water and afterwards slowly adds drop by drop into the polymeric solution and emulsified for about 20 minutes. Morphological observations have shown uniform nanofibres and no crystals of drug were detected on the nanofibre surface. Two different polymers as shell material were used. While 25% of the drug was released from Dox/PLLA nanofibres, in the first 50 minutes, only 9% was released from Dox/PEG-PLLA nanofibres. The higher encapsulation of the drug in the PEG-PLLA nanofibres was obtained due to the higher affinity and compatibility between PEG and DOX (both hydrophilic).

Even though emulsion electrospinning can be used when a hydrophilic therapeutic agent has to be encapsulated inside a hydrophobic polymer (Briggs & Arinzeh 2014; Xiaoqiang Li et al. 2010), the drug denaturation is more likely resultant from the emulsion electrospinning compared to the coaxial electrospinning. The shear forces applied during the emulsion preparation may generate heat which can be detrimental for the bioactive molecules (Hong Zhang et al. 2010; Briggs & Arinzeh 2014). Other limitations of the emulsion electrospinning are related to the types of surfactant and proper viscosity of the drop phase required to maintain a stable emulsion (Angeles et al. 2008).

2.3.2 Drug release mechanisms

For biomedical applications, such as tissue engineered scaffolds and drug delivery systems biodegradable polymer are preferable compared to non-biodegradable material, since they do

not require retrieval after the full release of the drug. The release of a drug from biodegradable polymer may be a combined effect of diffusion and degradation of the polymer matrix (Rathinamoorthy et al. 2012; Goddard et al. 2003).

There are several factors that contribute to the release mechanism (Liechty et al. 2010; Juergen Siepmann et al. 2011):

i. type of polymer matrix;
ii. polymer crystallinity;
iii. M_w of polymer and M_w drug;
iv. type of drug loading method;
v. hydrophilicity or hydrophobicity of the drug;
vi. morphology of polymer matrix, including shape, size, porosity;
vii. pH, temperature or enzymatic action.

If the polymer matrix is not soluble in the release medium and swelling and degradation do not occur, the drug is generally released by diffusion. The rate of diffusion depends on the type of interaction with the polymer matrix, the drug molecular weight and the diffusion coefficient (D), which is a measure of the molecule mobility in the medium. This mechanism is well described by the Fick's first law (Equation 5) where J is the rate of mass transport per unit area, dC/dx is the gradient of drug concentration and D is the diffusion coefficient.

$$J = -D \frac{dC}{dx}$$

Equation 5

Equation 6 is the Fick's second law of diffusion which has been derived from the first one, where C is the drug concentration, t the time, and , y, z are the three Cartesian coordinates.

$$\frac{\partial C}{\partial t} = D\left(\frac{\partial^2 C}{\partial x^2} + \frac{\partial^2 C}{\partial y^2} + \frac{\partial^2 C}{\partial z^2}\right)$$

Equation 6

A popular semi-empirical model that can be used to describe drug kinetics transport is based on the power-law expression (J. Siepmann & N.A. Peppas 2012). The well-known Korsmeyer-Peppas equation is given by Equation 7.

$$\frac{M_t}{M_\infty} = kt^n$$

Equation 7

M_t is the cumulative amount of drug released at time t, M_∞ is the total mass loaded into the polymer, k is the drug release rate which depends on the structural and geometric characteristics of the system, n is the release exponent suggesting the mechanism of release. Table 2.6 shows the values of n for different types of geometry.

Table 2.6 – Exponent n of the power law and drug release mechanism from polymeric controlled drug delivery system of different geometry.

Exponent, ***n***			
Thin film	Sphere	Cylinder	***Release mechanism***
0.5	0.43	0.45	Fick diffusion
0.5 < n < 1.0	0.43 < n < 0.89	0.45 < n < 0.89	Anomalous diffusion
1.0	0.85	0.89	Case-II transport

The Peppas equation can be applied if the drug is homogeneously distributed in the polymeric matrix and in the range of (M_t / M∞) lower than 0.60 (Pattama Taepaiboon et al. 2007). When n is equal to 0.5, the equation represents Equation 8, known as Higuchi's equation, a classical model that assumes drug diffusion for the release from a polymer insoluble in the solvent. The constant k_H depends on the geometry of the device. However this model is based on several assumption: the initial drug concentration in the matrix is much higher than drug solubility; drug diffusion takes place only in one dimension (edge effect must be negligible); matrix swelling and dissolution are negligible; drug diffusivity is constant and perfect sink conditions are maintained in the release environment (H. Sciences 2010).

$$\frac{M_t}{M_\infty} = k_H\sqrt{t}$$

Equation 8

Regarding the drug release from electrospun nanofibres, the Peppas equation has been generally employed (T. T. T. Nguyen et al. 2012; Chi Wang et al. 2010; Z. Li et al. 2014; D.-G. Yu, Chian, et al. 2013; Sohrabi et al. 2013). However the value of M_{∞} which is the actual amount of drug loaded, is not usually calculated (Chi Wang et al. 2010; Jannesari et al. 2011; D.-G. Yu, Chian, et al. 2013) suggesting that the efficiency of encapsulation is hypothesised to be 100%. Only a few researchers dissolved completely the nanofibrous samples in proper solvent to extract the drug and hence to determine the efficiency of encapsulation (Ranganath & C.-H. Wang 2008; P Taepaiboon et al. 2006).

3 GENERAL MATERIALS AND METHODS

3.1 Materials

Poly (lactic acid) 4060D was purchased from Nature Works LLC (Minnetonka, MN, USA). 4060D is fully amorphous grade (PDLLA), with a D-lactide content of about 11% to 13%, density of 1.24 g/cm^3 and it is provided in forms of pellets. In this thesis the term PLA is used for simplicity.

The weight average molecular weight (M_w) of PLA was measured by gel permeation chromatography (GPC) (Agilent 1260 Infinity). The column (PL gel mixed-B, length 30 mm, particle size 30 μm, Agilent) was calibrated by using poly(styrene) standards of known molecular weight within the range 3,770 – 2,950,000 g/L using tetrahydrofuran (THF, GPC grade, Sigma Aldrich). The flow rate was maintained at 1 ml/min at a column temperature of 30 °C. PLA was dissolved in THF at a concentration of about 1% w/v and approximately 20 μl of sample were injected into the column. Mark Houwink constants used are K 17.4e-05 dl/g and α 0.736. The molecular weight distribution of PLA 4060D is shown in Figure 3.1 and the results are reported in Table 3.1. M_w of PLA 4060D is approximately 100 000 g/mol.

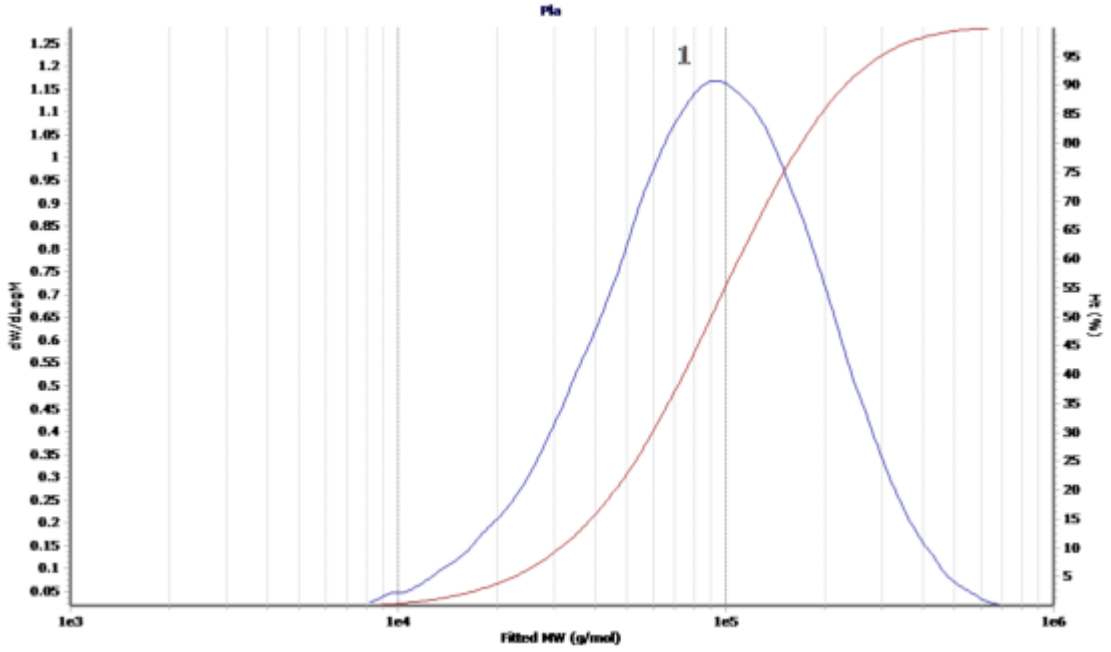

Figure 3.1 – Molecular weight distribution of PLA 4060D.

Table 3.1 – Average molecular weights of PLA 4060D: M_n is the number average molecular weight, M_w is the weight average molecular weight, M_z is the higher average molecular weight, M_v is the viscosity average molecular weight, PD is the polydispersity index (M_w/M_n).

M_n	M_w	M_z	M_v	PD
48399	99988	181683	169724	2.07

All solvents used for the production of PLA nanofibres (chapter 4, 5 and 6) are listed in Table 3.2 and were used without further purification.

For the production of core-shell nanofibres (chapter 7), poly (vinyl alcohol) (PVA) with M_w of 70000 g/mol (98% hydrolysed) and lidocaine hydrochloride monohydrate (LidHCl) (Sigma-Aldrich, UK) (M_w 288.81 g/mol) were used as core materials.

Figure 3.2 shows the chemical structure of LidHCl. Other materials and solvents purchased for the drug delivery studies are reported in Table 3.3.

Table 3.2 – List of solvents used to dissolve PLA (chapter 4, chapter 5, chapter 6).

Solvent	Abbreviation	Company
1,4-Dioxane	1,4-DX	Fisher Scientific, UK
Acetone	AC	Fisher Scientific, UK
Chloroform	CHL	Sigma-Aldrich, UK
Dichloromethane	DCM	Sigma-Aldrich, UK
Dimethylacetamide	DMAc	Sigma-Aldrich, UK
Dimethylformamide	DMF	Sigma-Aldrich, UK
Tetrahydrofuran	THF	Sigma-Aldrich, UK

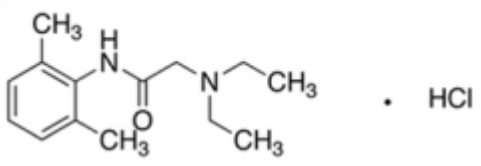

Figure 3.2 – Chemical structure of lidocaine hydrochloride.

Table 3.3 – List of chemicals used in chapter 7.

Solvent	Company
Rhodamine B	Sigma Aldrich, NL
Fluorescein isothiocyanate	Sigma Aldrich, NL
Acetonitrile	Fisher Scientific, UK
Diethylamine	Sigma-Aldrich, UK
Sodium phosphate monobasic dihydrate	Fisher Scientific, UK
Phosphate buffered saline tablets	Sigma-Aldrich, UK
Sodium acetate anhydrous	Sigma-Aldrich, UK

3.2 Electrospinning process

3.2.1 Electrospun PLA nanofibres

For the preparation of all PLA solutions, the solvent or mixture of solvents was/were added to a pre-weighted amount of PLA. All solutions were magnetically stirred at room temperature (20-22°C) for approximately 4 hours until complete dissolution of the polymer. Electrospinning of the solution was performed immediately after its preparation.

Figure 3.3 shows the electrospinning setup used for the experiments described in charter 4, chapter 5 and chapter 6. A 10 ml syringe (Becton Dickinson, Luer lock) was filled with the polymeric solution and connected to a metallic needle (outer diameter 0.9081 mm, inner diameter 0.603 mm, Fisher Scientific, UK) using a Teflon tubing. The flow rate was controlled using a syringe pump (PHD Ultra, Harvard Apparatus, Cambridge, UK), placed outside the electrospinning chamber. This chamber is connected to a ventilation system to remove solvent vapours. A copper plate wrapped with aluminium foil was used as collector for the deposition of nanofibres and a support is used to keep the collector in vertical position in front of the needle. The positive electrode of voltage was connected to the metallic needle, while the negative one was connected to the plate. The electrospinning experiments were performed at room temperature between 19 and 22°C. The humidity inside the electrospinning chamber was controlled using a hygrometer (DT-321 ATP Instrumentation, UK) and kept constant at 35% using dry compressed air.

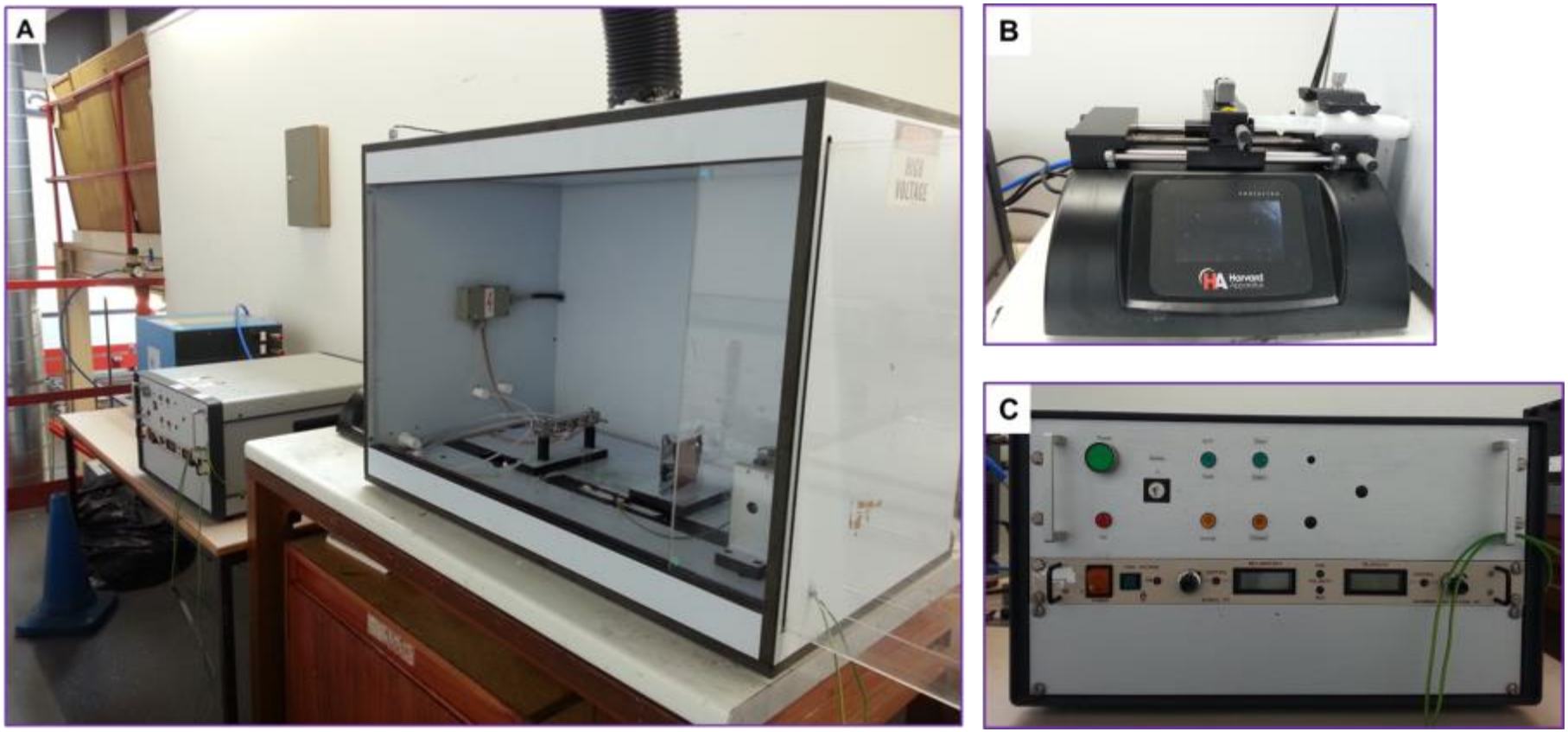

Figure 3.3 – Electrospinning setup (A), syringe pump (B), high voltage source (C) (Loughborough University).

3.2.2 Electrospun core-shell nanofibres

A vertical electrospinning setup (Figure 3.4) was used in the second part of this thesis (chapter 7) for the production of nanofibres with a core shell structure. The nanofibrous samples were prepared at the Dentistry-Biomaterials Department of Radboud University (The Netherlands), in collaboration with COST-Action MP1206 (Electrospun nanofibres for bio inspired composite materials and innovative industrial applications).

The shell material was a PLA solution prepared at room temperature. The core material was a PVA aqueous solution. A known amount of distilled water was first heated up to about 80°C and then PVA was slowly added to obtain a solution at polymer concentration of 10% w/v. The solution was magnetically stirred at 80°C until complete dissolution of the polymer. The water was from Millipore Milli-Q ultrapure water system.

Other core solution was prepared by addition of the model drug LidHCl to the PVA solution after its cooling. The amount of drug added was 50% weight by weight of PVA.

Two syringe pumps (Kd Scientific 100) were used to separately deliver shell and core solutions. The needle used has two concentric capillaries. The exit diameter of the outer capillary is 0.8 mm, while the inner capillary has a diameter of 0.5 mm. The flow rate of the shell was fixed at 2.1 ml/h, while the core flow rate was varied. Three core solution flow rate were selected: 0.3, 0.5, 0.7 ml/h. The distance was varied 15 to 22 cm and the voltage was changed between 12 and 21 kV, in order to obtain a stable electrospun jet. The nanofibrous samples, with and without drug, were collected on a static plate covered with aluminium foil.

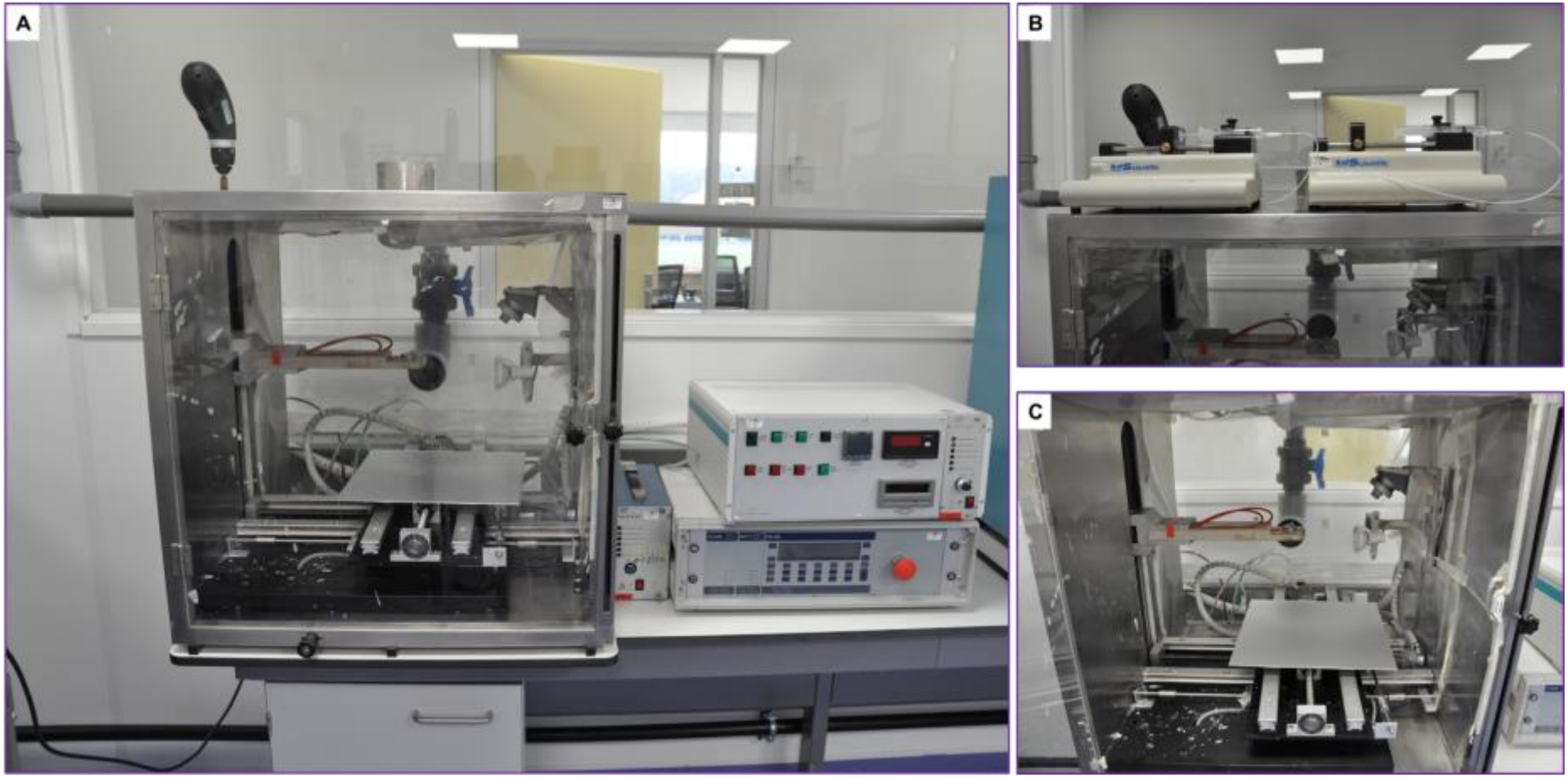

Figure 3.4 – Electrospinning setup (A), syringe pumps (B), high voltage source (C), (Radboud University, Biomaterials Department, Nijmegen, NL).

3.3 Characterisation of solution properties

As reported in the literature review of this thesis, several solution properties affect the morphology and the mean diameter of the electrospun nanofibres. Solution viscosity, surface tension and conductivity were therefore measured for all solutions.

The dependence of *shear solution viscosity* on shear rate was measured with a HAAKE VT550 rheometer equipped with a cone-plate measuring system (cone radius 40 mm, cone angle 1.59 degrees, truncation 56 μm). The steady state viscosity measurements were performed in the continuous ramp mode at constant temperature of 25°C. The solution was placed between the Peltier plate and the rotating cone attached to the driving motor spindle. The changes in viscosity were measured over a range of shear rate from 0.1 to 1000 s^{-1}. The test was repeated at least three times for each solution. The same rheometer was used to perform oscillatory tests and elastic (G') and plastic modulus (G'') of the solutions were measured. An amplitude sweep test over a stress range between 0.1 and 100 Pa at a constant frequency of 1Hz was first performed to find the linear viscoelastic region (LVR). Once LVR region was determined, a frequency sweep test was used to determine the nature of the material. The frequency was varied from 0.1 to 100 Hz at a value of shear stress in the LVR. All measurements were repeated three times for each solution.

The *surface tension* of the PLA solutions was measured with an electronic tensiometer (White Electric Instrument, DB2kS). All glassware was first cleaned with a mixture of aqua regia and water before performing the test. Aqua regia is a corrosive fuming yellow liquid made of nitric acid (HNO_3) and hydrochloric acid (HCl). HNO_3 (70% w/w, Fisher Scientific Ltd, UK) was slowly added to HCl (36% w/w, Fisher Scientific Ltd, UK) in a volume ratio 1:4. Then the mixture was diluted with deionized water in a volume ratio 1:9. For the analysis, a platinum ring is lowered on the surface of the polymeric solution and then slowly lifted. The force required to break the contact between the liquid's surface and the ring is related to the surface tension. Five measurements were taken for each solution.

The *conductivity* of the polymer solutions was determined using a conductivity meter (Jenway Model 470) with a cell constant K = 1.07 and accuracy of ± 0.5%.

3.4 Characterisation of electrospun nanofibres

3.4.1 Scanning electron microscopy (SEM)

The morphology of nanofibrous samples was observed using field emission scanning electron microscopy (FEG-SEM, LEO 1530VP) using an accelerating voltage of 5.0 kV. Before observation, the nanofibres collected on the aluminium foil were coated using a gold/palladium sputter coater for 2 min (SC7640, Emitech). The diameter of PLA nanofibres was measured using image software (AxioVision Rel 4.8). At least 150 diameters were measured and IBM SPSS Statistics 22.0 (a software package for statistical analysis) was used to calculate an average value and create diameter distribution graph. The results are presented as mean value ± standard deviation. The one-way ANOVA was used to test the statistical significance of the difference between the mean values assuming a confidence level of 95% ($p < 0.05$).

3.4.2 Transmission electron microscopy (TEM)

A transmission electron microscope (JEOL, JEM 2000FX) operated at an accelerating voltage of 100 kV was used to verify the core/shell structure of the nanofibres produced using coaxial electrospinning. The samples for TEM observations were prepared by collecting during the electrospinning process few nanofibres onto standard carbon-coated copper grids. Several images were then taken at different magnifications.

3.4.3 Confocal laser scanning microscopy (CLSM)

The core/shell structure of the nanofibres was also evaluated using a confocal scanning microscope (Nikon, Eclipse TE 300). Fluorescent dyes were first added to the polymeric solutions. Approximately 30 μg/ml of Rhodamine B was added to the PLA solution, while fluorescein (90 μg/ml) was added to the PVA solution (with and without drug) prior electrospinning. The fibres were then collected on glass slides for few minutes. Rhodamine B

and fluorescein have different excitation and emission wavelengths as reported in Figure 3.4. Two lasers were used for the analysis: Argon with emission of 488 nm and Helium-neon of emission 543 nm. The software Laser Sharp 2000 was used to obtain the images.

Table 3.4 – Emission and excitation λ_{max} of the fluorescent dyes incorporated in the solutions.

	Excitation λ_{max} (nm)	**Emission λ_{max} (nm)**
Rhodamine B	540	625
Fluorescein isothiocyanate	495	525

3.4.4 Focus ion beam-scanning electron microscopy (FIB-SEM)

A dual beam microscope system (FEI, Nova 600 Nanolab) was used to investigate the internal structure of the core/shell nanofibres. The nanofibres collected on the aluminium foil were coated using a gold/palladium sputter coater for 2 min (Emitech, SC7640).

Platinum was deposited on a fibre to 'glue' it to the underneath fibre. Platinum deposition was performed using a current of 30 pA in the ion beam for 30 seconds. Then the ion beam probe was used to cut the fibre and remove a part of the fibre through milling. The cross section of the fibre was imaged using the electron beam. The electron images were collected in the immersion mode, which is for non-magnetic samples.

3.4.5 Water contact angle measurements

The wettability of nanofibrous samples was evaluated by measuring the water contact angle using sessile drop technique (Kruss Instrument, DSA 100). The samples were removed from the aluminium foil and placed on a glass slide. A droplet of water (10 μl) was placed onto the sample surface and the angle was immediately measured by taking pictures of the droplet using an optical microscope and the software (DSA-4). The reported values are the average values of at least five measurements.

3.4.6 Differential scanning calorimetry (DSC)

The thermal properties of the bulk materials (PLA, PVA, LidHCl) and the nanofibrous samples were investigated using a differential scanning calorimeter (TA Instruments, model Q10). Samples of approximately 9 to 13 mg were hermetically sealed in aluminium pans and loaded into the chamber. Thermal measurements were performed in heat flux mode of nitrogen atmosphere at 60 ml/min. The sample was heated from 20°C to 250°C at a rate of 10°C/min, followed by cooling to 20°C and a second heating at the same rate. Data were analysed using the TA universal analysis software package. The test was repeated three times for each sample.

3.4.7 Fourier transform infrared spectroscopy (FTIR)

The chemical bonds in the molecule of PLA, PVA, LidHCl and in the nanofibrous webs were identified using FTIR. The spectra of bulk materials and nanofibrous samples, with and without drug, were obtained with a Nicolet iS50 FTIR spectrometer (Thermo Scientific) with a diamond ATR (attenuated total reflectance) accessory. The sample was placed onto the ATR crystal and the spectrum was collected. The scan was performed in the range 40 - 4000 cm^{-1}. For each electrospun nanofibrous mat the scan was repeated three times in three different regions of the sample.

3.4.8 X-ray photoelectron spectroscopy (XPS)

The chemical nature of the bulk materials (PLA, PVA, LidHCl) and core/shell nanofibres with and without drug, was also investigated with X-ray photoelectron spectroscopy (K-Alpha, Thermo Scientific, UK). XPS data were taken by a flood gun charge neutralizer system equipped with Al Kα micro-focused monochromator (hv = 1486.6 eV) with variable spot size (30-400μm in 5μm). In order to determine the surface elemental compositions wide energy survey scans of bulk materials and nanofibres were acquired over 0–1350 eV binding energy range, at pass energy of 200 eV with energy step size of 1 eV from 400 μm diameter circular spot size. The high resolution spectra were recorded for C 1s, O 1s region and Cl2p

(for lidocaine hydrochloride) at pass energy of 50 eV with energy steps of 0.1 eV in order to analyse the bonding states.

3.4.9 High performance liquid chromatography (HPLC)

A high performance liquid chromatography system (Agilent Technologies, Series 1100) was employed to assay lidocaine hydrochloride (LidHCl) in the release medium. The chromatographic column used is Gemini® C18 (Phenomenex, UK). The characteristics of the column are reported in Table 3.5.

Table 3.5 – Characteristics chromatographic column HPLC system.

Material	Porous organ-silica
Particle size	5 μm
Pore size	110 Å
Column length	250 mm
Column inner diameter	4.6 mm

The mobile phase was a mixture of an aqueous phase and acetonitrile at a ratio 65:35 volume by volume (Ricci Júnior et al. 2002). The aqueous phase was 0.05 M sodium phosphate buffer and 0.05% of diethylamine at pH 6.0. A sample volume of 20 μL was injected into the HPLC system and the drug detection was carried out at a wavelength of 210 nm at a column temperature of 28°C. From a stock solution of 250 ppm (250 mg/l = 250 μg/ml) of lidocaine hydrochloride in phosphate buffer solution (PBS) at pH 7.4 and acetate buffer solution at pH 5.5, two calibration curves were first prepared at concentration from 1 to 125 ppm. The drug retention time was approximately 4.8 minutes at a flow rate of 1 ml/h.

PBS solution was prepared by dissolution of one table (Sigma Aldrich, UK) in 200 ml of distilled water. One tablet dissolved in 200 mL of deionized water yields 0.01 M phosphate buffer, 0.0027 M potassium chloride and 0.137 M sodium chloride buffer, pH 7.4. The acetate buffer solution (0.1 M) was prepared by dissolution of sodium acetate anhydrous in distilled water followed by addition of acetic acid glacial. The pH of both solutions was controlled with a pH meter.

3.4.9.1 Efficiency of drug encapsulation

The actual content of drug LidHCl in the nanofibrous structures was determined as follow. The samples were first freeze-dried to eliminate eventual residual solvent or moisture. Then a disc with diameter of 1 cm was obtained from the nanofibrous web using a metal punch and it was dissolved in 1 ml of DMSO. 30 µl of this solution was withdrawn and added to 970 µl of PBS in a vial for HPLC analysis. The amount of drug was back-calculated from the obtained data against the predetermined calibration curve.

The theoretical amount of drug in the nanofibrous web was calculated considering the flow rate of the core solution and the total time of the electrospinning process. The efficiency of encapsulation was calculated using Equation 9.

$$Efficiency\ of\ encapsulation\ \% = \frac{\text{Actual drug content (from HPLC analysis)}}{\text{Theoretical drug content}}$$

Equation 9

3.4.9.2 Drug release studies

The electrospun samples were first cut into a disc with diameter of 1 cm using a metal punch. Each sample was placed into an individual 1.5 ml eppendorf tube containing 1 ml of release medium. Then the vials were placed in a shaking water bath at a 37°C and 100 rpm to simulate physiological conditions of the body. At specific time intervals, 700 µl of solution was withdrawn and an equal amount of fresh medium was added. The drug concentration in the release medium was determined according to the calibration curve of LidHCl in the same buffer (pH 7.4 or pH 5.5). The experiments were carried out in triplicate and the results were reported as mean values plotted as function of time. The release was investigated over a period of 7 days.

The cumulative percentage of the released drug was calculated based on the initial weight of the drug incorporated in the electrospun scaffold considering the efficiency of encapsulation, using Equation 10. V_t is the volume of the sample withdrawn (700 µl), C_i is the concentration

of the encapsulated compound in the previous sample, V_0 is the total volume of the release media (1 ml), C_n is the concentration of the drug release at a specific interval time, and m_{LidHCl} is the amount of lidocaine encapsulated (Morelli et al. 2016; Z. Li et al. 2014).

$$Cumulative\ drug\ release\ percentage\ \% = \left[\left(V_t \sum_{1}^{n-1} C_i + V_0 C_n\right) / m_{LidHCl}\right] * 100$$

Equation 10

4 EFFECT OF DIFFERENT SOLVENT SYSTEMS ON PLA NANOFIBRE MORPHOLOGY AND DIAMETER

4.1 Introduction

In electrospinning the selection of the solvent or mixed-solvent system to dissolve the polymer is one of the main factors influencing the solution properties and consequently the electrospinnability of the solution (K.H. Lee et al. 2003; Jarusuwannapoom et al. 2005; H. Liu & Y. L. Hsieh 2002; Choktaweesap et al. 2007). Although different solvents may be used to dissolve a polymer, the resultant electrospun nanofibres will present different morphologies and diameter as a result of the diverse interactions between polymer and solvent molecules. While several researchers have investigated the effect of solution properties such as polymer concentration and surface tension, a few authors reported the effects of different solvent systems on nanofibre morphology and diameter. Solutions of poly(caprolactone) (PCL), poly(styrene) (PS), polyamide-6 (PA6), poly(urethane) (PU), poly(methyl methacrylate) (PMMA) have been electrospun by several researchers and the morphology of the electrospun nanofibrous webs was examined (Megelski et al. 2002; Eda et al. 2007; Jarusuwannapoom et al. 2005; Wannatong et al. 2004; Gholipour Kanani & Bahrami 2011; K.H. Lee et al. 2003; X. Gu et al. 2014; Yener & Yalcinkaya 2013; Huan et al. 2015; Uyar & Besenbacher 2008).

For example Wannatong et al. (Wannatong et al. 2004) investigated the effect of six solvents (acetic acid, acetonitrile, m-cresol, toluene, tetrahydrofuran (THF) and dimethylformamide (DMF)) on the productivity and morphology of PS nanofibres. The main observations were related to the solvent boiling point and dielectric constant. Nanofibres with smaller diameter were collected with higher boiling point solvents, such as DMF (153°C) and m-cresol (203°C) because the gradual evaporation of the solvent from the polymeric jet causes the viscoelastic properties to change and therefore the charged jet is further stretched before reaching the collector. Moreover nanofibre productivity was enhanced using solvents with higher dielectric constant. During electrospinning an electric field is created and therefore viscous polymeric solutions are stretched due to the repulsion of the charges present on the jet surface. Since solutions with higher conductivity carry more charges consequently they are more susceptible to the electric field. Hence the mass throughput of the solutions from a spinneret

increases.

In addition to the type of solvent system, another parameter that has a significant influence on fibre formation during the electrospinning of polymeric solutions is the number of chain entanglements in the solution. Experimental observations have shown that a minimum amount of chain entanglements is required for the production of continuous fibres (Matthew G. McKee et al. 2004; R.H. Colby et al. 1991). A number of studies have shown that a minimum polymer concentration, known as the entanglement concentration (C_e), is required for beaded fibre formation (P. Supaphol et al. 2005; Chisca et al. 2012; C. Tang et al. 2010). Below C_e only droplets of the polymeric solution are collected because there are no entanglements. Above C_e nanofibres with beads start to be collected and the frequency of bead formation decreases on further increasing the polymer concentration. However at high concentration, no fibres are produced due to the high solution viscosity (K.H. Lee et al. 2003; H. Liu & Y. L. Hsieh 2002).

Although the effect of the polymer concentration on the shear viscosity has been investigated for a few polymers, the role of viscoelasticity of the polymer solutions on nanofibre morphology is rarely considered. Some studies have shown the effect of the elastic (G') and plastic modulus (G'') of the polymer solution on the electrospinning process (R. Rošic et al. 2012; Chisca et al. 2012). For a successful electrospinning the plasticity G'' of the solution has to dominate over the elasticity (G') (Regev et al. 2010; J. H. Yu et al. 2006). However the elasticity of the solution has to be low but still present due to the fact that the increased elastic force increases the tendency of the jet to contract (R. Rošic et al. 2012). A higher degree of elasticity is needed to suppress the breakup of the jet into droplets by the Rayleigh instability and therefore to allow the production of nanofibres. Correlations between rheological parameters of polymer solutions and the electrospinnability of the solutions and the resultant nanofibre morphology are required to understand the mechanisms underlying jet stabilization.

Regarding the production of poly (lactic acid) (PLA) nanofibres the most common solvents used to dissolve the polymer and produce electrospun nanofibrous webs are dichloromethane (DCM), chloroform (CHL), 2,2,2-trifluoroethanol (TFE), hexafluoroisopropanol (HFIP) and tetrahydrofuran (THF), and a number of mixtures, such as CHL/AC, CHL/DMF, DCM/DMF (S. Shao et al. 2011; H. W. Kim et al. 2008; Sung In Jeong et al. 2008; McCullen et al. 2007; J. Qin et al. 2013). A large number of scientific publications regarding electrospun PLA nanofibres for mainly biomedical applications have been reported in the literature (E. S. Kim

et al. 2010; F. Yang et al. 2005; Zong et al. 2002; Thorvaldsson et al. 2008). However no systematic review or scientific publication about the effects of different solvent systems on PLA nanofibre morphology, mean diameter and diameter distribution, has been reported.

4.2 Aims and objectives

The main aims of the work presented in this chapter were:

- To investigate the effect of solution properties on the morphology, diameter and diameter distribution of poly(lactic acid) electrospun nanofibres
- To identify a relationship between chain entanglements and electrospinnability of PLA solution

The achievement of these aims was possible through the realisation of the following objectives:

- Electrospinning of several PLA solutions in different solvent systems at a fixed polymer concentration and process parameters
- Optimization of the best solvent system in terms of production of defect-free nanofibres with thinner diameter and narrow diameter distribution
- Measurements of shear viscosity and viscoelasticity of PLA solution at several polymer concentrations

4.3 Results and discussion

4.3.1 Effect of single solvents on nanofibre morphology and diameter

Seven solvents were selected to dissolve PLA and electrospun PLA solutions. In Table 4.1 some physical and chemical characteristics of the selected solvents are reported. The first reason of solvent selection was the different physical and chemical characteristics of these solvents. For example the viscosity varies from 0.308 cP of AC to 1.960 cP of DMAc. Furthermore solvents have different dielectric constant (ε) which reflects the solvent polarity. In fact ε changes from 2.21 (DX) to 37.80 (DMAc). AC, DMF, DMAc are polar solvent as shown by the high dielectric constant, while DX, THF, DCM, CHL are non-polar. The second reason is related to the solubility parameters which are close to the solubility parameter of PLA (which is approximately 10 $cal^{1/2}\,cm^{-3/2}$) (Garlotta 2002). All solvents were able to dissolve the polymer and form homogenous solution. A polymer concentration of 10% w/v was chosen for all solvent systems and the process parameters were kept constant: voltage (*V*) of 20 kV, flow rate (*Q*) 1 ml/h, distance between needle and collector (*d*) of 15 cm. Each experiment last 15 minutes. The values of voltage and collection distance were fixed for the electrospinning of all PLA solutions. However, acceptable performance using for example the solvent DMF has been found for other polymer solutions operating with lower values of *V* and *d*. For example W. Liu (Wanjun Liu et al. 2015) used 12 kV, 15 cm and 1.5 ml/h for the electrospinning of polystyrene (PS) solution at concentration of 15% w/v in single solvents (DCM, AC, THF, DMF, cyclohexanone and 1-butanol) and binary solvent systems. Only DMF was found to produce beaded free nanofibres, while the other solvents produced beaded PS fibres with different morphologies. Similarly, a 10% w/v PS solution in DMF was electrospun by Wannatong et al (Wannatong et al. 2004) using an applied potential ranging from 10 to 30 kV over a collection distance of 10 cm. Defect free electrospun PS nanofibres with narrow diameter distribution were produced using a rotational speed of the collector of 1500 rev/min, under an applied potential in the middle range of 15-20 kV, while larger nanofibres with broad diameter distribution were formed at voltage of 10 kV, 25 and 30 kV. Hence, lower voltage and collection distance for the electrospinning of PLA solution in DMF may influence the following results in the chapter.

Table 4.1 – Physical and chemical properties of the solvents used (BP is the boiling point, η is the viscosity (at 25°C), γ is the surface tension (at 20°C), K is the electrical conductivity, ε is the dielectric constant (at 20°C, δ is the solubility parameter) (Smallwood 1996).

Solvent	**BP** **°C**	**η** **cP**	**γ** **mN/m**	**K** **μS/cm**	**ε**	**δ** **$cal^{1/2} \cdot cm^{-3/2}$**
Acetone AC	56	0.308	23.3	5E-03	20.60	10.0
1,4 Dioxane DX	101	1.177	40.0	5E-09	2.21	10.0
Tetrahydrofuran THF	66	0.480	28.0	4.5E+01	7.60	9.1
Dichloromethane DCM	40	0.449	28.1	4.3E-05	9.10	9.7
Chloroform CHL	61	0.563	27.2	1.0E-04	4.80	9.3
Dimethylformamide DMF	153	0.920	35.0	6.0E-02	36.70	12.1
Dimethylacetamide DMAc	166	1.960	43.7	/	37.80	11.0

Among single solvents only acetone (AC) was found to produce PLA nanofibrous mat probably due to its relatively high dielectric constant and low surface tension compared to the other solvents. In the electrospinning process the surface tension force is the cause of Rayleigh instability which leads to droplets of the polymeric solution. If the surface tension is low the electrical forces prevails and are able to stretch the polymeric jet, therefore the Raleigh instability is suppressed and nanofibres may be produced. However the PLA nanofibrous web collected using AC has bead-string morphology as shown in Figure 4.1.

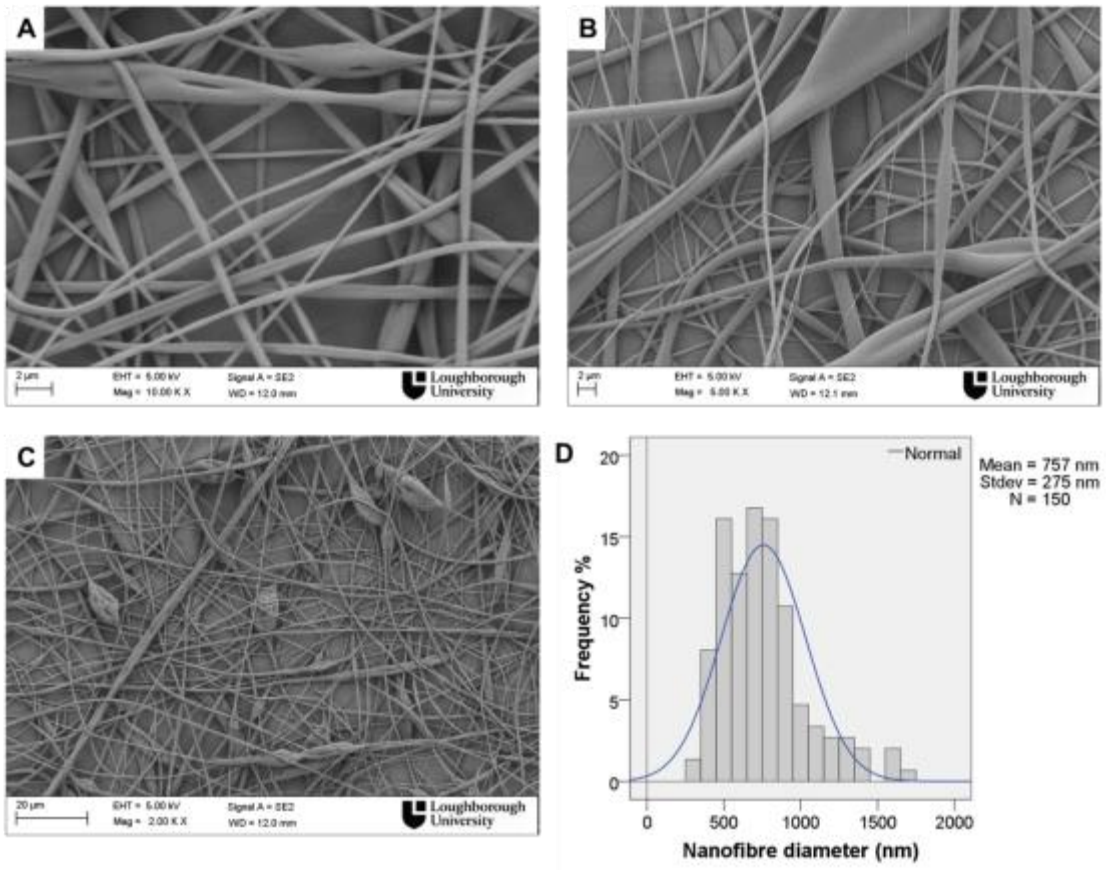

Figure 4.1 – Scanning electron micrographs of PLA nanofibres from solutions of 10% (w/v) of PLA in acetone: (a) 10,000X (b) 5,000X (c) 2,000X (d) nanofibre diameter distribution.

The mean nanofibre diameter was 757 nm with a standard deviation of 275 nm and beads have an elongated shape along the nanofibre axis. There are several factors that may be responsible of bead formation: high solution surface tension, low polymer concentration and hence solution viscosity, or low charge density (Fong et al. 1999). Generally high polymer concentration results in high solution viscosity and hence the polymeric electrospun jet is uniformly stretched by the electrical forces. As reported in paragraph 2.1.2.1, a sufficient number of entanglements between the polymer chains in solution needed to first produce nanofibres is defined by a value of concentration called entanglement concentration (C_e). While nanofibres with many beads are formed at C_e, on further increasing polymer concentration nanofibres with fewer beads may be formed as a result of more entanglements. Hence the bead structure of Figure 4.1 D may be due to low entanglements density.

Viscosity, surface tension and conductivity of PLA solution in single solvent systems were

measured and the results are reported in Table 4.2. The value of viscosity was taken from the log-log plot of the shear rate dependence of the solution viscosity at a shear rate of 400 s^{-1} because strong shear forces are imposed to the polymer chains during the electrospinning process (Doshi & D.H. Reneker 1995). Different solvents may dissolve completely PLA but they probably interact differently and this leads to solutions with unique and specific properties. Hence electrospun nanofibres with different morphologies may be produced.

Table 4.2 – Viscosity, surface tension and conductivity of PLA solution at concentration of 10% w/v in single solvents.

Solvent system	Viscosity (cP)	Surface tension (mN/m)	Conductivity (μS/cm)
AC	102±10	25.5±0.9	1.30
DX	531±26	36.8±1.3	0.01
THF	280±31	30.4±1.0	0.03
DCM	167±67	30.2±0.9	0.04
CHL	372±47	31.0±0.6	0.01
DMF	155±90	38.3±1.3	4.00
DMAc	210±21	37.7±1.0	2.60

The low solution conductivity of PLA solution in AC (1.30 μS/cm) may also explain the bead on string morphology of the nanofibres collected. Low charge density may lead to less repulsion between charges on the polymer jet surface and therefore decreased stretching of the electrospun jet.

When PLA solution in DX, THF, DCM, CHL, DMF and DMAc were electrospun, mainly droplets were collected as shown in Figure 4.2, Figure 4.3 and Figure 4.4. Most probably the higher surface tension of PLA solution in these solvents, ranging from approximately 30 to 38 mN/m compared with that of PLA solution in AC (25.5 mN/m) inhibited the formation of nanofibres and therefore only beads with different size and shapes were formed. Although solutions in DMF and DMAc have the highest conductivity, 4.0 and 2.6 μS/cm, respectively, (Table 4.2), no nanofibres were collected. This could be explained by either the extremely high solution surface tension or the polymer concentration lower than C_e. If the concentration is higher the C_e but the electric field strength is not sufficiently strong to overcome the high surface tension, a discontinuous jet may be emitted resulting in the collection of solution

droplets instead of nanofibres.

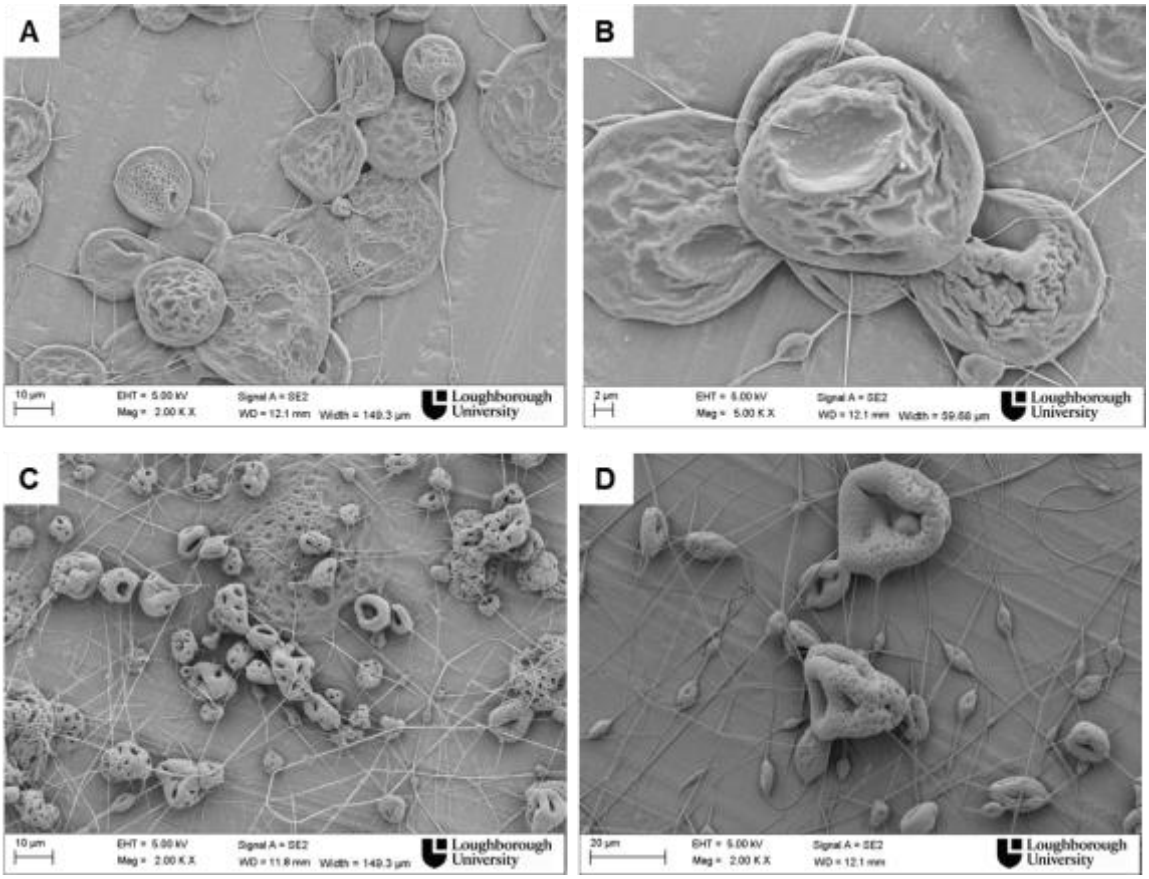

Figure 4.2 – Scanning electron micrographs of PLA nanofibres from PLA solutions at a PLA concentration of 10% (w/v) in: (a, b) 1,4-dioxane (2,000X and 5,000X); (c, d) tetrahydrofuran (2,000 X).

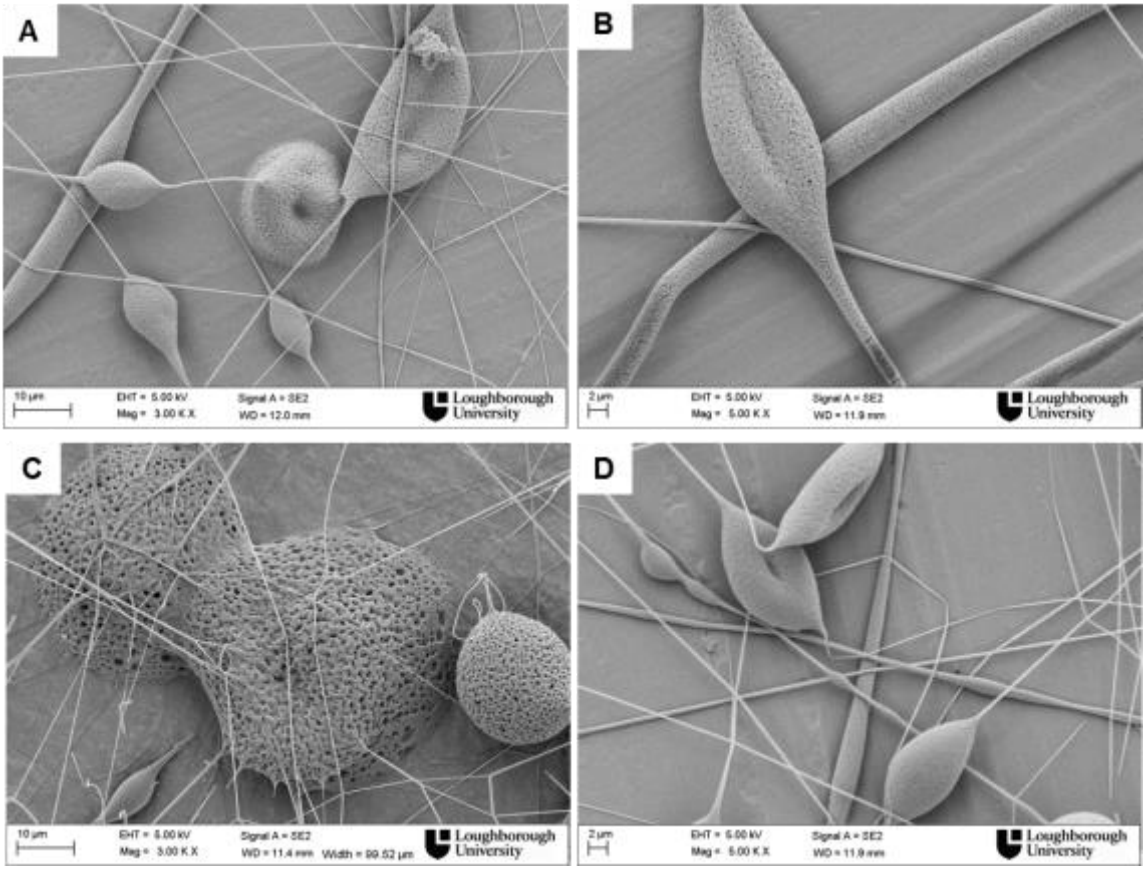

Figure 4.3 – Scanning electron micrographs of PLA nanofibres from PLA solutions at a PLA concentration of 10% (w/v) in: (a, b) dichloromethane (3,000X and 5,000X), (c, d) chloroform (3,000 X and 5,000 X).

The beads collected from PLA solution in DX and THF (Figure 4.2) have different shapes and sizes with a collapsed surface, while those from PLA solution in DMF and DMAc presented a circular shape and more uniform morphology (Figure 4.4). Unlike the previous observations, elongated droplets with a porous structure and a few fine nanofibres were formed using PLA solution in DCM and CHL as shown in Figure 4.3. The formation of pores may be explained with two main mechanisms, phase separation and breath figures. Thermodynamic instability is the driving force of a phase separation process. During the electrospinning process temperature decrease of the electrospun jet surface between the needle and the collector (thermally induced phase separation) or penetration of a non-solvent in the jet (vapour induced phase separation) could induce phase separation. On the other hand breath figures are formed when the reduction of temperature due to rapid evaporation of the

solvent leads to condensation of the water vapour from the environment to the jet surface. In this work both mechanisms may explain the formation of pores using PLA solutions in DCM and CHL. PLA is a hydrophobic polymer which does not dissolve in water, and DCM and CHL are high volatile solvents poorly miscible with water. Hence an imprint is left on the bead surface in the form of pores as a result of condensation of water molecules from the air on the jet surface followed by solvent and water (non-solvent for PLA) evaporation.

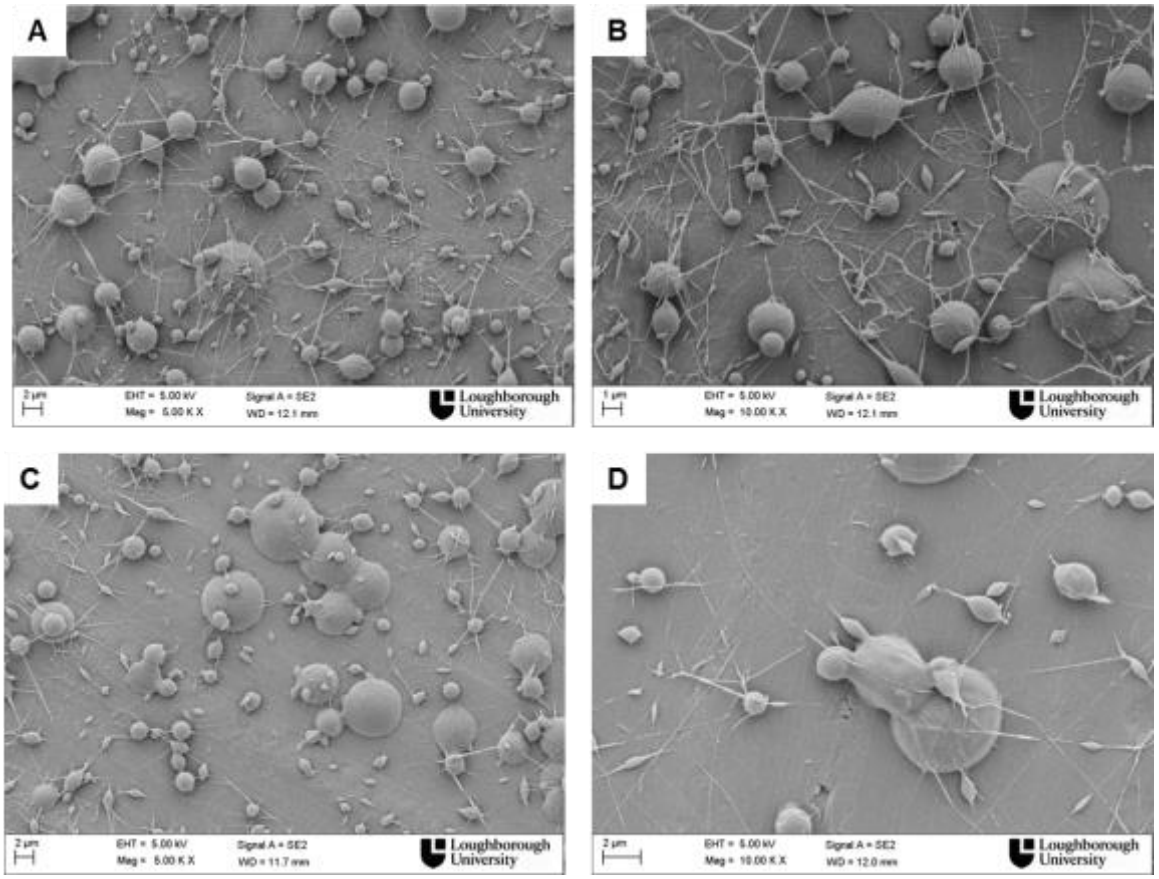

Figure 4.4 – Scanning electron micrographs of PLA nanofibres from PLA solutions at a PLA concentration of 10% (w/v) in: (a, b) dimethylformamide (5,000 X and 10,000 X); (c, d) dimethylacetamide (5,000 X and 10,000 X).

As relatively large nanofibres (757±275 nm) with some defects were obtained using AC, the next step was the preparation of PLA solution in binary solvent systems to improve the nanofibre production. Defect-free PLA electrospun nanofibres with narrow diameter distribution are required for many applications.

4.3.2 Effect of binary solvent systems on nanofibre morphology and diameter

Binary solvent systems were prepared by mixing acetone and one of the other solvents (DX, THF, DCM, CHL, DMF, DMAc) in a ratio 50/50 volume by volume to produce electrospun smooth and defect-free nanofibrous mats. SEM morphological observations of nanofibres collected using binary solvent systems have shown that the addition of acetone to the other solvents enabled the production of nanofibres demonstrating therefore enhancement of the electrospinning process. The electrospinning process parameters were the same to those used for the electrospinning of PLA solution in single solvent systems. The solvent systems AC/DX, AC/THF, AC/DCM and AC/CHL produced nanofibres with a bead-string morphology as shown in Figure 4.5, Figure 4.6, Figure 4.7 and Figure 4.8, respectively, while smooth defect-free nanofibres were collected using the solvent systems AC/DMF and AC/DMAc (Figure 4.9 and Figure 4.10). The mean diameter of nanofibres collected from PLA solution in each binary solvent system was calculated and its value is reported together with the diameter distribution in each figure.

Figure 4.5 shows SEM images of the nanofibres collected using the PLA solution in AC/DX. Many beads were collected within the electrospun mat and nanofibres have shown a diameter of 494±180 nm. Unlike the previous observations, a few beads but bigger nanofibres, with a mean diameter of 587 nm and a diameter distribution of 313 nm were formed from the electrospinning of PLA solution in AC/THF (Figure 4.6).

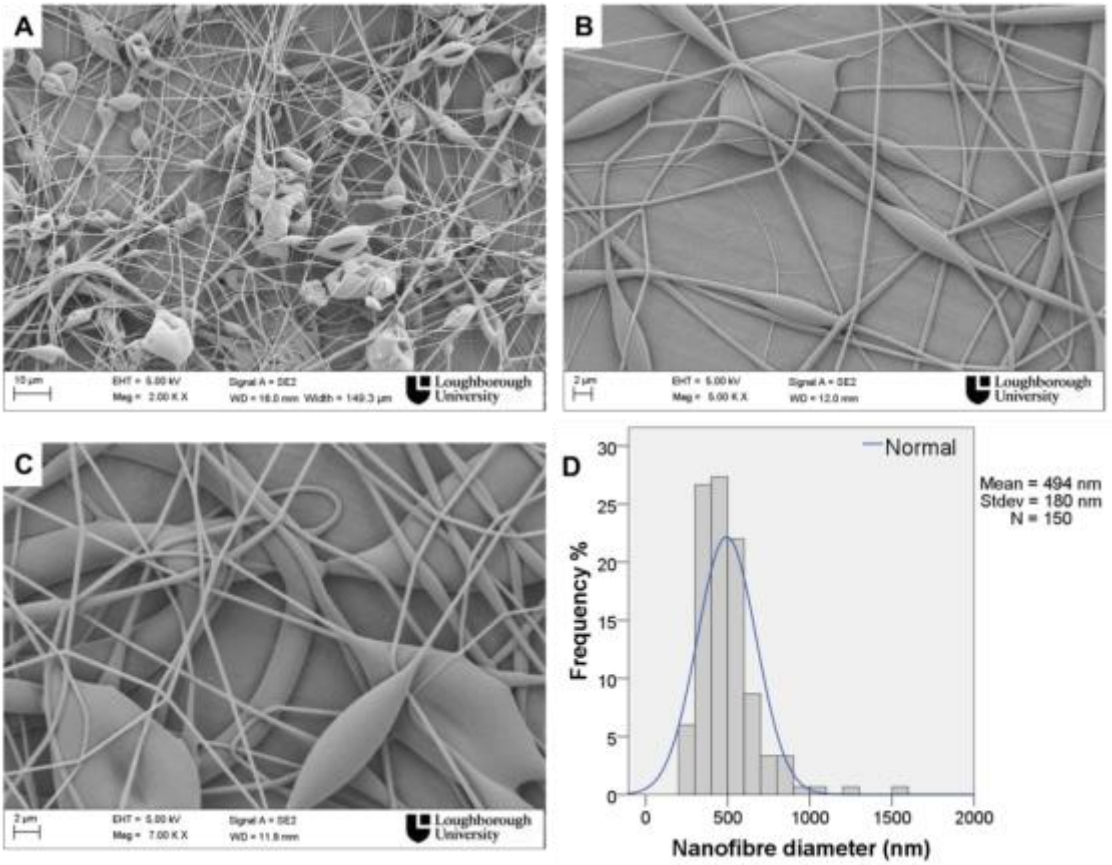

Figure 4.5 – Scanning electron micrographs of PLA nanofibres from solutions of 10% (w/v) of PLA in AC/1,4-DX at magnification of (a) 2,000 X (b) 5,000 X (c) 7,000 X (d) nanofibre diameter distribution.

Beads formed along the nanofibres had different shapes and sizes. This could be due to the different solution properties and interactions between polymer and solvent molecules in solution. Therefore measurements of solution viscosity, surface tension and electric conductivity were performed and they may be useful to understand the different nanofibre morphologies, mean diameter and diameter distribution. The results are reported in Table 4.3. The addition of AC to PLA solution in DX, THF, DCM and CHL led to a reduction of surface tension, while solution conductivity slightly increased. On the other hand AC/DMF and AC/DMAc solutions presented lower surface tension and lower conductivity compared to the DMF and DMAc solutions. For example PLA solution in DX has surface tension (γ) of 36.8 mN/m and conductivity (K) of 0.01 μS/cm (Table 4.2). The addition of AC to this solution resulted in lower surface tension of 30.10 mN/m, but higher electrical conductivity (0.17 μS/cm) was measured. Differently, both γ and K of PLA solution in DMF dropped as a

result of the addition of AC; the conductivity decreased from 4.0 to 2.8 μS/cm, and the surface tension had a fall from 38.3 to 30.6 mN/m.

Table 4.3 – Viscosity, surface tension and conductivity of PLA solution at concentration of 10% w/v in binary solvent systems.

Solvent system	**Viscosity (cP)**	**Surface tension (mN/m)**	**Conductivity (μS/cm)**	**Nanofibre diameter (nm) (mean±stdev)**
AC/DX	305±15	30.10±0.7	0.17	494±180
AC/THF	221±14	26.90±0.9	0.40	587±313
AC/DCM	133±64	27.60±1.2	0.62	1181±381
AC/CHL	169±15	27.30±0.7	0.65	679±296
AC/DMF	252±53	30.60±0.8	2.80	210±36
AC/DMAc	296±47	29.40±1.5	3.22	357±75

As discussed in paragraph 4.3.1, several factors may be the cause of bead formation within the nanofibrous samples: low polymer concentration (low solution viscosity), high solution surface tension and low solution conductivity. In this work, the lower surface tension and lower viscosity of PLA solution in AC/THF (221 cP) compared to that of PLA solution in AC/DX (305 cP) may be the main reason of the different morphologies of the electrospun mats. During the electrospinning process of solution in AC/THF the electrical forces have to overcome lower surface tension and viscosity forces and therefore beads appeared more elongated along the nanofibres as a result of higher degree of stretching.

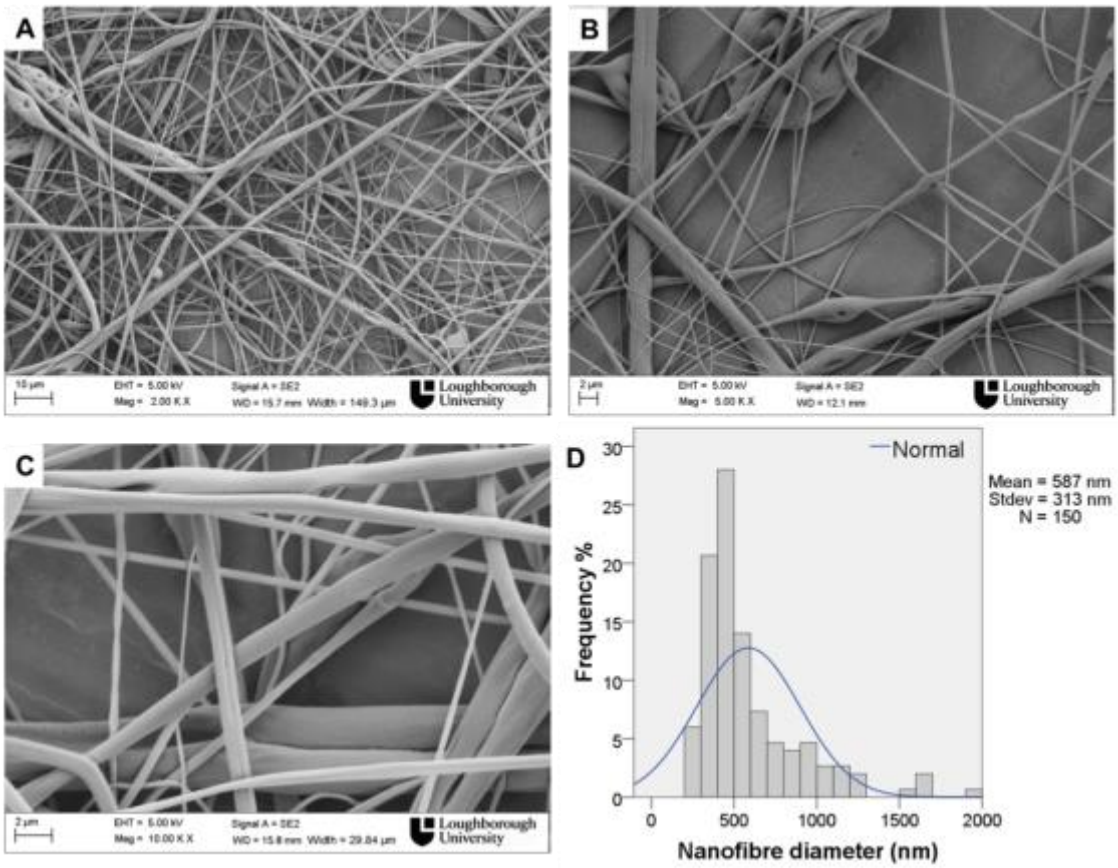

Figure 4.6 – Scanning electron micrographs of PLA nanofibres from solutions of 10% (w/v) of PLA in AC/THF at magnification of (a) 2,000 X (b) 5,000 X (c) 10,000 X (d) nanofibre diameter distribution.

Morphological analysis have also shown that the biggest nanofibres with broad diameter distribution (1181±381 nm) were collected using the solvent system AC/DCM (Figure 4.7). While few nanofibres and many beads were collected from PLA solution in DCM and CHL (Figure 4.3), the addition of AC in solution resulted in denser nanofibrous mats as shown in Figure 4.7 and Figure 4.8. However nanofibres still presented bead-string morphology. Figure 4.7 C shows that a large bead with porous structure within the nanofibrous web which may indicate that phase separation occurred during the electrospinning of PLA solution in AC/DCM similarly to the observations reported for the samples collected from PLA solution in the single solvent (paragraph 4.3.1).

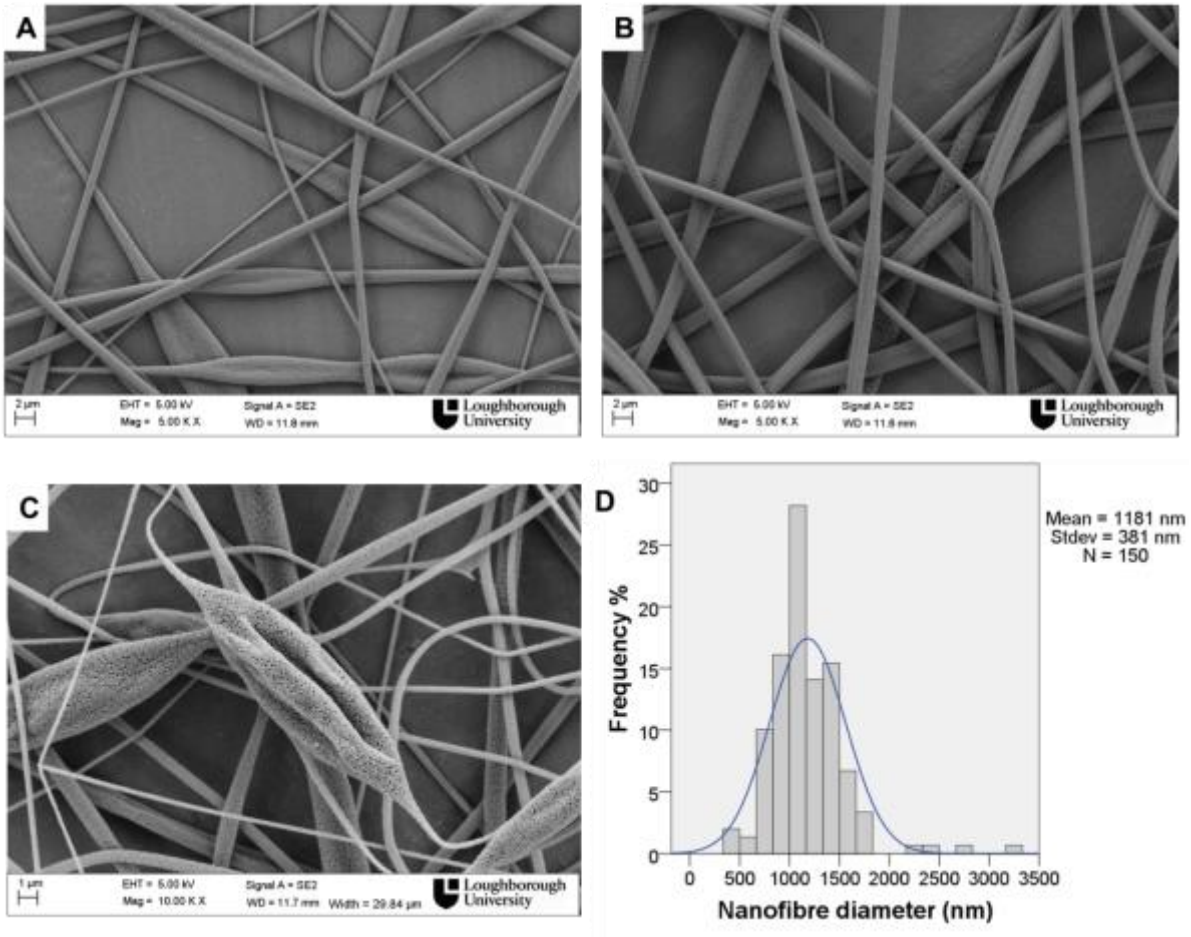

Figure 4.7 – Scanning electron micrographs of PLA nanofibres from solutions of 10% (w/v) of PLA in AC/DCM at magnification of (a, b) 5,000 X (c) 10,000 X (d) nanofibre diameter distribution.

The porosity on the surface of nanofibres collected from PLA solution in AC/CHL was less evident than that of nanofibres from solution in AC/DCM, but it was still observed (Figure 4.8). Although DCM has lower boiling point than CHL (40°C compared to 61°C), PLA solutions in binary solvent systems have similar physical characteristics as shown in Table 4.3. Most probably the faster evaporation of DCM from the electrospun jet compared to that of CHL is responsible for the higher porosity on the nanofibre surface.

As reported in the literature review of this thesis (chapter 2), the formation of nanofibres with porous structures has been related to the relative humidity in the electrospinning chamber and the types of polymer-solvent system (J. Zheng et al. 2012; L. Huang et al. 2011; Casper et al. 2004). In most scientific publications, pores are observed on the surface of nanofibres of

hydrophobic polymers. While nanopores were observed on electrospun PCL nanofibres, smooth nanofibres were collected from PEG solution in CHL and PCU solution in DMAc, (Nezarati 2013). Although CHL is a highly volatile solvent, PEG is water soluble polymer, therefore this indicates that no phase separation occurred and in turn no pores were left on the fibre surface.

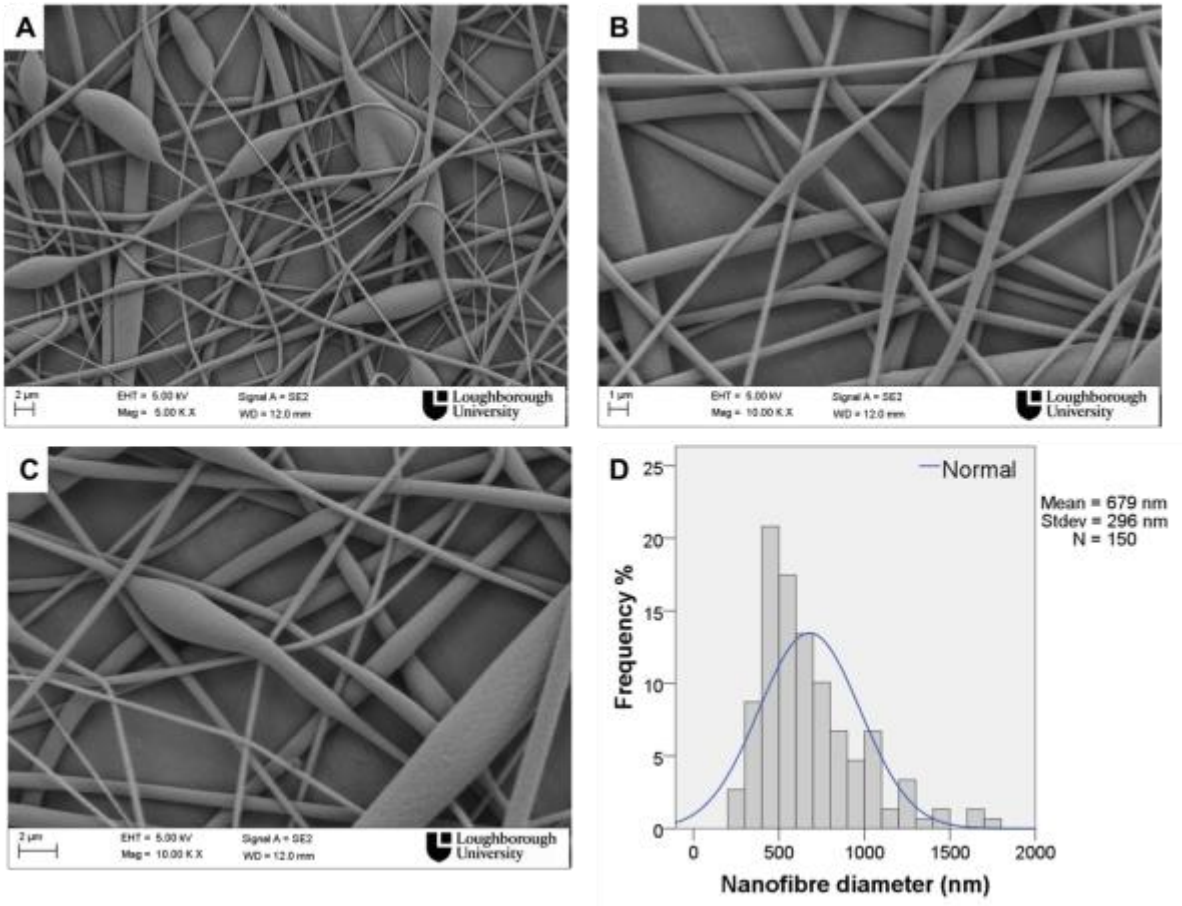

Figure 4.8 – Scanning electron micrographs of PLA nanofibres from solutions of 10% (w/v) of PLA in AC/CHL at magnification of (a) 5,000 X (b, c) 10,000 X (d) nanofibre diameter distribution.

The thinnest nanofibres with mean diameter of 210 nm and narrow distribution (36 nm) were instead collected using AC/DMF as shown in Figure 4.9. Furthermore from the optical observations the electrospun nanofibrous mats collected from solutions in AC/DMF and AC/DMAc (Figure 4.9 and Figure 4.10, respectively) appeared much denser between all nanofibrous mats collected. This could be explained by the highest conductivity of PLA solution in AC/DMF (2.80 μS/cm) and AC/DMAc (3.20 μS/cm) as shown in Table 4.3.

Higher amount of charges on the electrospun jet surface due to the higher solution conductivity leads to stronger jet elongation and therefore thinner nanofibres are collected. In addition high density of chain entanglements in PLA/DMF solution could be also responsible of the defect-free nanofibrous structure observed in Figure 4.9.

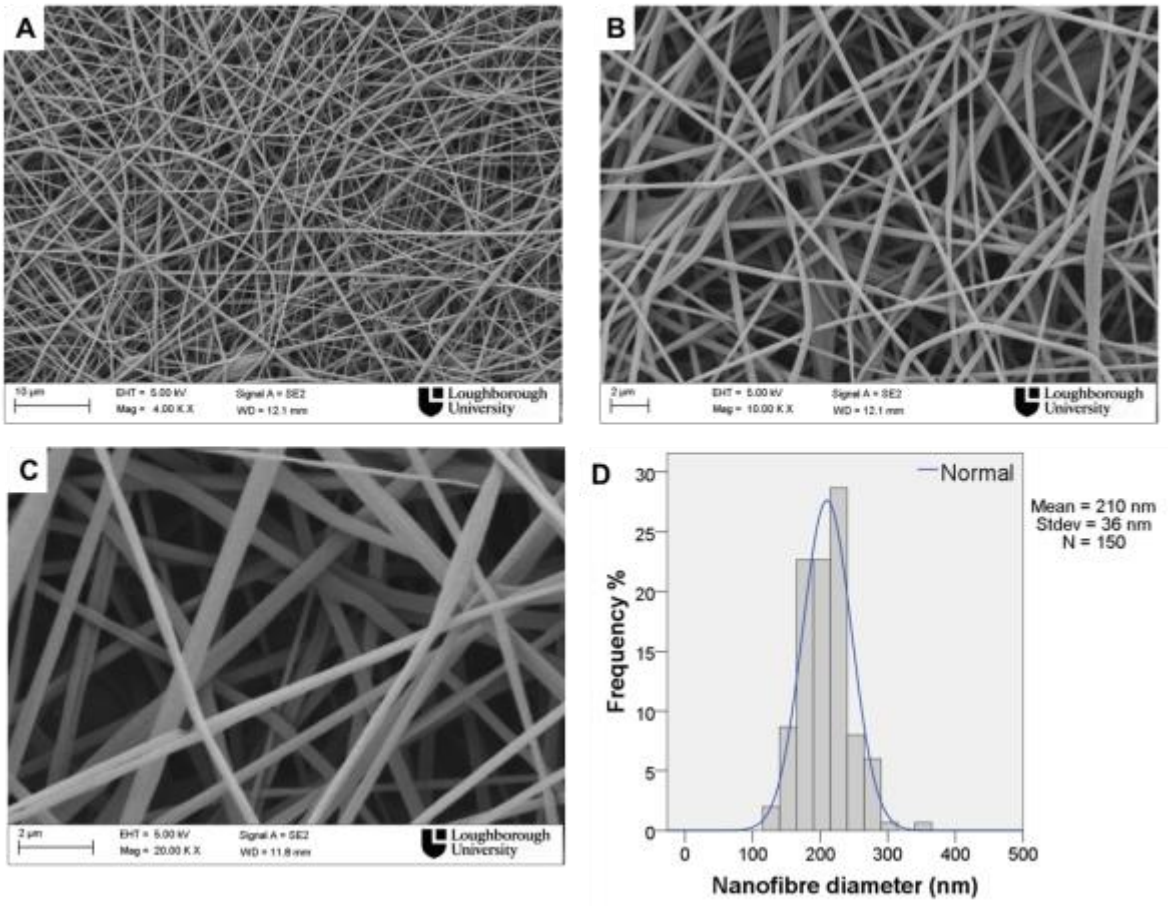

Figure 4.9 – Scanning electron micrographs of PLA nanofibres from solutions of 10% (w/v) of PLA in AC/DMF at magnification of (a) 4,000 X (b) 10,000 X (c) 20,000 X (d) nanofibre diameter distribution.

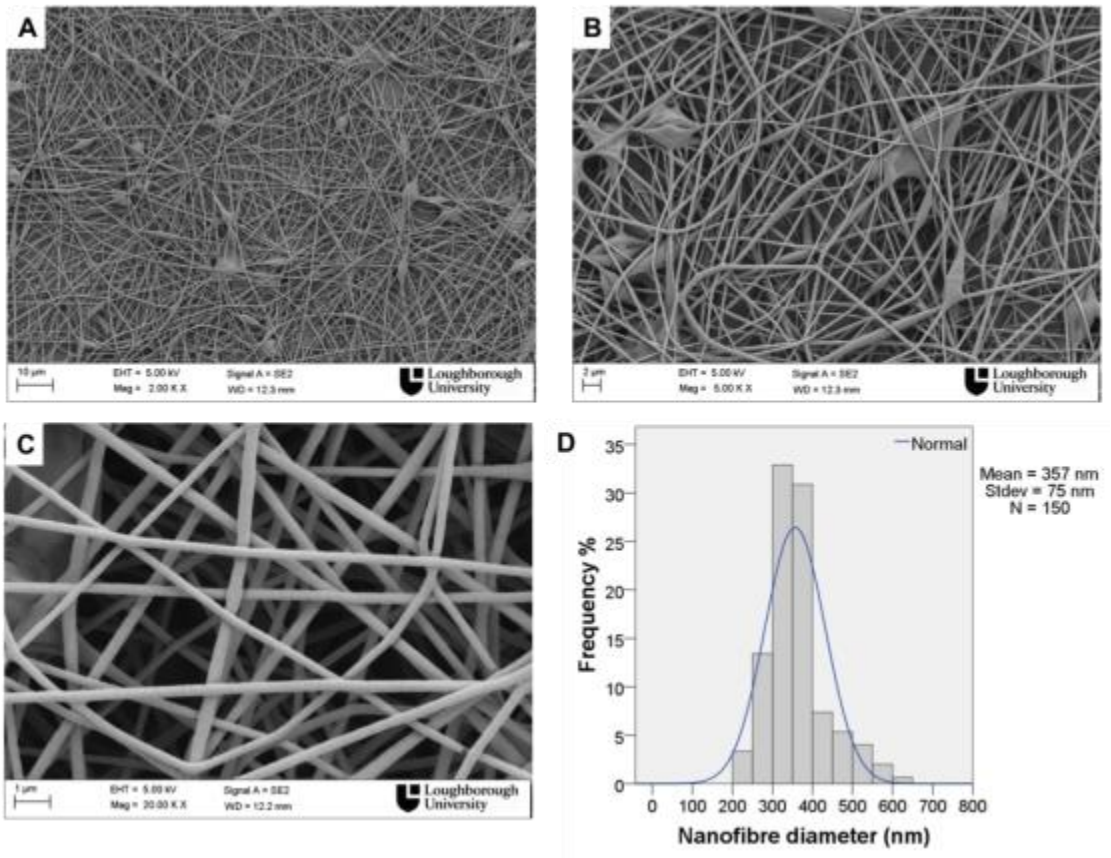

Figure 4.10 – Scanning electron micrographs of PLA nanofibres from solutions of 10% (w/v) of PLA in AC/DMAc at magnification of (a) 2,000 X (b) 5,000 X (c) 20,000 X (d) nanofibre diameter distribution.

Unlike the previous observations, beaded nanofibres with larger diameter and wider diameter distribution were collected from electrospinning of PLA solutions in AC/DCM and AC/CHL which have lower solution conductivity (Figure 4.7 and Figure 4.8, respectively). However although AC/DX and AC/THF had lower conductivity (0.17 mS/cm and 0.40 μS/cm, respectively) than AC/DCM and AC/CHL (0.62 and 0.65 μS/cm, respectively), nanofibres with slightly small diameter were produced. This observation may be related to the lower evaporation rate of the solvent mixture AC/DX and AC/THF compared to that of AC/DCM and AC/CHL. DX and THF have boiling point of 101°C and 66°C, respectively, that are lower than those of DCM (40°C) and CHL (61°C) (Table 4.3). Although fewer charges are presented on the jet surface due to the lower conductivity, the slow evaporation of the solvent from the electrospun jet resulted in a greater extent of stretching imposed by the electrical forces.

Figure 4.11 shows the effect of surface tension, viscosity and conductivity of PLA solution in binary solvent systems on the mean nanofibre diameter. While no relationship was found between each parameter and the mean diameter, it was found that an increase of the boiling point of the second solvent in the mixed-solvent system led to smaller nanofibre diameter (Figure 4.12). These observations are similar to those reported by Wannatong et al (Wannatong et al. 2004). A relationship between boiling point of the solvent and fibre diameter for the electrospinning of poly (styrene) in m-cresol, toluene, DMF and THF was described. Solvents with higher boiling point evaporate slower from the ejected charged jet. Therefore charges remain for longer time in the polymeric jet resulting in higher stretching and in turn thinner nanofibres can be produced.

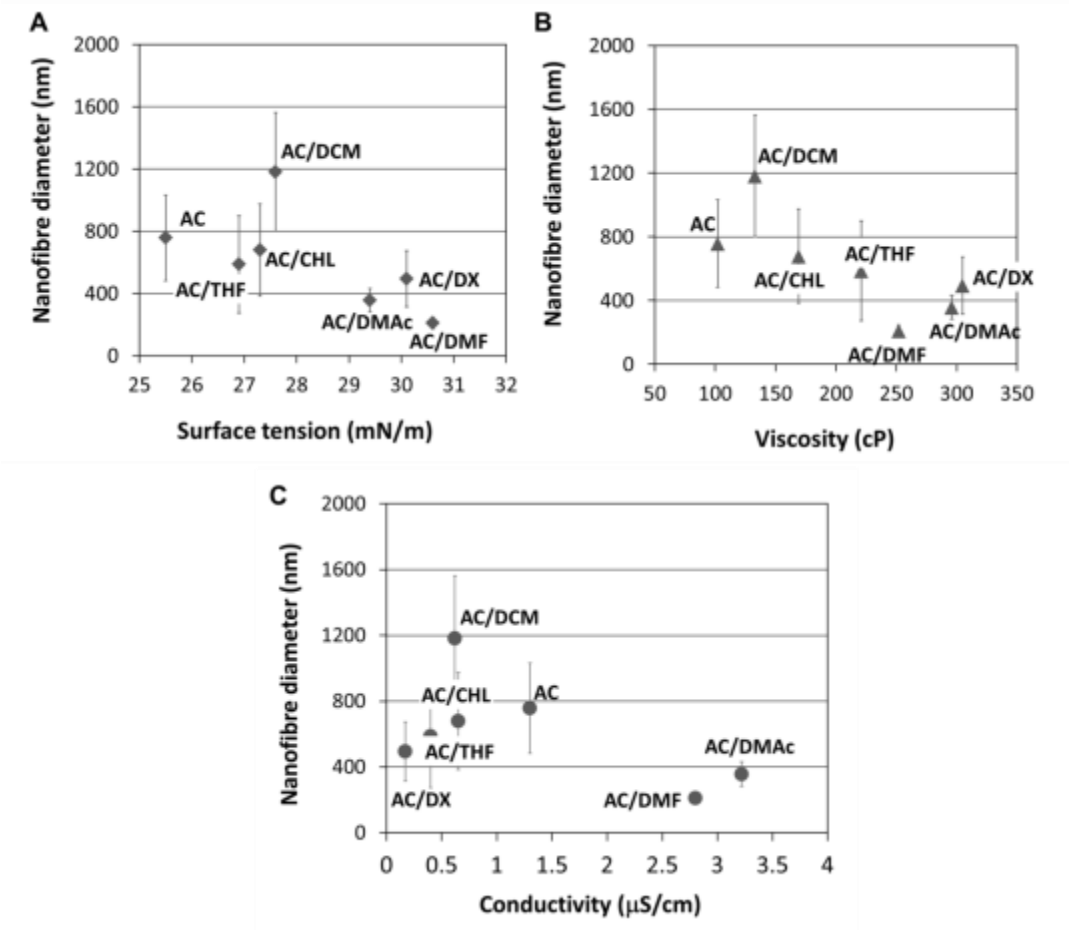

Figure 4.11 – Effect of (a) surface tension, (b) viscosity and (c) conductivity of PLA solution in binary solvent system on mean nanofibre diameter.

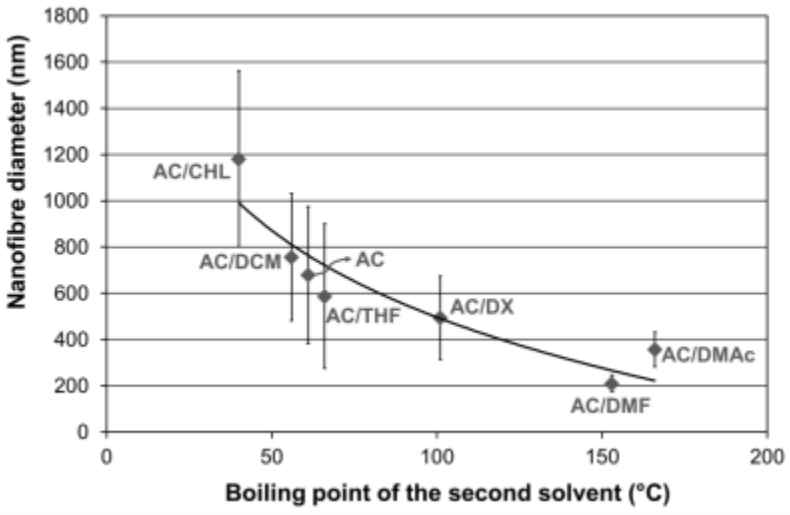

Figure 4.12 – Effect of the boiling point of the second solvent in binary solvent systems on mean nanofibre diameter.

Thus far, the results have shown that the effect of solution viscosity, conductivity and surface tension on the resultant nanofibre morphology and diameter cannot be studied separately. The electrospinning process is a very complex electrohydrodynamic phenomenon. PLA solution in different binary solvent systems has its unique properties that lead to a specific effect on the nanofibre morphology depending on viscosity, surface tension and electric conductivity. In this work PLA solution with high viscosity, low surface tension and high conductivity appeared to be the best choice to produce defect-free nanofibres with small diameter and narrow diameter distribution. AC/DMF results to be the most appropriate solvent system for the electrospinning of PLA solution.

4.3.3 Effect of solvent ratio AC/DMF on nanofibre morphology and diameter

Acetone/dimethylformamide (AC/DMF) was the solvent system to produce defect-free PLA nanofibres with the smallest mean diameter and narrow diameter distribution. Hence the next step focused on changing the ratio between the two solvents (AC, DMF) and investigating the effects on solution properties, nanofibre morphology and mean diameter. Figure 4.13 and

Figure 4.14 shows SEM images of the nanofibres produced at different solvent ratios (AC/DMF). Morphological observations have shown that mainly beads were collected with few short nanofibres using the solvent ratio 20/80 and 40/60 (Figure 4.13). On further increasing the amount of acetone in the solvent mixture, smooth nanofibres were first produced using the solvent ratio 50/50 v/v as shown in Figure 4.14. In addition while the solvent ratio 50/50 and 60/40 led to dense nanofibrous webs with no defects, a few number of beads were observed using the solvent ratio (80/20), most probably due to the faster evaporation rate of the solvent mixture on increasing AC.

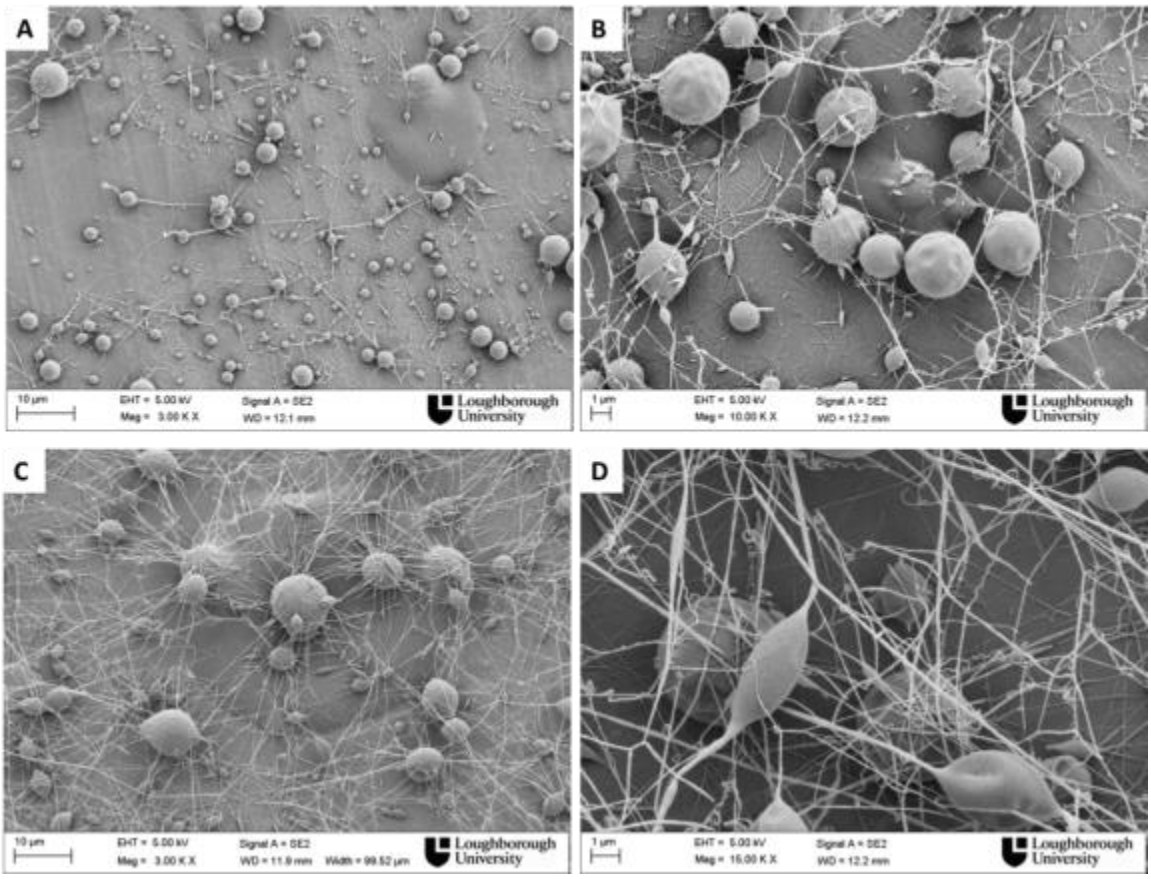

Figure 4.13 – Effect of solvent ratio (AC/DMF) on nanofibre morphology: scanning electron micrographs of PLA nanofibres from solutions of 10% (w/v) of PLA in AC/DMF at a ratio of 20/80 (v/v) (a) 3,000 X (a) 10,000 X; 40/60 (c) 5,000 X (d) 15,000X.

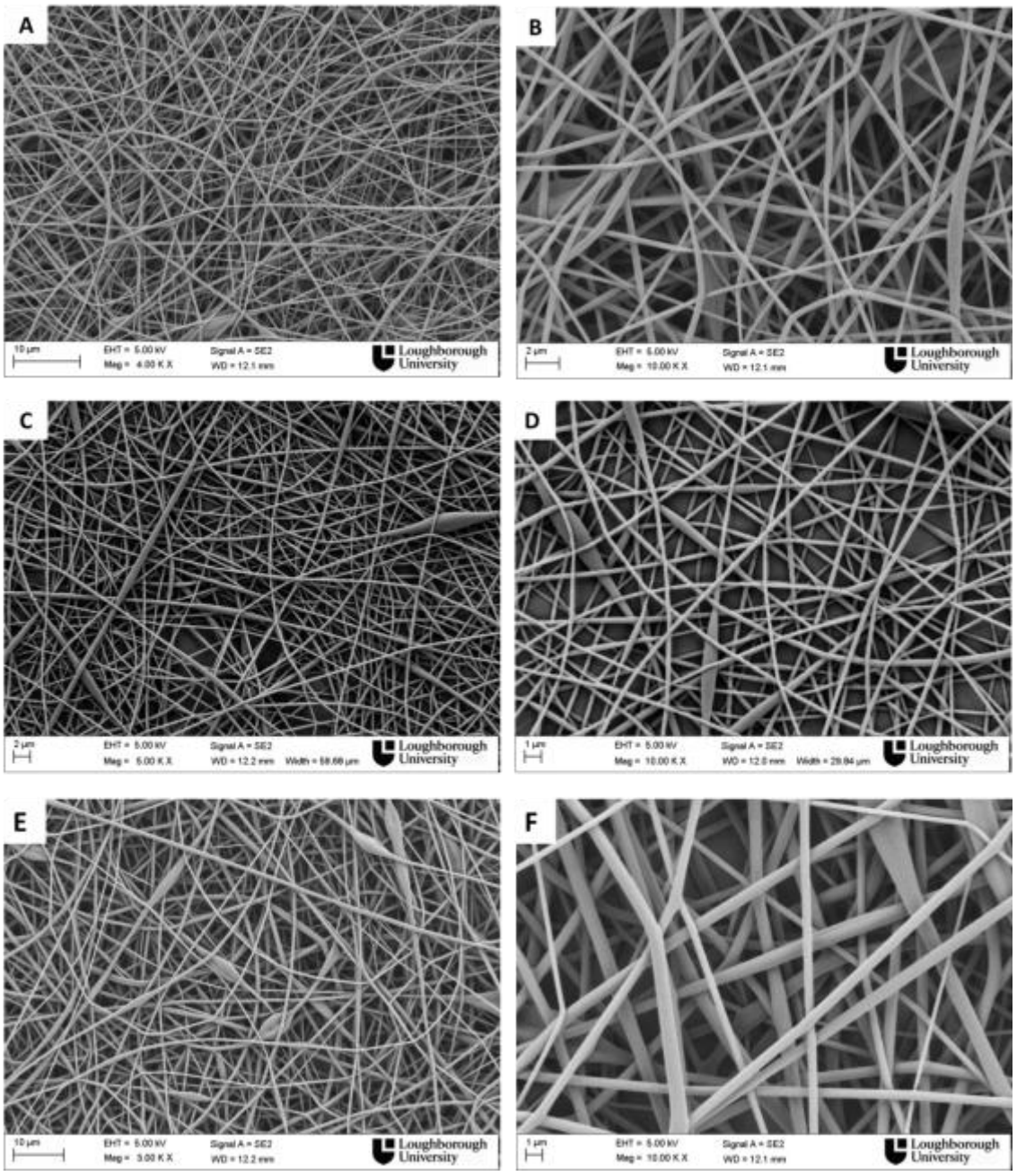

Figure 4.14. Effect of solvent ratio (AC/DMF) on nanofibre morphology: scanning electron micrographs of PLA nanofibres from solutions of 10% (w/v) of PLA in AC/DMF at a ratio of (a-b) 50/50 v/v (4,000 X - 10,000 X); (c-d) 60/40 v/v (5,000 X - 10,000 X); (e-f) 80/20 v/v (3,000 X - 10,000 X).

Measurements of viscosity, surface tension and conductivity of PLA solutions in AC/DMF at all solvent ratios were performed and the results are presented in Table 4.4 together with the mean diameter of the electrospun nanofibres collected.

Table 4.4 – Solution viscosity, surface tension and conductivity of PLA solution at concentration of 10% w/v in AC/DMF at different ratios.

AC/DMF (v/v)	Viscosity (cP)	Surface tension (mN/m)	Conductivity (μS/cm)	Nanofibre diameter (nm) (mean±stdev)
100/0	102±10	25.5±0.9	0.07	1360±521
80/20	347±42	27.6±0.3	1.34	557±176
60/40	303±82	30.0±0.3	2.42	272±58
50/50	252±53	30.6±0.3	2.80	210±36
40/60	229±22	32.6±0.3	3.22	No nanofibres
20/80	170±12	35.8±0.1	3.32	No nanofibres
0/100	155±9	38.4±0.3	3.31	No nanofibres

An increase of DMF in the solvent mixture results in higher surface tension and higher conductivity of the PLA solution. The image A of Figure 4.15 shows the effect of the solvent ratio on solution surface tension, while image B presents the effect of the solvent ratio on the nanofibre diameter. Most likely the higher surface tension of the PLA solution in AC/DMF at ratios of 20/80 and 40/60 compared to solutions at solvent ratios 50/50, 60/40 and 80/20 inhibited the formation of nanofibrous structures. Morphological observations have shown that only beads were collected from 20/80 and 40/60 (Figure 4.13) and this could be due to the higher Rayleigh instability which breaks down the polymeric jet into droplets. Defect-free nanofibres were then collected when the solution surface tension dropped to about 30 mN/m at ratios 50/50 and 60/40 although a reduction of solution conductivity (2.4 and 2.8 μS/cm, respectively) was also measured. However the ratios 80/20 and 100/0 led to nanofibres with few beads, although also lower solution surface tension was measured.

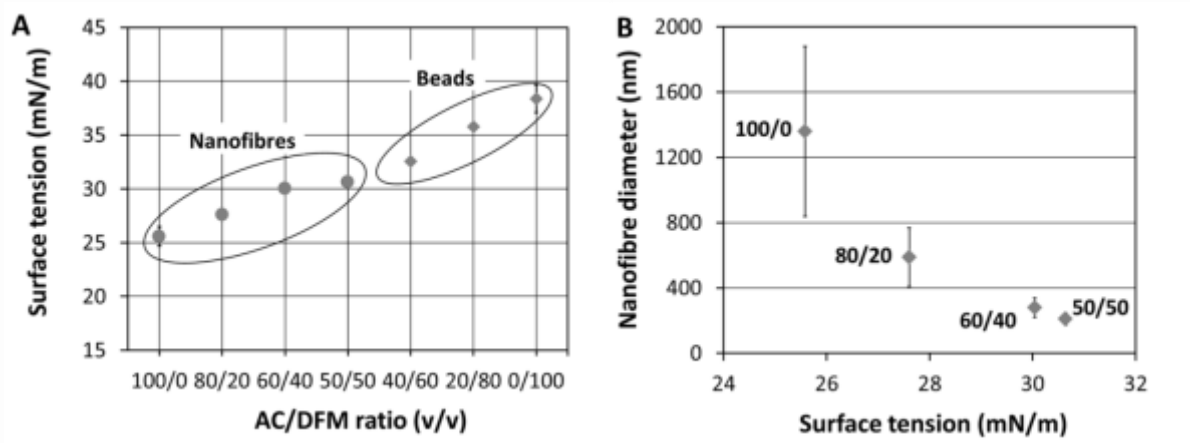

Figure 4.15 – (A) Effect of solvent ratio (AC/DMF) on surface tension of PLA solutions, (B) effect of surface tension on nanofibre diameter.

The application of a lower surface tension to get defect-free nanofibres is not a general rule, but depends on the type of solvent and polymer. While defect-free PEO nanofibres were collected on increasing the amount of ethanol in the PEO solution (Fong et al. 1999), beaded nanofibres were formed with the addition of ethanol in PVA solution (C. Zhang et al. 2005). Ethanol is a solvent for PEO, while it is a non-solvent for PVA. The reduction of surface tension was accompanied by the reduction of viscosity of PVA solution and this resulted in the production of beaded nanofibres most probably due to fewer entanglements in solution.

In paragraph 4.3.2 it was shown that although AC/DMF and AC/DMAC (50/50 v/v) had the highest solution surface tension (30.6 and 29.4 mN/m, respectively) between the binary solvent systems, the thinnest nanofibres were formed from these solutions compared to the other binary solvent systems as a result of the higher solution conductivity of about 3 μS/cm compared to values lower than 1 μS/cm for the other solutions. The effect of solvent ratio AC/DMF on solution conductivity and on nanofibre diameter is reported in Figure 4.16 A and Figure 4.16 B, respectively. Higher solution conductivity was measured on increasing the amount of DMF in the mixed solvent system AC/DMF. Hence this led to the production of nanofibres with smaller diameter.

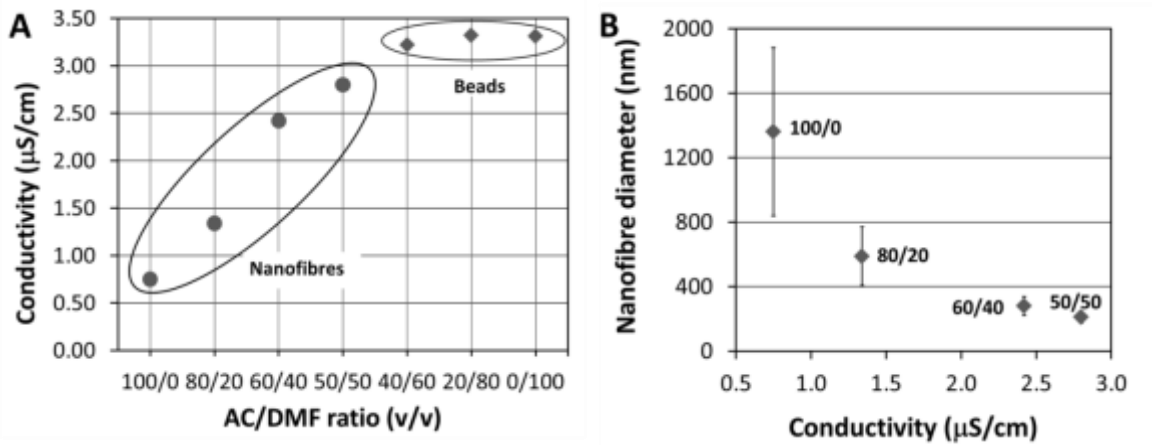

Figure 4.16. (A) Effect of solvent ratio (AC/DMF) on conductivity of PLA solutions, (B) effect of conductivity on nanofibre diameter.

Previous studies also reported that the production of thinner smooth fibres with fewer defects may be achieved on increasing solution conductivity (X.-H. Qin et al. 2007; Zuo et al. 2005). The addition of salts has been found to increase the solution conductivity and hence the charge density. The higher whipping instability which dominates at higher charge density leads to higher drawing ratio of the polymeric jet because more charges are presented at the jet surface (Hohman et al. 2001a; Hohman et al. 2001b). This explains the production of smooth nanofibres with few or no defect, if sufficient number of entanglements is formed in solution.

To summarise, PLA solution in AC/DMF at ratios of 50/50 and 60/40 v/v were the most suitable solutions for the production of defect-free nanofibres with small diameter and narrow diameter distribution. Although these solutions have high surface tension than the solution at ratio 80/20 (Table 4.4), the high electric conductivity and high viscosity enhance the formation of uniform nanofibrous mats. Overall it has been shown that the effect of solution viscosity, conductivity and surface tension on the resultant nanofibre morphology and diameter cannot be studied separately.

4.3.4 Effect of polymer concentration on nanofibre morphology and diameter

AC/DMF solvent ratios 50/50 and 60/40 were found to be the most promising solvent ratio to produce the thinnest nanofibres with few or no defects. The next step involved the preparation of PLA solution in AC/DMF 50/50 v/v at different polymer concentrations to examine the effect on solution properties and nanofibre morphology. As mentioned previously in this chapter, the polymer concentration is one of the key parameter together with the solvent type for the electrospinnability of polymeric solutions and successful production of nanofibres. A sufficient number of entanglements is needed to form continuous nanofibres. Therefore the PLA concentration was varied from 5 to 15% w/v and all solutions were electrospun using the same process parameters: voltage 20 kV, flow rate 1 ml/h and distance between the needle and collector of 15 cm.

Figure 4.17 shows SEM images of electrospun samples collected using a PLA concentration of 3% w/v (A, B), 4% w/v (C, D), and 5% w/v (E, F). Only beads were collected from the electrospinning of these solutions due to insufficient chain entanglements. On increasing the polymer concentration to 6% w/v nanofibres were first produced even thought a lot of beads were observed within the electrospun web (Figure 4.18 A, B). In addition the shape of the beads changed from more circular to spindle-like with an increase of PLA concentration. While nanofibres with bead string morphology were formed up to a concentration of 10% w/v (Figure 4.18 E, F), defect-free nanofibres were successfully collected from PLA solution at concentration of 12.5% w/v and 15% w/v (Figure 4.19).

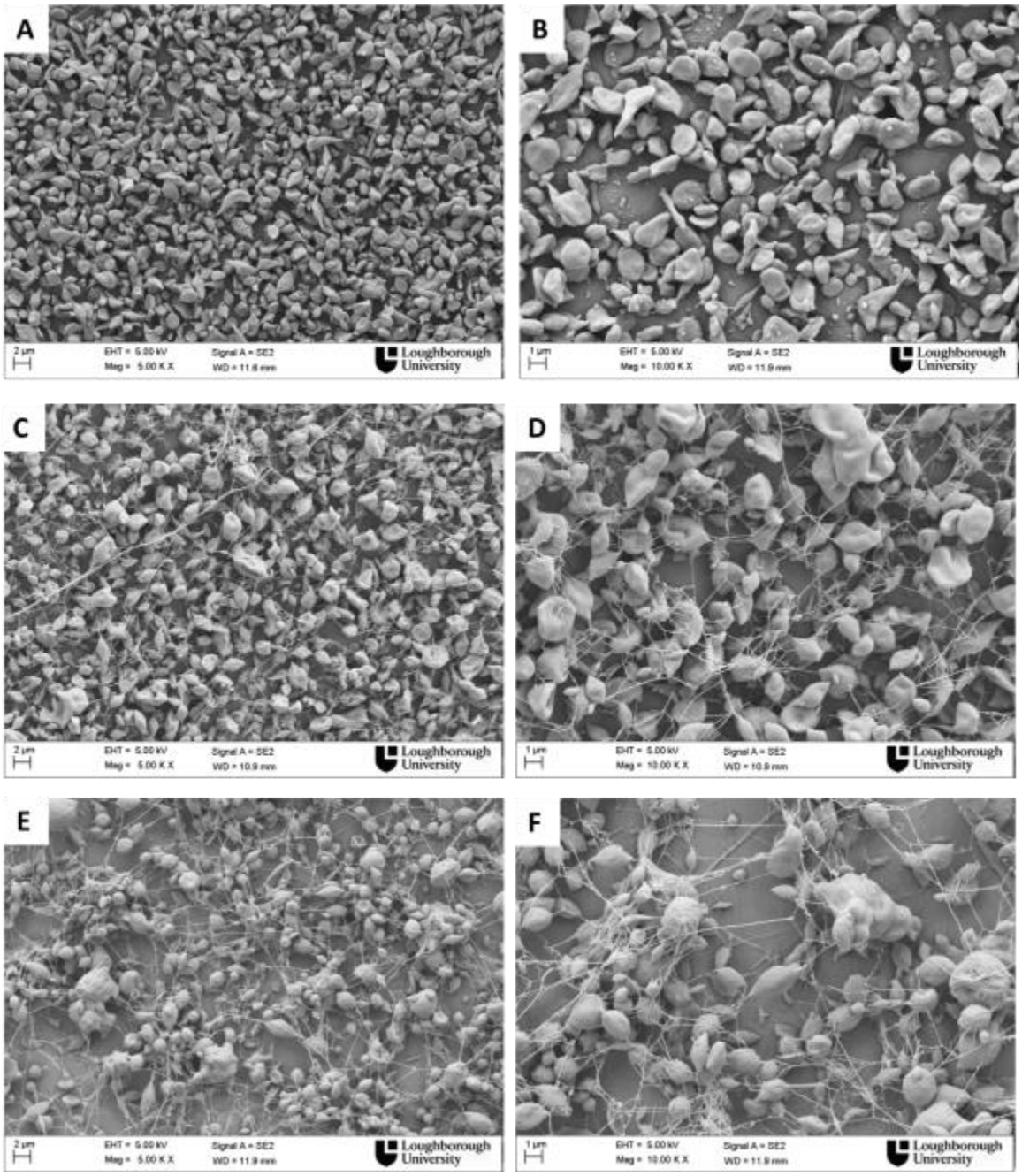

Figure 4.17 – Effect of polymer concentration on nanofibre morphology: scanning electron micrographs of PLA nanofibres from solutions of PLA in AC/DMF at a ratio of 50/50 v/v at concentration of (a, b) 3% w/v (5,000 X - 10,000 X); (c, d) 4% w/v (5,000 X - 10,000 X); (e, f) 5% w/v (5,000 X - 10,000 X).

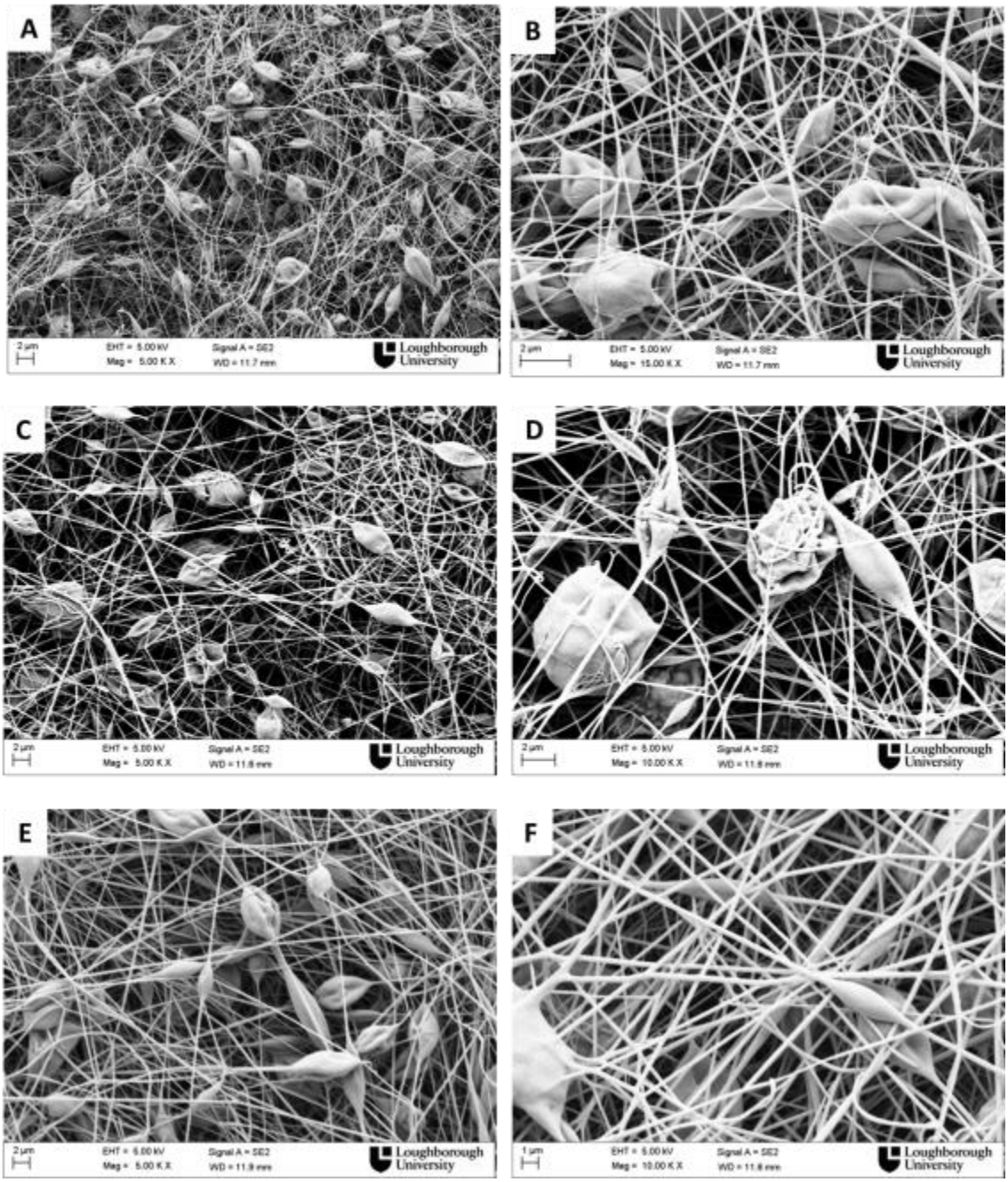

Figure 4.18. Effect of polymer concentration on nanofibre morphology: scanning electron micrographs of PLA nanofibres from solutions of PLA in AC/DMF at a ratio of 50/50 v/v at concentration of (a, b) 6% w/v (5,000 X - 15,000 X); (c, d) 7.5% w/v (5,000 X - 10,000 X); (e, f) 10% w/v (5,000 X - 10,000X).

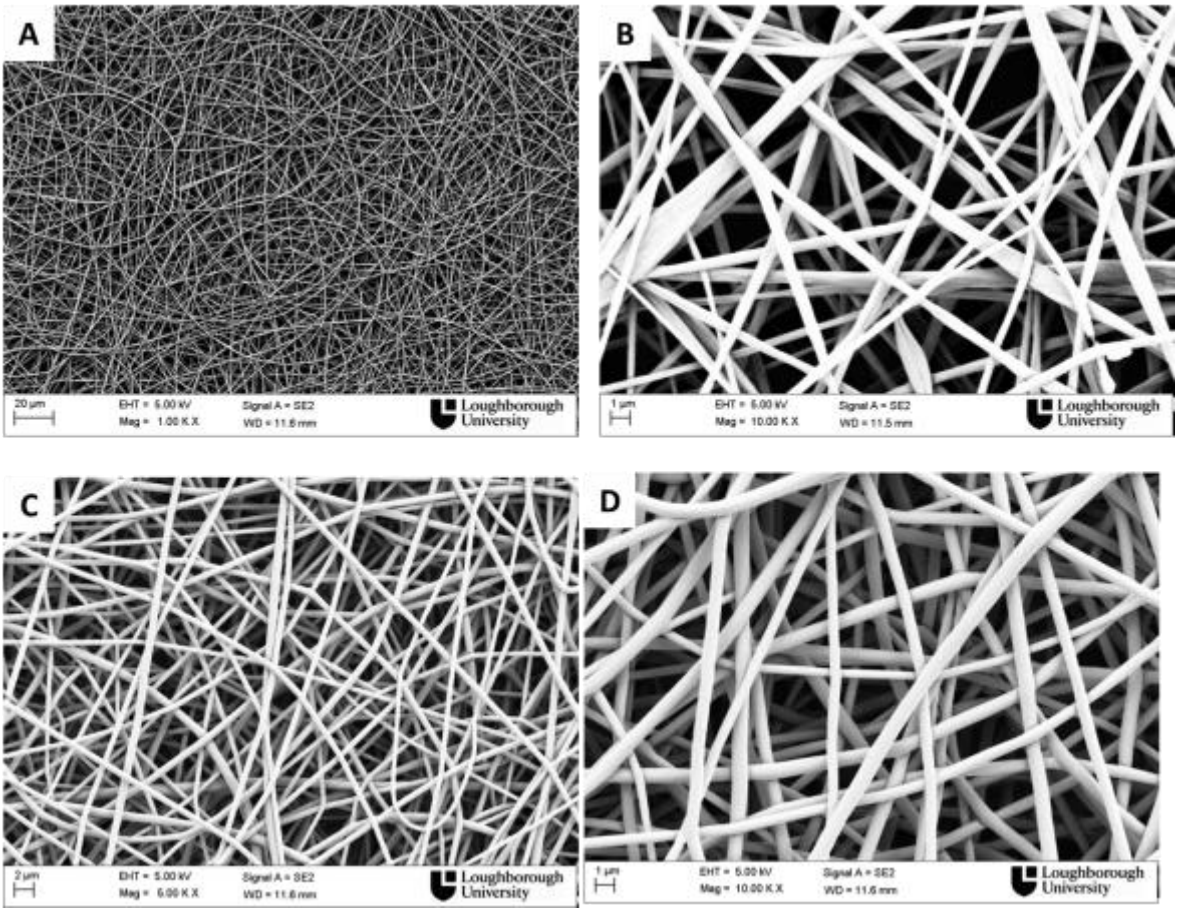

Figure 4.19. Effect of polymer concentration on nanofibre morphology: scanning electron micrographs of PLA nanofibres from solutions of PLA in AC/DMF at a ratio of 50/50 v/v at concentration of (a, b) 12.5% w/v (1,000 X - 10,000 X); (c, d) 15% w/v (5,000 X - 10,000 X).

Next, the diameter of nanofibres collected from PLA solutions at concentration of 7.5, 10, 12.5 and 15% w/v was measured and the results are reported in Figure 4.20. The smallest nanofibres with diameter of 131 nm were produced using a PLA concentration of 7.5% w/v although a mixture of nanofibres and beads were collected as shown in Figure 4.18 C and D. On increasing the polymer concentration the morphology was changed from beaded nanofibres to uniform fibre structure and the mean diameter gradually increased from 131 to 489 nm as shown in Figure 4.20. This may be explained by an increase of solution viscosity on increasing polymer concentration. The chain entanglements density increases and hence the electrical forces were not sufficiently strong to stretch a more viscous polymeric jet. Therefore this resulted in the production of nanofibres with bigger diameter and wider diameter distribution. Similar observations were reported for example for PEO aqueous

solutions (Chowdhury & G. K. Stylios 2012), PVA aqueous solutions (Ding et al. 2002) and PCL solution in DCM/DMF (Gholipour Kanani & Bahrami 2011).

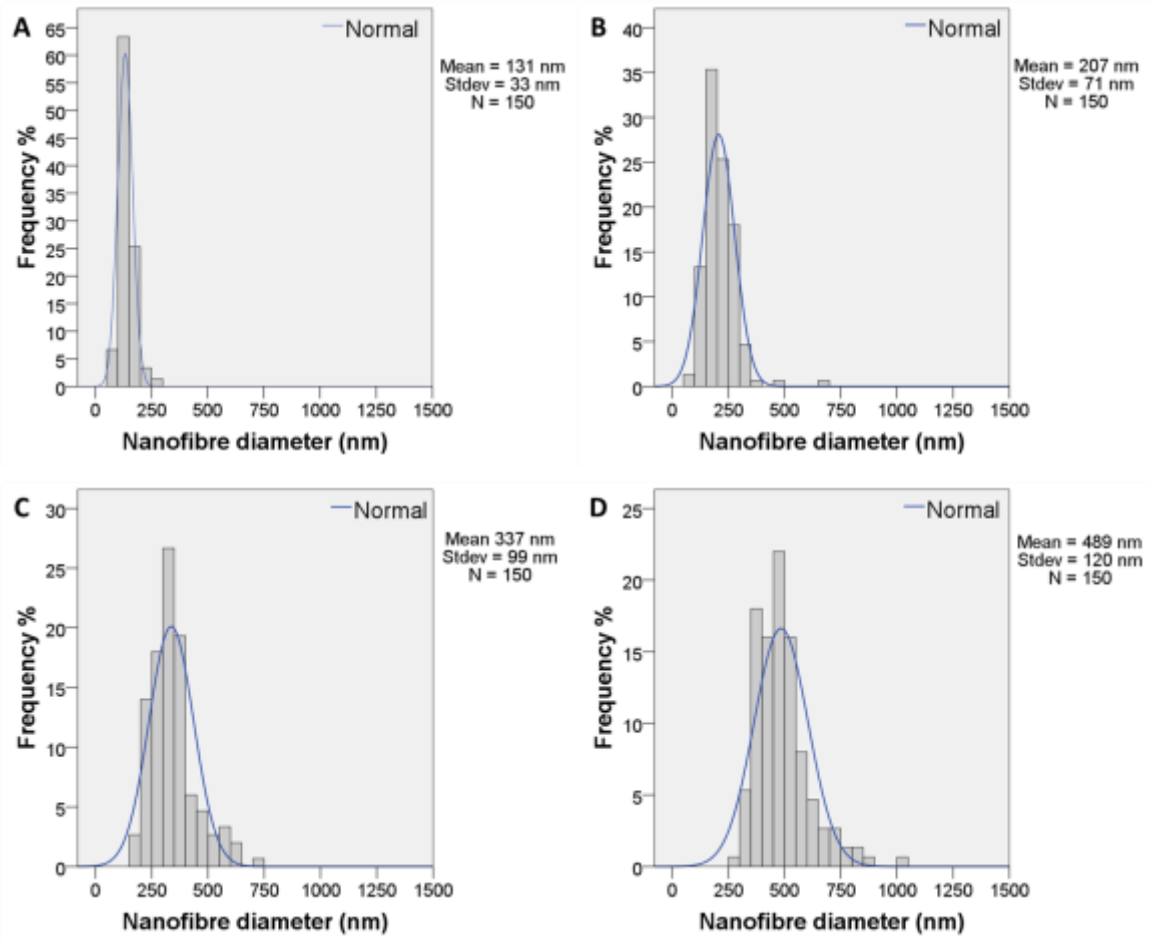

Figure 4.20. Effect of PLA concentration on mean nanofibre diameter (a) 7.5% w/v (b) 10.0% w/v (c) 12.5% w/v (d) 15% w/v.

Surface tension and conductivity of PLA solution at 5, 7.5, 10, 12.5 and 15 % w/v were also measured. The results presented in Table 4.5 show a slight increase of both surface tension and conductivity on increasing the polymer concentration. Although higher solution conductivity should result in the production of thinner nanofibres due to the higher charge density, in this work PLA nanofibres with larger diameter were formed at higher polymer concentration. This indicates that the solution viscosity has more significant effect on the nanofibre morphology than the increase conductivity. Hence the rheological behaviour of PLA solution was investigated on a wide concentration range in order to identify the different concentration regimes in which polymer chain entanglements dominate the flow behaviour.

Table 4.5 – Surface tension and electrical conductivity of PLA solution in AC/DMF at several polymer concentrations.

PLA concentration (% w/v)	Conductivity (μS/cm)	Surface tension (mN/m)
5	2.82±1.18	29.3±0.3
7.5	3.74±1.14	29.5±0.2
10	3.86±0.64	29.0±0.6
12.5	4.36±0.69	29.6±0.9
15	3.94±0.47	29.9±0.9

Figure 4.21 shows a log-log plot of the concentration dependence of the viscosity for PLA solutions in AC/DMF (50/50 v/v). Three regimes were found from the log-log plot. The first change in slope occurred at a concentration of approximately 4% w/v and it represents the transition between the dilute regime and the semidilute unentangled regime named critical concentration C*. A second change in slope at concentration of approximately 7% w/v (marked C_e) is the boundary between the semidilute unentangled and entangled regimes. The results are in good agreement with the morphological observations. In fact Figure 4.18 has shown that nanofibres with beads were first formed between 6 and 7% w/v.

While rotational tests were used to determine the viscosity of the solutions at several polymer concentrations as a function of shear rate, oscillatory tests were performed to determine both dynamic moduli, elastic (storage, G') and plastic (loss, G''). The main reason of the evaluation of these moduli is due to the stretching of polymeric jet imposed by the electrical forces during the electrospinning process.

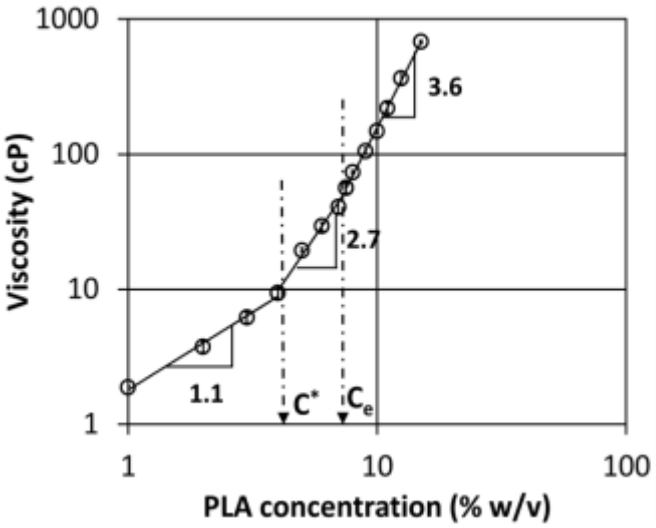

PLA concentration (% w/v)	Viscosity (cP)
1	1.87±0.05
2	3.74±0.34
3	6.21±0.57
4	9.37±0.91
5	19.46±0.63
6	29.30±2.03
7	40.77±4.93
7.5	56.46±2.092
8	73.49±5.69
9	105.1±3.7
10	147.9±19.8
11	219.1±42.6
12.5	364.6±15.7
15	679.9±45.9

Figure 4.21. Effect of PLA concentration on viscosity of PLA solution in AC/DMF (50/50 v/v).

Higher viscoelasticity may enhance the stretching of a polymer solution as it travels to the collector. There is competition between the Rayleigh instability that tends to form droplets and the viscoelasticity of the polymer that wants to suppress the Rayleigh instability (T. Lin et al. 2004; Y. Liu et al. 2008; Zuo et al. 2005).

Figure 4.22 shows a log-log plot of the values of G' and G'' versus the polymer concentration. It can be seen that G' and G'' both increased with increasing the polymer concentration, but the difference between the G' and G'' values became larger at higher concentration. This may indicate that the elastic property of the PLA solution was more significant due to the increased entanglements density. A clear change in slope of the elastic component (G') was observed at a concentration of approximately 7% w/v. This observation was in agreement with the morphological observations and shear viscosity measurements, indicating that nanofibres are first produced at concentration higher than the entanglement concentration (C_e).

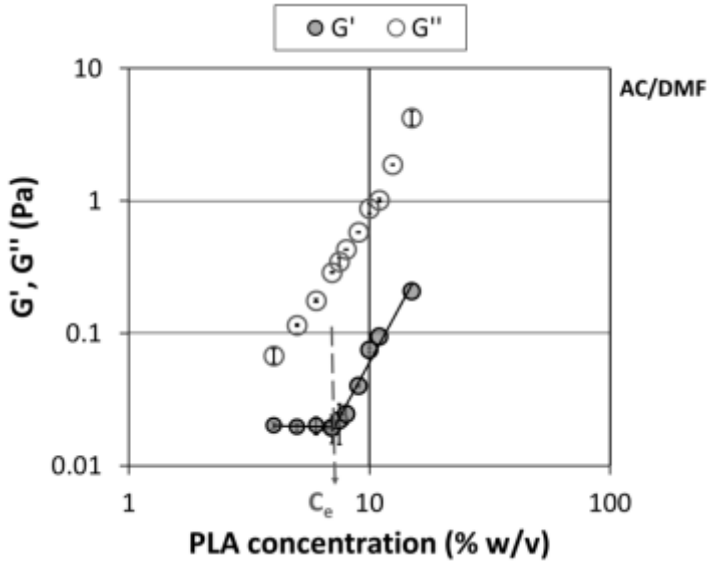

Figure 4.22. Effect of PLA concentration in acetone/dimethylformamide (50/50 v/v) on the elastic (G') and plastic (G'') modulus at 1 Hz.

To summarise, both shear viscosity and viscoelasticity measurements of PLA solution at several polymer concentration may be a useful approach to predict the concentration at which electrospun nanofibres are first collected, named C_e. In addition the selection of a polymer concentration of 2 or 2.5 times C_e will most probably allow the production of defect-free uniform electrospun nanofibrous mats.

4.4 Conclusion

The effect of different solvent systems on the PLA nanofibre diameter and morphology of the electrospun webs was investigated in this chapter. Among the PLA-solutions in single solvents, only the PLA solution in 10% w/v acetone produced PLA nanofibres. Therefore binary solvent systems were based on mixtures of acetone and another solvent. All the PLA solutions in binary solvent systems of 10% w/v were spinnable and nanofibres could be collected. The effect of different binary solvent systems on nanofibre morphology and diameter was observed by scanning electron microscopy (SEM). Results have shown that beaded nanofibres were collected using the solvent systems AC/DX, AC/THF, AC/DCM and AC/CHL, while defect-free nanofibres were collected using the solvent systems AC/DMF

and AC/DMAc, most probably due to the higher electrical conductivity of PLA solutions.

Next, the effect of the amount of AC in PLA solution AC/DMF solvent ratios of acetone/dimethylformamide (AC/DMF) on nanofibre morphology and diameter was examined. Thinner nanofibres with a narrow diameter distribution were produced using the solvent ratios 60/40 v/v and 50/50 v/v. An increase of AC in the mixture AC/DMF enhanced the electrospinning process and defect-free nanofibre were first produced at solvent ratio of 50/50 v/v, although on further increasing the amount of AC caused higher bead formation and an increase of the mean nanofibre diameter and diameter distribution.

The last step focused on changing PLA concentration in AC/DMF (50/50 v/v) solution to investigate its effect on solution viscosity, nanofibre morphology and diameter. Above 12.5% w/v PLA concentration uniform defect-free nanofibres could be produced. Hence the chain entanglement concentration, C_e, was taken as 7% w/v, which corresponds to the concentration at which nanofibres are first observed. Also rotational and oscillatory tests revealed a chain entanglement concentration of approximately 7% w/v.

In this chapter it was demonstrated that viscosity, surface tension and conductivity cannot be studied separately for the production of homogeneous electrospun nanofibrous mats. Of all solution properties, the polymer concentration is the most significant parameter to enable the production of nanofibres and a clear relationship between the arrangements in solutions and the production of defect free nanofibres was established. Measurements of the elastic modulus of the polymer solution at several concentrations are useful tool to predict the value of the entanglement concentration (C_e). The transition from beads and beaded nanofibres was observed at concentration C_e, then defect free nanofibres were collected using a polymer concentration about 2 or 2.5 times higher than C_e. After polymer concentration, solution surface tension and electrical conductivity should be measured. High electrical conductivity helps the formation of thinner nanofibres and low surface tension reduces the bead formation in the nanofibrous network.

5 THREE STEP METHODOLOGY TO ENSURE SOLUTION ELECTROSPINNABILITY AND SUCCESSFUL PRODUCTION OF DEFECT-FREE PLA NANOFIBRES

5.1 Introduction

The understanding of the interactions between solvent and polymer, and hence of the polymer dissolution, is extremely important in determining the solution electrospinnability, because it allows optimization of the processing conditions. The chemical structure of a specific polymer determines its solubility in various solvents and a specific polymer will dissolve in solvents with similar solubility parameters to its own (Antoniou & Alexandridis 2010; Miller-Chou & Koenig 2003). The Flory–Huggins chi parameter [χ] is generally used to indicate the compatibility of solvent and polymer (De Gennes 1979; Flory 1953). It uses the Hildebrand solubility parameter of solvent (δ_S) and polymer (δ_P), as shown in Equation 11 (Guarino et al. 2011; Koenhen & Smolders 1975) where M_s is the molecular weight of the solvent (g/mol), R the universal gas constant (MPa·cm^3·K^{-1}·mol^{-1}), T the absolute temperature (K), and ρ_s is the density of the solvent (g/cm^3), the value 0.34 represents a lattice parameter.

$$[\chi] = (\delta_S - \delta_P)^2 \frac{M_S}{RT\rho_S} + 0.34$$

Equation 11

If χ is lower than 0.5 indicates that there are favourable solvent-polymer interactions, whereas if χ is greater than 0.5 then polymer-polymer interactions are favoured (Ferdinand Rodriguez 1996; Pattamaprom et al. 2006). Therefore the strength of the interactions between polymer chains and the solvent molecules can be estimated by the Flory-Huggins parameter.

However the Hildebrand solubility parameter is only applicable for non-polar system. In 1967 Hansen during his PhD studies (Ferdinand Rodriguez 1996) broke down the Hildebrand solubility parameter into three components, δ_D, δ_P, δ_H, representing the dispersive (nonpolar), polar and hydrogen bond interactions, respectively. The polymer solubility can be represented by using a three-dimensional model. A sphere with radius R_{AO}, known as the interaction radius, could be formed for each polymer. Equation 12 represents the distance between the polymer and solvent, called R_A, which is a measure of how alike they are.

$$R_A^2 = 4(\delta_{D,p} - \delta_{D,s})^2 + (\delta_{P,p} - \delta_{P,s})^2 + (\delta_{H,p} - \delta_{H,s})^2$$

Equation 12

If the solvent lies inside the polymer sphere, dissolution occurs. On the other hand, no homogeneous solution can be prepared if the solvent falls outside the domain. The ratio R_A/R_{AO} represents the relative energy difference (RED), which is a parameter to describe the solvent quality. If its value is lower than 1, this indicates that there is high affinity between polymer and solvent and therefore the liquid is a solvent for the polymer, whereas higher values indicate non-solvents and consequently phase separation will occur (Gedde 1995). However in most scientific publications about electrospinning of polymeric solutions, the selection of solvents to dissolve a polymer has been based on experience from similar polymer-solvent systems. Only in the last years a few scientific publications have reported the great significance of the Hansen solubility parameters for the selection of a suitable solvent and electrospinning of the resultant solution (Lubasova & Martinova 2011; Yener & Yalcinkaya 2013; L. Li, Z. Jiang, et al. 2014; L. Li, R. Li, et al. 2014).

In chapter 4 it has been shown the effect of different solvent systems on the properties of PLA solution and on nanofibre morphology and diameter. The solvents were initially selected based on the electrospinning of PLA or polymer blends reported in the literature (F. Yang et al. 2005; E. S. Kim et al. 2010; H.-W. Kim et al. 2006). Solution viscosity, surface tension and electric conductivity cannot be studied separately and different solvents or mixtures of solvents affect differently the solution properties, and hence the outcome of the electrospinning process. In addition the optimization of the polymer concentration is a crucial factor for the production of defect-free nanofibres (Hohman et al. 2001a; Deitzel et al. 2001). The number of entanglements in solution for the selected concentration has to support sufficient chains overlap and an entangled network should be formed. In section 4.3.4 of chapter 4, the value of concentration at which this takes place, called the entanglement concentration, C_e, was determined by measurements of shear viscosity and viscoelasticity for a PLA solution in AC/DMF. It would be worthwhile to develop a complete and efficient procedure for the selection of an appropriate solvent system and therefore solution properties for the production of defect free uniform nanofibres. A theoretical approach would be very useful in order to reduce the number of solubility test and trial and error experiments,

especially when a ‘new’ polymer or polymer blends are electrospun.

5.2 Aims and objectives

The main aim of the work presented in this chapter was the development of a general methodology to select a solvent or a mixture of solvents to ensure the preparation of electrospinnable solutions for the production of defect-free nanofibres.

The achievement of this aim was possible through the realisation of the following objectives:

- Selection of solvents for poly (lactic acid) by using a thermodynamic approach
- Selection of solvents by using solution conductivity and dielectric constant criteria
- Determination of entanglement concentration (C_e) by shear viscosity and viscoelasticity measurements.

5.3 Results and discussion

In the following paragraphs the solubility of poly (lactic acid) in terms of Flory Huggins and RED parameters, the relationship between polymer concentration and viscoelasticity, in different solvents together with the electrical properties of PLA solution are discussed.

5.3.1 Thermodynamic criterion: solubility parameters

For all solvents used in this work, the Flory-Huggins parameter χ was calculated using Equation 11, with R of 8.314 $MPa \cdot cm^3 \cdot K^{-1} \cdot mol^{-1}$ and T of 283.15 K. The solubility parameter (δ_p) used for PLA was determined from an average of values found in the literature (A. Agrawal et al. 2004). The value calculated was 20.18 $MPa^{1/2}$. Table 5.1 shows the solubility parameter, molecular weight and density of all solvents with the correspondent Flory-Huggins parameter.

Table 5.1 – List of solvent properties: Hildebrand solubility parameter (δ), density (ρ_s), molecular weight (M_w) and Flory-Huggins parameter (χ).

Solvent	**AC**	**THF**	**DX**	**DCM**	**CHL**	**DMF**	**DMAc**
δ (MPa) $^{1/2}$	20.2	19.5	20.5	20.20	19.0	24.8	22.8
Density (ρ_s) (g/m^3)	0.791	0.889	1.033	1330	1.483	0.948	0.937
Molecular weight (M_w) (g/mol)	58	72	88	85	119	73	87
χ	**0.34**	**0.36**	**0.34**	**0.34**	**0.39**	**1.03**	**0.60**

While a χ value lower than 0.5 was obtained using AC, THF, DX, DCM, CHL, a higher value was calculated for DMF and DMAc. This means that AC, CHL, DX are good solvents for PLA and allow the polymer chains to expand in solution, while the value of $\chi_{(PLA\text{-}DMF)}$ of 1.03 represents poor interactions between the two components.

However homogeneous solutions were prepared using all single solvents at PLA concentration of 10% w/v as reported in paragraph 4.3.1 of chapter 4. Similar findings were reported by Pattamaprom et al (Pattamaprom et al. 2006). The authors dissolved poly (styrene) (PS) in DMF and nitrobenzene at all concentrations (10, 20, and 30% w/v), despite the fact the χ parameter was much higher than 0.5. These observations may be due to the dependence of χ on temperature and on concentration over a wide range of polymer concentration (Koenhen & Smolders 1975). Therefore the next step involved the creation of a tri-dimensional space with orthogonal axes δ_D, δ_P, δ_H as shown in Figure 5.1, which defines the PLA solubility sphere. The radius of the sphere is the PLA interaction radius (R_{AO}) of 11.26 $MPa^{-1/2}$ (A. Agrawal et al. 2004) and the centre is represented by its Hansen solubility parameter. Table 5.2 presents the solubility parameters of each solvent.

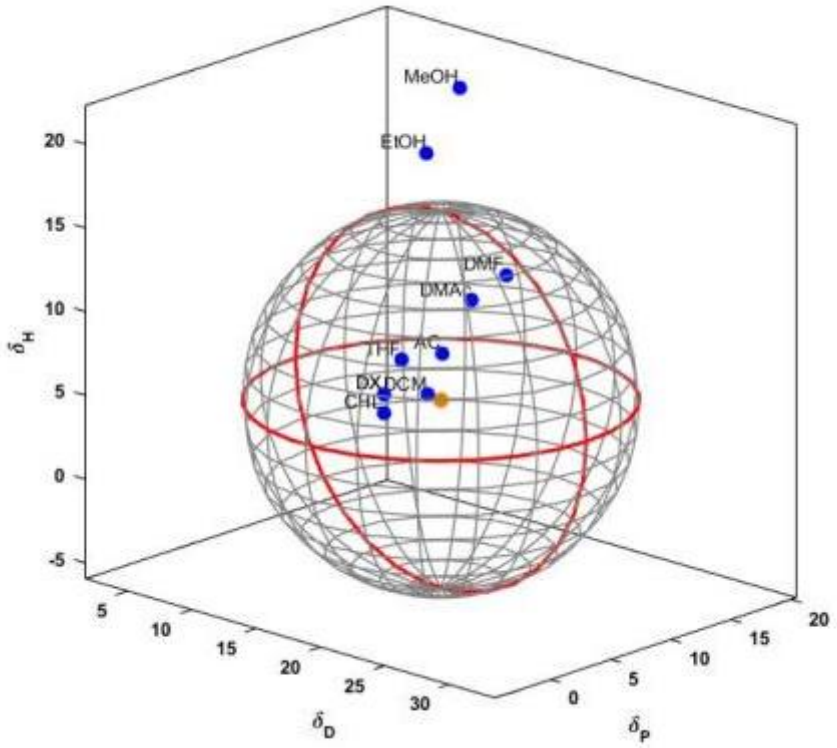

Figure 5.1 – Representation of solvents and PLA in the Hansen tridimensional space.

Table 5.2. Hansen solubility parameters of PLA and all solvents (Hansen 2007).

Solubility parameter (MPa) $^{1/2}$	**PLA**	**AC**	**THF**	**DX**	**DCM**	**CHL**	**DMF**	**DMAc**
δ_d dispersion	17.65	15.50	16.80	19.00	18.20	17.80	17.40	16.80
δ_p polar	8.00	10.40	5.70	1.80	6.30	3.10	13.70	11.50
δ_h hydrogen	5.28	7.00	8.00	7.40	6.10	5.70	11.30	10.20

Figure 5.1 shows that all solvents lay inside the sphere therefore indicating that they are good solvents and are able to dissolve PLA. The solubility parameter distance (R_A) was then calculated using Equation 12. The results are reported in Table 5.3 together with the relative energy difference (RED) calculated as the ratio between R_A and the radius of the polymer sphere (R_{AO}).

All solvents have shown RED value lower than 1. The lowest RED values were obtained for DCM (0.19) and THF (0.35), while the highest values were obtained for DX (0.63) and DMF

(0.74). The higher the RED value, the more favourable are polymer-polymer interactions compared to the polymer-solvent interactions.

Table 5.3. R_A and RED value for solvents used in this work.

Solvent	**R_A**	**R_A/R_{AO} = RED**
DCM	2.18	2.18/11.26 = 0.19
THF	3.95	3.95/11.26 = 0.35
CHL	4.93	4.93/11.26 = 0.44
AC	5.22	5.22/11.26 = 0.46
DMAc	*6.04*	*6.04/11.26 = 0.54*
DX	*7.09*	*7.09/11.26 = 0.63*
DMF	*8.29*	*8.29/11.26 = 0.74*

Thus far, it has been shown that all solvents chosen to prepare PLA solutions in chapter 4 meet the first thermodynamic criterion since the RED values are lower than 1 and in fact homogeneous PLA solutions were prepared. DMF and DMAc also lay inside the solubility sphere of PLA, although the Flory-Huggins parameters higher than 0.5 indicate most probably weak interactions between polymer and solvents.

The next paragraph will introduce the second step of the methodology and it will be focused on solvent dielectric constant and solution conductivity.

5.3.2 Electrical criterion: solvent dielectric constant

After the first criterion was met, the next step of the proposed methodology was the adjustment of the solution conductivity. Although polymeric solutions are electrically neutral, with the application of an electric field separation of positive and negative ions in solution will occur (Collins et al. 2012). The solvent ability of dissociation depends on its polarity and so high value of dielectric constant indicates high ability of dissociation. If the needle is positively charged, the negative ions migrate to the inner surface of the needle, while the bulk of the solution is left with an excess of positive charges which are attracted to the collector of opposite sign (negative) (D.H. Reneker & A.L. Yarin 2008). The repulsion of these positive

charges is responsible of the jet bending as its travel towards the collector. Therefore if the solution has higher charge density, a higher extent of stretching of the electrospun jet is imposed by the electrical forces resulting in the production of thinner nanofibres.

The most common solvents used for electrospinning of PLA solution are organic and fluorinated solvents which have a certain degree of toxicity. For this work, acetone (AC) was initially chosen for its low boiling point and lower toxicity compared with the other solvents, because the use of electrospun nanofibrous structures in tissue engineering applications, as scaffolds or drug delivery systems, require particular attention to organic solvents residue which can cause adverse reactions with cells. The χ and RED value determined for AC indicate that it is a good solvent for PLA (Table 5.1 and Table 5.3) and it has a dielectric constant of 20.6. However although DMF has the highest dielectric constant (36.7) between all single solvents used in this work, it was shown that no nanofibres were formed from electrospinning of PLA solution at a polymer concentration of 10% (paragraph 4.3.1). On the other hand, the addition of AC to DMF enhanced the electrospinning process resulting in defect-free and thinner nanofibres (paragraph 4.3.2) compared to the bead string morphology of the nanofibrous mats formed from PLA solution in AC. The solution conductivity was measured and it is about 1.30 μS/cm in AC, 4.0 μS/cm in DMF and 2.80 μS/cm in the mixture AC/DMF. As a result, thinner nanofibres would be expected using solution in DMF, but the morphological observations have shown only beads (paragraph 4.3.1). This may be explained by the weak interactions between PLA and DMF, as indicated by the high RED value of 0.74.

In the next paragraphs the effect of PLA concentration on the electric conductivity of PLA solution in single solvents, AC and DMF, and on the resultant nanofibre morphology and mean diameter, will be investigated. Figure 5.2 shows how the PLA concentration affects solution conductivity.

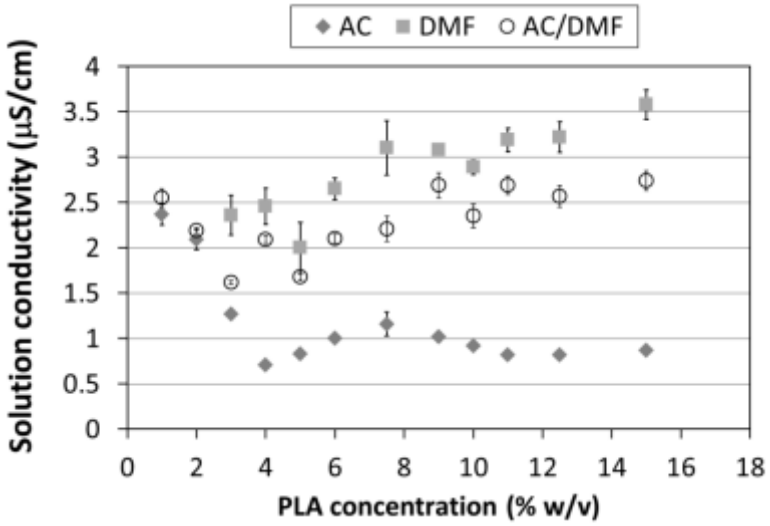

Figure 5.2 – Solution conductivity (K) of PLA solutions in AC, DMF, and AC/DMF at several polymer concentrations.

An increase of polymer concentration from 1% to 6% led to a reduction of conductivity from about 2.5 to approximately 1.0 µS/cm in PLA solution in AC. This may be explained by the restricted mobility of ions in more viscous solution on increasing the PLA concentration. However on further increasing polymer concentration no significant variation was measured. The reduction of conductivity resulted from an increase of polymer concentration was also reported for poly(methyl-phenyl-siloxane) (PMPS) solution in chloroform by Nakano et al (Nakano et al. 2012). The opposite trend was observed for PLA solution in DMF and in the mixture AC/DMF most probably due to the weaker interactions between PLA and DMF. Similar findings were reported by Lin et al (T. Lin et al. 2005) for PAN solution in DMF. The authors stated that the increased polymer concentration led to higher conductivity due the existence of a strong polar group, nitrile group, in every repeat unit of PAN. However with the addition of a cationic surfactant (dodecyltrimethylammonium bromide, DTAB) in the PAN solution, the conductivity was found to decrease on increasing the PAN concentration. This was attributed to the fact that more polymer entanglements restrict the movement of surfactant ions in the solution.

The effect of polymer concentration on the nanofibre morphology for PLA solution in AC and DMF will be discussed in the next section and the results will be compared with the

previous findings for PLA solution in the solvent mixture AC/DMF (refer to chapter 4).

5.3.3 Rheological criterion: critical entanglement concentration (C_e) determination

Once the thermodynamic criteria and the electrical property criteria are met, the third step involves the prediction of the entanglement concentration for the production of defect-free nanofibres. First PLA was dissolved in each single solvent, AC and DMF, at several polymer concentrations and the solution was electrospun using the same process parameters: an applied voltage of 20 kV, flow rate of 1 ml/h and collection distance of 15 cm. Next, morphological analysis of the nanofibrous samples collected was performed.

Figure 5.3, Figure 5.4 and Figure 5.5 show how the polymer concentration for PLA solution in AC affects the nanofibre morphology. While only beads with irregular shapes were formed using a polymer concentration of 3 and 4% w/v (Figure 5.3 A-D), a mixture of beads and few nanofibres was formed on increasing the polymer concentration to 5% w/v (Figure 5.3 E and F). A further increase of concentration to 6% and 7.5% resulted in collection of more nanofibres but a lot of beads were still produced (Figure 5.4 A-D). This may indicate that more entanglements between polymer chains are formed and hence higher viscoelastic forces favour the formation of a continuous polymer jet. Figure 5.4 E and F show that denser nanofibrous mat was first formed from the electrospinning of PLA solution at concentration of 10% w/v and in addition the beads shape changed from irregular to spindle-like. The successful production of defect-free nanofibres was achieved using the PLA solutions at 12.5 and 15% w/v (Figure 5.5), but the electrospinning of solutions at concentration higher than 15% was not possible due to the very high solution viscosity.

The change in the fibre morphology with increasing PLA concentration can be attributed to the competition between surface tension and viscoelastic forces. If the solution viscosity is low, the surface tension force prevails and therefore the Rayleigh instability tends to form beads. An increase in polymer concentration results in more chain entanglements and hence an increase in solution viscosity occurs. When enough entanglements are formed between the polymer chains and the electrical forces are sufficiently strong to overcome the surface tension force, defect-free nanofibres may be collected.

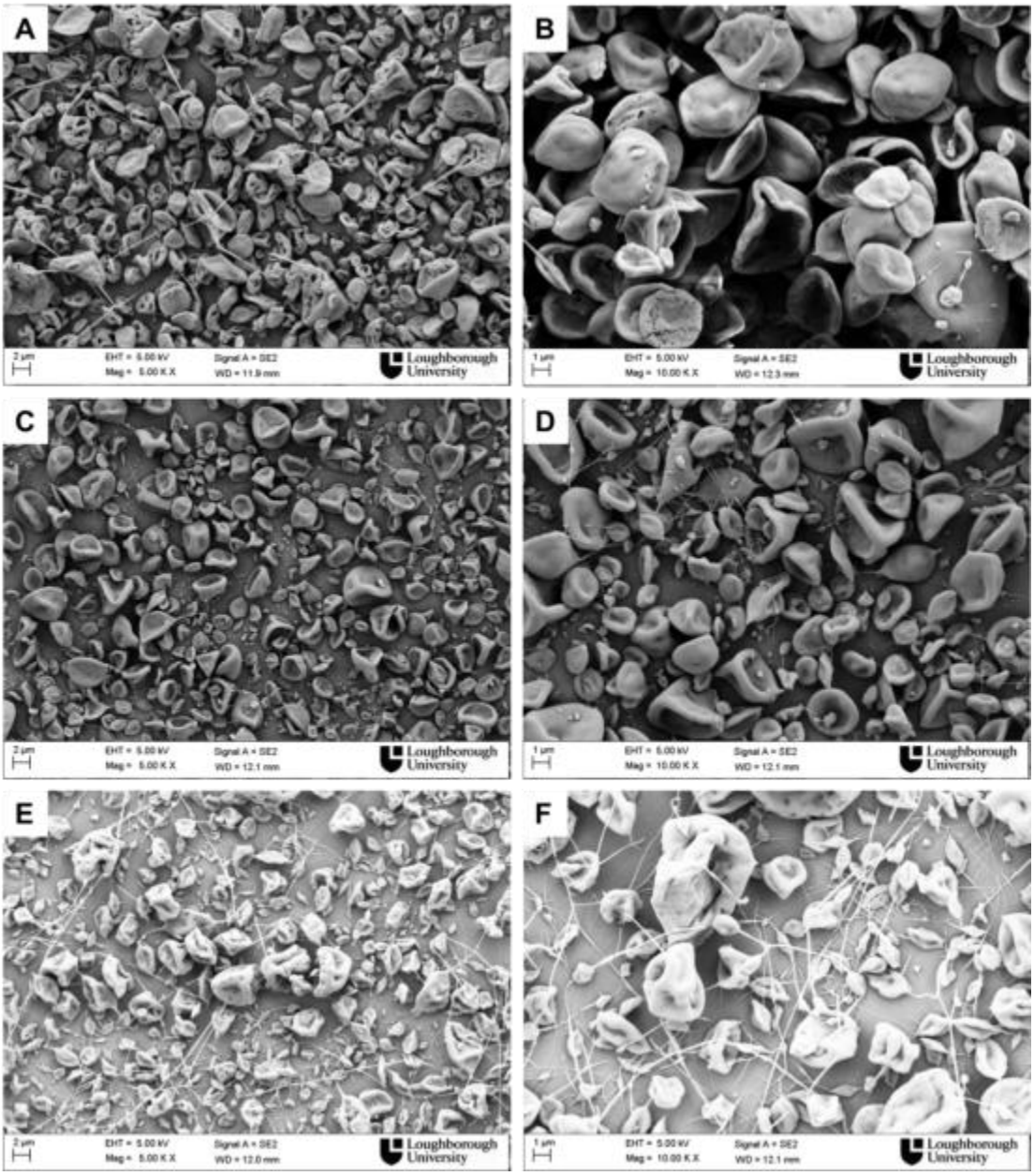

Figure 5.3 – Effect of polymer concentration on nanofibre morphology - scanning electron micrographs of PLA nanofibres from solutions of PLA in AC at concentration (A, B) 3% w/v (5,000 and 10,000 X), (B, C) 4% w/v (5,000 and 10,000 X), (E, F) 5% w/v (5,000 and 10,000 X).

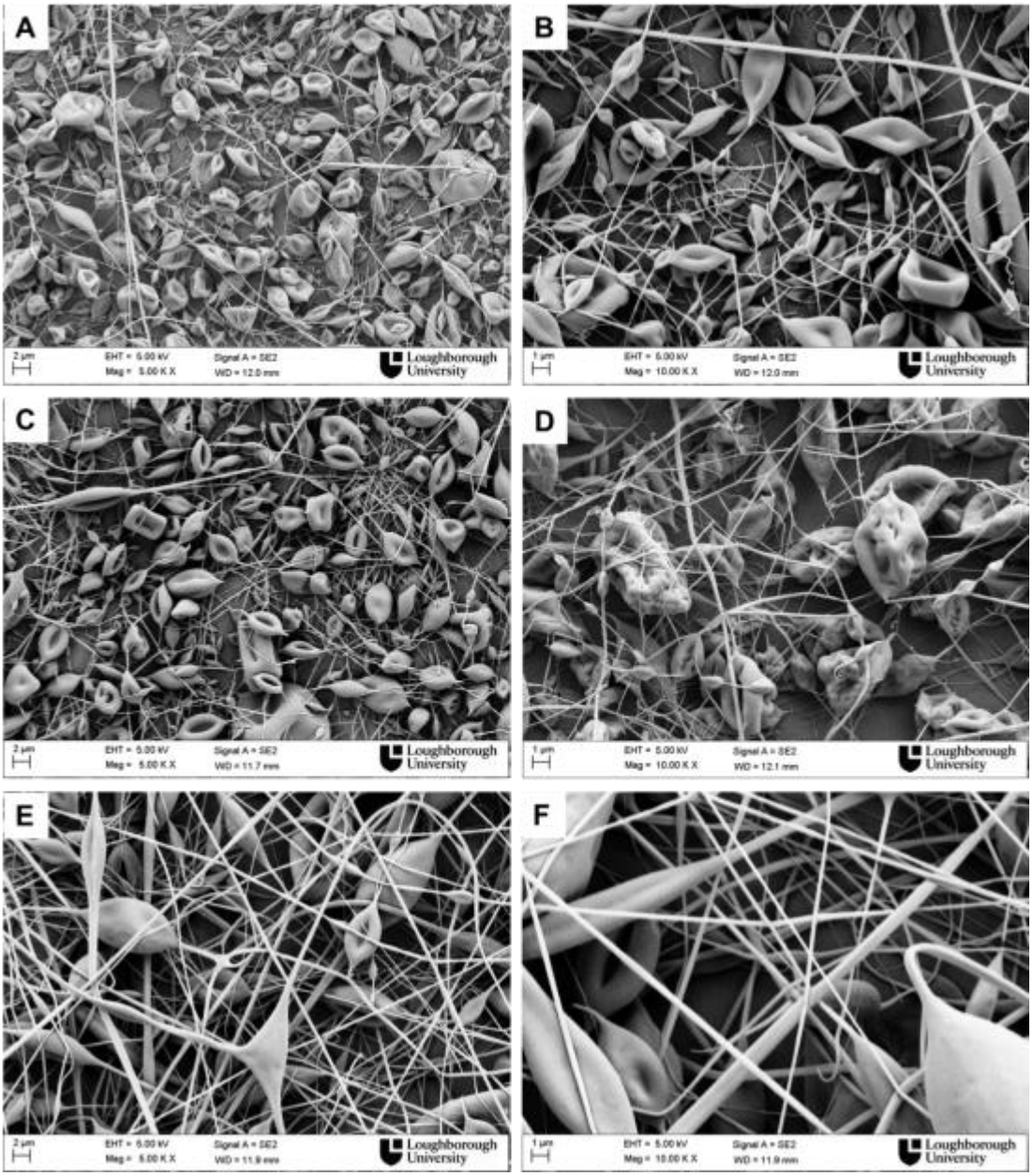

Figure 5.4 – Effect of polymer concentration on nanofibre morphology - scanning electron micrographs of PLA nanofibres from solutions of PLA in AC at concentration (A, B) 6% w/v (5,000 and 10,000 X), (C, D) 7.5% w/v (5,000 and 10,000 X), (E, F) 10 % w/v (5,000 and 10,000 X).

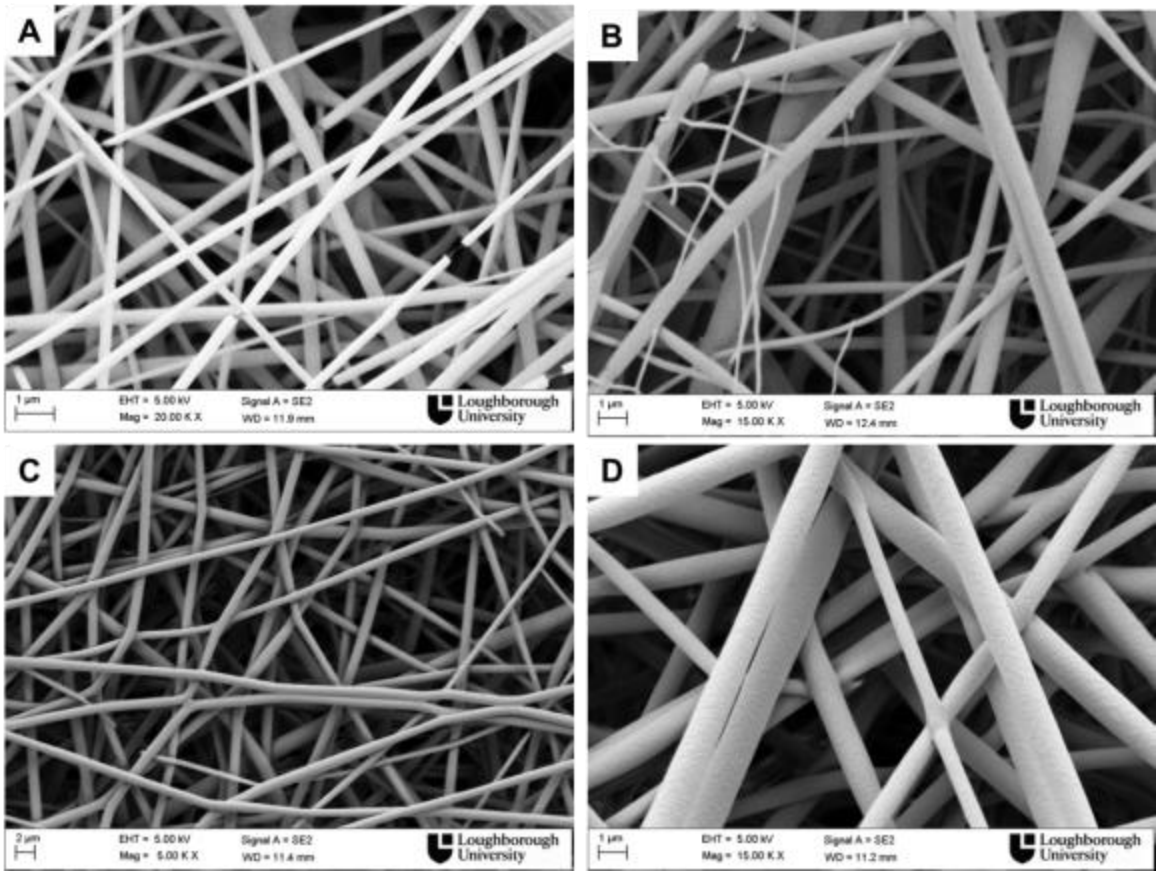

Figure 5.5 – Effect of polymer concentration on nanofibre morphology - scanning electron micrographs of PLA nanofibres from solutions of PLA in AC at concentration (A, B) 12.5% w/v (10,000 and 15,000 X), (C, D) 15.0% w/v (5,000 and 15,000 X).

Figure 5.6 shows the effect of polymer concentration on the mean nanofibre diameter. An increase from 10% to 15% led to an increase of mean diameter from 220 nm to 915 nm, and the bead density is reduced as a result of the higher entanglements density. The electric field strength was fixed, and therefore less degree of stretching imposed by the electrical forces to a more viscous electrospun jet resulted in the production of larger nanofibres.

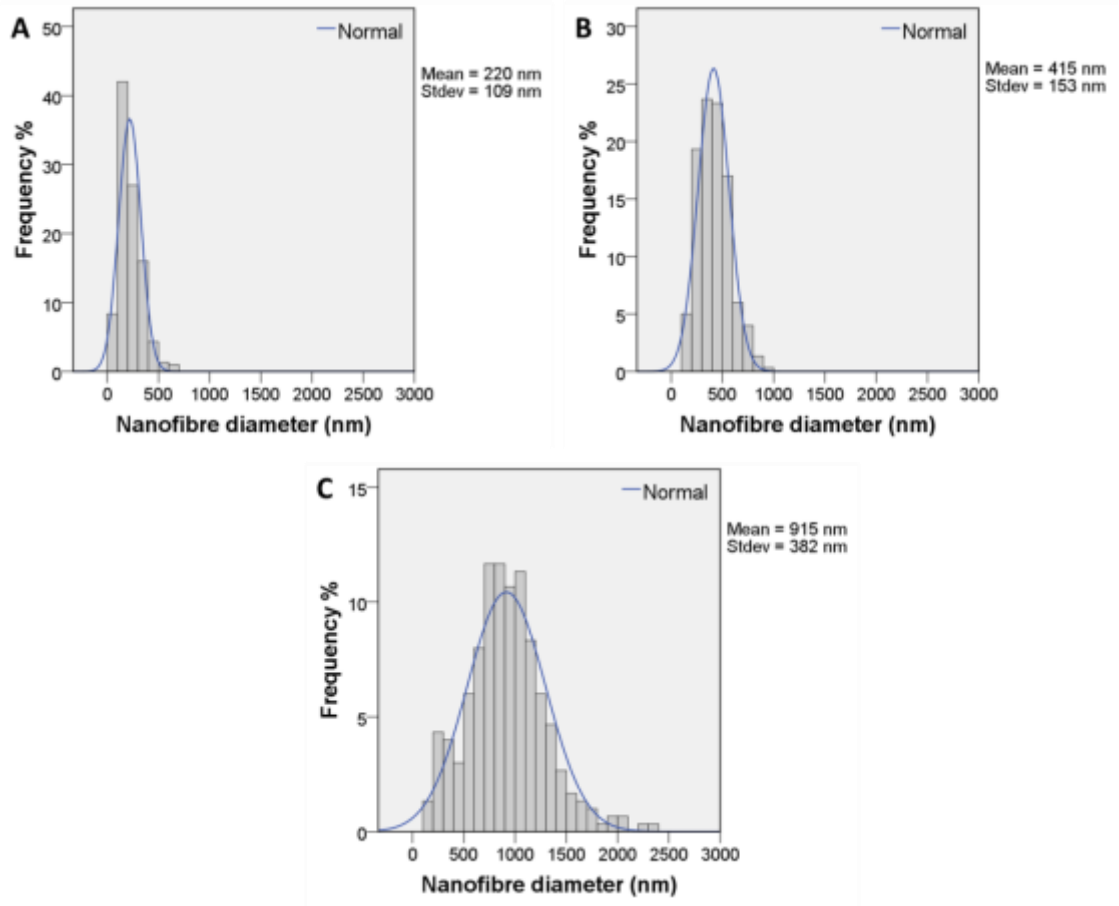

Figure 5.6 – Effect of PLA concentration in AC solution on nanofibre diameter (A) 10% (B) 12.5% (C) 15%.

Similarly PLA concentration was varied from 3% to 20% w/v in PLA solution in DMF and SEM images of the electrospun samples are shown in Figure 5.7. Only beads were collected using solution of concentrations lower than 7.5% w/v and the shape of these beads looks different from those collected from PLA solution in AC. Beads from DMF solution had regular and spherical shape, while those from AC solution had irregular and elliptical shapes. A possible explanation could be related to the lower surface tension of AC (23 mN/m) compared to that of DMF (37 mN/m). During electrospinning the electrical forces have to overcome the surface tension force to form a continuous jet. Therefore the higher surface tension of PLA solution in DMF may lead to a smaller surface area thus resulting in the production of beads with a spherical shape. A few short fibres with a lot of beads were first collected from PLA solution at polymer concentration of 10% (Figure 5.7 B), while a further increase of concentration to 15% gave more nanofibres and some beads (Figure 5.7 D).

Denser nanofibrous mats were formed using a polymer concentration of 17.5% but bead-string morphology was still observed up to 20% w/v as shown in Figure 5.7 F. At concentration higher than 20% w/v the electrospinning process was hard to maintain due to the high viscosity of the solution.

From the morphological analysis it was observed that using DMF as solvent system, a high amount of polymer is needed to form a sufficient entanglements density in solution and therefore to produce continuous nanofibres. Though the RED value for DMF lower than 1 (Table 5.3) indicates the possibility of dissolution of PLA in DMF, the Flory-Huggins value of 1.03 may indicate the poor interactions between the polymer and solvent molecules. Therefore defect-free nanofibres were not collected using only DMF to dissolve PLA at any polymer concentrations. These findings indicate that polymer dissolution in a specific solvent, solution surface tension, conductivity and viscosity cannot be studied separately. Although PLA solutions in DMF have higher conductivity than PLA solution in AC, the higher surface tension together with poor polymer-solvent interactions led to fine nanofibres with many beads. In addition wet nanofibrous mat were formed as a result of the low evaporation rate of DMF from the electrospun jet during its travel towards the collector. DMF has a much higher boiling point compared to AC.

Despite DMF being unsuitable for the production of defect-free PLA nanofibres as a single solvent, the preliminary studies reported in chapter 4 have shown that the addition of DMF to AC at a polymer concentration of 10% w/v was beneficial for the production of thin nanofibres with a narrow diameter distribution.

Results have shown a significant decrease in nanofibre diameter and more uniform diameter distribution for nanofibres produced from PLA solutions in AC/DMF compared to those collected from solutions in AC. For example, the mean fibre diameter for nanofibres produced from AC/DMF solution at 15% w/v was 489±120 nm (refer to paragraph 4.3.4), whereas it was 915±382 nm for nanofibres produced from AC solution at the same polymer concentration. The higher dielectric constant of DMF is responsible for the greater dissociation of positive and negative ions which increases conductivity of AC/DMF solutions. Hence the polymer jet is subjected to higher stretching that led to the production of nanofibres with smaller diameter.

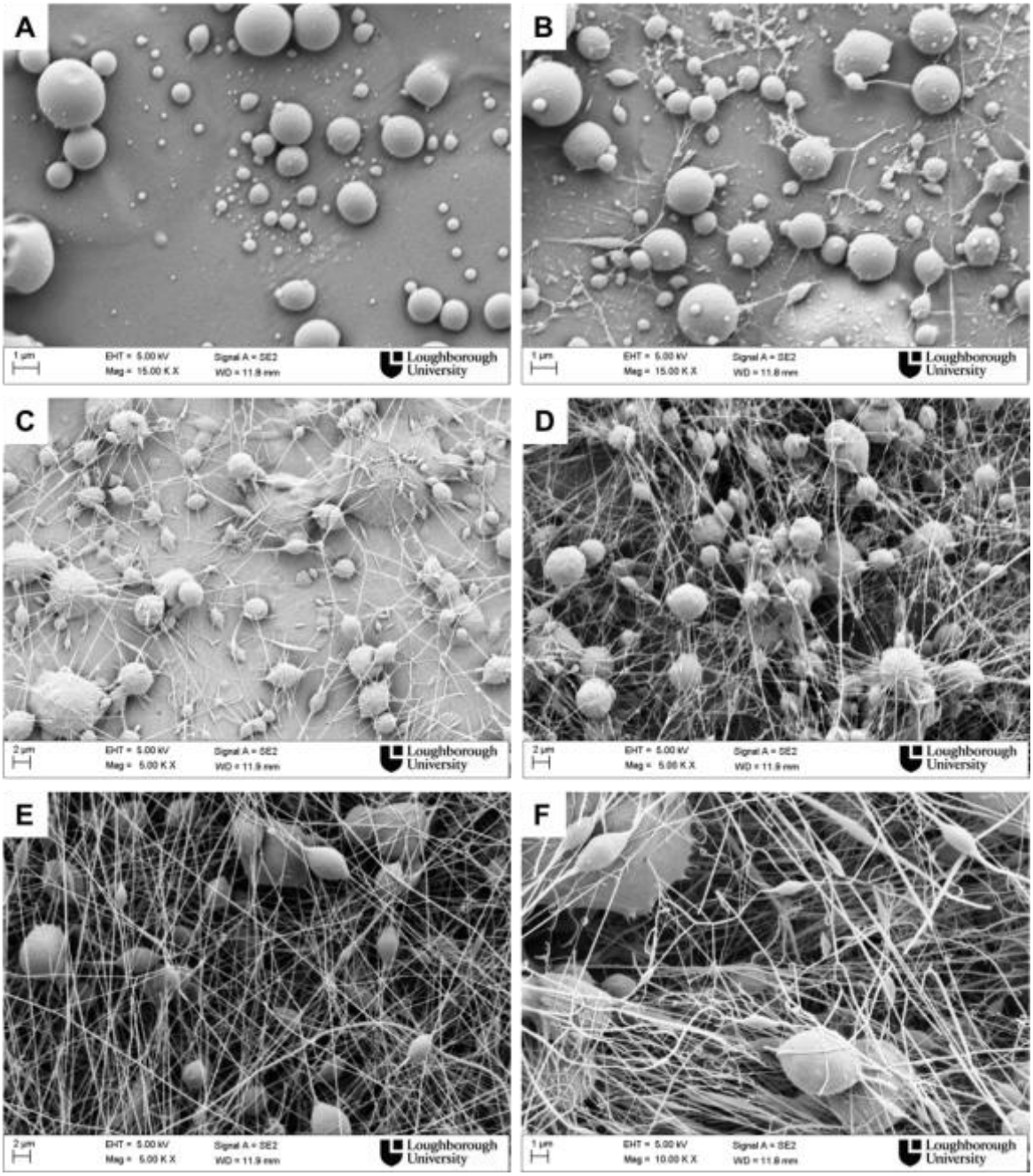

Figure 5.7 – Effect of polymer concentration on nanofibre morphology - scanning electron micrographs of PLA nanofibres from solutions of PLA in DMF at concentration (A) 7.5% w/v (15,000 X), (B) 10% w/v (15,000 X), (C) 12.5% w/v (5,000), (D) 15% w/v (5,000), (E) 17.5% w/v (5,000), (F) 20% w/v (10,000).

The third step of the methodology proposed for the collection of defect-free PLA nanofibres, involved the evaluation of C_e for PLA solution in single solvents, AC and DMF, by rotational and oscillatory tests. An entanglement concentration, C_e, was calculated from shear viscosity and viscoelasticity measurements of PLA solution in the mixture AC/DMF (paragraph 4.3.3). Similarly, oscillatory and rotational test were performed for PLA solutions in AC and DMF. Figure 5.8 A and B show the log-log plot of shear viscosity as a function of PLA concentration in solutions AC and DMF, respectively. Three regimes were found from the log-log plot. The first regime represents the dilute regime, where polymer chains do not overlap and there are no entanglements. The transition between the dilute and semidilute unentangled regime is defined by the critical concentration C^* that occurs at approximately 3% for PLA solution in AC, while at 4% for DMF. Then the rapid viscosity increase suggests the existence of chain entanglements occurring around this concentration, C_e. The value of C* and C_e for PLA solution in the different solvent systems are reported in Table 5.4.

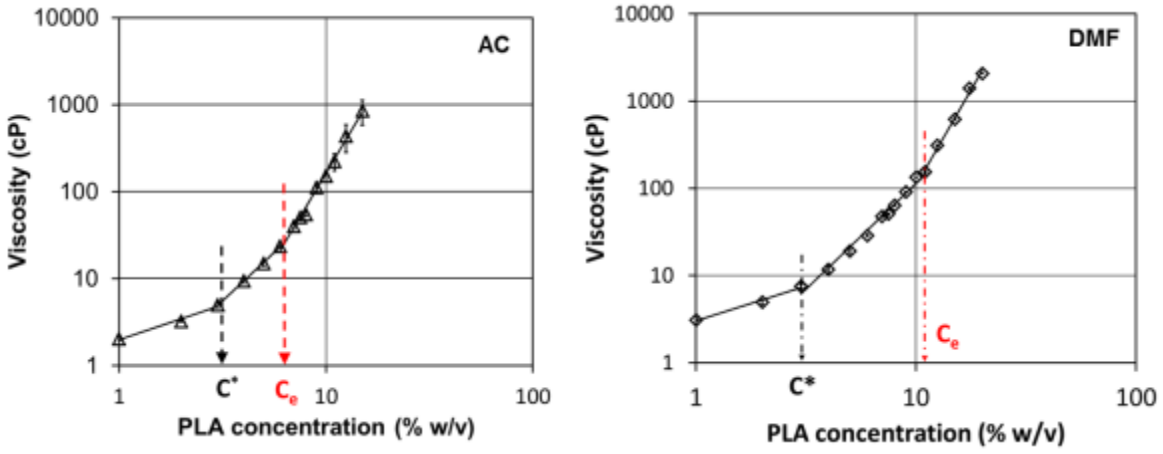

Figure 5.8. Effect of the polymer concentration on the shear viscosity of PLA solution in (A) AC and (B) DMF.

Table 5.4 – Value of overlap (C*) and entanglement (C_e) concentration for all solvent systems.

Solvent	C*(% w/v)	C_e (% w/v)
AC	3.0	**6.3**
DMF	4.0	**10.2**
AC/DMF	3.7	**7.1**

The viscosity of PLA solution in AC (Figure 5.8 A) is proportional to $C^{0.8}$ in the dilute regime, to $C^{2.2}$ in the semidilute unentangled regime, and thereafter is proportional to $C^{4.1}$ in the semidilute entangled regime. The morphological observations of nanofibrous mats collected from PLA solution in AC are consistent with the prediction from the solution viscosity data. In fact, Figure 5.4 A has shown that nanofibres are first formed at a concentration of 6% w/v and the optimum concentration for defect-free nanofibre production is between 2 and 2.5 times the entanglement concentration i.e. 12.5% w/v (see Figure 5.5 A).

Similar to the previous observations, three regimes were found for PLA solutions in DMF as shown in Figure 5.8 B. The entanglement concentration, found to be about 10% w/v, is higher than the concentration found for PLA solution in AC (6%) and that one determined for PLA solution in AC/DMF (7%). As stated in the previous paragraphs, the higher RED value for DMF compared to AC indicates poor interactions between PLA and DMF. Therefore this explains the higher C_e. Figure 5.7 shows that nanofibres are first collected at a concentration between 10 and 12.5% w/v, indicating good agreement of the prediction of C_e between the morphological observations and the solution viscosity data. The PLA concentration needed to produce defect-free nanofibres should be around 25% w/v, but this solution was too viscous to electrospun.

The next step involved the measurements of elastic and plastic moduli of PLA solution in single solvents, AC and DMF. However no results are reported for solution in AC due to the high volatility of AC which resulted in no reproducible oscillatory measurements. Figure 5.9 shows a log-log plot of the values of G’ and G’’ versus the polymer concentration, where the plasticity (G”) of the solution is always higher than the elasticity (G’) at any concentration. A linear relationship between G’’ and the polymer concentration was observed, while a change of slope was evaluated for the elastic modulus G’ at a concentration around 9.8% w/v. This value was approximately the same as the entanglement concentration (C_e) found from the

log-log plot of viscosity reported in Figure 5.4 (10.2% w/v). The change in slope occurred at a concentration of 7.7% w/v for PLA solution in AC/DMF (paragraph 4.4.4), in good agreement with the value of 7.1% w/v for the entanglement concentration (C_e) found from the viscosity measurements (Table 5.4).

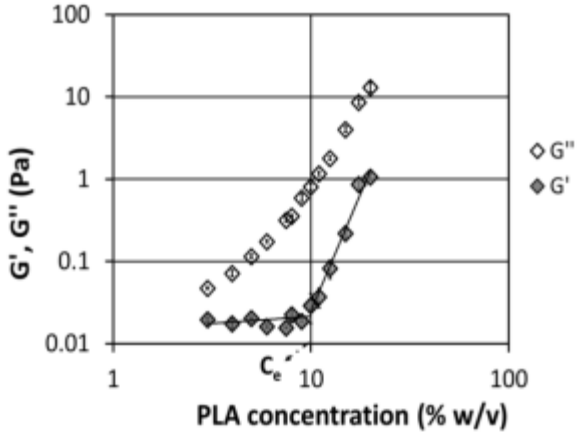

Figure 5.9. Effect of PLA concentration on elastic (G') and plastic (G") modulus of PLA solution in DMF.

To summarise, a three step integrated methodology has been proposed for the selection of solvent systems to produce electrospinnable solutions that form defect-free poly (lactic acid) nanofibres with narrow diameter distribution. The methodology includes 1) initial choice of solvent by solubility evaluation to meet thermodynamic criteria 2) solution conductivity adjustment by using solvent mixtures to meet electrical property criteria, and 3) critical entanglement concentration (C_e) determination by viscosity measurements, supported by elastic and plastic moduli measurements, followed by concentration adjustment to meet rheological criteria.

5.3.4 Validation of the methodology

DX and CHL were selected as solvents for PLA. These solvents have Flory-Huggins parameter lower than 0.5 and RED values lower than 1 indicating therefore they are good solvents for PLA (Table 5.1 and Table 5.3) and in fact homogeneous PLA solutions were prepared. However no nanofibres were collected using PLA solution in DX at a concentration

of 10% w/v, as shown in Figure 5.10 A and as initially found (refer to 4.3.1). Only beads were formed most probably due to the combined effect of high solution surface tension and very low electric conductivity (0.01 μS/cm) (Table 5.5). In addition, the solution accumulated at the needle tip as a result of the low volatility of the solvent and therefore it was necessary to stop the experiment and clean the needle to avoid its clogging. On increasing the polymer concentration to 15% w/v very few nanofibres were collected (Figure 5.10 B), but the higher solution viscosity of 2073 cP (Table 5.5) inhibited the electrospinning process and consequently dense nanofibrous mat was not formed.

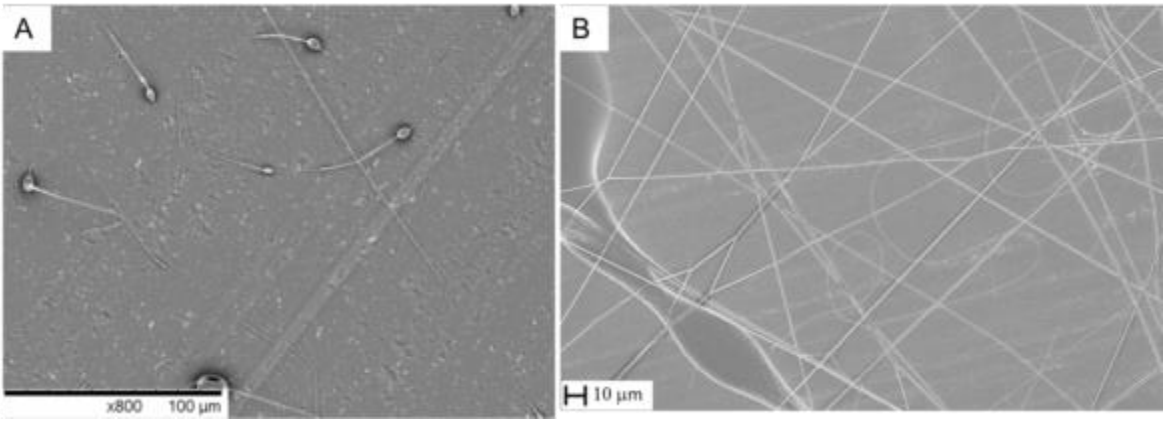

Figure 5.10 – Scanning electron micrographs of PLA nanofibres from solutions of PLA in DX at a concentration of (A) 10% w/v and (B) 15% w/v.

Table 5.5 – Viscosity, surface tension and conductivity of PLA solution in DX and CHL.

Solvent system	PLA concentration (% w/v)	η (cP)	σ (mN/m)	K (μS/cm)
DX	10	435.3±10.7	35.52±0.26	0.01
	15	2073±460.7	36.02±0.36	0.01
CHL	10	354.9±17.5	30.80±0.27	0.01
	15	1427±165	31.62±0.23	0.01

Figure 5.11 shows SEM micrographs of the samples collected from electrospinning of PLA solution in CHL. Although few nanofibres were collected using solution at concentration of 10%, only few fibres were formed as a result of the high solvent volatility, and a further increase of the polymer concentration to 15% did not enhance the electrospinning process. However, a few more nanofibres seemed to be collected using CHL as solvent system compared to DX. This could be due to the slightly lower surface tension of about 31 mN/m of

PLA solution in CHL compared to 35 mN/m of PLA solution in DX. However no dense nanofibrous webs were collected from both solutions in DX and CHL.

When comparing CHL and AC, it can be observed that they have a similar boiling point (61°C and 56°C, respectively), but there is a large difference in the dielectric constant. AC is more polar solvent with dielectric constant of 20.6 compared to that of CHL (4.8). The successful production of nanofibres with bead string morphology from PLA solution in AC at polymer concentration of 10% (Figure 5.4 E, F) can be explained by the higher dielectric constant and hence higher charge density on the electrospun jet.

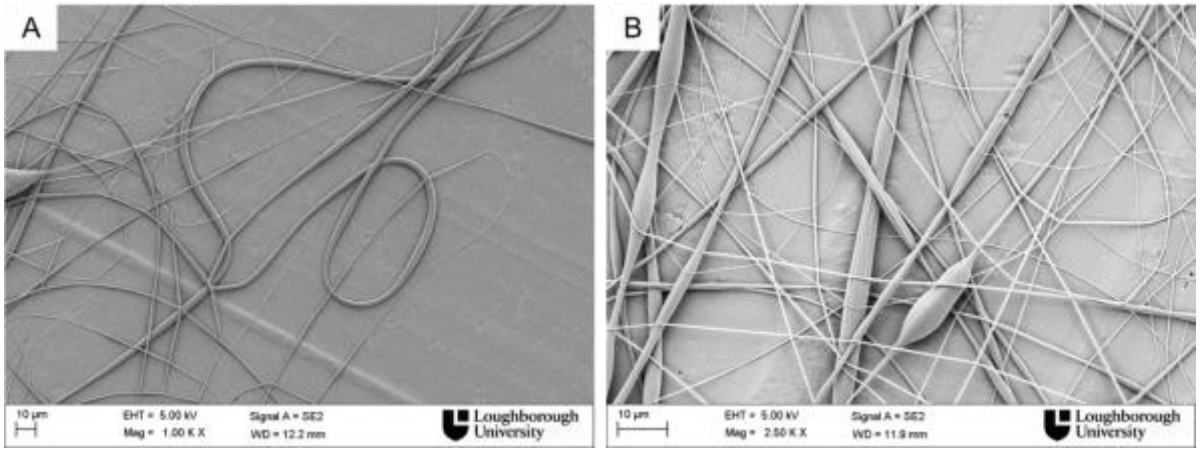

Figure 5.11. Scanning electron micrographs of PLA nanofibres from solutions of PLA in CHL at a concentration of (A) 10% w/v and (B) 15% w/v.

In the next paragraph, the second step of the methodology is implemented by addition of DMF to DX and CHL. A significant increase of solution conductivity to about 3 μS/cm was measured for PLA solution in DX/DMF (Table 5.6), together with an increase of surface tension from 30 to 36 mN/m but a decrease of solution viscosity from 354 cP to 205 cP. Morphological analysis on the samples collected was performed and the results are shown in Figure 5.12. Dense nanofibrous mats were collected from PLA solutions at polymer concentration of 10 and 15%, although a few beads were detected using the lower concentration of 10%. This may indicate these concentrations are higher than an entanglement concentration C_e, resulting therefore in the collection of uniform smooth nanofibres.

Table 5.6. Viscosity, surface tension and conductivity of PLA solution in DX/DMF and CHL/DMF.

Solvent system	PLA concentration (% w/v)	η (cP)	σ (mN/m)	K (μS/cm)
DX/DMF	10	275.4±24.2	36.32±0.51	3.08±0.10
	15	1031±51.2	36.96±0.30	2.77±0.11
CHL/DMF	10	205.1±6.3	33.64±0.38	1.68±0.05
	15	980.1±75.0	34.24±0.17	1.23±0.03

Similarly to the previous observations, the addition of DMF to PLA solution in CHL improved the electrospinning process and led to defect-free nanofibres as shown in Figure 5.13. The increase amount of electric charges with the addition DMF resulted in higher solution conductivity in both solution in DX and CHL. Hence under the electric field, higher electrostatic forces are responsible of the higher stretching of the electrospun polymeric jet, and the sufficient entanglements between the polymers chains can resist the stretching imposed by the electrostatic forces. This led to a continuous jet emitted from the needle tip resulting in the formation of dense uniform defect-free electrospun webs.

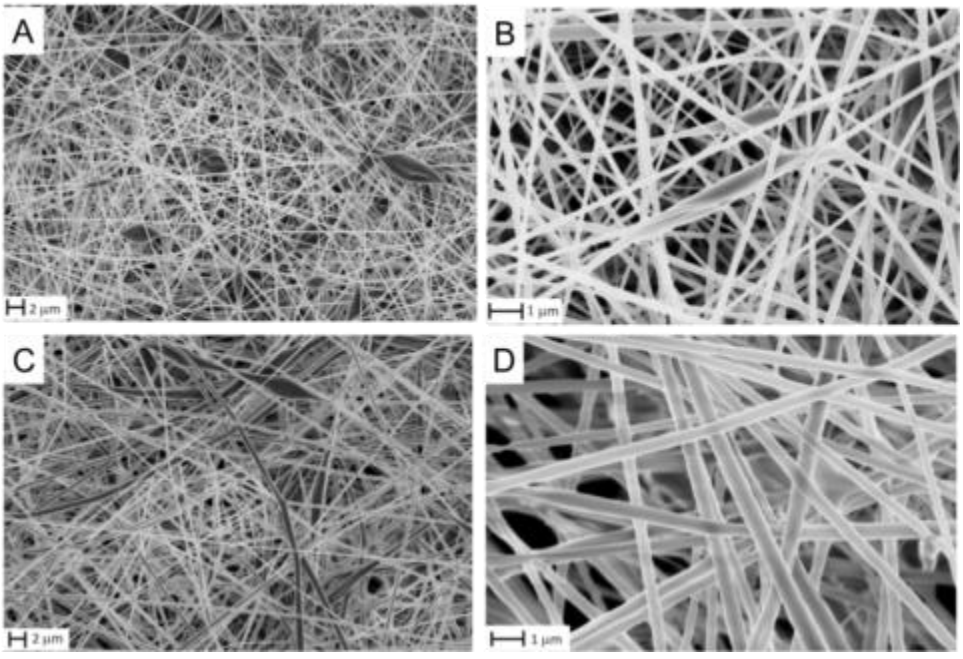

Figure 5.12. Scanning electron micrographs of PLA nanofibres from solutions of PLA in DX/DMF (50/50 v/v) at concentration of 10% w/v 5000x (A) and 20000x (B), and concentration of 15% w/v 5000x (C) and 20000x (D).

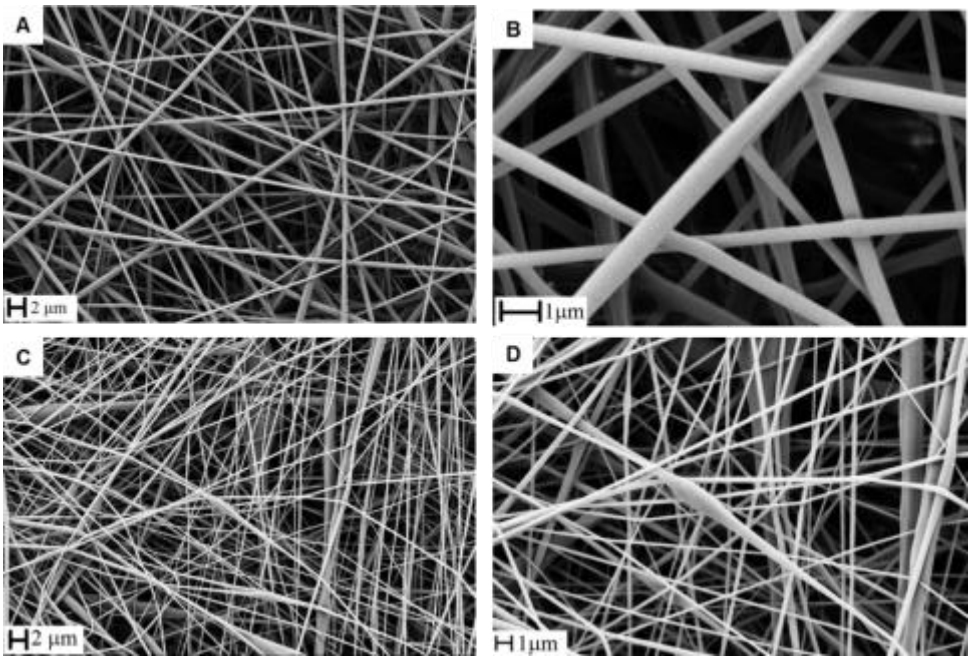

Figure 5.13. Scanning electron micrographs of PLA nanofibres from solutions of PLA in CHL/DMF (50/50 v/v) at concentration of (A, B) 10% w/v (5000x and 25000x), (C, D) 15% w/v (5000x and 10000x).

Next, measurements of nanofibre diameter were carried out and the diameter distribution is reported in Figure 5.14. Nanofibres with diameter of 262±70 nm and of 153±28 were formed from 10% PLA solution in DX/DMF and CHL/DMF, respectively, while larger nanofibres (377±89 nm and 466±118 nm) were formed at 15%, as a result of the higher solution viscosity (Table 5.6).

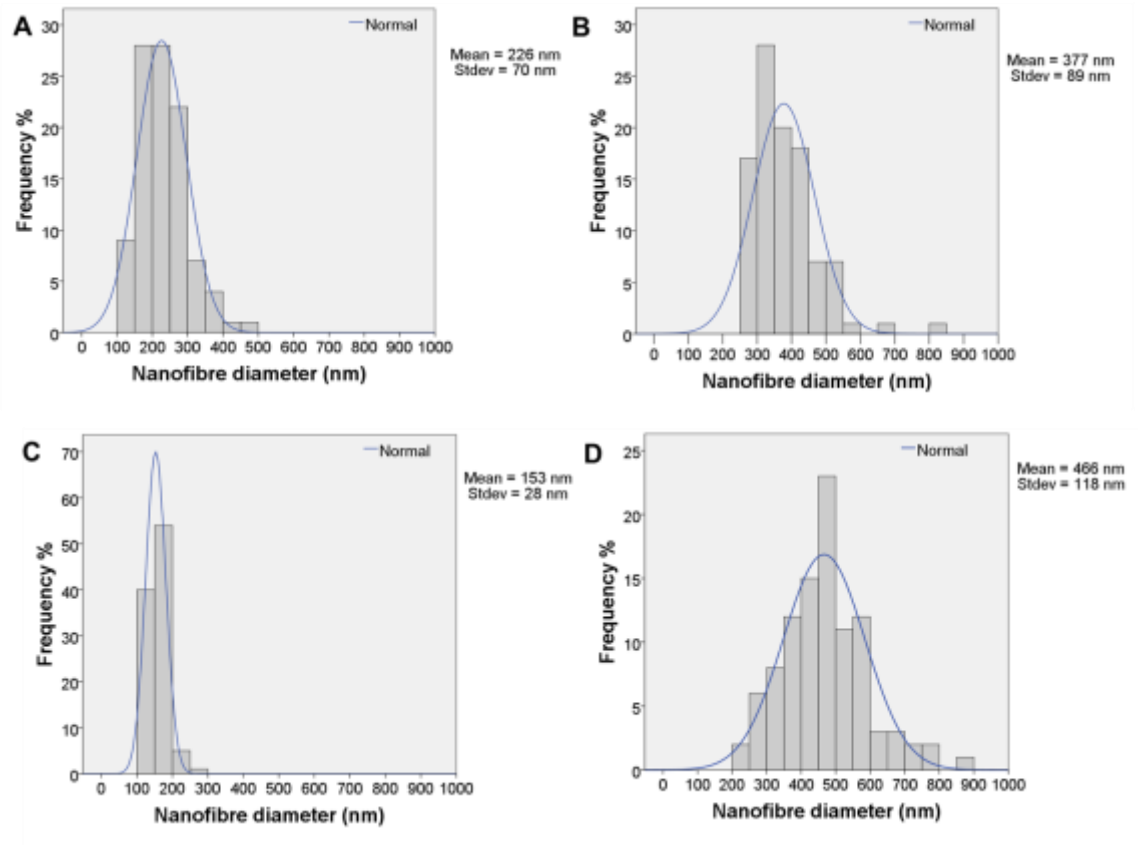

Figure 5.14. Diameter distribution of nanofibres collected from PLA solution in DX/DMF at concentration of (A) 10% and (B) 15%, and PLA solution in CHL/DMF at concentration of (C) 10% and (D) 15%.

These results suggest that the requirements for successful solution electrospinnability and hence the production of thinner defect-free nanofibres, are: low RED value, high dielectric constant of the solvent, low solution surface tension and sufficient chain entanglements density.

5.4 Conclusion

The main objective of this study was to propose a methodology for the selection of solvent systems to produce electrospinnable solutions that form defect-free nanofibres with narrow diameter distributions.

The first step was to select the most suitable solvent using a thermodynamic approach. The

Flory-Huggins parameter is lower than 0.5 for PLA solution in AC, CHL and DX, indicating that they are good solvents for PLA, whereas χ is higher than 0.5 for PLA solution in DMF representing poor interactions between solvent molecules and polymeric chains. However the RED values are a better indication of the polymer solubility. All solvent systems used in this work present RED values lower than 1 indicating good dissolution of the polymer. In fact, it was possible to dissolve PLA in all solvent system and form homogeneous solutions.

The second step was to optimise the solution electrical properties to produce defect-free nanofibres with narrow diameter distribution. DX, CHL and DMF did not produce defect-free fibres when used as single solvents, the first two due to their low dielectric constant and the last one probably due to its high boiling point and χ parameter. However, when DX and CHL were combined in a binary mixture with DMF defect-free fibres were produced. The addition of a solvent with high dielectric constant enables the formation of defect-free fibres. Similarly, the addition of DMF to PLA solution in AC enhanced the electrospinning process and the thinner nanofibres were collected.

The third step was to choose the optimum polymer concentration to collect defect-free nanofibres. The effect of the polymer concentration on the solution viscosity showed a sharp increase of viscosity and the elastic modulus at chain entanglement concentration, C_e, of approximately 6% w/v and 7% w/v for PLA solution in AC and AC/DMF, respectively, whereas higher entanglement concentration (10.2% w/v) was found for PLA solution in DMF. Nanofibres were first formed at a concentration about C_e as shown from the morphological observation, while defect-free nanofibres at a concentration about 2 or 2.5 times C_e. The important finding is the higher entanglement concentration for PLA solution in DMF. AC is solvent better solvent for PLA than DMF. Hence the polymer coils in DMF solution will contract and the entanglements between the polymer chains are weak. Therefore the formation of beads or beaded nanofibres occurred. On the other hand, for a good solvent (AC) interaction between polymer chains and solvent molecules are energetically favorable. This causes polymer coils to expand, entanglements are strong and therefore nanofibres can be produced.

Summarizing the observations, the methodology proposed in this work follows three steps:

1- solubility parameter criteria (χ and RED);

2- high dielectric constant (polar solvents);

3- polymer concentration higher than the entanglement concentration C_e.

This methodology was applied for poly (lactic acid), but it would very useful for many other polymers. The methodology takes into account thermodynamic and rheology. It would allow the selection of the most appropriate solvent or mixture of solvents for a specific polymer or polymer blends and may consent to simplify the solvent selection process and improve current 'trial and error' practices used. Additionally the methodology may allow the selection of greener solvents which is still one of the main challenges of solution electrospinning.

6 ANALYSIS OF THE EFFECT OF ELECTROSPINNING PROCESS PARAMETERS ON THE JET ELECTRIC CURRENT AND ON NANOFIBRE MORPHOLOGY AND MEAN DIAMETER

6.1 Introduction

The output of an electrospinning process is affected by several parameters, which have been divided in three groups, solution, process and ambient parameters as reported in the literature review of this thesis. After selection of an appropriate solvent system and hence solution properties, the process parameters may be optimised for the production of dense uniform nanofibrous webs. The effect of process parameters including voltage, flow rate and collection distance on the electrospun nanofibre morphology and mean diameter has been investigated for several polymers such as PCL, PEO, PA6 and PHBV (Bosworth & Downes 2012; Chowdhury & G. K. Stylios 2012; Chowdhury & G. Stylios 2010; Zuo et al. 2005). However depending on the type of polymer and polymer-solvent system, different results have been reported. In particular, the effect of voltage on nanofibre diameter and morphology has shown controversial results. Even though the majority of the studies have presented a reduction of the nanofibre diameter with an increase of the applied voltage, it has been also reported that nanofibres with larger diameter may be formed at higher voltages.

Table 6.1 presents a summary of the effect of the applied voltage for different polymer-solvent systems. In addition different observations have been reported for the same polymer at different polymer concentrations and process conditions. An increase of applied voltage from 12 to 18 kV led to the production of PEO nanofibres with smaller diameter using PEO solution at polymer concentration of 12% w/w (Chowdhury & G. K. Stylios 2012), while a 5% w/w PEO solution resulted in nanofibres with larger diameter on increasing applied voltage from 3 to 7 kV (Morota et al. 2004). This may be due to several factors including different polymer molecular weights, solution flow rates and ambient conditions.

Table 6.1 – List of scientific publications investigating the effect of applied voltage on the nanofibre morphology and diameter.

Polymer	**M_w**	**Solvent**	**Concentration**	**Distance**	**Flow rate**	**Voltage**	**Effect on nanofibre diameter** **increasing applied voltage**	**Reference**
	kg/kmol		**% w/w**	**cm**		**kV**		
PVA	Mn 65, 96% DH	H_2O	11	8	/	from 7 to 19	DIAMETER DECREASES	Ding et al 2002
PVA	/	H_2O	10	10	/	from 10 to 25		Lee et al 2004
PCL	40	CHL	5	7.5	0.1 ml/min	from 20 to 40		Hsu & Shivkumar 2004
PDLA	100	CHL:AC (3:1)	3, 5, 7	15	/	10, 14, 18		Gu & Ren 2005
PA6	/	TFE	11	14	/	from 12 to 21		Li et al 2006
PA6	/	FA	20	/	/	12, 15, 18		Chowdhury & Stylios 2010
PEO	300	H_2O or (H_2O+EtOH)	12	11	/	12, 15, 18		Chowdhury & Stylios 2012
PEO	20, 500, 4000	H_2O	5	7	/	from 3 to 7	DIAMETER INCREASES	Morota 2004
PMMA	135, 150	EtOH	10, 15, 20	15	/	from 7.5 to 22.5		Pornsopone 2005
PVA	DH 98%	H_2O	7	15	0.2 ml/h	from 5 to 13		Zhang 2004
PLGA	from 15 to 81	THF/DMF (3:1)	10	15	1 ml/h	from 14 to 22	↑ from 14 to 20 kV, then ↓ at 22 kV	Liu et al 2009

Electrospinning is a complex electrohydrodynamic process where many factors can affect the final morphology and diameter of the nanofibres and some of these factors are closely dependent on each other. The derivation of one universal correlation between the nanofibre diameter and all parameters affecting the electrospinning process is a major challenge. Moreover control over the diameter of electrospun nanofibres is still a bottleneck. So far only one group of researchers proposed a simple equation to predict the final diameter of the nanofibres collected (Sergey V Fridrikh et al. 2003) which is function of flow rate Q, electric current I, surface tension γ, dielectric permittivity of the surrounding air and the whipping instability. This equation was determined by the balance between solution surface tension and electrostatic charge repulsion, but polymer concentration, solvent evaporation and viscoelastic effects were neglected (refer to paragraph 2.1.1.1, Equation 2). In order to use this equation the value of electric current *I* should be measured, but in most scientific publications the electric current is not usually recorded. There is still a lack of experimental studies about the effect of electric current on the nanofibre morphology and diameter. Different electrospinning setups have been used when measuring the electric current by a few researchers. A plate-plate electrospinning apparatus consists of two aluminium disks and a small needle was used by Fridrikh and Fallahi (Sergey V Fridrikh et al. 2003; Delaram Fallahi et al. 2008), while a needle-plate configuration was employed by other researchers (Samatham & K. J. Kim 2006; Demir et al. 2002; S. A. Theron et al. 2004; S. J. Kim et al. 2004). An integrated current measurement system in the electrospinning apparatus would be very useful resulting in a qualitative approach to predict the final morphology of the nanofibrous webs. Moreover the prediction of the mean nanofibre diameter would offer a great advantage because nanofibrous structures with reproducible properties including diameter, porosity and mechanical properties, are required in many applications.

6.2 Aims and objectives

The aims of the work presented in this chapter consisted in investigating the effect of process parameters on the morphology of electrospun PLA nanofibre and mean diameter, and on comparing the experimental fibre diameter versus the predicted value.

The achievement of these aims was possible through the realisation of the following objectives:

- Electrospinning of poly (lactic acid) solution in AC/DMF by varying applied voltage, solution flow rate and collection distance;
- Measurements of electric current *I* for all experiments to improve the understanding of the process by using the proposed model and to determine the factors that cause deviations from the predicted behaviour.

6.3 Results and discussion

6.3.1 Effect of process parameters on the nanofibre morphology and mean diameter

The results reported in chapter 4 have shown that defect-free uniform nanofibres with narrow diameter distribution (210±36 nm) were produced using PLA solution in AC/DMF 50/50 at concentration of 12.5% w/v. Therefore the effect of process parameters on nanofibre morphology and mean diameter was investigated for this solution. The experiments performed in this section are reported in Table 6.2. The value of applied voltage was 7.5, 10, 15 and 20 kV, the flow rate set by the syringe pump was 0.5, 1 and 2 ml/h, and the collector was placed at 10 and 15 cm from the needle tip.

Table 6.2 – List of experiments performed.

N. EXPERIMENT	VOLTAGE	FLOW	DISTANCE
	kV	ml/h	cm
1	20	1	15
2	20	1	10
3	20	0.5	10
4	20	0.5	15
5	15	1	15
6	15	0.5	15
7	15	0.5	10
8	15	1	10
9	10	0.5	10
10	10	0.5	15
11	10	1	10
12	10	1	15
13	7.5	0.5	10
14	7.5	0.5	15
15	7.5	1	15
16	7.5	1	10
17	7.5	2	10
18	7.5	2	15
19	10	2	10
20	10	2	15
21	15	2	10
22	15	2	15
23	20	2	10
24	20	2	15

Morphological analysis of the electrospun nanofibrous mats was performed using scanning electron microscopy (SEM). Figure 6.1, Figure 6.2, Figure 6.3 and Figure 6.4 show micrographs of PLA nanofibres produced using voltage of 7.5, 10, 15 and 20 kV, respectively, at several flow rates and collection distances. The applied voltage has an influence on the stretching and acceleration of the jet towards the collector. Hence different morphologies of the electrospun webs and nanofibres with different diameters may be formed with variation of applied voltage.

Overall the nanofibres produced at 7.5 kV and 10 kV had a cylindrical and smooth morphology with very few or no defects within the mats as shown in Figure 6.1 and Figure 6.2. At voltage of 7.5 kV and flow rate 0.5 ml/h, the PLA solution accumulated at the needle tip and a stable electrospun jet was emitted resulting in the formation of defect-free nanofibres (Figure 6.1 A-D). However, on increasing flow rate from 0.5 to 1 ml/h the

electrically charged drop was elongated and few solution droplets were seen in front of the collector. Figure 6.1 E-H show the formation of few defects within the nanofibrous mats and similarly beaded nanofibres were collected on further increasing flow rate to 2 ml/h as shown in Figure 6.5 A-D.

With an increase of applied voltage to 10 kV, successful production of defect-free nanofibres was achieved at flow rate of 0.5 and 1 ml/h (Figure 6.2). The increase of applied voltage from 7.5 to 10 kV at 1 ml/h led to a more stable electrospun jet towards the collector and this may explain the reduction of bead formation within the nanofibrous mats collected. As reported in chapter 2, the electric field strength (E) is defined as the ratio between applied voltage and collection distance. Therefore an increase of voltage leads to an increase of E at a fixed collection distance and consequently higher electrostatic forces are responsible for higher degree of stretching of the electrospun jet. Nevertheless, when the flow rate was doubled (2 ml/h), a few droplets were seen in front of the collector similarly to the observations at 7.5 kV and 2 ml/h (Figure 6.5).

PEO aqueous solution was electrospun at several flow rates and nanofibrous mats were collected (Chowdhury & G. K. Stylios 2012). While beaded nanofibres were collected using the lowest and highest flow rate, 0.2 ml/h and 0.3 ml/h, respectively, efficient production of smooth defect-free nanofibres was achieved at 0.25 ml/h. Only few scientific publications have reported the effect of flow rate on the nanofibre morphology and diameter (Chowdhury & G. K. Stylios 2012; Megelski et al. 2002; C. Zhang et al. 2005).

SEM micrographs in Figure 6.3 and Figure 6.4 show the morphology of the nanofibrous mats collected using applied voltage of 15 and 20 kV, respectively. At the lowest flow rate few more beads were formed in the electrospun webs compared to the defect-free mats collected at voltages of 7.5 and 10 kV. During the electrospinning process an increase of voltage led to a reduction of the volume of the drop and the Taylor cone. Most probably the higher electrostatic forces removed the polymeric solution at a rate much higher than the flow rate set from the syringe pump. With increasing applied voltage higher repulsion of the charges on the jet surface occurs and hence stronger whipping jet instability is developed. This may explain the formation of a few beads.

Dietzel et al (Deitzel et al. 2001) reported similar findings for the electrospinning of PEO aqueous solutions. The authors collected smooth nanofibres at low voltage (5.5 kV), while

highly beaded fibres were produced on increasing applied voltage (9 kV). As the electric field strength became too high, increased instabilities of the jet may increase bead density (Mazoochi et al. 2012). An increase of voltage leads to more rapid evaporation of the solvent from the jet and therefore the formation of smooth fibres could be impeded because beads on the electrospun jet may be not given time to be stretched.

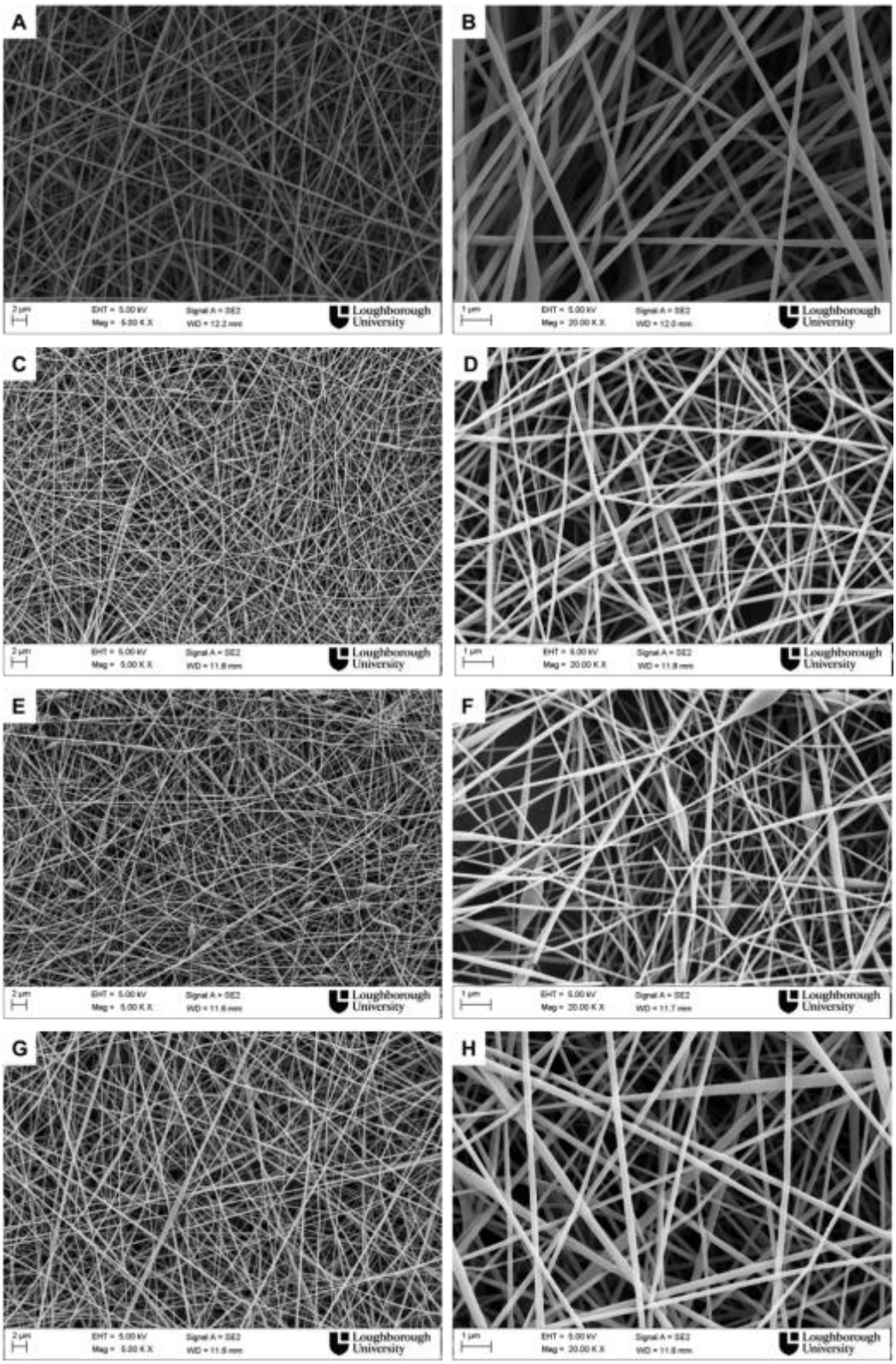

Figure 6.1 – Scanning electron micrographs of PLA nanofibres from solutions of 12.5 % (w/v) of PLA in acetone/dimethylformamide (AC/DMF) (50/50 v/v) at voltage of 7.5 kV (A, B) 0.5 ml/h, 10 cm, (C, D) 0.5 ml/h, 15 cm, (E, F) 1.0 ml/h, 15 cm, (G, H) 1.0 ml/h, 10 cm.

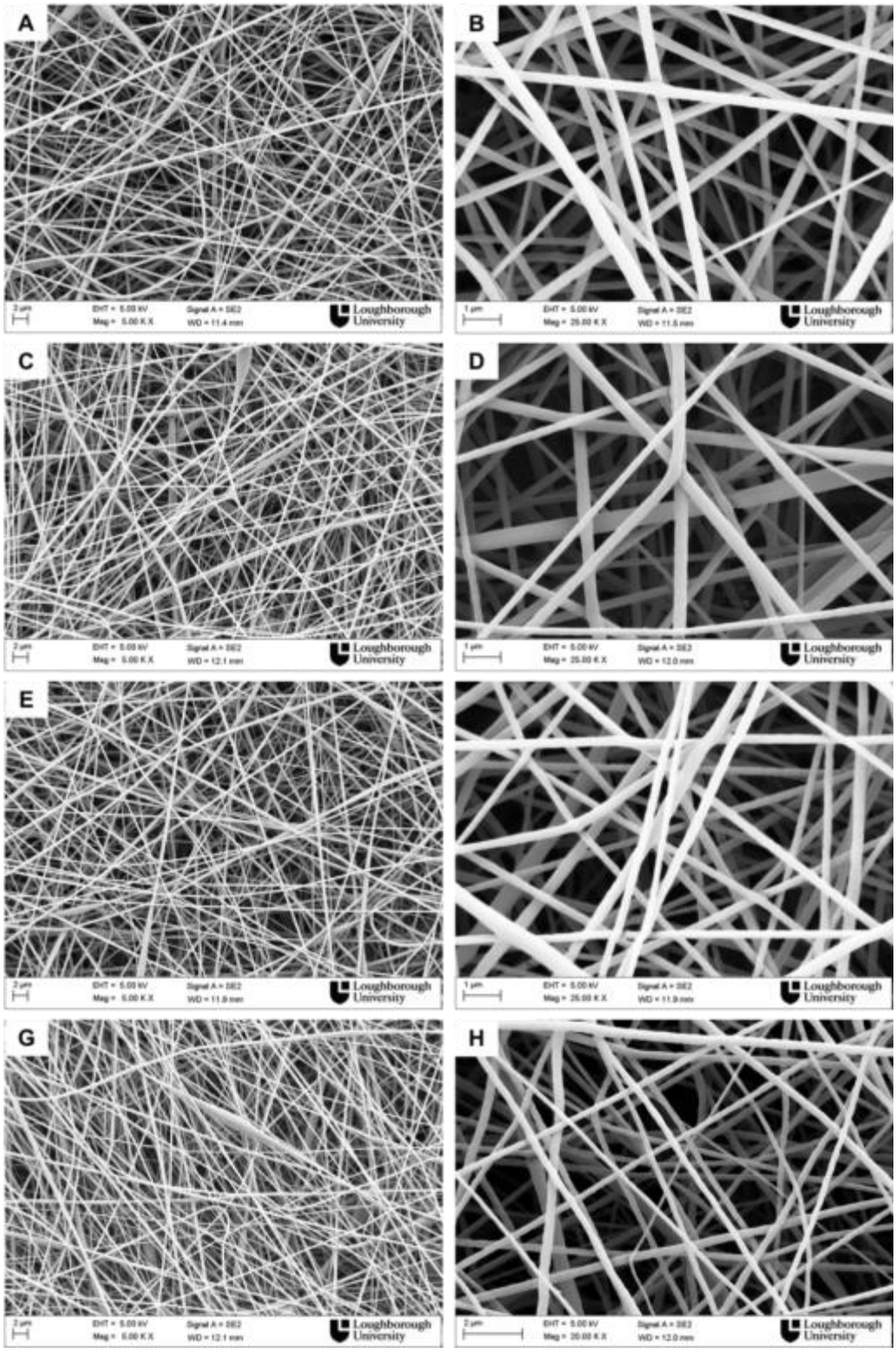

Figure 6.2 – Scanning electron micrographs of PLA nanofibres from solutions of 12.5 % (w/v) of PLA in acetone/dimethylformamide (AC/DMF) (50/50 v/v) at voltage of 10 kV and (A, B) 0.5 ml/h, 10 cm, (C, D) 0.5 ml/h, 15 cm, (E, F) 1.0 ml/h, 10 cm, (G, H) 1.0 ml/h, 15 cm.

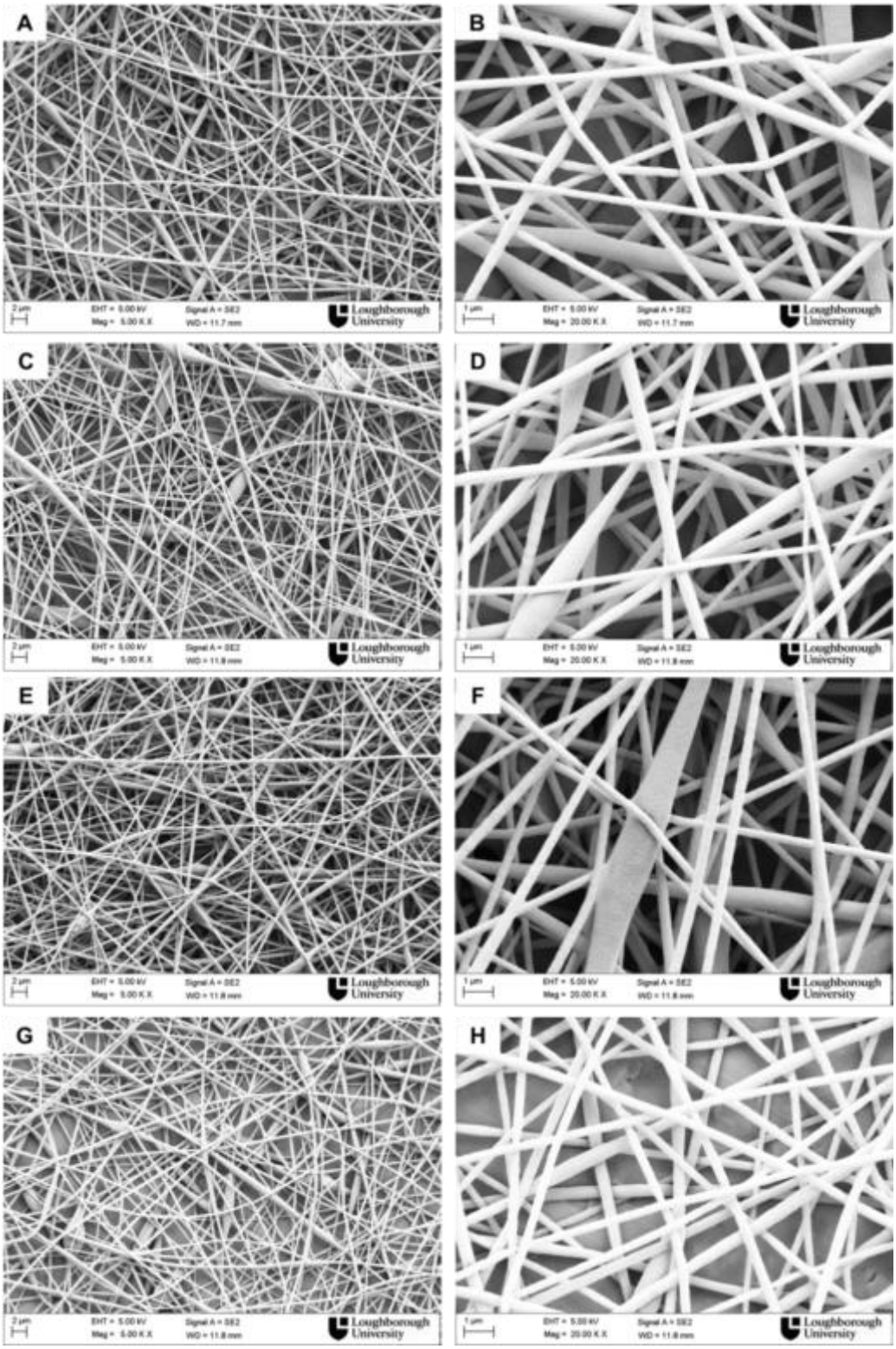

Figure 6.3 – Scanning electron micrographs of PLA nanofibres from solutions of 12.5 % (w/v) of PLA in acetone/dimethylformamide (AC/DMF) (50/50 v/v) at voltage of 15 kV and (A, B) 0.5 ml/h, 10 cm, (C, D) 0.5 ml/h, 15 cm, (E, F) 1.0 ml/h, 10 cm, (G, H) 1.0 ml/h, 15 cm.

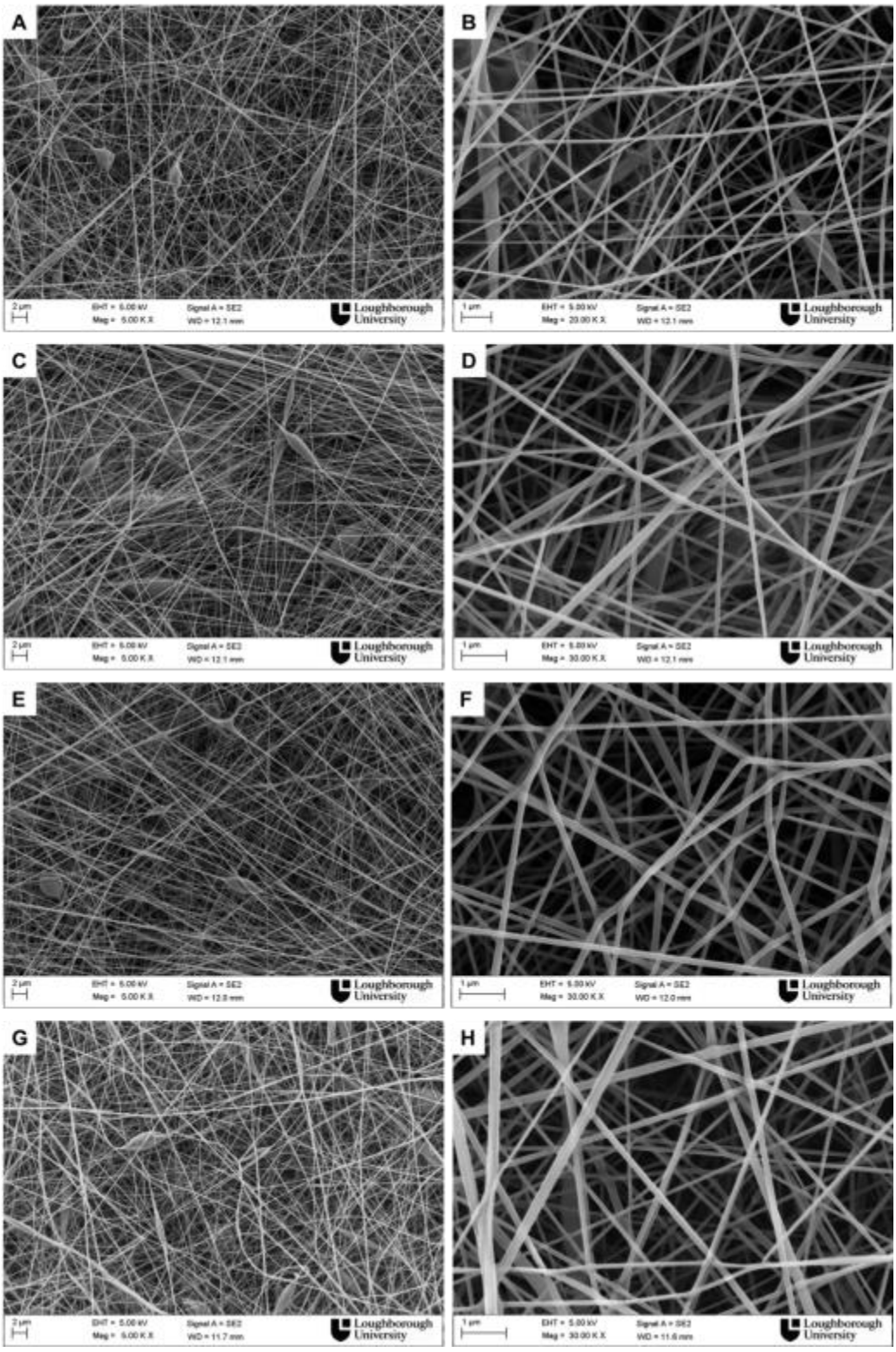

Figure 6.4 – Scanning electron micrographs of PLA nanofibres from solutions of 12.5 % (w/v) of PLA in acetone/dimethylformamide (AC/DMF) (50/50 v/v) at voltage of 20 kV and (A, B) 1 ml/h, 15 cm, (C, D) 1 ml/h, 10 cm, (E, F) 0.5 ml/h, 15 cm, (G, H) 0.5 ml/h, 10 cm.

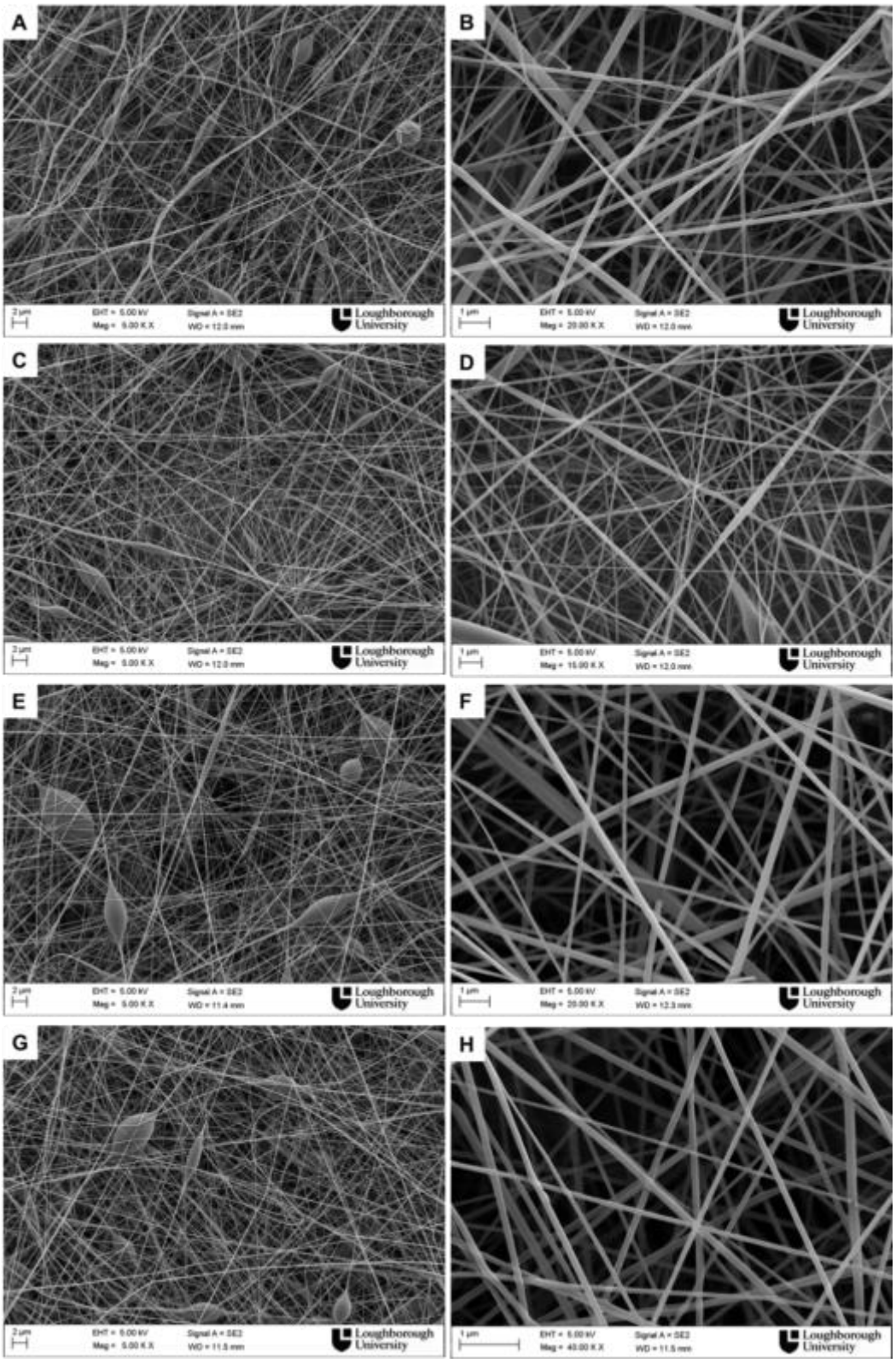

Figure 6.5 – Scanning electron micrographs of PLA nanofibres from solutions of 12.5 % (w/v) of PLA in acetone/dimethylformamide (AC/DMF) (50/50 v/v) at 2 ml/h (A, B) 7.5 kV, 10 cm, (C, D) 7.5 kV, 15 cm (E, F) 10 kV, 10 cm (G, H) 10 kV, 15 cm.

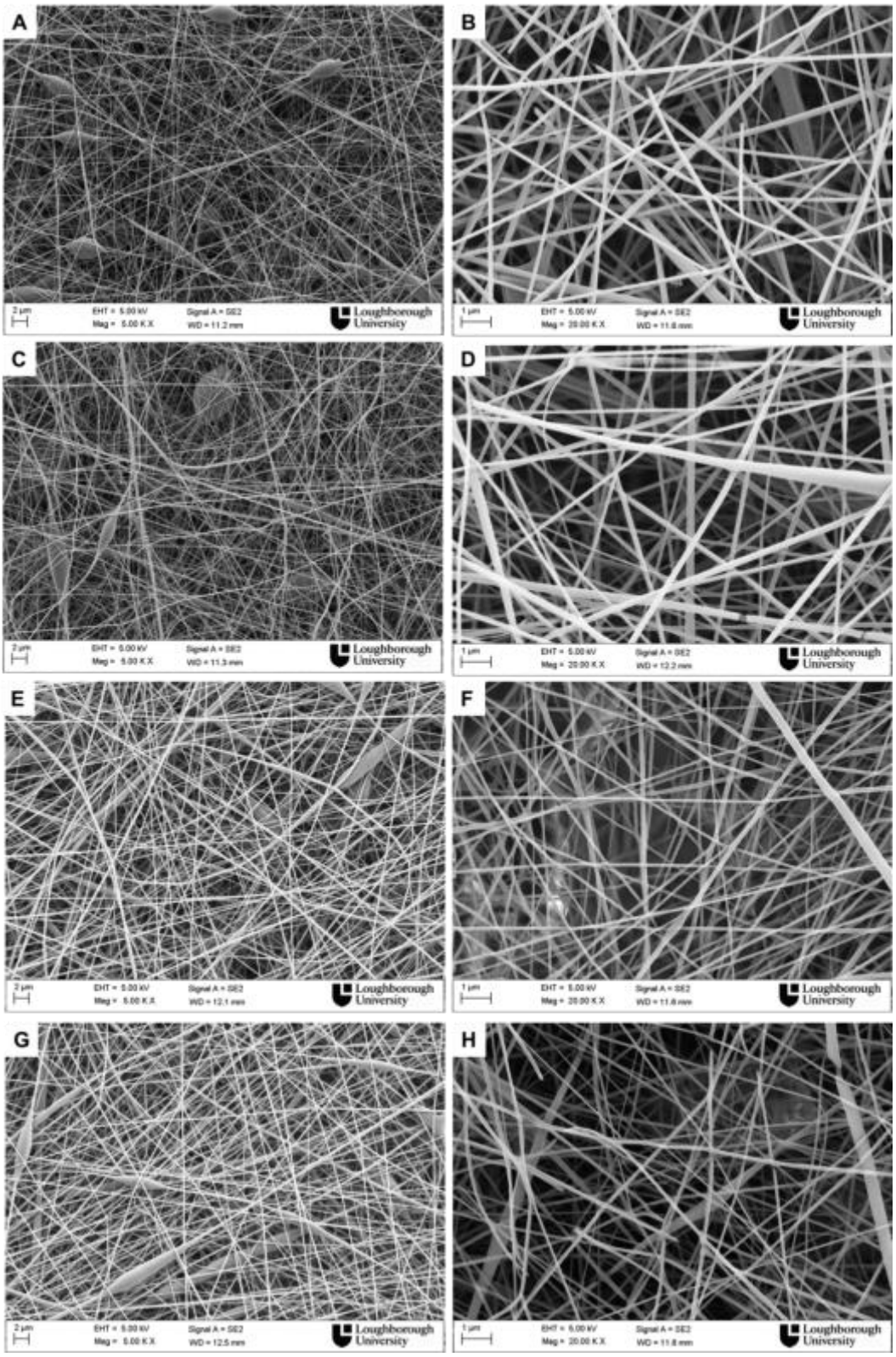

Figure 6.6 – Scanning electron micrographs of PLA nanofibres from solutions of 12.5 % (w/v) of PLA in acetone/dimethylformamide (AC/DMF) (50/50 v/v) at 2 ml/h (A, B) 15 kV, 10 cm, (C, D) 15 kV, 15 cm (E, F) 20 kV, 10 cm (G, H) 20 kV, 15 cm.

To summarize, defect-free PLA nanofibres were produced from PLA solution in AC/DMF at concentration of 12.5% using applied voltage of 7.5 and 10 kV. However the bead formation was enhanced at the highest flow rates of 1 and 2 ml/h. Generally the production of beads within the electrospun nanofibrous web has been related to both solution and process parameters. In chapter 4, it has been reported that low solution viscosity, high surface tension or low solution conductivity may lead to beaded nanofibres (Zuo et al. 2005; Y. Liu et al. 2008). Low solution viscosity leads to beaded nanofibres as a result of the insufficient entanglements density, and solution with high surface tension may be responsible of bead formation if the electrostatic force cannot overcome the surface tension force. In this chapter the bead density may be related to a variation of charge density, because the same solution was used for all experiments so the solution properties including viscosity, surface tension, conductivity, were not varied. The diameter of the nanofibres was measured and the results are reported as mean ± standard deviation as shown in Table 6.3. In the next paragraphs the effect of each parameter (applied voltage, flow rate and collection distance) on the mean nanofibre diameter and diameter distribution is described.

Table 6.3 – Mean nanofibre diameter and standard deviation for all experiments.

N. EXPERIMENT	Voltage	Flow rate	Distance	Nanofibre diameter (mean ± stdev)
	kV	ml/h	cm	nm
1	20	1	15	157±56
2	20	1	10	172±62
3	20	0.5	10	355±90
4	20	0.5	15	223±79
5	15	1	15	142±46
6	15	0.5	15	145±49
7	15	0.5	10	151±45
8	15	1	10	128±36
9	10	0.5	10	151±49
10	10	0.5	15	153±42
11	10	1	10	264±67
12	10	1	15	154±38
13	7.5	0.5	10	259±45
14	7.5	0.5	15	180±48
15	7.5	1	15	245±51
16	7.5	1	10	151±37
17	7.5	2	10	312±74
18	7.5	2	15	486±117
19	10	2	10	201±42
20	10	2	15	154±38
21	15	2	10	150±53
22	15	2	15	138±36
23	20	2	10	182±52
24	20	2	15	152±46

6.3.1.1 Effect of applied voltage (V)

The effect of the applied voltage on the PLA nanofibre diameter is discussed in this section. Figure 6.7 shows the variation of mean nanofibre diameter on increasing applied voltage from 7.5 to 20 kV at all flow rates and collection distances.

Using a flow rate of 0.5 ml/h and collection distance of 10 cm, an increase of voltage from 7.5 to 15 kV led to a reduction of the diameter from 259±45 nm to 151±45 nm as shown in Figure 6.7 A. However nanofibres with larger diameter (355±90 nm) were produced on a

further increasing voltage to 20 kV. The lowest and the highest voltage caused the collection of bigger nanofibres. These observations could be explained by the effect of two phenomena. If the applied voltage increases, higher electric field strength (E) and higher electrostatic forces cause higher drawing ratio of the solution from the needle tip. The electric field strength is defined as the ratio between the applied voltage and the collection distance (V/d). Stretching and whipping instability of the electrospun jet are controlled by the forces due to the external electric field and the Coulomb repulsion force between charges on the jet surface. Therefore this explains the production of PLA nanofibres with smaller diameter on increasing voltage from 7.5 to 15 kV. On the other hand at 20 kV, although the electric field strength is further increased, the rapid evaporation of the solvent may lead to a faster solidification of the polymeric jet. Consequently the jet resists further stretching and PLA nanofibres with larger diameter are eventually formed at the highest applied voltage. Similar trend was observed using collection distance of 15 cm (Figure 6.7 A).

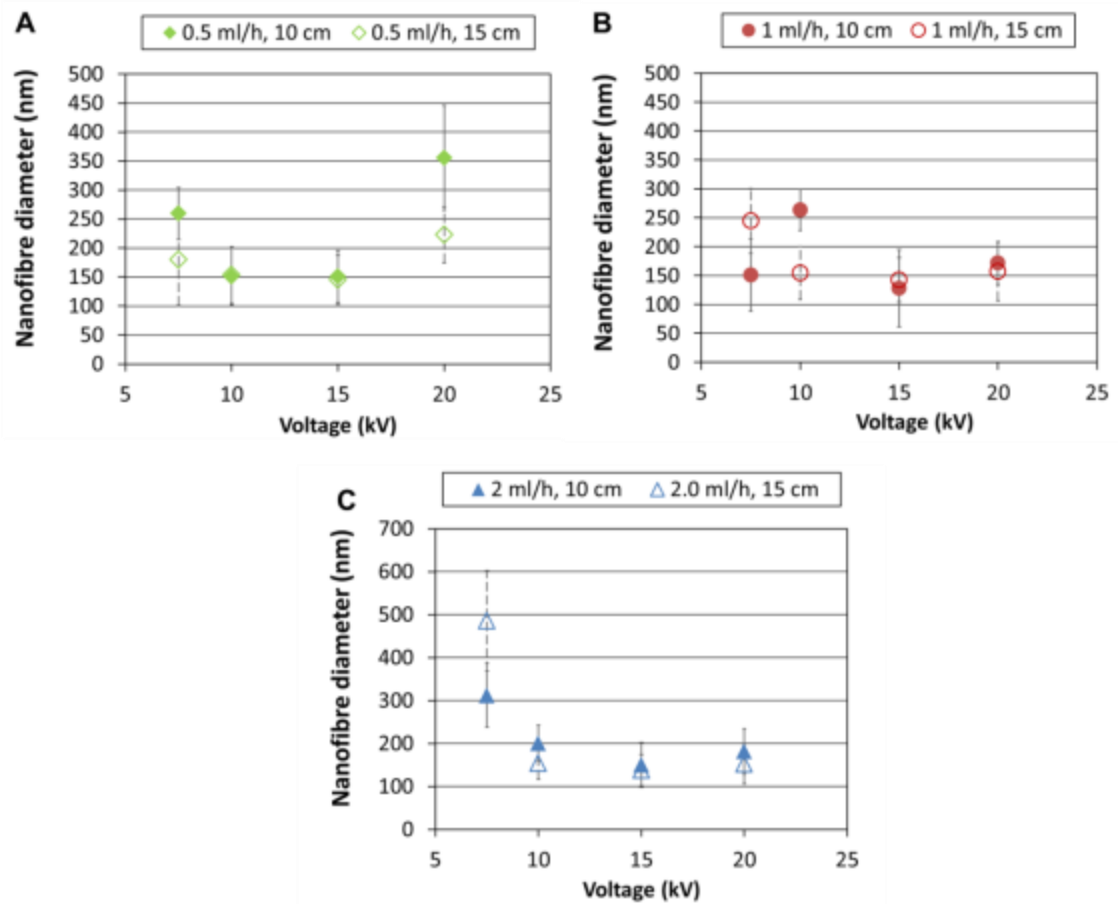

Figure 6.7 – Effect of voltage on mean nanofibre diameter at flow rate of (a) 0.5 ml/h, (b) 1 ml/h, (c) 2 ml/h.

Unlike the previous observations, Figure 6.7 B shows that using flow rate of 1 ml/h and collection distance of 15 cm, a significant reduction of the mean diameter from 245±51 nm to 157±56 nm was observed from the lowest to the highest applied voltage. Similar trends were identified for the electrospinning of the PLA solution at flow rate of 2 ml/h (Figure 6.7 C). However, the diameter of the fibres increases non-linearly with the voltage using flow rate of 1 ml/h and collection distance of 10 cm.

As mentioned in the introduction of this chapter, the effect of voltage on the nanofibre diameter has shown different trends. While a reduction of fibre diameter is easily understood due to the higher electric field strength (E) as the voltage increases, the opposite effect is somewhat unclear from the literature. Poly(sulfone) (PSF) and PVA nanofibrous structures with thicker diameter were formed on increasing applied voltage (Mazoochi et al. 2012; C. Zhang et al. 2005). Kanani et al reported that an increase of voltage from 10 to 20 kV led to larger PCL nanofibres, and this effect was observed using different solvent systems, however no explanations were given (Gholipour Kanani & Bahrami 2011).

One-way ANOVA analysis was performed on the data to verify the statistical significance of the effect of voltage on the mean nanofibre diameter depending on flow rate and collection distance. The *P*-value of hypothesis was computed as 0.05. Therefore a value of P lower than 0.05 indicates a statistical significance at the 95% confidence level. The P value is lower than 0.05 for all conditions as shown in Table 6.4, indicating therefore there is a significant difference between the mean nanofibre diameter at the different levels of voltage.

Table 6.4 – P-value of the ANOVA analysis for the voltage effect on the mean diameter.

Flow rate, collection distance	P-Value
0.5 ml/h, 10 cm	2.24E-95
0.5 ml/h, 15 cm	1.86E-27
1 ml/h, 10 cm	3.30E-65
1 ml/h, 15 cm	1.02E-48
2 ml/h, 10 cm	9.65E-72
2 ml/h, 15 cm	1.69E-128

To summarise, an increase or decrease of the electrospun nanofibre diameter on increasing applied voltage is dependent of the flow rate and the different results depends on which phenomenon prevails. Higher voltage causes an increase of the intensity of the electric field

(E) and an increase of the electrostatic repulsive forces. Hence nanofibres with smaller diameter may be produced as a result of the higher charge density with increasing applied voltage that leads to higher drawing ratio. On the other hand, higher voltage can increase the nanofiber diameters if the solvent evaporates quickly from the polymeric solution also as a result of an increase of temperature of the surface of the electrospun jet. In turn the polymeric jet cannot be further stretched before reaching the collector and nanofibres with larger diameter are collected.

These findings contribute to the clarification of the controversy encountered in the literature about the effect of the applied voltage on the diameter for various polymer-solvent systems under various electrospinning conditions.

6.3.1.2 Effect of collection distance (d)

It has previously mentioned that the electric field strength (E) can increase by increasing applied voltage (V) or decreasing collection distance (d). In addition the collection distance affects the flight time available for the stretching of the polymeric solution and therefore the time for the nanofibre collection. For this study the collector was place at 10 and 15 cm from the needle tip. Figure 6.8 shows the effect of the collection distance on the mean nanofibre diameter at different flow rates and applied voltages. Even though the morphological analysis did not show significant difference between the nanofibrous samples collected at different collection distances, a reduction in the mean diameter was overall determined with increasing *d* as reported in Table 6.3. The effect for specific conditions of flow rate and voltage are presented in the next sections.

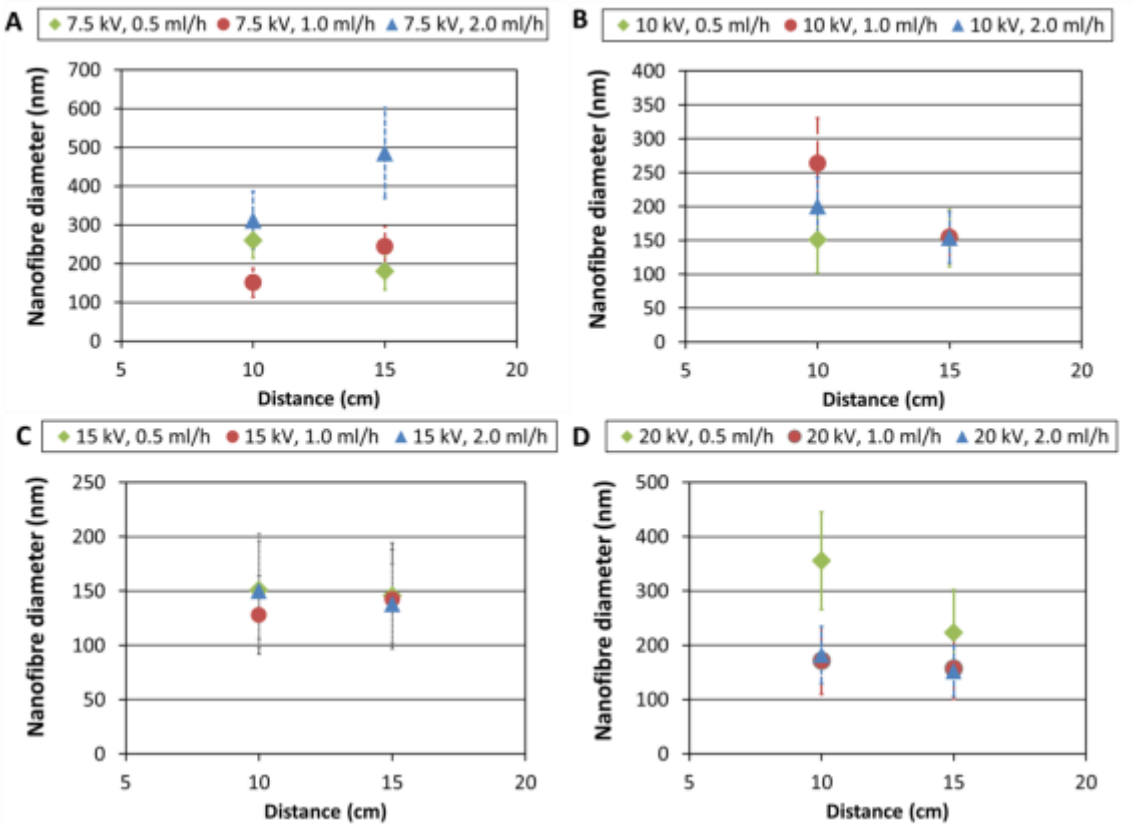

Figure 6.8 – Effect of collection distance on mean nanofibre diameter at voltages of (a) 7.5 kV (b) 10 kV (c) 15 kV (d) 20 kV.

Figure 6.8 A shows a flow rate dependence of the effect of the distance on the mean diameter at voltage of 7.5 kV. While an increase of distance at 0.5 ml/h led to a significant drop of the mean nanofibre diameter from approximately 260 nm to 180 nm, larger nanofibres were produced on increasing *d* at flow rate of 1 and 2 ml/h. The elongated Taylor cone observed and some droplets of polymeric solution collected in front of the collector using 7.5 kV and 1 and 2 ml/h are indication of the reduced electric field strength. Therefore this results in weaker electrostatic forces and hence in the production of nanofibrous structures with larger diameter. On the other hand, a more stable solution drop was maintained at the needle tip during the electrospinning process using 7.5 kV and 0.5 ml/h. At the lowest flow rate, even though the electric field strength is lowered on increasing d, the flight time available for the collection of PLA nanofibres is increased. Hence thinner nanofibres were collected. Similar to the voltage effect, ANOVA analysis was performed and the results are reported in Table 6.5. P-value lower than 0.05 at all flow rates was determined for voltage of 7.5 kV,

indicating the significant difference in the mean diameter of the nanofibres collected using 10 and 15 cm.

Table 6.5 – P-value from the ANOVA analysis for the collection distance effect on the mean diameter.

Voltage (kV)	Flow rate (ml/h)	P-Value	Fibre diameter
7.5	0.5	7.05E-27	↓
7.5	1	8.41E-36	↑
7.5	2	1.35E-24	↑
10	***0.5***	***0.82***	**-**
10	1	1.86E-36	↓
10	2	4.13E-13	↓
15	***0.5***	***0.38***	**-**
15	1	7.60E-03	↑
15	***2***	***0.054***	**-**
20	0.5	1.31E-17	↓
20	***1***	***0.06***	**-**
20	2	2.69E-08	↓

Unlike the previous observations, opposite trends were observed using higher applied voltages. When voltage of 10 kV was applied, Figure 6.8 B shows that an increase of collection distance did not show any significant difference in the mean nanofibre diameter using flow rate of 0.5 ml/h (P-value of 0.82, Table 6.5), whereas a considerable reduction in the mean diameter of 42% and 23% was observed at flow rate of 1 and 2 ml/h, respectively. These observations indicate that the effect on the flight time for the electrospun jet prevails over the reduction of the electric field strength as the collection distance is increased from 10 to 15 cm. Hence thinner fibres are collected. Figure 6.8 C and Figure 6.8 D present the effect of the collection distance for PLA nanofibres collected using 15 and 20 kV, respectively. While the mean diameter increase was 10% using 15 kV and 1 ml/h, an increase of *d* led to nanofibres with smaller diameter using voltage of 20 kV.

In most scientific publications it has been generally reported that higher collection distance enables the production of thinner nanofibres due to more time available for the solvent evaporation and bending and whipping of the jet (Yan Li et al. 2006). In other cases, although the fibre size did not change with an increase of distance, some elongated beads were observed along the fibres at the lowest collection distance (Megelski et al. 2002). This may

be explained by the fact that even though the electrostatic forces are stronger at lower *d*, the electrospun flight time is too short for the solvent to evaporate.

To summarise, the reduction or the increase of the mean diameter of PLA fibres depends on both electric field strength (E) and flight time available for the polymeric jet to be stretched before reaching the collector. If electric field strength does not drastically decrease when the collection distance is increased and stable Taylor cone is maintained, nanofibres with smaller diameter may be produced as a result of the more time given for stretching and solvent evaporation. On the other hand, a significant reduction of electric field strength (E) may lead to the collection of nanofibres with larger diameter as observed in this work for PLA nanofibres produced using 7.5 kV and 1 and 2 ml/h.

6.3.1.3 Effect of flow rate (Q)

The third process parameter investigated for the electrospinning of PLA solution in AC/DMF is the solution flow rate (*Q*) set by the syringe pump. Figure 6.9 shows the effect of *Q* on the mean diameter of PLA nanofibres for all values of voltage and both collection distances.

Comparing Figure 6.9 A and Figure 6.9 B, it can be observed that the effect of the flow rate at the lowest and the highest voltages led to opposite results. The mean diameter increased from 259±45 nm to 312±74 nm with increasing Q from 0.5 to 2 ml/h at the lowest voltage of 7.5 kV. However, the opposite trend was observed at the highest voltage of 20 kV where the mean diameter decreased from 355±90 nm to 182±52 nm. In the middle range of voltage, 10 and 15 kV, no significant variation in the mean diameter was observed, but at 10 kV and 10 cm a non-linear relationship was determined. The results from the ANOVA analysis performed to investigate the significance of the flow rate on the variation in the mean diameter are reported in Table 6.6. The effect of *Q* is significant at 7.5 kV and 20 kV and both collection distances as demonstrated by the P-value lower than 0.05. The phenomena that lead to the different effects are discussed in the following paragraphs.

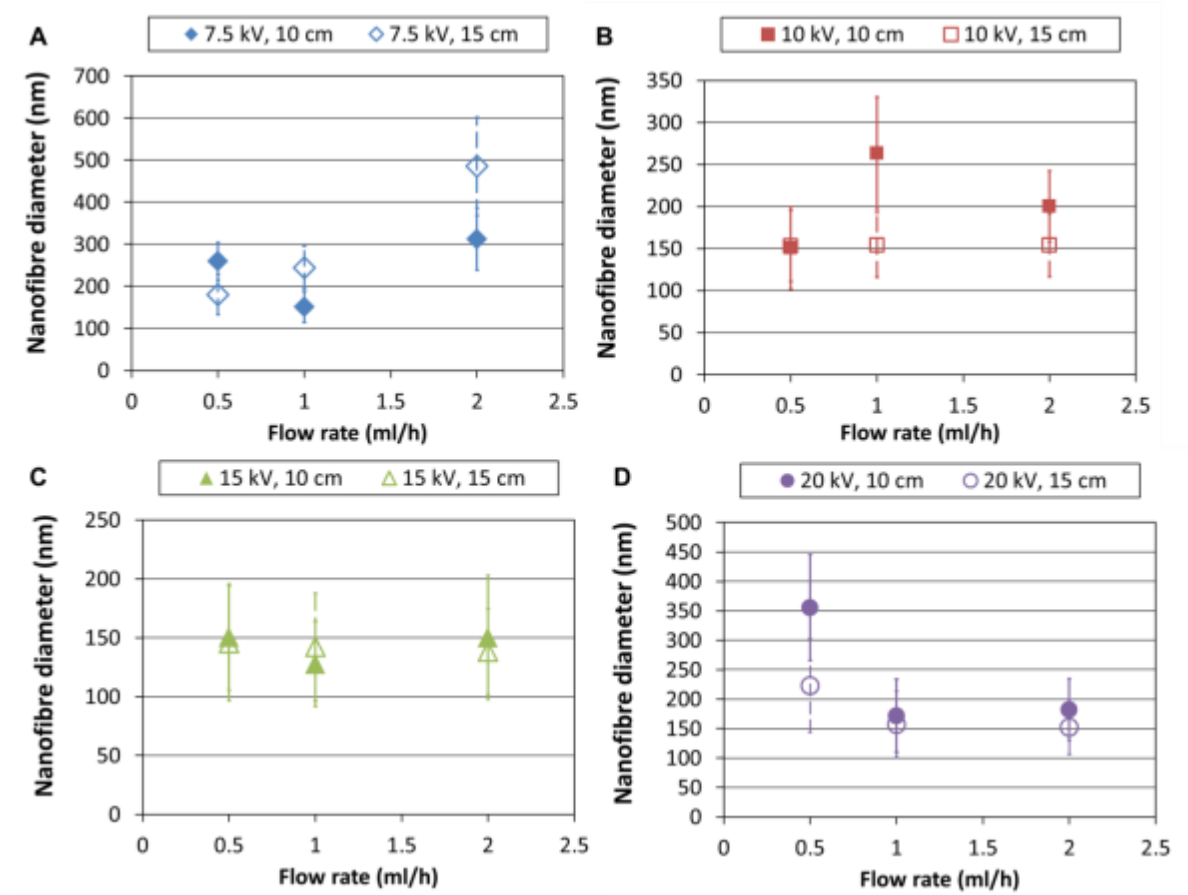

Figure 6.9 – Effect of flow rate on mean nanofibre diameter at voltages of (a) 7.5 kV (b) 10 kV (c) 15 kV (d) 20 kV.

Table 6.6 – P-value from the ANOVA analysis for the flow rate effect on the mean diameter.

Voltage (kV)	Distance (cm)	P-Value	Fibre diameter
7.5	10	4.48E-68	↑
7.5	15	5.45E-74	↑
10	10	1.71E-43	↑ then ↓
10	***15***	***0.97***	-
15	10	4.62E-05	↓ then ↑
15	***15***	***0.48***	-
20	10	6.72E-43	↓
20	15	5.27E-18	↓

As previously reported during the electrospinning at 7.5 kV the solution drop at the needle tip was observed to slightly elongate on increasing flow rate and some droplets were collected at 1 and 2 ml/h. This indicates that the electrostatic forces were not sufficiently strong to stretch more polymeric solution that became available at the needle tip on increasing flow rate.

Therefore nanofibres with larger diameter were produced. The electric field strength was unable to maintain a stable electrospinning jet most probably due to insufficient surface charge density as the diameter increases with increasing *Q* (Baumgarten 1971; Zargham et al. 2012). In addition the morphological analyses have shown an increase of bead formation (Figure 6.5) at high flow rate of 2 ml/h. On the other hand, thinner PLA nanofibres were produced with an increase of flow rate from 0.5 to 2 ml/h at 20 kV. This observation may be due to the solvent evaporation rate. At 20 kV and 0.5 ml/h, the solvent evaporates quickly as soon as the solution reaches the needle tip and the electrostatic forces are unable to stretch the solidified jet leading to nanofibres with mean diameter of 355±90 nm. On increasing *Q* smaller diameter (182±52 nm) was measured.

To summarise, there is a competition between the electric field strength and the solvent evaporation in a similar manner to what previously reported for the voltage effect in paragraph 6.3.1.1. At low Q the solvent evaporation effect prevails over the strength of the field and increasing the voltage results in fast solvent evaporation and jet solidification leading to the formation of larger fibres. At high Q, the effect of the field strength prevails and stronger forces are exerted on the jet leading to the formation of smaller fibres. Between the three process parameters investigated for the electrospinning of the PLA solution in AC/DMF the most significant factor that affected nanofibre morphology and mean diameter is the applied voltage. The increase or decrease of the diameter on increasing flow rate and collection distance was found to be dependent on the applied voltage.

The effect of solvent evaporation rate and the charge density on the nanofibre morphology and diameter have been not investigated in depth, although several models have shown the importance of these two parameters for understanding the mechanisms of the electrospinning process and prediction of the drawing ratio of the electrospun jet in the electric field (A.L. Yarin et al. 2001a).

6.3.2 Measurements of electric current I

The section will focus on the validation of an equation proposed by Fridrick et al (Sergey V Fridrikh et al. 2003) for a PLA solution in AC/DMF at polymer concentration of 12.5 % w/v. Fridrikh's equation was introduced to predict the final diameter of the jet close to the

collector and therefore the final nanofibre diameter. However a few polymer-solvent systems were investigated by the authors. The measurement of electric current (*I*) is necessary in order to apply the equation. Therefore the current was recorded using a digital multimeter (Fluke 289 True RMS). The mean value of current is reported in Table 6.7 for all experiments. It was observed that *I* varied between approximately 130 nanoampere (nA) and 3800 nA depending on the process conditions. The last column presents the values of volume charge density (ρ) defined as the ratio between electric current (*I*) and volumetric flow rate (*Q)* (S. A. Theron et al. 2004).

Table 6.7 – Mean value of electric current (I) recorded during all experiments with correspondent volume charge density.

V (kV)	Q (ml/h)	d (cm)	mean I (nA)	ρ = I/Q (C/l)
7.5	0.5	10	151	1.087
7.5	0.5	15	136	0.979
7.5	1	15	137	0.493
7.5	1	10	178	0.640
10	1	10	286	1.030
10	1	15	233	0.840
10	0.5	15	165	1.190
10	0.5	10	190	1.367
15	0.5	10	1307	9.410
15	0.5	15	520	3.743
15	1	15	481	1.732
15	1	10	569	2.048
20	1	10	3402	12.248
20	1	15	1599	5.756
20	0.5	15	2279	16.412
20	0.5	10	3777	27.192
7.5	2	10	137	0.246
7.5	2	15	137	0.247
10	2	10	260	0.468
10	2	15	185	0.333
15	2	10	504	0.908
15	2	15	354	0.636
20	2	10	3419	6.154
20	2	15	1174	2.113

Most of the models proposed to understand the mechanism and the behaviour of the electrically charge jet during the electrospinning process, are quite complex for numerical

solutions. In their model Reneker et al (D.H. Reneker et al. 2000) estimated the charge carried by the jet of a PEO aqueous solution to be 1 C/l. However the use of the quantity charge per unit volume (C/l) does not imply that the charge density is distributed uniformly throughout the jet. In fact far from the nozzle the rapid thinning and whipping of the jet as it travels to the collector suggests that most of the charges are located near the jet surface.

Even though Theron and Fridrikh only reported average values of current, in this thesis the current was recorded during the process.

Figure 6.10 shows the measured current as a function of process time at the different applied voltages and fixed collection distance of 10 cm. Overall a very little change of current was recorded using the lowest voltages of 7.5 and 10 kV (Figure 6.10 A and B), whereas the highest voltages of 15 and 20 kV led to larger fluctuations (Figure 6.10 C and D). These observations may be related to the whipping instability of the electrospun jet. An increase of voltage leads to an increase of electric charges and therefore stronger charge repulsion may be responsible of the larger current fluctuations.

Regarding the nanofibre morphology it has been shown that defect-free nanofibres were produced at voltages of 7.5 and 10 kV at the lowest flow rate (0.5 ml/h), whereas few beads were observed in the nanofibrous structures at 15 and 20 kV, although nanofibres with smaller diameter were formed at 15 kV. These observations could be related to the types of current fluctuations. High applied voltage leads to higher whipping instabilities and hence to the production of less uniform electrospun nanofibrous mats.

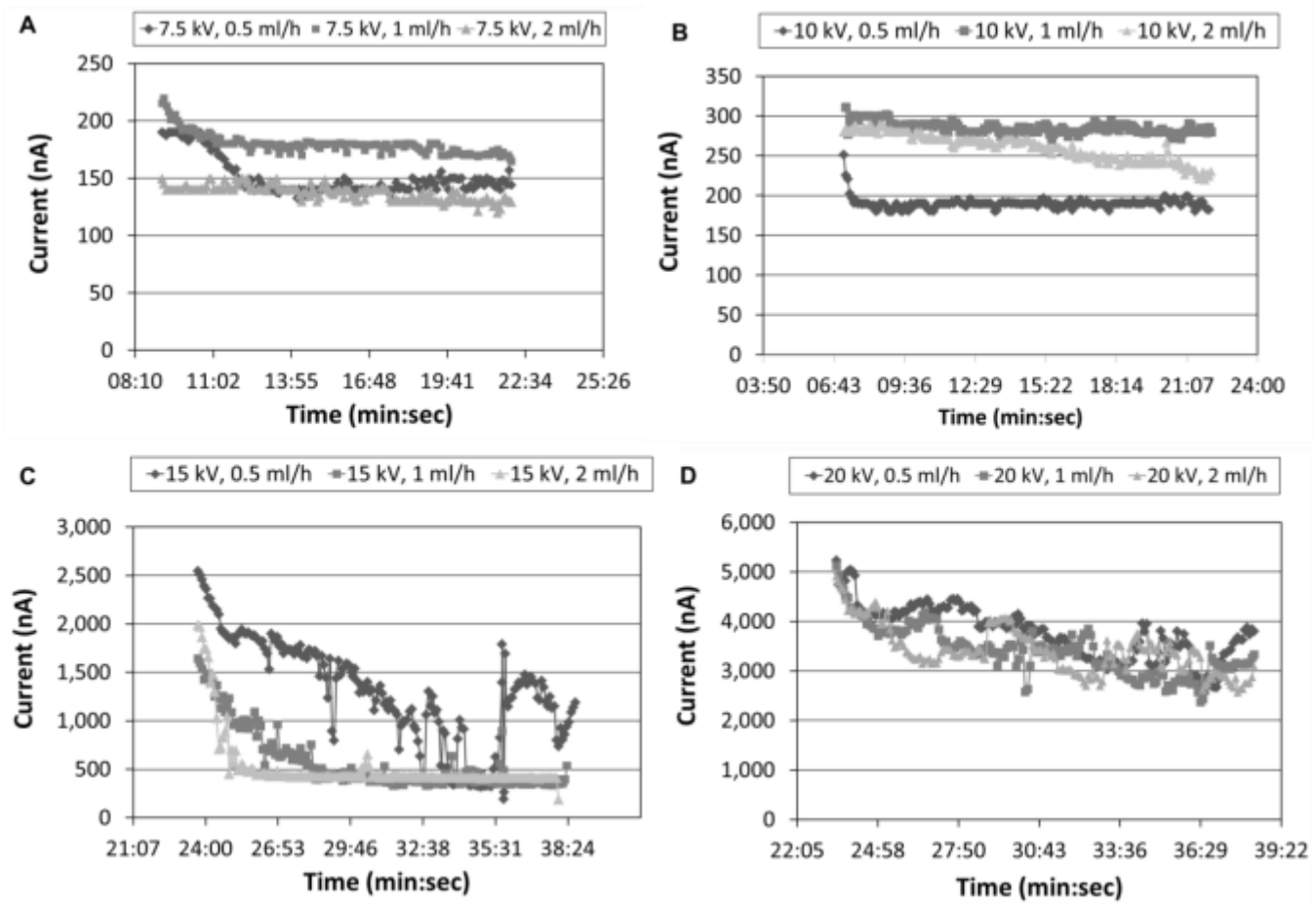

Figure 6.10 – Current measured as a function of the electrospinning process time at collection distance of 10 cm and voltage of (A) 7.5 kV, (B) 10 kV (C) 15 kV (D) 20 kV.

By recording the variation of electric current during the electrospinning process, it would be possible to ascertain approximately the quality of the electrospun nanofibrous mats and determine the highest voltage that could lead to the smallest diameter without affecting the bead formation. Additionally, the value of current can be used to predict the final nanofibre diameter.

The effect of each process parameter, i.e. voltage, collection distance and flow rate, on both jet electric current (I) and volume charge density (ρ) are examined and discussed in the next sections.

6.3.2.1 Current-voltage (I-V) relationship

The effect of voltage on electric current (I) and volume charge density (ρ) was first examined. Figure 6.11 A shows a log-log plot of applied voltage versus *I*. An increase of current was recorded on increasing voltage from 7.5 to 20 kV at any collection distances and flow rates, and a similar relationship was observed for the electric field strength (E) (Figure 6.11 B). For example using a flow rate of 0.5 ml/h and distance of 10 cm, the current increased from 151 nA to 3777 nA. The scaling exponent value was found between 2.1 and 3.5 (Table 6.8) and this indicates that PLA solution in AC/DMF is a non-Ohmic conductor because it does not follow the Ohm's law. A material is considered 'Ohmic' when the ratio between current and voltage is constant over a wide range of voltage values. This is not the case for polymeric electrospun jets. Similar values of the exponent have been reported for different types of polymer-solvent systems: $I \sim E^3$ for PCL solution in DCM/DMF (Ji Huan He & Yu Qin Wan 2004), $I \sim E^{2.6}$ for poly (acrylonitrile) (PAN) in DMF (Delaram Fallahi et al. 2008) and $I \sim E^{2.7}$ poly(urethane) in DMF (Demir et al. 2002). As a result of the increased electric current, the volume charge density was found to increase as shown in Figure 6.11 C, since it was calculated as the ratio between current and volumetric flow rate (S. A. Theron et al. 2004).

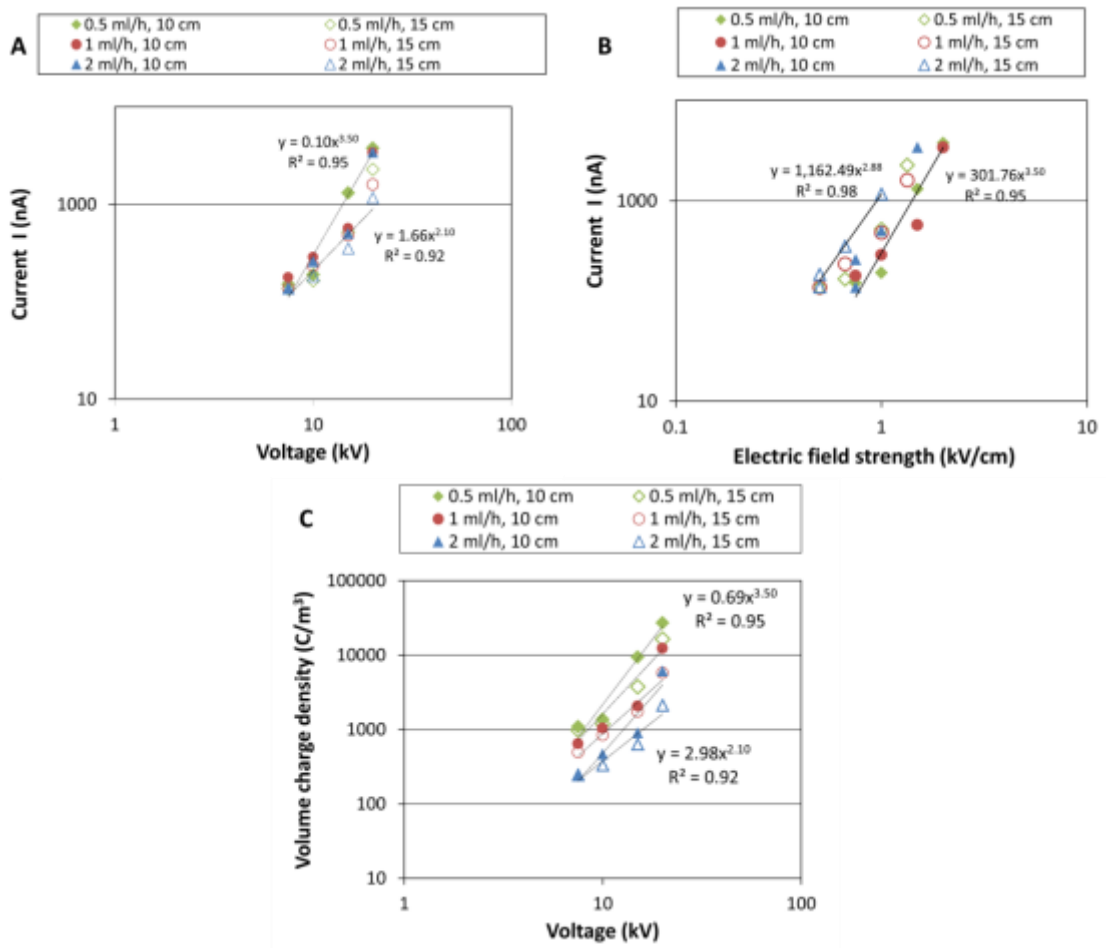

Figure 6.11 – Effect of (A) applied voltage and (B) electric field strength on the electric current (C) effect of applied voltage on volume charge density.

Table 6.8 – Exponent value of the power law relationship between voltage (or electric field strength) and current.

Flow rate, collection distance	Exponent value
0.5 ml/h, 10 cm	3.5
0.5 ml/h, 15 cm	2.9
1 ml/h, 10 cm	2.8
1 ml/h, 15 cm	2.4
2 ml/h, 10 cm	3.0
2 ml/h, 15 cm	2.1

The next step involved the calculation of the predicted fibre diameter using Equation 2 and Equation 3 proposed by Fridrikh (Sergey V Fridrikh et al. 2003).

$$h_t = \left(\gamma\bar{\varepsilon}\frac{Q^2}{I^2}\frac{2}{\pi(2ln\chi - 3)}\right)^{1/3}$$

Equation 2

$$d_t = h_t * c^{1/2}$$

Equation 3

First, the mean value of jet current was used to calculate the jet diameter close to the collector h_t using Equation 2. The whipping instability value χ is defined as the ratio between R and h, with R being the radius of curvature of the whipping jet and h is the jet diameter. Fridrikh et al (Sergey V Fridrikh et al. 2003) stated that the exact value of χ is not critical since ln χ varies slowly and a value of 100 was used. Figure 6.12 presents the results of the effect of the applied voltage on the nanofibre diameter. The predicted values of the fibre diameter are represented as a curve, while the experimental values are shown by markers. A value of χ of 10, 100 and 1000 was used to determine the predicted diameter. Overall while no significant difference in the predicted nanofibre diameter is observed using a value of χ of 100 and 1000, bigger diameter is determined using a value of 10. For example at voltage of 7.5 kV and flow rate of 2 ml/h, χ of 10 resulted in predicted diameter of 400 nm, while 250 and 200 nm are the values predicted using 100 and 1000, respectively. However it is highly unlikely that a value of 10 is determined during an electrospinning process, since the radius of curvature of the whipping jet (R) is much higher that the jet diameter (h). The whipping instabilities are responsible for the jet thinning and therefore they are essential for the production of ultrafine nanofibers as described in section 2.1.1. Hence a value of 100 is selected and used in the next sections.

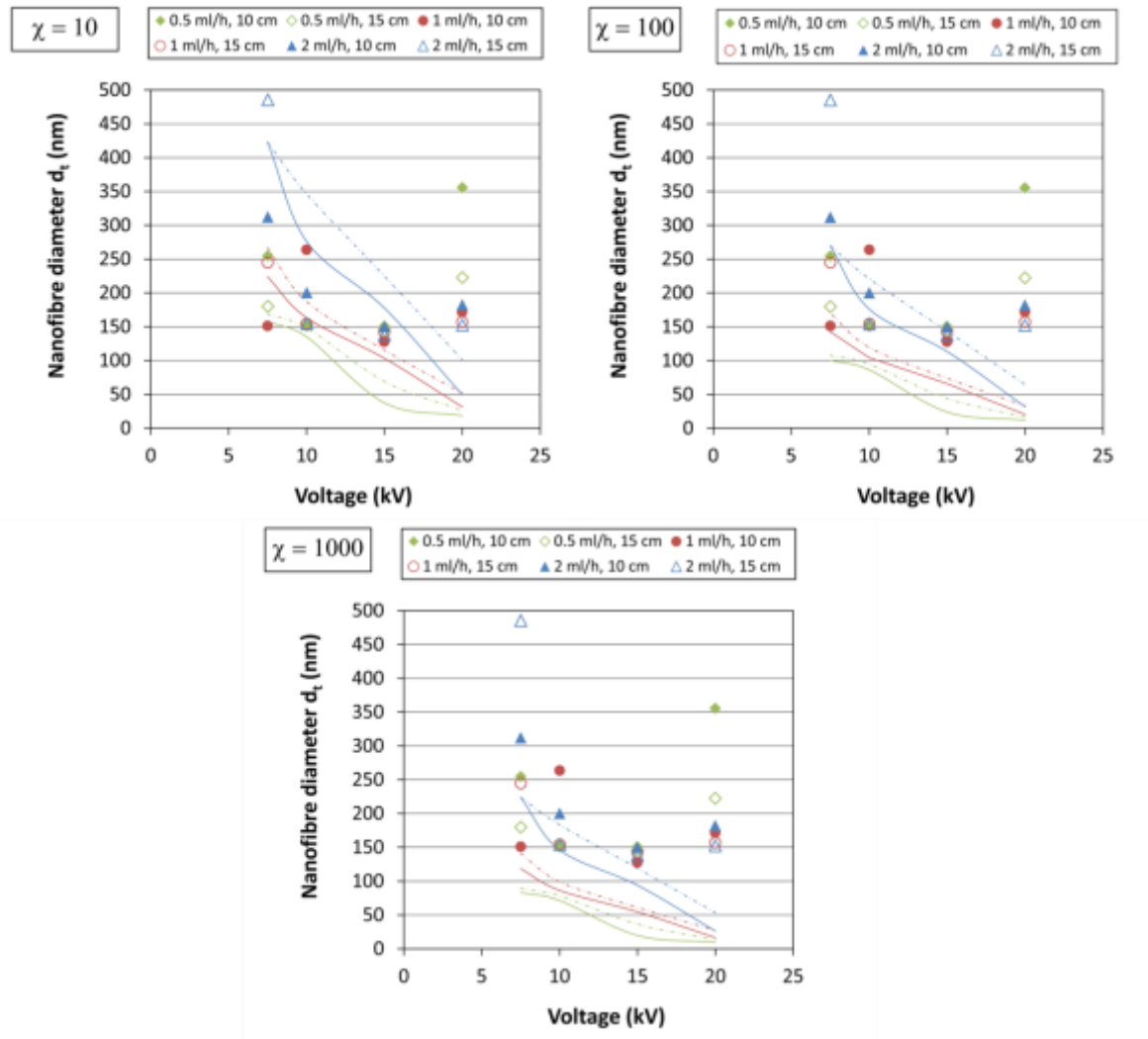

Figure 6.12 – Effect of the applied voltage on the nanofibre diameter.

A reduction in the nanofibre diameter would be expected on increasing applied voltage at all flow rates and collection distances as shown by the curves. The higher number of charges per volume (ρ) causes an increase of repulsive forces which stretch the electrospinning jet and therefore thinner nanofibres may be collected. Overall these results are in good agreement with the morphological observations. Nevertheless at the lowest flow rate of 0.5 ml/h the mean nanofibre diameter initially decreased from 7.5 to 15 kV, but a further increase of voltage to 20 kV led to the production of larger nanofibres (Figure 6.7 A paragraph 6.3.1.1). This indicates that the measured electric current probably ignores the dynamics of the charge transfer mechanism.

6.3.2.2 Current-distance (I-d) relationship

In this section the relationship between current and collection distance will be investigated. At a fixed voltage and constant flow rate, the electric field strength (E) decreases on increasing the distance between the needle tip and the collector. Figure 6.13 presents the effect of the collection distance on the measured electric current of the electrospun jet. Overall an increase of collection distance resulted to lower values of electric current I and also lower volume charge density. The reduction of I is a result of the decrease in the electric field strength (E).

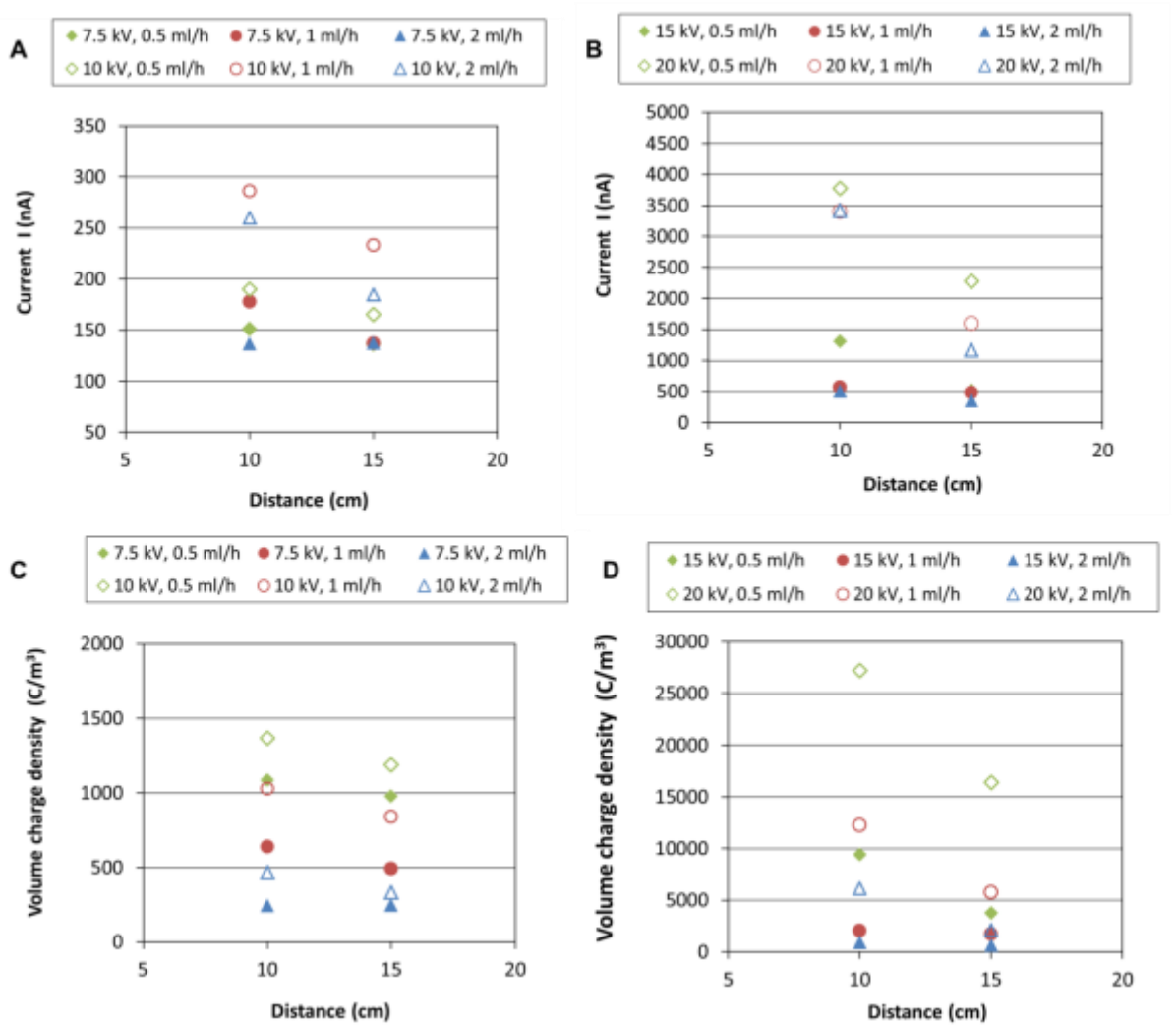

Figure 6.13 – Effect of collection distance on current (A, B) and volume charge density (C, D) for applied voltage of 7.5, 10, 15 and 20 kV.

The predicted nanofibre diameter was calculated and the results are shown in Figure 6.14 and Figure 6.15. While an increase of applied voltage has shown a reduction of the predicted diameter, an increase of collection distance shows an increase of the predicted diameter as a result of the reduction of electric current at all process conditions. In paragraph 6.3.2.2 it has been shown that an increase of *d* may lead to either reduction or increase in the mean diameter of PLA nanofibres depending on the value of applied voltage. Larger nanofibres were collected on increasing collection distance at the lowest applied volte of 7.5 kV and flow rate of 1 and 2 ml/h, which is in good agreement with the effect of *d* on the predicted diameter (Figure 6.14). Nevertheless, thinner fibres were collected on increasing collection distance at the highest applied voltage (20 kV) (Figure 6.8 D).

Similar to the observations for the effect of applied voltage, these discrepancies between the predicted nanofibres and the experimental values are most probably due to the fact that the model proposed ignores the dynamics of the charge transfer mechanism and the effect of the solvent evaporation which is not taken into account.

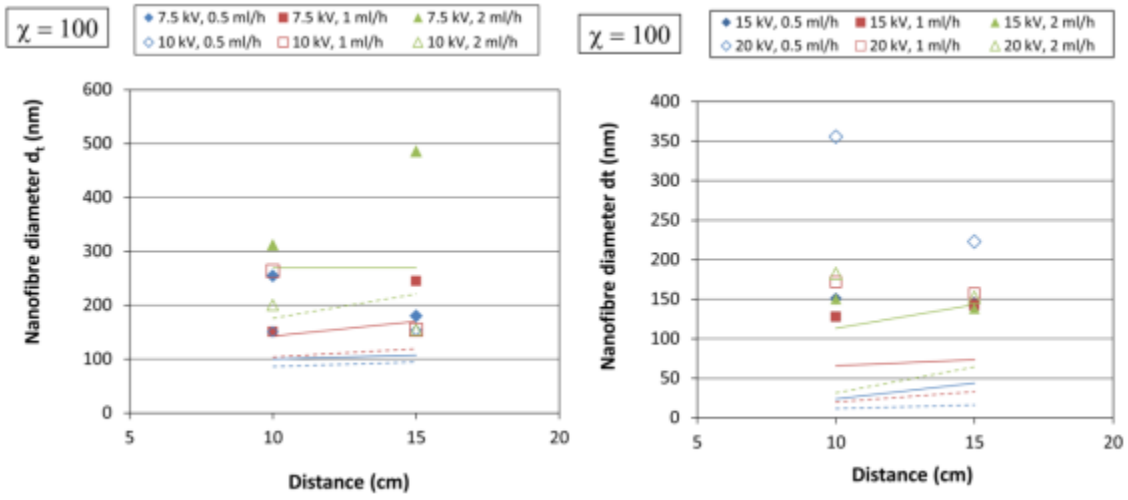

Figure 6.14 – Effect of the collection distance on the predicted diameter.

6.3.2.3 Current-flow rate (I-Q) relationship

The flow rate has also shown to have an effect on the current measurement and on the volume charge density. Figure 6.16 A shows that a non-linear relationship between the flow rate and the current was determined for the lowest values of voltage (7.5 and 10 kV), whereas

Figure 6.16 B shows a reduction of current as the flow rate increases from 0.5 to 2 ml/h at 15 and 20 kV. The variation of current may result from variations in the number of injected charges with solution flow rate. The volume charge density was also calculated as shown Figure 6.16 C and D. Even though the current has shown a non-linear relationship at 7.5 kV, the volume charge density decreases on increasing flow rate from 0.5 to 2 ml/h for all values.

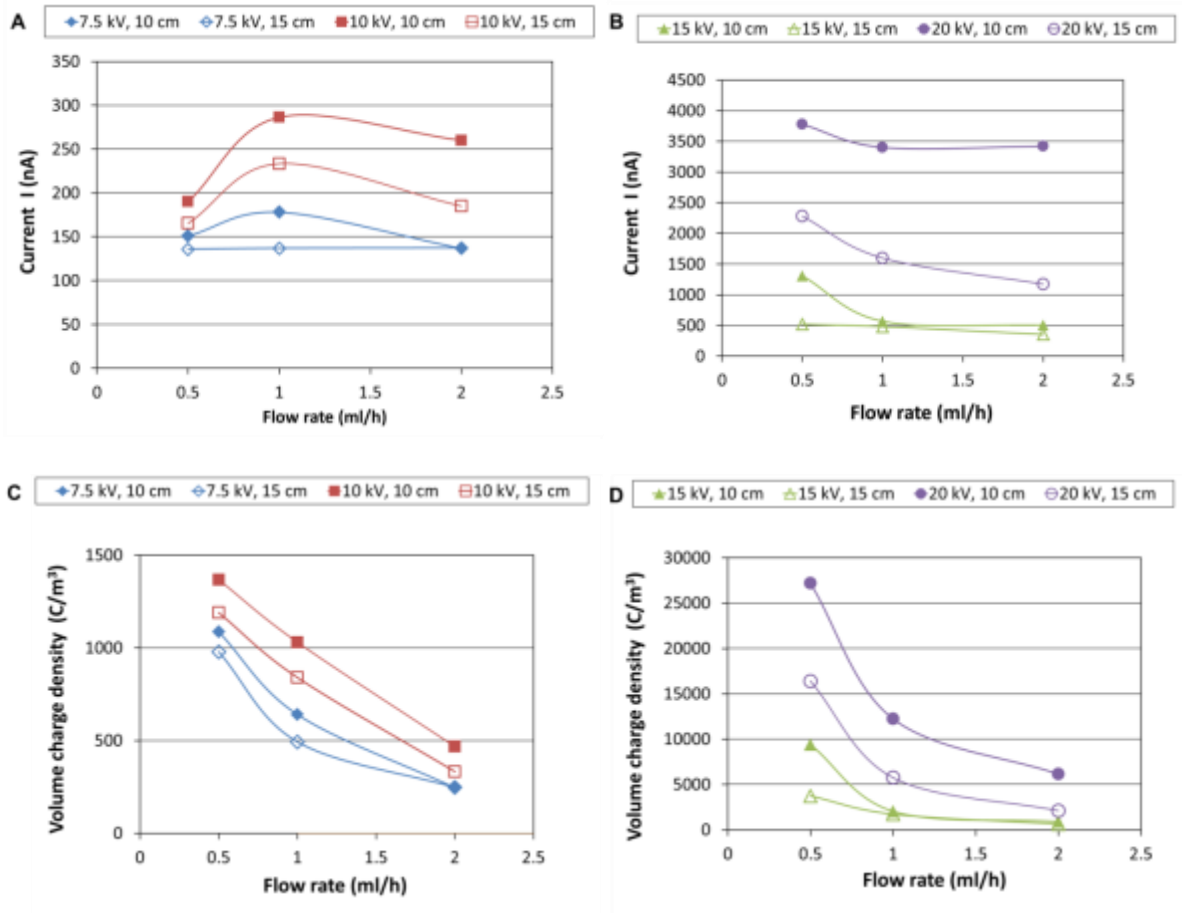

Figure 6.15 – Effect of flow rate on current (A, B) and volume charge density (C, D) for applied voltage of 7.5, 10, 15 and 20 kV.

Figure 6.17 shows that overall larger diameter of PLA nanofibres would be expected on increasing flow rate. This is in good agreement with the morphological observations of the electrospun nanofibrous mats collected using 7.5 kV. At fixed collection distance of 10 cm nanofibres with diameter of 259±45 nm were produced at 0.5 ml/h, whereas larger nanofibres (312±74 nm) were collected at 2 ml/h. Nevertheless, an increase of flow rate resulted in thinner nanofibres at the highest voltage of 20 kV, although a reduction of volume charge

density was calculated Figure 6.16 D.

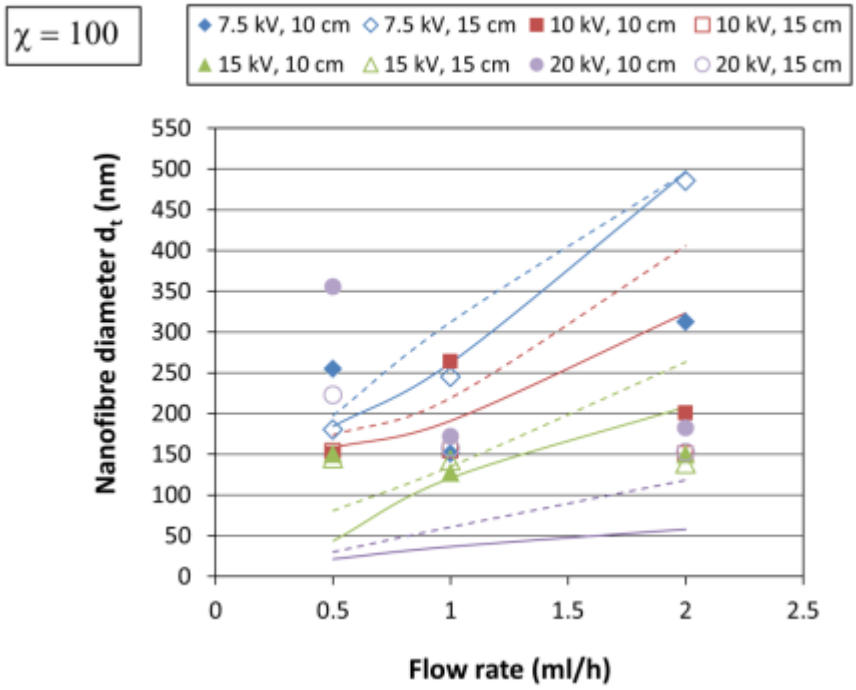

Figure 6.16 – Effect of flow rate on the predicted nanofibre diameter.

In their studies, Theron et al (S. A. Theron et al. 2004) reported that the electric current *I* increases with *Q* for some solutions, while it decreases for others. PEO solution in ethanol/water (40/60) and PVA in ethanol/water (50/50) have shown overall an increase of electric current on increasing volumetric flow rate at several applied voltages from 10 to 21 kV, whereas PCL solution in a mixture of DCM and DMF (40/60) led to opposite trend. But explanations of the different trends of the electric current were not given. A possible reason may be related to the types of solvent used for the polymer-solvent systems investigated. The aqueous solutions have much higher electric conductivity than the PCL solutions.

In the next section the predicted diameter for PLA nanofibres is compared with the experimental diameter and possible explanations are given.

6.3.2.4 Predicted vs experimental nanofibre diameter

The experimental nanofibre diameter was plotted versus the predicted nanofibre diameter as shown in Figure 6.18. Different results were obtained depending on the process conditions. Good agreement between the predicted and experimental values was found for some experiments, whereas the predicted value for the PLA nanofibres is much smaller than the experimental value in other experiments which indicates that the stretching of the PLA nanofibres is over predicted.

In this thesis, the over predicted stretching was observed mostly for the nanofibres collected at the highest voltage of 20 kV. This may be explained by the high whipping instabilities resulted from the increase of charge density. During the electrospinning of PLA solution at 20 kV and 0.5 ml/h the volume of solution drop at the needle was lower compared to 7.5 kV indicating that the electrospun jet was probably withdrawn at a rate much higher than the solution flow rate set by the syringe pump. This suggests that the value of flow rate Q used in the model to predict the diameter is not correct. At high voltage the solvent evaporates fast and most probably more charges are being removed from the surface, they leaves with the solvent molecules and contribute to the measure current I. Hence the loss of surface charges led to variation in the measured current as shown in fact in Figure 6.10. Furthermore the value of χ defined as the ratio between the radius of curvature of whipping and the jet diameter, may be affected due to the much higher jet instabilities at 20 kV. Splitting of the jet in multiple jets may also occur contributing therefore to explain the wide difference between predicted and experimental diameter.

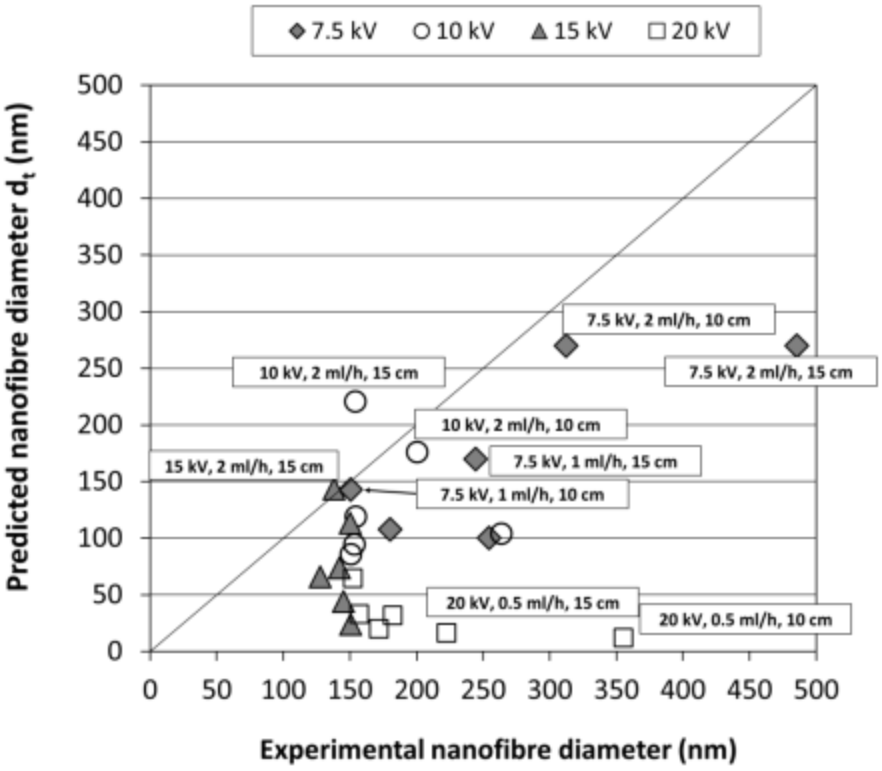

Figure 6.17 – Experimental versus predicted nanofibre diameter for PLA solution in AC/DMF using a value of χ of 100.

Fridrikh et al (Sergey V Fridrikh et al. 2003) observed deviation of the predicted diameter from the experimental diameter for PCL nanofibres (Figure 6.19). The authors stated that the over predicted stretching of PCL nanofibres compared to the good agreement for PAN and PEO aqueous solution was due to the difference in charge carrier and solvents. For PEO and PAN solution the main charge carrier is the polymer, because the solvent (water) evaporates slowly from the jet, and therefore the charges care carried by the electrospun jet until it reaches the collector. On the other hand, the mixture chloroform/methanol carries most of the charges for PCL solution due to the high solvent volatility. Hence the charges contribute to the value of current *I*, the charge density is over predicted, resulting therefore in under prediction of the diameter of the PCL nanofibres. Nevertheless, no information about the value of applied voltage, flow rate, collection distance and solution properties, such as solution conductivity or viscosity, was given by the authors (Sergey V Fridrikh et al. 2003).

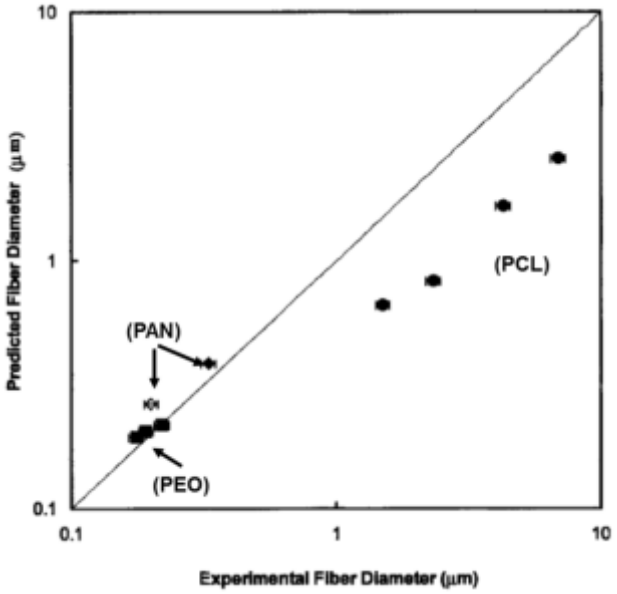

Figure 6.18 – A comparison of the experimental and predicted fibre diameters (Sergey V Fridrikh et al. 2003).

The jet diameter h_t is plotted as a function of (Q/I) as shown in Figure 6.20. The results show that good agreement with the theory is achieved considering the lowest voltages of 7.5 and 10 kV and some experiments at 15 kV. Fridrikh et al have shown that the theoretical curve for h_t is shifted below the experimental data by a constant factor of about 2 (Figure 6.21) for PCL solutions. This was explained by the high volatility of the solvent mixture chloroform/methanol which is the main charge carrier. Even though Fridrikh et al used plate-plate geometry, in this thesis needle-plate geometry was used and good prediction of the fibre diameter was determined in some experiments.

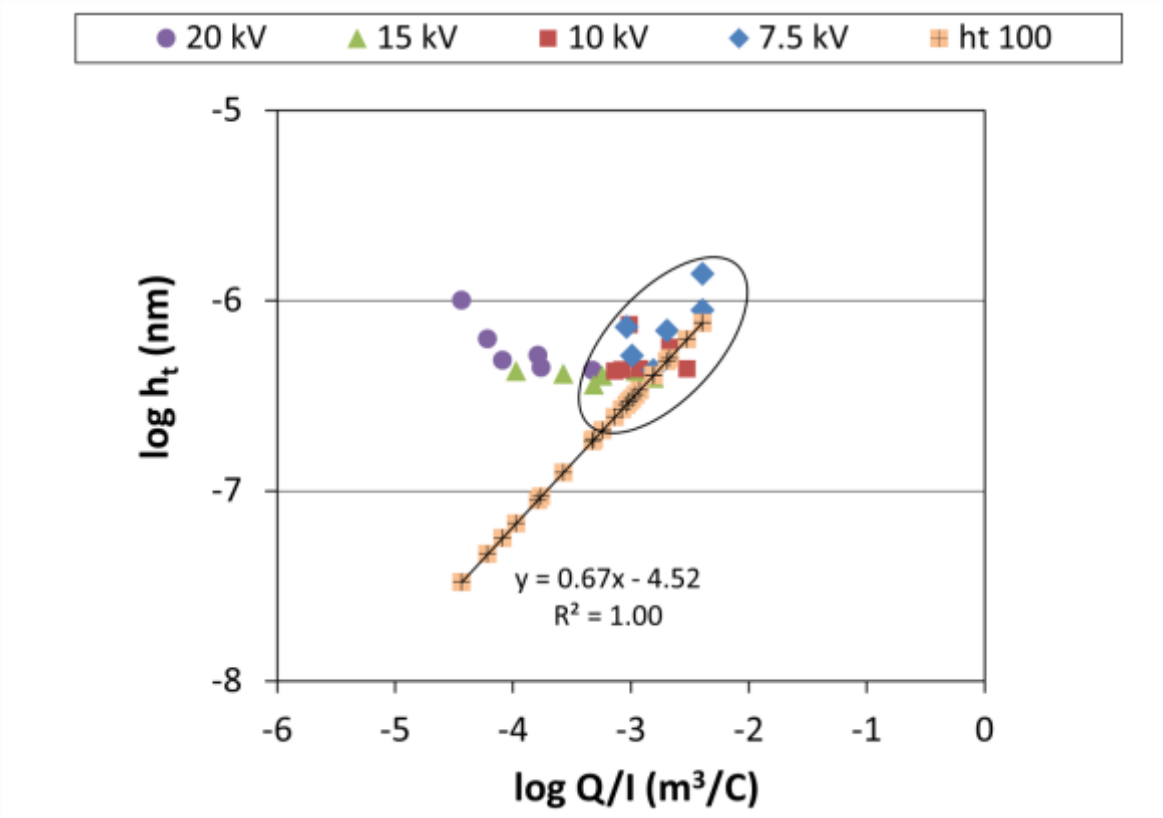

Figure 6.19 – The terminal jet diameter h_t as a function (Q/I) compared to the theory.

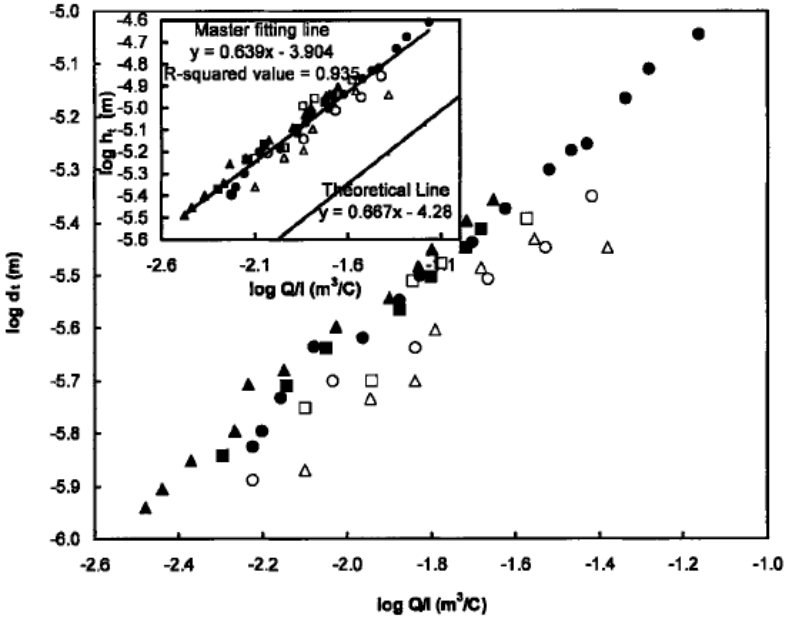

Figure 6.20 – The log of fibre diameter versus the log of (Q/I) for several PCL concentrations (Sergey V Fridrikh et al. 2003).

It can be concluded therefore the solvent evaporation rate should be taken into account for the prediction of the fibre diameter. More studies should be then carried out to understand how the solvent evaporation affects the electrospinning process and how the equation could be modified. It is also well known that other solution properties strongly affect the morphology of the electrospun mats and the nanofibre diameter. According to Fridrikh's model the relationship between jet current and diameter is monotonic. However a more complex relationship was recently reported between the jet current and the fibre diameter by Angammana et al (Angammana & Jayaram 2011b). The diameter of PEO nanofibres electrospun from a 5% PEO aqueous solution was found to decrease with increasing jet current within a range of solution conductivity, whereas it increases with an increase of *I* for higher solution conductivity. The conductivity affects the distribution of the electric charges on the jet surface and the tangential electric field forces exerted on the jet (Moutsatsou et al. 2015; A.L. Yarin et al. 2001a). Furthermore, as reported in the literature of this thesis, Kim et al (S. J. Kim et al. 2004) have shown that a maximum value for the current *I* was recorded for the middle value of polymer concentration (6% w/v) and thinner nanofibres with narrow diameter distribution were collected as a results of a balance between the ion mobility and the number of charged ions. This suggests that most probably the solution viscosity should be also introduced.

There is a lack of scientific publications on the influence of the solution and process parameters on the jet electric current and charge density and consequently on the fibre morphology and diameter (S. A. Theron et al. 2004; Delaram Fallahi et al. 2008; D. Fallahi et al. 2010). The model proposed by Fridrikh neglects the volatility of the solvents, the elastic effect due to solvent evaporation, charge carrying ability of the polymers and solution conductivity. Solution viscosity and conductivity are significant parameters in the electrospinning process, and therefore should be introduced in the scaling formula. In addition the model was proposed considering that the collector is a stationary plate, but in some scientific publications nanofibres with smaller diameter have been produced using a rotating drum as collector compared to the static plate (Z. X. Meng et al. 2010; D. Gupta et al. 2009) as a result of the drawing effect given by the rotation of the drum. The rotation may also affect the solvent evaporation. Hence these effects should be considered for the prediction of the final diameter.

An integrated current measurement system could be useful to verify the stability of the electrospinning process, to detect any current variations that may lead to beaded structures.

6.4 Conclusion

The research described in this chapter was conducted to give a better insight in the effect of the process parameters on the morphology and diameter of PLA nanofibres, and to identify the factors that hinder the prediction of the diameter of electrospun nanofibres. A PLA solution in AC/DMF was prepared and the electric current was recorded during each experiment.

Between the process parameters investigated in this work, applied voltage and flow rate were found to be the most significant factors affecting the morphology of the electrospun nanofibrous mats. An increase of voltage led to an increase of bead density within the webs due to an increase of jet instabilities and to more rapid solvent evaporation which causes a shorter time for the stretching of beads along the electrospun jet. Defect free nanofibres were formed at 7.5 and 10 kV at the lowest flow rate of 0.5 ml/h and the Taylor cone appeared more stable during the electrospinning process. On increasing applied voltage the mean nanofibre diameter was found to increase or decrease depending on the value of solution flow rate set by the syringe pump. A non-linear relationship was found between diameter and voltage using the lowest flow rate of 0.5 ml/h, while using 1 and 2 ml/h constant reduction of the mean diameter was determined as the applied voltage increases. Uniform defect free nanofibrous sample were collected at the lowest voltages using the lowest flow rate, independently of the collection distance.

The competitive action of two phenomena is responsible of the reduction or increase of the mean diameter. If the electric field strength is increased on increasing applied voltage without affecting too much the solvent evaporation rate, then thinner nanofibres may be formed as a result of the higher electrostatic force that stretched the polymeric jet. On the other hand, if the solvent evaporates quickly from the electrospun polymeric jet, the jet solidifies faster and so nanofibres with larger diameter are collected at higher voltages. This was observed at the lowest flow rate (0.5 ml/h). First the jet diameter decreased from about 260 nm to 150 nm, then it increased to 355±90 nm as the voltage increased to 20 kV.

The electric current *I* was measured for each experiment and the observations have shown significant oscillations of *I* at the highest applied voltages, while stable value was recorded using 7.5 and 10 kV. Monitoring the current would be possible to test the process stability with respect to time. At the highest applied voltages the value of current oscillates as a result of the stronger whipping instabilities of the jet. An increase of voltage resulted in higher electric current, while reduction of current was determined on increasing collection distance. Then, the electric current values were used to verify the validity of Fridrikh's equation and predict the final diameter of the electrospun PLA nanofibres. The results have shown that the equation is able to predict the fibres diameter for some experiments, while it was not successful in others especially at 20 kV. More systematic studies should be carried out for different polymer-solvent systems to determine a universal correlation between the final nanofibre diameter and the solution and process parameters.

7 PRODUCTION OF CORE-SHELL NANOFIBRES BY COAXIAL ELECTROSPINNING FOR ENCAPSULATION OF HYDROPHILIC DRUG

7.1 Introduction

Blend, coaxial or emulsion electrospinning have been employed by researchers to incorporate drugs into the nanofibres. While the blend electrospinning has generally shown an initial burst drug release, when for example a hydrophilic drug is blended with a hydrophobic polymer, coaxial electrospinning and emulsion electrospinning were demonstrated to produce loaded nanofibres with a sustained drug release (Zamani et al. 2013; Chong Wang et al. 2011). By changing the core solution flow rate in the coaxial electrospinning, different drug release profiles could be achieved and also multiple drugs could be incorporated (W. Song et al. 2013; Y. Su et al. 2012; Yazhou Wang et al. 2010). On the other hand, emulsion electrospinning is a more complex process where the concentration of an emulsifier has an important effect on the emulsion stability and therefore on the nanofibre morphology (Badawi & El-Khordagui 2014; Pal et al. 2014). Emulsion consists of immiscible liquids, while in coaxial electrospinning the same solvent for shell and core solutions can be used since the solutions are delivered through different channels (Chi Wang et al. 2010; T. T. T. Nguyen et al. 2012). Moreover, core-shell nanofibres can protect biomolecules or active agents (such as DNA) from being influenced by the environment, maintaining their activity.

There are different views regarding the selection of miscible or immiscible core and shell solutions. Some researchers reported that the same solvent for core and shell solutions would reduce the interfacial tension between the two solutions and this would therefore be beneficial for the formation of a core (J. H. Yu et al. 2004; L. Cheng et al. 2014). On the other hand, Sohrabi and his group of researchers (Sohrabi et al. 2013), for example, speculated that the production of core-shell nanofibres was successful probably due to the immiscibility of PA6 solution in formic acid (shell material) and PMMA solution in chloroform (core material), and also the fast processing of the electrospinning could significantly prevent the mixing of the two solutions.

Aqueous solutions have been used as core material to incorporate proteins and growth factors

in nanofibres made of hydrophobic shell. Table 7.1 presents a list of scientific publications. It can be observed that both miscible and immiscible core and shell solutions have been employed.

Table 7.1 – List of scientific publications regarding the production of core/shell nanofibres loaded with hydrophilic molecule.

Shell solution	Core solution	Miscibility	Reference
PCL CHL/DMF (7/3)	PEG+BSA (10%w/w) Water	PCL no soluble in water ***CHL and water: non miscible*** DMF and water: *miscible*	Jiang, 2005
PCL TFE	PEG+BSA Water	PCL no soluble in water TFE and water: *miscible*	Zhang, 2006
PCL CHL:Ethanol (3:1 w/w)	Gentamicin Water	PCL no soluble in water ***CHL and water: non miscible*** Ethanol and water: *miscible*	Z-M. Huang, 2006
PLLA-CL TFE	BSA+NGF Water	PLLACL no soluble in water TFE and water: *miscible*	S. Yan, 2009
PLGA DCM/DMF (7/3 v/v)	HA (hyloronic acid)+BSA Water	PLGA no soluble in water ***DCM and water: non miscible*** DMF and water: *miscible*	Y.K. Joung, 2011
PCL + collagen (90/10 v/v) CHL:DMF 1:1 v/v	PVA + HA (hydroxyapatatite) (90/10 v/v) Water	PCL no soluble in water ***CHL and water: non miscible*** DMF and water: *miscible*	W. Song, 2013
PLLCL + Gelatin (60/40 w/w) HFIP	BSA + growth factor Water	PLLCL no soluble in water HFIP and water: *miscible*	Jin, 2013
PCL HFIP	Laminin Water	PCL no soluble in water HFIP and water: *miscible*	E. Kijen´ska, 2014

Similarly to the single electrospinning, the jet may undergo instabilities as it travels to the collector, therefore a great challenge in core-shell electrospinning is the ability to get consistent core-shell morphology throughout the length of the nanofibre. The most common technique used to verify the formation of core-shell structure is transmission electron microscope (TEM). However, only a segment of the nanofibres is often shown (C. He et al. 2006; Z.-M. Huang et al. 2006) and during the electrospinning process it is impossible to verify that there is no disruption to the core solution supply. Therefore more techniques should be used to confirm the formation of a continuous core-shell structure in the nanofibres in order to understand the drug release profile.

A balance between surface tension, viscoelastic and electrostatic forces is required for the successful production of defect-free nanofibres from electrospinning. But, while the effect of

solution and process parameters has been investigated on the production of electrospun nanofibres using a single nozzle, there is a lack of information on solution properties of core and shell solutions, including viscosity, surface and interfacial tension, and solution conductivity. The selection of solution and process parameters is still based on trial and error experiments. In coaxial electrospinning the two solutions first come in contact at the end of the needle tip. Therefore the type of solvents used and the compatibility between polymers and solvents certainly have an effect on the result of the electrospinning process. However there is no systematic methodology that could be used for the selection of the electrospinning parameters for successful production of core shell nanofibres. The work reported here in this chapter describes an attempt to improve the understanding of the important criteria for successful coaxial electrospinning.

7.2 Aims and objectives

The main aims of the work presented in this chapter were:

- To produce core/shell nanofibres made of hydrophobic shell and loaded with a hydrophilic model drug in the core
- To verify the core-shell structure of the nanofibres using different techniques.

The achievement of these aims was possible through the realisation of the following objectives:

- Coaxial electrospinning of PLA solution as shell material and PVA solution as core component, varying the core solution flow rate
- Coaxial electrospinning of PLA solution as shell material and PVA/LidHCl solution as core component, varying the core solution flow rate
- Drug release studies over a period of 7 days using two release medium (pH 7.4 and pH 5.5).

7.3 Results and discussion

In the previous chapters of this thesis, defect free PLA nanofibres with diameter between 150 and 250 nm were produced from PLA solution in AC/DMF (50/50 v/v). Therefore this solution was initially prepared and used as shell solution for coaxial electrospinning, while PVA aqueous solution was delivered in the inner core of the needle. However, clogging of the needle occurred and electrospinning was unsuccessful. PLA is not soluble in water; therefore this could explain the precipitation of PLA and hence clogging of the needle.

When trifluoroethanol (TFE) was selected as a solvent to dissolve PLA the jet stability was enhanced and nanofibrous structures were collected. The reason may be related with the solvent evaporation rate and the miscibility of solvents with water. Though all solvents (AC, DMF, TFE) are miscible with water, they have different boiling points and vapour pressure. TFE has a boiling point (BP) of 78°C and a vapour pressure of 70 mmHg. On the other hand, the boiling point of AC is 56°C (194 mmHg), while that of DMF is 153°C (3.8 mmHg). This suggests that the evaporation rate of the solvent mixture probably have an important effect on the stability of the electrospinning process.

The applied voltage and the collection distance were varied to obtain a stable electrospun jet. 12 kV and 15 cm were found to be suitable for the coaxial electrospinning when no drug was loaded in the core solution, whereas an increase of applied voltage to 21 kV and collection distance to 22 cm were used when the drug was loaded in the core PVA solution. By the simultaneous feeding of two solutions through a coaxial needle, a Taylor cone made of an inner and an outer component is formed at the needle tip and eventually nanofibres with a core-shell structure could be formed. The stability of the jet of two liquids is strongly affected by the physical properties of the two liquids, such as solution viscosity, interfacial tension, conductivity, as well as the feed rates and applied voltage. Therefore the characterisation of the solution properties is essential in order to better understand the multiple effects that occur simultaneously and determine the fibre morphology.

7.3.1 Characterization of solution properties

Viscosity, surface tension and conductivity of shell and core solutions, with and without drug, were measured and the results are reported in Table 7.2. PLA solution in AC/DMF has a lower solution viscosity than PLA solution in TFE, but higher solution conductivity and surface tension. The higher viscosity of the shell solution compared to that one of PVA solution is probably one of the key requirements for the core shell electrospinning. In conventional electrospinning the polymer concentration and hence the solution viscosity is key element for the formation of sufficient chain entanglements between the polymer chains. The viscoelastic force counteracts the electrostatic force responsible of the stretching of the solution. During coaxial electrospinning the shell fluid surrounds the core fluid and stabilises it against break-up into droplets due to the Rayleigh instability (J. H. Yu et al. 2004). Therefore a high viscosity of the shell solution together with a low interfacial tension between core and shell solutions is essential to maintain a stable Taylor cone at the end of the needle tip (Díaz et al. 2006; Moghe & B. S. Gupta 2008; Hong Zhang et al. 2010).

On the other hand, both conductivity and surface tension of the core solution are much higher than those of PLA solution in TFE. Water is a polar solvent with high dielectric constant which leads to high electric conductivity of about 422 μS/cm. The addition of lidocaine hydrochloride to the PVA solution significantly increases the conductivity to 6890 μS/cm, as a result of the drug ability of forming ions when dissolved in water.

Table 7.2 – Solution properties of core and shell solutions.

	Shell solution	
	PLA in AC/DMF (12.5% w/v)	PLA in TFE (14% w/)
Viscosity (cP)	252±53	513.7±18.4
Surface tension (mN/m)	30.6±0.8	23.0±0.22
Conductivity (μS/cm)	2.80±0.01	0.66±0.04
	Core solution	
	PVA in water (10% w/v)	(PVA + LidHCl) in water (10% w/v, drug 50% w/w)
Viscosity (cP)	301.5±18.5	316.0±6.29
Surface tension (mN/m)	60.3±0.36	55.7±0.55
Conductivity (μS/cm)	422.6±4.51	6980±40.0

During the electrospinning process the elongation of the shell solution is mainly driven by electrostatic repulsion between the charges on the jet surface. However, in most scientific publication the solution properties of core and shell solution are not measured. Poly(L-lactide-co-caprolactone) (PLLACL) solution in trifluoroethanol (TFE) and bovine serum albumin (BSA) in water were used as shell and core material, respectively, by Yan et al (S. Yan et al. 2009). Successful production of core-shell nanofibres was demonstrated and sustained release of BSA determined. The authors mentioned the formation of electrospun nanofibres and the morphologies may be affected by the presence of water in core solution, because of its low volatility. Wet fibres may be collected if water does not completely evaporate from the electrospun jet as it travels towards the collector, but the low flow rate of the core solution limited this problem. However solution properties were not measured and the conductivity was not taken into account.

7.3.2 Physical characterisation of nanofibres

The morphology of the core-shell nanofibres produced was investigated using several techniques, including scanning electron microscopy (SEM), transmission electron microscopy (TEM), confocal laser scanning microscopy (CLSM) and focus ion beam (FIB). A number of other techniques were employed to examine both chemical composition of the nanofibrous mats and interactions between core and shell materials. Each analysis will be discussed in the next paragraphs.

7.3.2.1 Scanning electron microscopy (SEM) analysis

Morphological analyses of the surface of the nanofibrous structures with and without drug were performed using scanning electron microscope. Figure 7.1 shows the nanofibres collected without drug, while Figure 7.2 shows the nanofibres loaded with LidHCl. SEM micrographs show that nanofibres with no beads were collected from all formulations. The viscoelastic force of the shell solution was able to counteract the electrostatic forces due to charge repulsion, as a result of sufficient entanglements between PLA polymer chains. However, very few imperfections were detected in all electrospun samples. The micrographs

shown in Figure 7.3 and Figure 7.4 were taken at high magnification.

Branching of the jet is shown in Figure 7.3 A and Figure 7.4 A corresponding to nanofibres formed using a core flow rate of 0.3 ml/h. A branched fibre is formed by the ejection of a secondary jet from the primary jet during electrospinning. Similar observations have been reported by Reneker and Yarin (D.H. Reneker & A.L. Yarin 2008) and this phenomenon is generally due to non-uniform distribution of the charges along the electrospun jet. Probably this is due to the much higher conductivity of the core solution compared to the shell solution. Furthermore, Figure 7.3 B shows a protuberance on the fibre surface, while the fibres indicated with arrows in Figure 7.3 C and D presents wrinkled surfaces. This observation could be a consequence of different and changing combinations of solvent transport and fluid properties.

An increase of core flow rate to 0.5 and 0.7 ml/h led to the formation of some flat nanofibres as shown in Figure 7.4 C and D. This observation could be explained by the formation of a skin on the fibre surface and it may an indication of non-uniform solvent evaporation. TFE has a much higher evaporation rate than water. Therefore this may affect the fibre structure, as water may continue to evaporate after the fibre is collected.

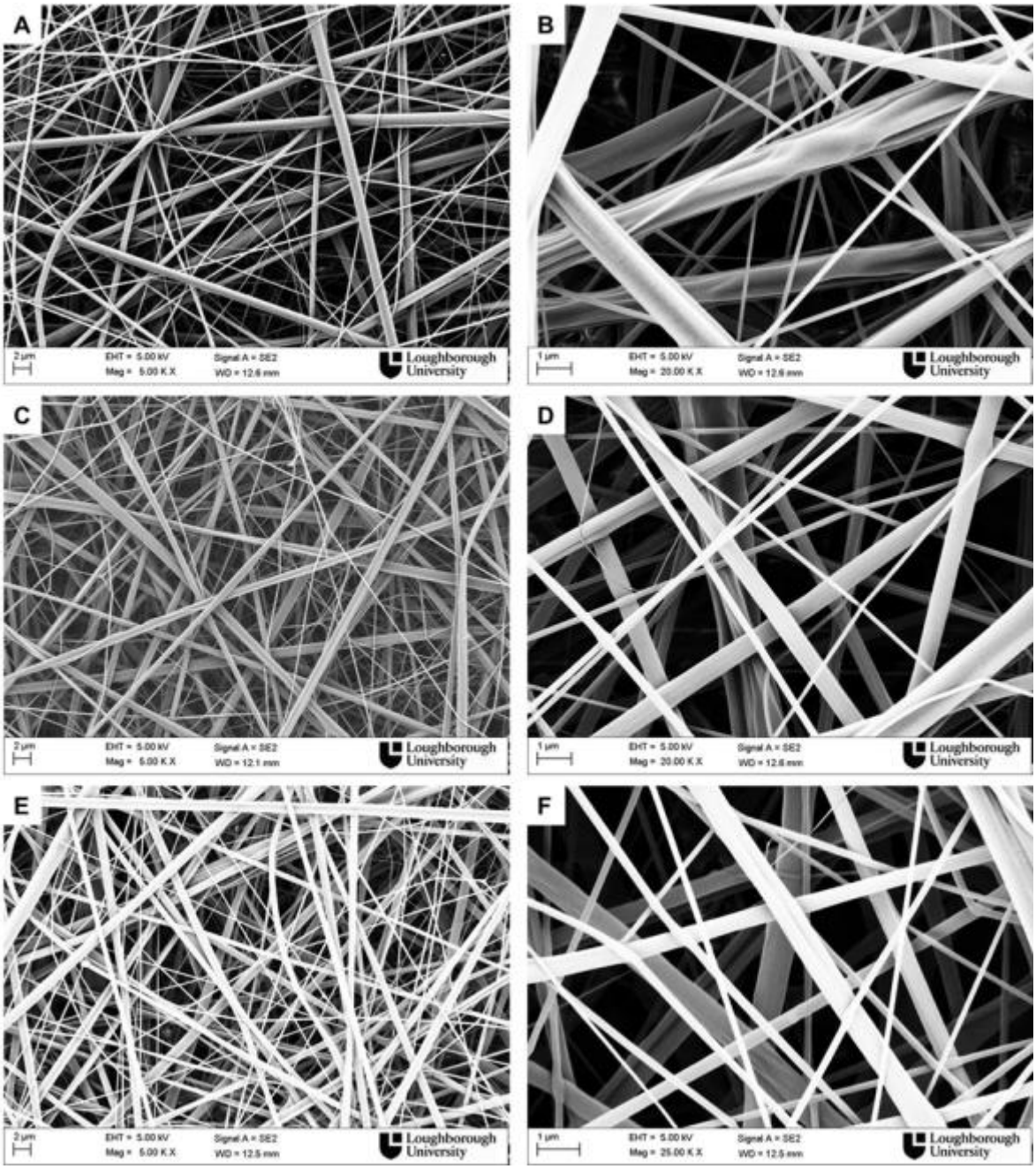

Figure 7.1 – Scanning electron micrographs of core-shell nanofibres with no drug at different core flow rates (A, B) 0.3 ml/h, (C, D) 0.5 ml/h, (E, F) 0.7 m/h.

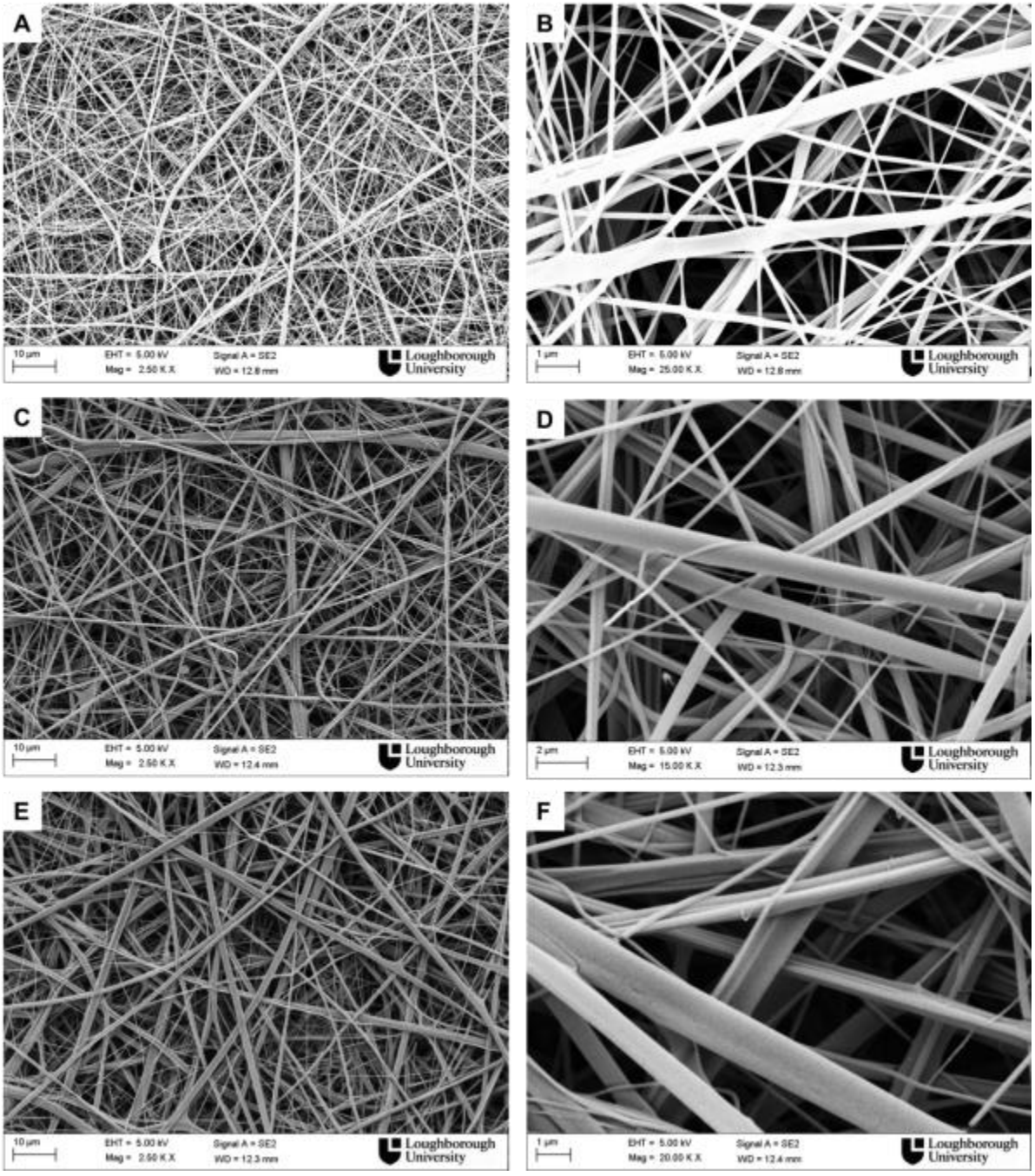

Figure 7.2 – Scanning electron micrographs of core-shell nanofibres with drug loaded in the core at different core flow rates (A, B) 0.3 ml/h, (C, D) 0.5 ml/h, (E, F) 0.7 m/h.

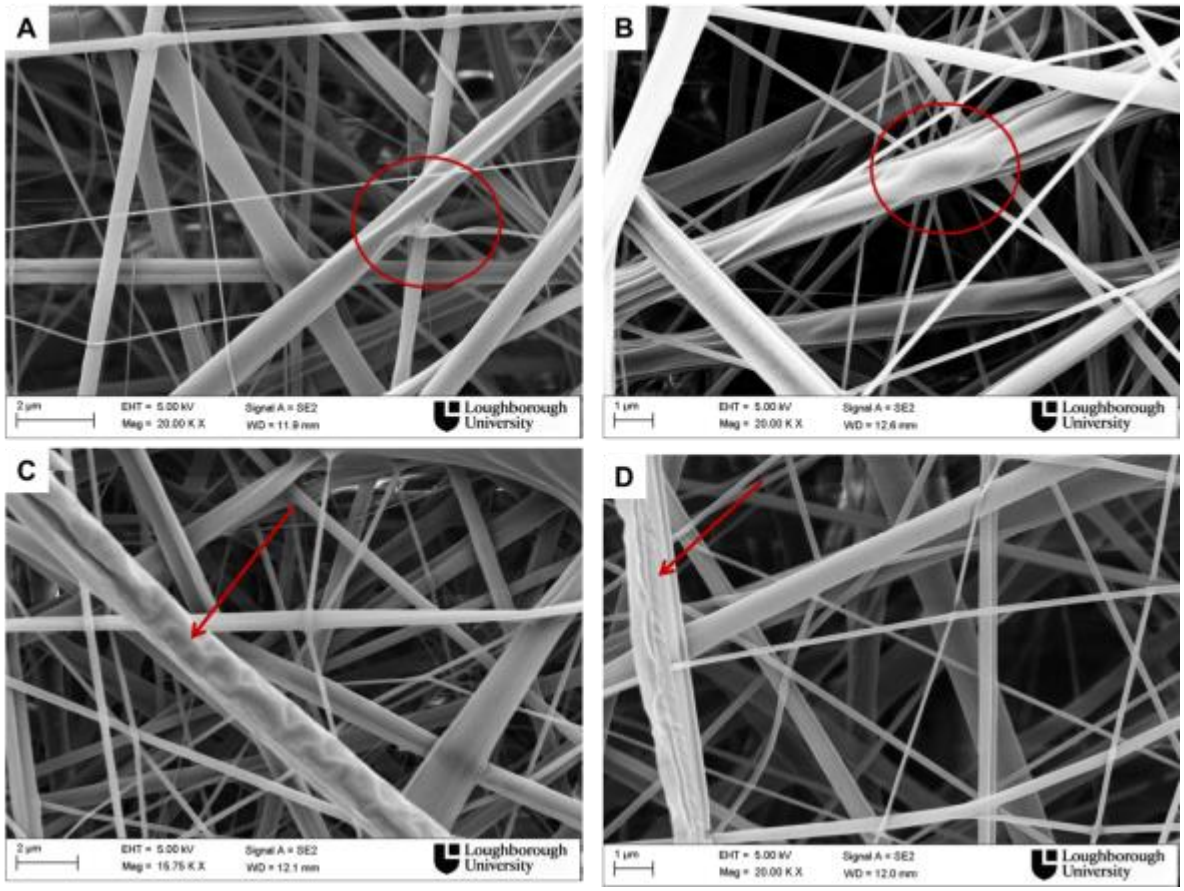

Figure 7.3 – Core shell nanofibres (no drug) presented (A, B) 2.1-0.3 ml/h, (C) 2.1-0.5 ml/h, (D) 2.1-0.7 ml/h.

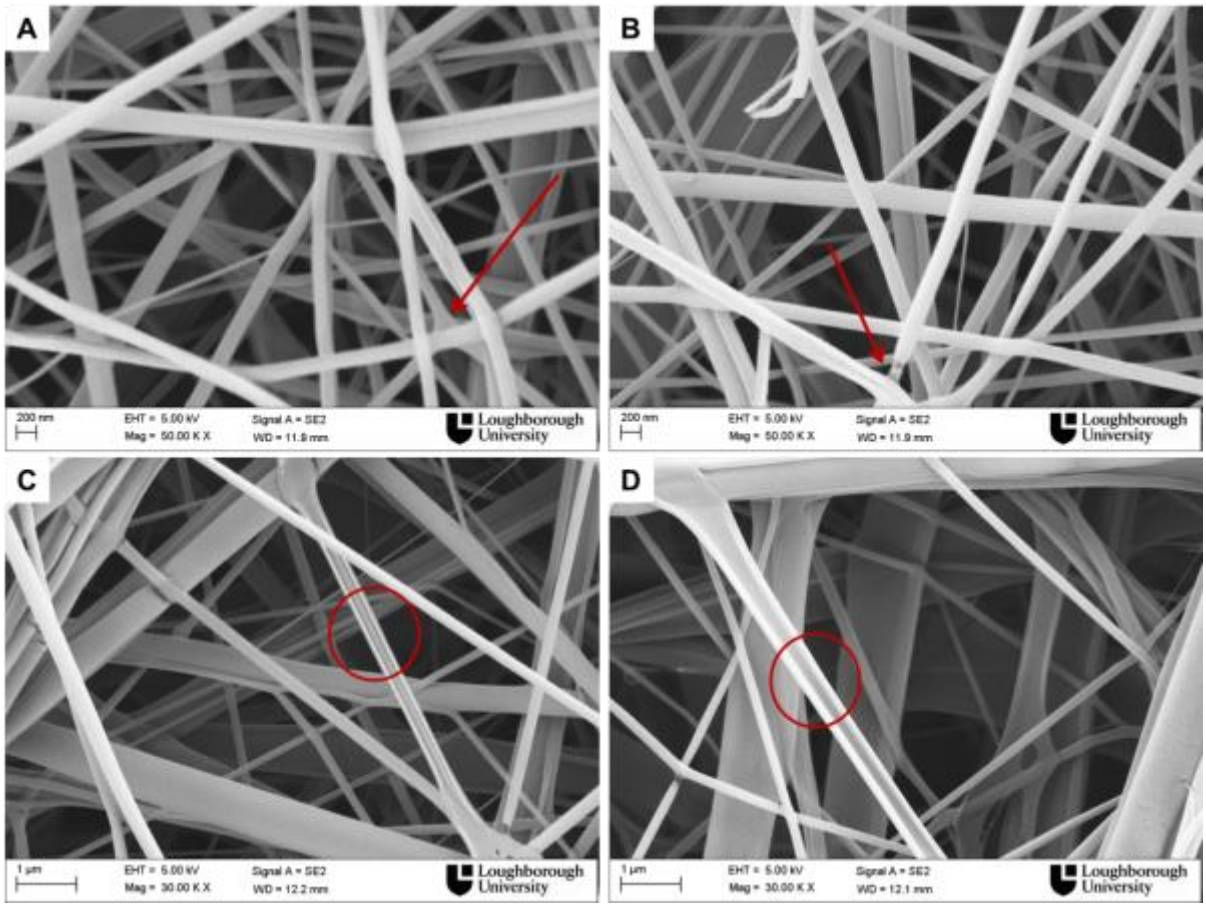

Figure 7.4 – Core-shell nanofibres loaded with drug (A, B) 2.1-0.3 ml/h, (C) 2.1-0.5 ml/h, (D) 2.1-0.7 ml/h.

Next, measurements of nanofibre diameter were performed. The results are reported in Figure 7.5. Statistical significance was determined by one-way ANOVA analysis. While the mean diameter of nanofibres with no drug does not significantly vary on increasing the core solution flow rate from 0.3 to 0.7 ml/h (p value=0.08>0.05), when the drug was incorporated in the core solution a significant difference in the mean diameter was determined (p value=4.16E-26<0.05). The diameter increases from 164 to 403 nm as the flow rate increases. This may be related to the increase of conductivity of the PVA solution resulting from the addition of the drug. In this case, the jet is most probably more unstable and hence small variations of the solution core flow rate lead to larger difference in the mean diameter.

Comparing the value of diameter of nanofibres with and without drug produced using a core of flow rate of 0.3 ml/h, a significant difference was observed (p value=3.36E-18<0.05). The diameter of the sample without drug is just over 300 nm whereas when drug is added at the same flow rate the diameter decreases to about 160 nm. This could be explained by the higher conductivity of the core solution when LidHCl is incorporated as shown in Table 7.2, while solution viscosity and surface tension did not significantly vary when drug is added. In simple electrospinning, an increase of solution conductivity usually leads to higher amount of electrical charges resulting therefore in thinner nanofibres (You et al. 2006). Here, the reduction of the diameter of PLA nanofibres with the addition of LidHCl may suggest that the higher amount of charges of core solution leads to higher total amount of charges (shell+core) and it is responsible of the higher degree of jet stretching imposed by the electrical forces. It is not fully understood how the electrical charges affect the coaxial electrospinning process, although some authors stated that the electric charges are located predominantly at the outer fibre surface (Pham, U. Sharma & A.G. Mikos 2006; Greiner et al. 2006).

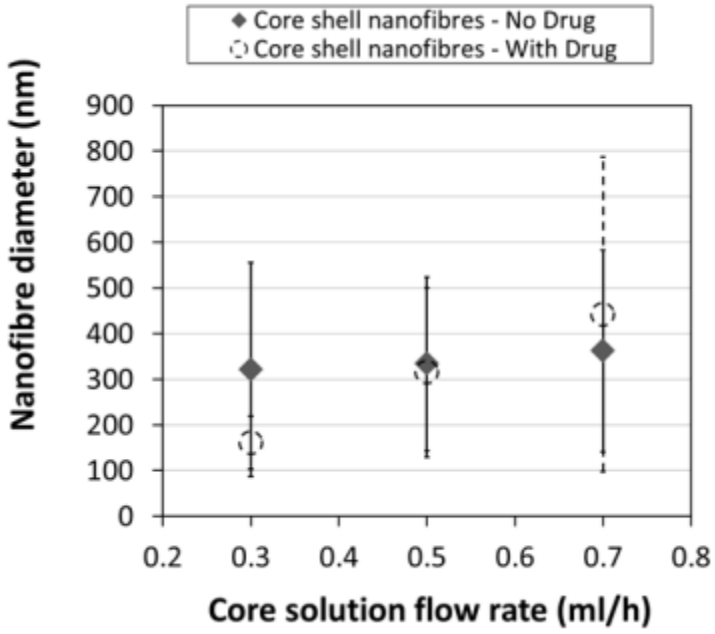

Figure 7.5 – Mean diameter for core-shell nanofibres.

As the core solution flow rate is increased to 0.5 ml/h, no significant difference was observed between the mean diameter of the nanofibres with and without drug, which was 313±180 and

335±192 nm, respectively (p value=0.24>0.05). Similarly, at the highest flow rate (0.7 ml/h) p value of 0.10 indicates there is no significant difference.

A few scientific publications reported the effect of core flow rate on the shell and core thickness (H. Jiang et al. 2005; Chi Wang et al. 2010; Joung et al. 2011). For example Wang et al (Chi Wang et al. 2010) have reported that an increase of core flow rate leads to an increase of core diameter, while no effect was observed on the shell thickness by SEM analysis. On the other hand, other researchers (Y Z Zhang et al. 2006; H. Jiang et al. 2005) found that the shell diameter increases with increasing core flow rate, but no explanations have been proposed. For example Zhang et al (Y Z Zhang et al. 2006) reported that the fibre diameter for samples produced using core flow rate of 0.2, 0.4, and 0.6 ml/h were 277±140, 330±167, and 378±149 nm, respectively. The different trends are most probably due the different types of core and shell solutions. At constant applied voltage, an increase of core flow rate may affect the solvent evaporation rate of the solvent in the core but also that one of the solvent in the shell solution. The effect of drug incorporation in the core solution on the solution properties including viscosity, conductivity and surface tension has not been fully investigated. It would be really important to understand how the drug affects the solution properties of the core solution and hence the coaxial electrospinning.

7.3.2.2 Transmission electron microscopy (TEM) analysis

As the SEM images cannot provide evidence of the formation of core shell structure, several means were employed to characterize the encapsulation effect. First, the core-shell nanofibres were examined by using TEM. The sample collected using core solution flow rate of 0.3 ml/h has shown overall a monolayer structure, although a thin core was observed as shown in Figure 7.6. This could be due to the low flow rate of the core solution and hence the TEM cannot clearly detect the boundaries.

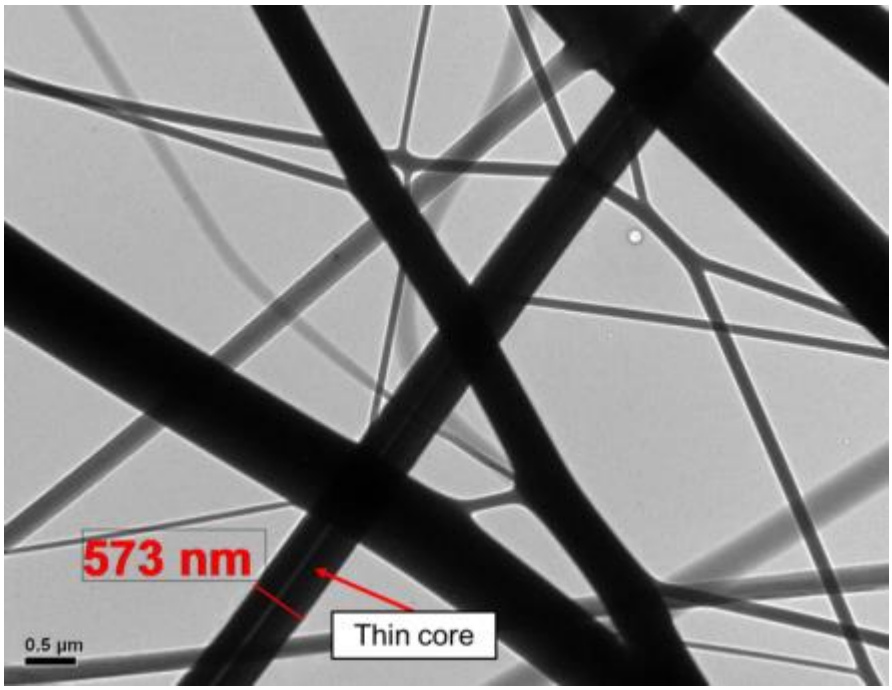

Figure 7.6 – Core-shell nanofibres produced at core-shell flow rate ratio 0.3/2.1 ml/h.

Different structures were instead observed on increasing the flow rate to 0.5 and 0.7 ml/h, as shown in Figure 7.7 and Figure 7.8, respectively. TEM investigations of the PVA-PLA core-shell nanofibres collected using a flow rate of 0.5 ml/h have shown that some nanofibres had a distinct core shell structure, as the interface between core and shell is clearly visible. The colour of the inner part is lighter than that one of the external shell. But some imperfections were detected. The formation of nanofibres with branches shown by arrows in red is most probably an indication of splitting of the jet during the experiment.

On increasing core solution flow rate to 0.7 ml/h different types of morphology could be observed as shown in Figure 7.8. Images A and B show defect-free core shell fibres whereas images C and D show some defects or imperfections in the samples. The core shell structure is clearly visible in the first two images where nanofibres presents core and shell diameter of 638 nm and 485 nm, 559 and 437 nm, respectively. On the other hand, a large nanofibre with no core but two branches is shown in Figure 7.8 C, as a result of splitting of the electrospun jet. Similar to the previous observations of nanofibres produced using a flow rate of 0.5 ml/h, this phenomenon is most probably due to irregular distribution of charges on the jet surface which are responsible of the jet stretching imposed by the electric forces. The different colour of the main fibre and the branches combined with the lack of any core shell visible structure

might indicate that the branches are formed by the core solution.

Other imperfections are shown in Figure 7.8 D. A nanofibre looks flat and the deformation (shown by arrows in red) is probably caused by non-uniform solvent evaporation. Overall the thickness of both shell and core appeared larger than that of nanofibres formed using flow rate of 0.5 ml/h, although more imperfections were also detected.

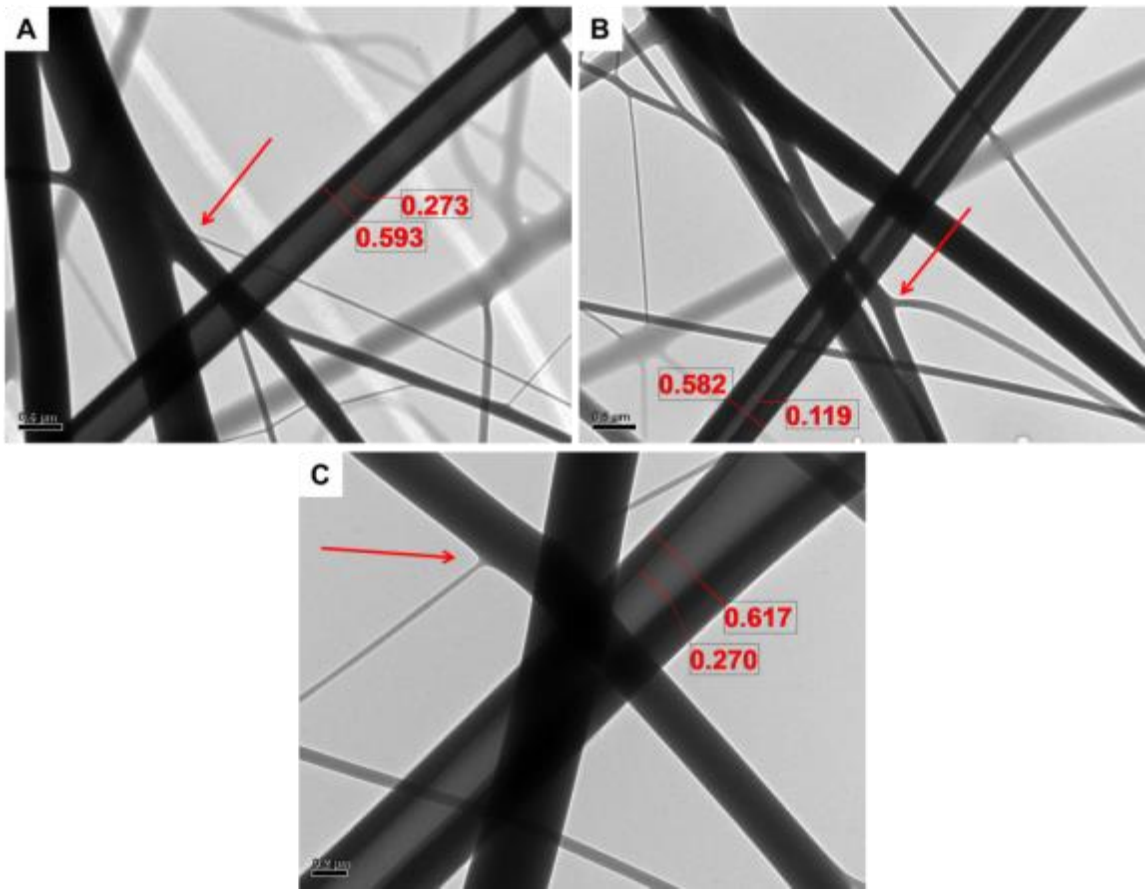

Figure 7.7 – Core-shell nanofibres produced at core-shell flow rate ratio 0.5/2.1 ml/h.

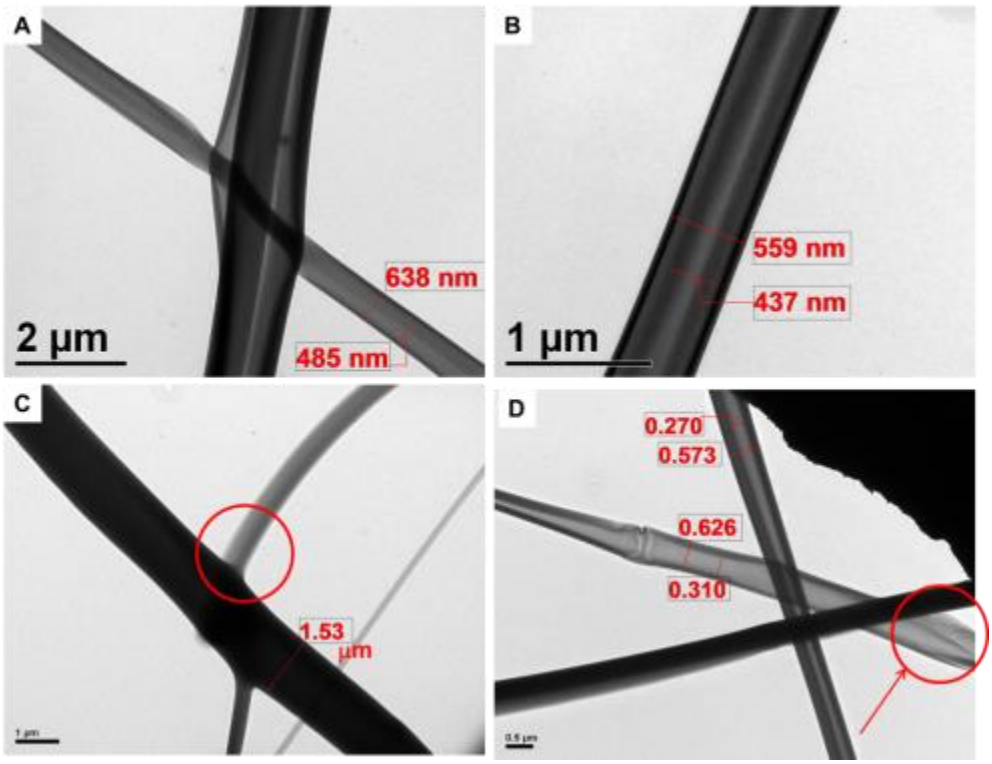

Figure 7.8 – Core-shell nanofibres produced at core-shell flow rate ratio 0.7/2.1 ml/h.

Nanofibres with monolayer structures and splitting of the jet are a phenomenon that have been observed and reported by few researchers (C. He et al. 2006; Y Z Zhang et al. 2006; Z. Sun et al. 2003; J. H. Yu et al. 2004). Yu et al (J. H. Yu et al. 2004) observed that a third of the fibres did not exhibit core shell structure when a poly(aniline) (PANi) aqueous solution was used as core material and a PVA aqueous solution as shell component. Even though the solution properties were not reported, the author suggested that the PANi solution is pulled out by the electrostatic forces at higher rate than the flow rate set by the syringe pump (0.005 ml/min), as result of its higher charge density compared to the PVA shell solution. In fact PANi is more conductive polymer compared to PVA.

Hence the splitting observed in some PVA/PLA nanofibres is probably due to the higher conductivity of PVA/LidHCl solution (6980 µS/cm) compared to that of the PLA solution in TFE (0.66 µS/cm). Zhang and his colleagues (Y Z Zhang et al. 2006) electrospun PCL solution in TFE as shell material and PEG with bovine serum albumin (BSA) in aqueous solution as core component. The results have shown some monolayer nanofibres, but no information about solution conductivity was given by the authors.

In most scientific publications about co-axial electrospinning, the solution properties such as viscosity, conductivity and surface tension are not reported. Coaxial electrospinning is far more complex than normal single fluid electrospinning. During the coaxial electrospinning process, the shell solution is elongated due to repulsion of charges on the jet surface, but it is not clear how the charges of the core solution affect the electrospinning process. The core solution is stretched together with the shell due to viscous dragging and contact friction (D. Li & Y. Xia 2004). Therefore a better understanding of the electrohydrodynamics involved in coaxial electrospinning may be gained by measuring the solution properties of both core and shell solutions.

7.3.2.3 Confocal laser scanning microscopy (CLSM) analysis

To support TEM images, an optical imaging technique was applied to verify the formation of nanofibres with a core shell structure. In most scientific publications, TEM is generally used to verify the core shell morphology (D.-G. Yu, Williams, et al. 2013; Yajing Li et al. 2012; Kijeńska et al. 2014), but confocal laser scanning microscope have been also employed in the last years by few researchers (Joung et al. 2011; Maleki et al. 2013; Benada et al. 2012; G. Jin et al. 2013) for nanofibrous structures.

The samples were prepared by addition of green dye in the core solution and red in the shell solution to enable the visualisation of the core shell structure. A number of images of the PVA/PLA nanofibres collected on a glass slide were taken as shown in Figure 7.9, Figure 7.10 and Figure 7.11. In each figure the first and the second columns present the contribution of the green and red dye in core and shell, respectively, while the third column is the overlay of the first two. The last column shows the image in natural light. The evidence of both red and green colours proved the contribution of both dyes and the formation of core shell fibres, but the detection of the boundaries between core and shell was sometimes challenging.

Overall no or few beads were observed in the nanofibres collected from coaxial electrospinning of PLA solution as shell material and PVA solution without drug as core material (Figure 7.9, Figure 7.10). Figure 7.9 shows images of nanofibres collected using core flow rate of 0.3 ml/h. Although the core-shell nanofibres are extremely small and

detailed layer structures of the inner component distribution could not be identified by CLSM, Figure 7.9 (E-H) shows the formation of a bead along the electrospun nanofibres. The green signal of fluorescein is observed in the inner part of the bead (image E), while the stronger red signal (image F) is observed in the shell. Therefore this may suggest that core shell structure was formed. In the image L the nanofibre presents a thin dark shell, while the arrows indicate discontinuous distribution of the core. This could be explained by the smaller flow rate of the core solution compared to that of the shell solution. Core and shell solutions have different viscoelastic properties, so when stretching is applied the core may not withstand this stretching and may break up. Therefore the discontinuous core may be the result of the low flow rate combined with the different concentration and viscoelastic properties of the core.

An increase of flow rate to 0.5 ml/h resulted in more homogenous fibres as shown in Figure 7.10, although some elongated beads were seen in image B. In addition, the highest core solution flow rate of 0.7 ml/h led probably to jet splitting. The white arrow in the image G shows a green fibre from the merged image (third column) which could indicate that the core solution is pulled out due to higher amount of charges (higher solution conductivity) compared to the shell solution.

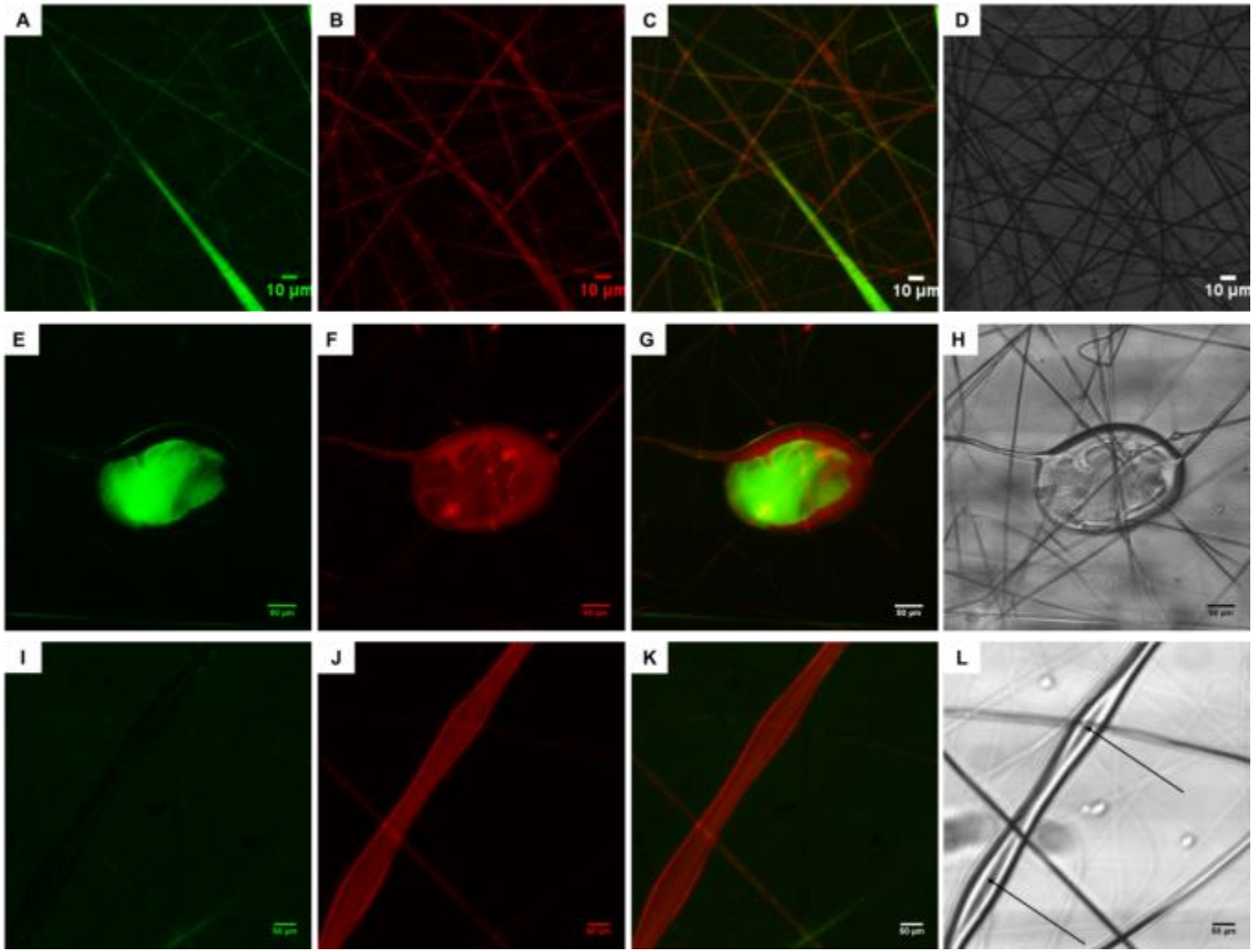

Figure 7.9 – CLSM images of nanofibres (**no drug)** collected using a core-shell flow rate of 0.3-2.1 ml/h (A-D) 10 µm, (E-L) 50 µm.

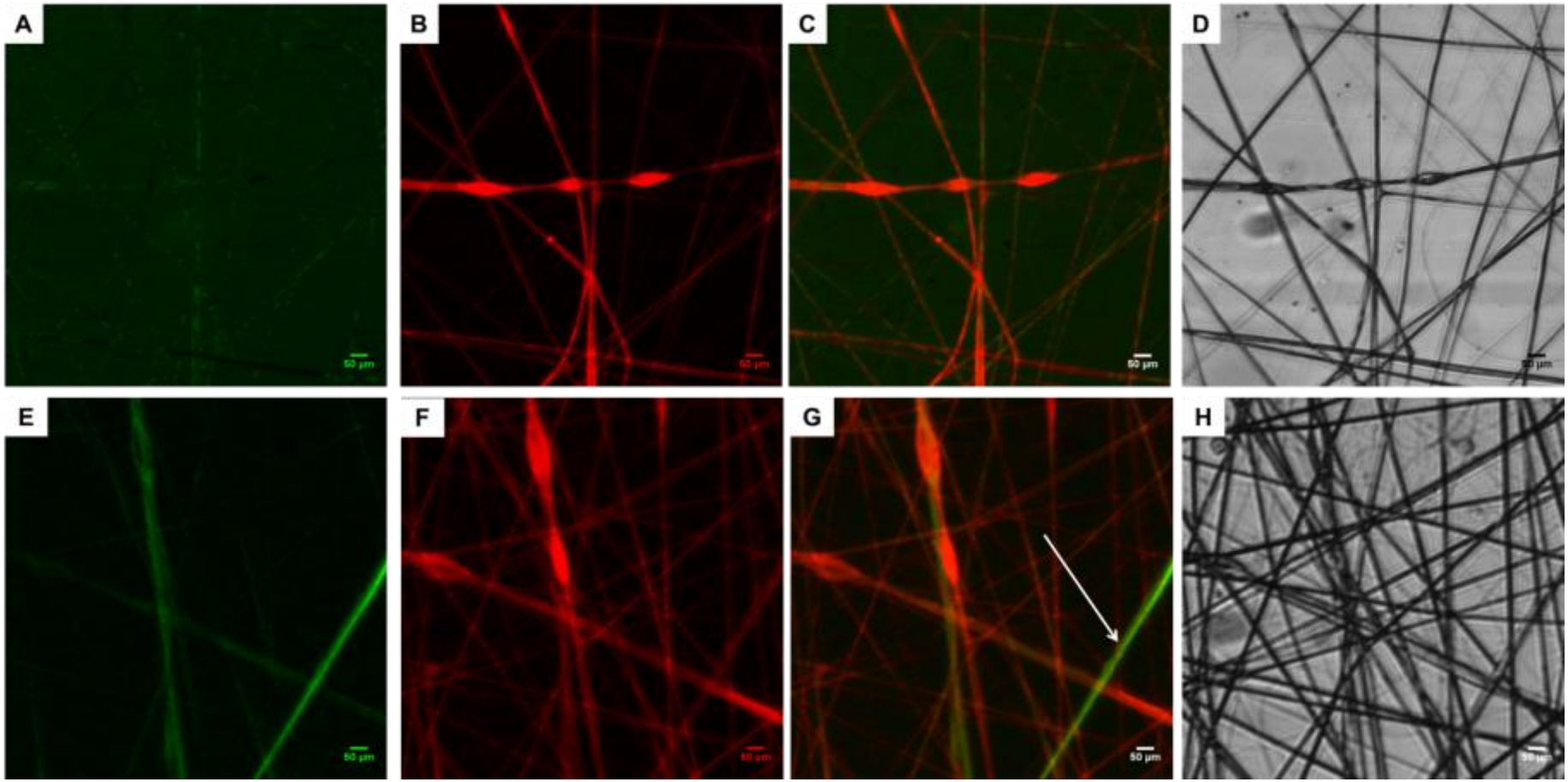

Figure 7.10 – CLSM images of nanofibres (**no drug**) collected using core-shell flow rate of (A-D) 0.5-2.1 ml/h, (E-F) 0.7-2.1 ml/h.

CLSM images of nanofibres loaded with LidHCl in the core are shown in Figure 7.11. Similar to the observations of nanofibres without drug, the detection of the two layers was challenging. In Figure 7.11 G a fibre with a yellow core and very thin red shell is observed. The yellow colour is most probably a result of the similar signal intensity of the fluorescein and rhodamine. An increase of core solution flow rate to 0.7 ml/h result in a defect along the fibre. The inner part of this defect is yellow (image K), whereas the shell is red. Therefore this could again suggest that core shell structure is formed.

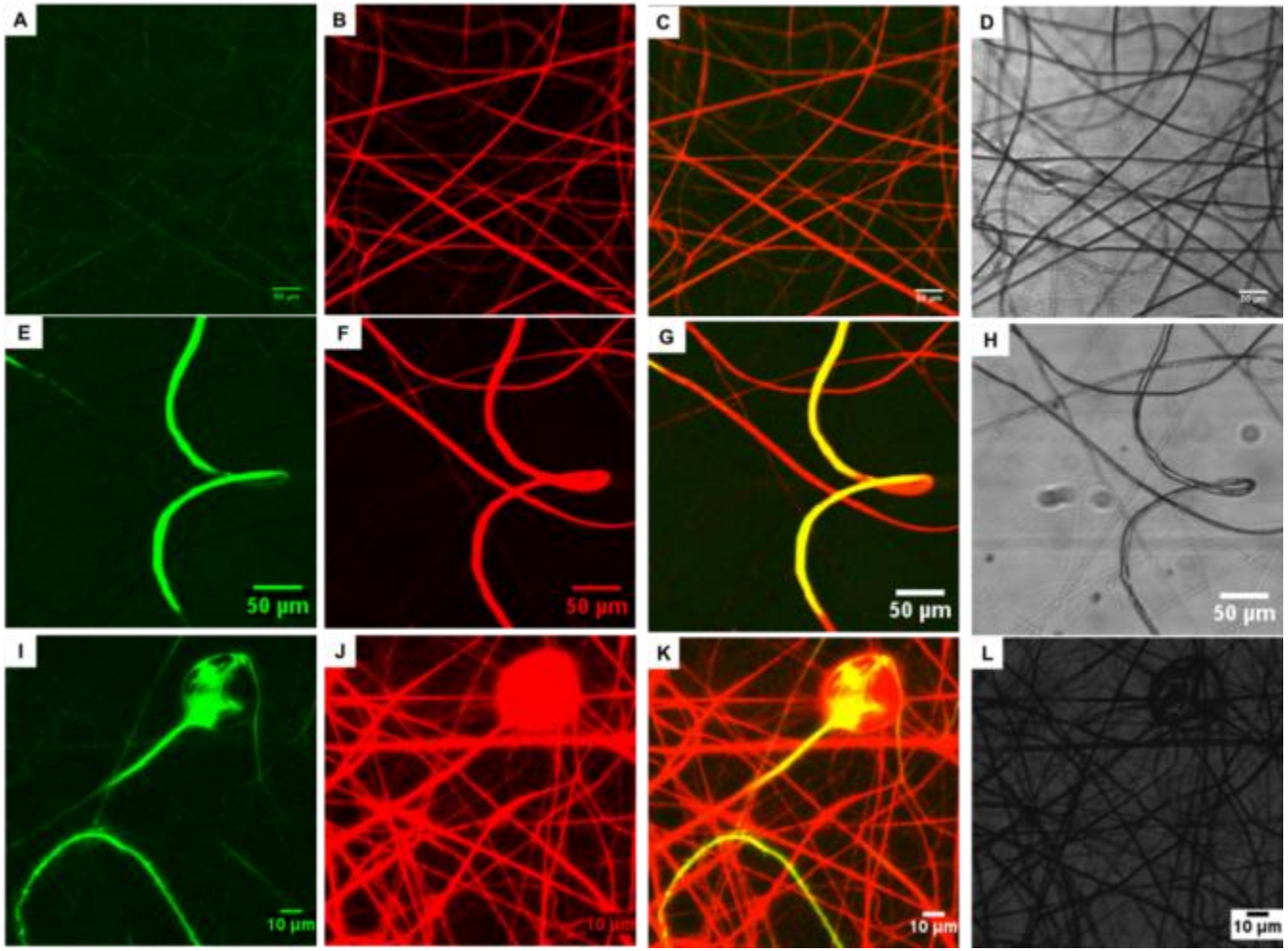

Figure 7.11 – CLSM images of nanofibres **loaded with drug** collected using core-shell flow rate of (A-D) 0.3-2.1 (E-H) 0.5-2.1 (I-L) 0.7-2.1 ml/h.

To summarise, sharp boundaries in the TEM images due to the difference in electron transmission ability between the core and shell materials were indicative of the core shell structure of the fibres and it was possible in some cases to measure the thickness of core and shell layers. On the other hand, CLSM was challenging and different distributions of fluorescein in the core suggested that different morphologies co-existed such as core shell fibres, hollow fibres and monolayer structures. Similarly, Ji et al (Ji et al. 2010) used confocal microscopy to observe the protein distribution, although it was not an acceptable method for measurement of the different core and shell fibre diameters.

7.3.2.4 Focus ion beam-scanning electron microscopy (FIB-SEM)

A less commonly used method of analysis was employed to verify the formation of a core shell structure, the focused-ion beam milling process for characterization of the fibre cross section (S. Choi et al. 2011; Wenwen Liu et al. 2013; Abidian et al. 2006). An ion beam probe is used to cut the nanofibre and remove a part of it through milling. Then the cross section of the nanofibre is imaged under the SEM. Figure 7.13 shows some of the nanofibres observed with this analysis. Different morphologies have been detected. Even though Figure 7.13 A, B and C may suggest the formation of either a hollow or a core shell structure, due to the darker inner region of the fibre, Figure 7.13 D shows probably buckled fibres.

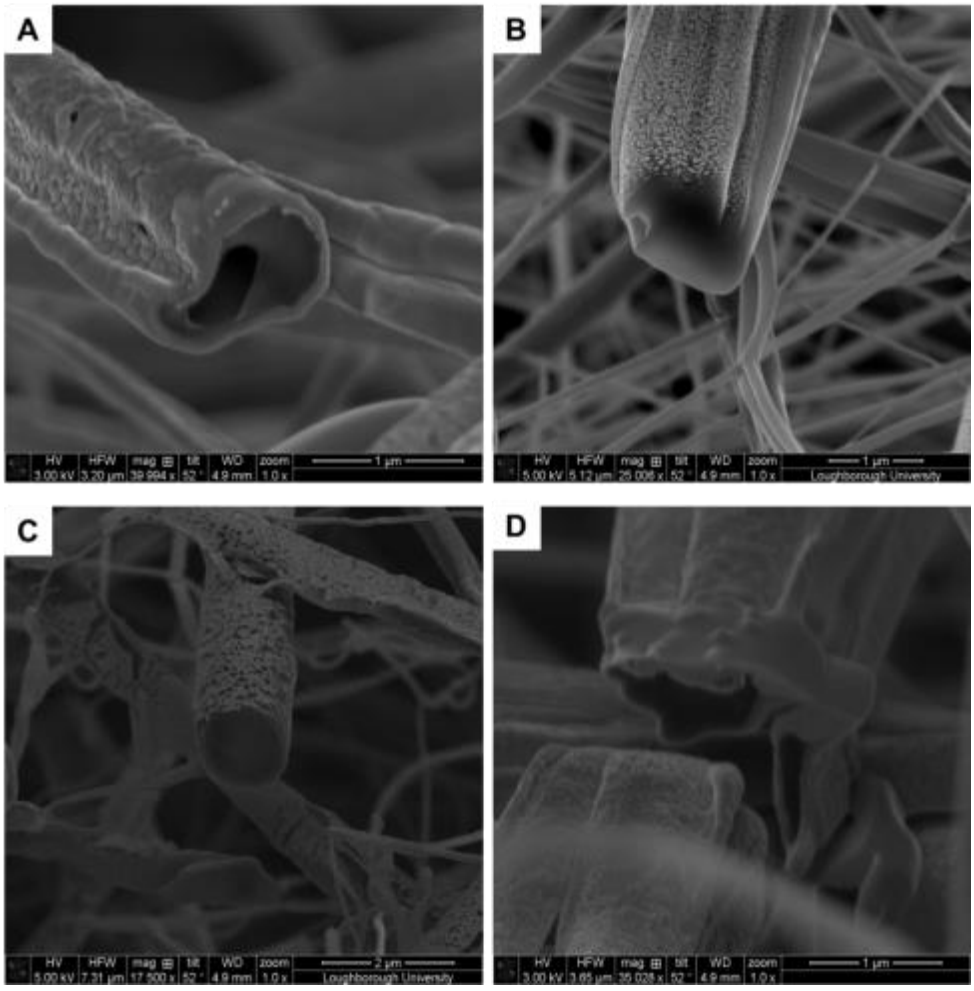

Figure 7.12 – FIB-SEM images of nanofibres collected using core solution flow rate of 0.5 ml/h.

As reported in chapter 2, a buckling effect may lead to the formation of microtubules or micro ribbon instead of uniform core shell structures, as a result of the slower evaporation of solvent in the core compared to the fast evaporation of the solvent from the shell (Dror et al. 2007). Different polymer-solvent systems were selected as core and shell solutions by Arinstein et al (Arinstein et al. 2009). The results have shown that immiscible core and shell solutions, PEO in ethanol/water and PCL in CHL/DMF, respectively, lead to production of hollow nanofibres. On the other hand, collapsed and less uniform tubes were observed when the core material was a PEO solution in DMF, miscible with the shell.

In this work of thesis PLA and PVA solutions are immiscible, because water is non-solvent for PLA, although the solvent of the shell solution (TFE) is completely miscible with water. As the aqueous solution gets in contact with the shell during the electrospinning process,

precipitation of the inner layers may occur unless the electrostatic forces are able to stretch quickly the shell solution and so no enough time is given for the precipitation. Hence this phenomenon may explain the observations of some fibres with discontinuous core, shown from CLSM images. The discontinuous core could be formed if precipitation of the polymer occurs before the fibre is stretched to its full length. Hence when the fibre is further stretched after precipitation, the core breaks and forms a discontinuous morphology. Furthermore, Figure 7.3 B from the SEM analysis has shown a protuberance on the fibre surface, which could be an indication of the buckling effect. In several scientific publications an aqueous solution has been used as core material and the authors confirmed the production of core shell nanofibres by TEM analysis (S. Yan et al. 2009; Z.-M. Huang et al. 2006; Kijeńska et al. 2014). Poly (L-lactide-co--caprolactone) (PLLACL) solution in trifluoroethanol (TFE) and bovine serum albumin (BSA) in water were used as shell and core material, respectively, by Yan et al (S. Yan et al. 2009). Nevertheless, no clear evidence of the core shell structure was reported by the authors with TEM analysis and no measurements of solution properties was reported, although the wide shell diameter distribution was related to splitting of the electrospun jet.

In conclusion, TEM analysis has been found to be the most appropriate technique to show the core shell structure in nanofibres. Nanofibres can be collected on copper grid and directly observed under the microscope, while dyes are required for CLSM analysis. But, it is probably important to collect several samples in order to have an average of the core thickness. In coaxial electrospinning, the entrainment of the core in the shell solution and hence production of fibres with the core-shell configuration may be guaranteed by both the control of solution chemistry and interactions between core and shell solutions, and also the fast processing which may prevent mixing of the solution and/or polymer precipitation.

7.3.2.5 Water contact angle (WCA) measurements

The surface wettability of the nanofibrous samples was investigated by measuring the water contact angle for pure PLA and PVA nanofibres, and PVA-PLA nanofibres with and without drug. The results are reported in Figure 7.14. Contact angles lower than 90° correspond to high wettability and hydrophilic surfaces, while large contact angles than 90° correspond to

low wettability and hydrophobic surfaces.

PVA is a hydrophilic polymer, which indicates good compatibility with water due to the ability of forming hydrogen bonding (-OH). Therefore this explains the contact angle of approximately 60° for PVA nanofibres. However the measurement of this angle was challenging, because in many occasions the drop was immediately adsorbed into the nanofibrous mat as a result of the high PVA hydrophilicity. On the other hand, a mean value of 126° for PLA nanofibres was observed and it is strong indication of the hydrophobicity of the material. PLA is non-soluble in water.

Next, the water contact angle was measured for core/shell PVA/PLA nanofibrous samples with and without drug. The mean values varied between 122 and 128° regardless of the drug addition, indicating, therefore, the hydrophobicity of the membrane. The contact angle value for the core shell samples are very close to the contact angle value of pure PLA nanofibres. Hence these observations suggest that PLA is the outer layer of the nanofibrous mat. Considering that pure PVA nanofibrous mat have clearly shown hydrophilicity with a contact angle of 60°, the value of about 125° of the core/shell nanofibres may also suggest that PVA is incorporated in the core, and hence core-shell structure is formed. In fact, if PVA is not incorporated in a core, the contact angle should decrease due to the PVA hydrophilicity.

The WCA analysis was used to verify the encapsulation of the core material by few researchers (T. T. T. Nguyen et al. 2012; Maleki et al. 2013; W. Song et al. 2013). Nguyen et al (T. T. T. Nguyen et al. 2012) have shown that on increasing core flow rate from 0.1 ml/h to 0.4 ml/h, the WCA of the resultant nanofibrous membrane slightly from 103° to 0°. The authors stated that this is due to the exposure of the core material on the fibre surface. At the highest core flow rate (0.4 ml/h), the shell material (PLA) with flow rate of 1.5 ml/h is not able to encapsulate the core material (PEG and drug, salicylic acid). In this work of thesis the core flow rate did not show to reduce the contact angle value indicating therefore that PVA is incorporated in the PLA shell. These observations indicate that the core/shell flow rate ratio is together with the solution properties an important parameter in coaxial electrospinning.

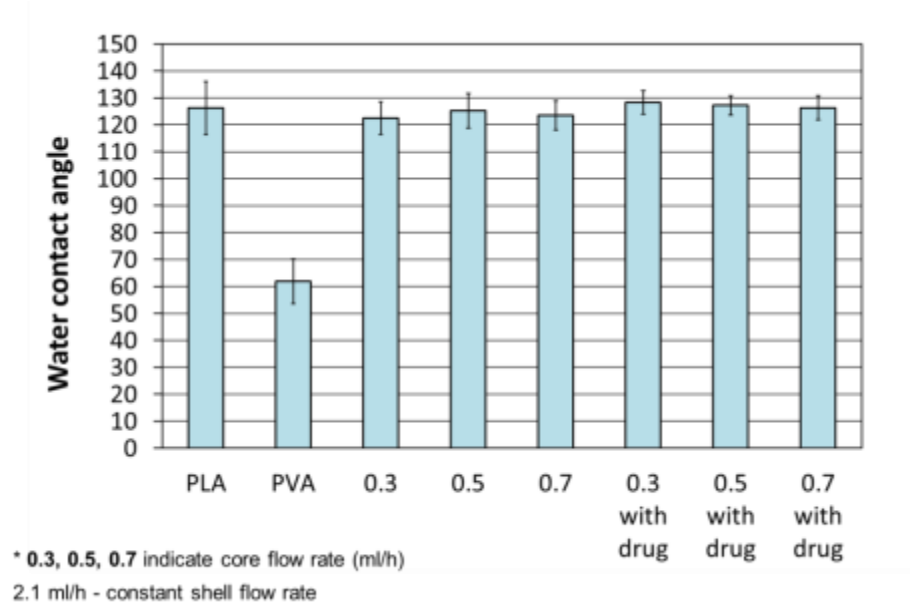

Figure 7.13 – Water contact angle values of PLA and PVA nanofibres and core shell nanofibres, with and without drug.

To summarise, so far it has been shown that relatively uniform defect-free nanofibrous mats were produced from coaxial electrospinning using PLA solution in TFE as shell material and PVA aqueous solution, as core material. Overall mats are most probably made of core-shell nanofibres, but some hollow nanofibres and also monolayer structure were detected depending on the core solution flow rate.

7.3.2.6 Differential scanning calorimetry (DSC) analysis

In most scientific publications, differential scanning calorimetry has been used to investigate the crystalline structures of the electrospun nanofibrous samples (T. T. T. Nguyen et al. 2011; Muller et al. 2009; Dhandayuthapani et al. 2010; X. Qin et al. 2012). It is an important issue to check the thermal characteristics of the electrospun nanofibres after electrospinning in order to compare them with the pure polymers. Changes in glass transition temperature, melting temperature, degree of crystallinity, enthalpy of fusion and thermal degradation are a sign of possible structural changes which might occur after electrospinning and blending. Thermal analysis was performed for the bulk materials, PLA and PVA, and all nanofibrous

samples produced with and without drug. No significant difference was observed between the the thermograms of bulk PLA and PLA nanofibres as shown in Appendix (Figure A.1), indicating therefore that the electrospinning process does not change the polymer structure. The analysis was repeated three times for both samples. The step change at about 59ºC during the heating cycle corresponds to the glass transition temperature (T_g) of the polymer. No cold crystallisation peak (T_c) or any melting point (T_m) were detected, thus confirming the completely amorphous nature of PLA. The values of T_g for PLA powder and PLA nanofibres are reported in Table A.1. Differently, in their studies Zong et al (Zong et al. 2002) found lower T_g for PLLA electrospun membrane as a result of higher surface area to volume ratio, and lower crystallinity due to the high elongation rate during electrospinning. DSC and XRD analysis have shown that the polymer chains were non crystalline but highly oriented. A certain level of chain alignment for PLLA electrospun fibres was also found by Oliveira (Oliveira et al. 2013).

Similarly, DSC thermogram for PVA powder and PVA nanofibres were obtained as shown in Figure A.2. The curve of PVA powder presents a slight reduction of heat flow as the temperature increases from 50°C to 150°C. This denotes moisture lost from the sample. Then further increasing temperature, an endothermic peak is shown at about 226°C indicating the melting process of PVA. The theoretical melting peak of fully hydrolysed PVA found in the literature is between approximately 190°C and 235°C (Jelinska et al. 2010; Parparita et al. 2012). In the following cooling cycle the DSC curve presents an exothermal crystallization peak that is shifted slightly to a lower temperature compared with the melting peak, between approximately 183 and 186°C. However, PVA nanofibres presented a different thermogram to that of PVA powder (Figure A.2). Loss of moisture was clearly distinguished between 90°C and 150°C indicating therefore that after the electrospinning process a certain amount of water remained in the nanofibrous mat. The second feature is the presence of a double peak at the melting point, the first one at about 227°C and the second one at 233°C. The analysis was repeated three times and the double peak was detected in all samples. In some cases the double peak has been related to the formation of imperfect crystals (Muller et al. 2009). During the cooling step the crystallization peak was found at higher temperature, approximately 194°C. The results reported in Table A.2 (see Appendix) show that the crystallinity of the nanofibres samples is slightly lower than that of the PVA powder (about 60 J/g). These observations may be due to the strong elongation stress imposed on the

electrospun jet by the electrostatic forces. During the electrospinning process nanofibres solidify quickly and therefore the molecular chains may not have enough time to form perfect crystals (Muller et al. 2009; G.-M. Kim et al. 2008).

Next, the thermal analysis was performed for the electrospun core/shell nanofibrous samples with and without drug. The analysis was performed on three samples. The thermograms are shown in Figure 7.14, while Table 7.3 shows the values of T_g, T_m, H_m for each samples. In the curve of nanofibres with no drug, the first peak at around 61°C represents the glass transition temperature of PLA, while the endothermic peak (T_m) at approximately 220°C indicates the presence of PVA. Slightly lower T_m of core-shell nanofibres was found compared to T_m of PVA nanofibres (about 227°C), which may reveal an increase of crystal imperfections when PVA is used as core material, similar to the previous observations, although only one peak is detected. The shell solution is exposed to the higher shear stress, while the core is subjected to a viscous stress due to the interface interactions with the shell. This may hinder the formation of perfect crystals.

Regarding the thermogram of core-shell nanofibres loaded with LidHCl, similar value of T_g was recorded compared to the samples with no drug, while much lower T_m of about 201°C was detected. LidHCl has a melting point of about 85°C (Wei et al. 2015; Klaus Florey 1985; Riga et al. 2007). This may therefore suggest that the incorporation of lidocaine in the sample reduces T_m. (Figure 7.14). The value of T_m was found to be between 224 and 232°C for PVA nanofibres, while approximately 220°C and 202°C for the core/shell PVA/PLA nanofibres with and without drug, respectively.

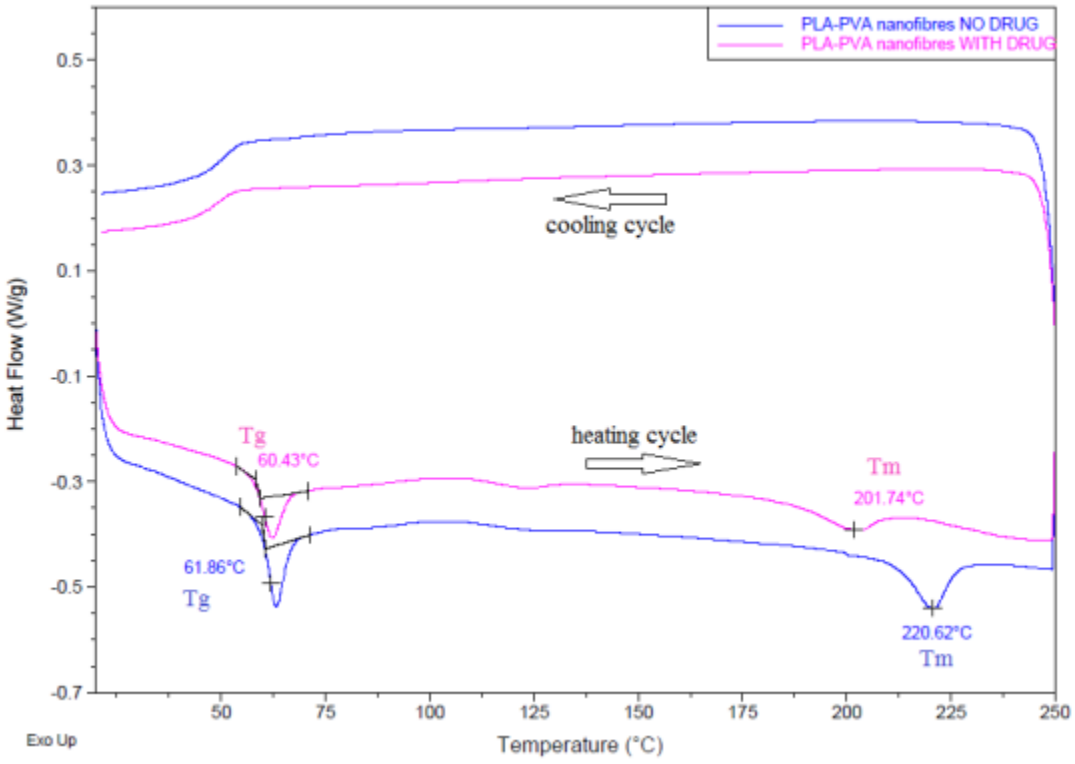

Figure 7.14 – DSC thermogram of core shell PVA/PLA nanofibres with and without LidHCl.

Table 7.3. Glass transition temperature (T_g), melting point (T_m) and heat of fusion (ΔH_m) of core shell nanofibres with and without drug.

Sample	T_g (°C)	T_m (°C)	ΔH_m (J/g)
Nanofibres - no drug	61.0±1.0	220.0±0.9	4.5±0.3
Nanofibres - with drug	60.0±0.5	201.6±1.6	3.2±0.4

To summarise, DSC analysis has shown two peaks in the thermogram of the core-shell nanofibrous samples which is therefore an indication that both PLA and PVA are within the electrospun structures. Additionally, the lower melting temperature of the nanofibrous samples loaded with drug (about 202°C) compared to that of nanofibres with no drug (220°C) suggest the presence of LidHCl.

7.3.2.7 Fourier transform infrared spectroscopy (FTIR) analysis

FTIR spectroscopy was carried out to analyse any structural changes upon electrospinning as well as interactions between PLA, PVA and LidHCl in the core/shell nanofibres. Figure 7.15 shows FTIR spectra of the bulk materials, PLA, PVA and LidHCl, and the electrospun nanofibrous samples with and without drug.

The PLA spectrum shows peaks at the bands at 2,999 and 2,949 cm^{-1} from symmetric and asymmetric valence vibrations of C-H, respectively. A peak at 1,746 cm^{-1} indicates the C=O stretching, while bending vibrations of CH from CH_3 (asymmetric and symmetric) were found at 1,452 and 1,380 cm^{-1}. At 1,364 cm^{-1} the C-O-C stretching vibration is detected. The overlap of the C-H bending vibration and the C-O-C stretching vibration were seen at 1,269 cm^{-1}. Asymmetrical and symmetrical valence vibrations C-O-C of the aliphatic chain appeared at 1,181 cm^{-1}, and 1,080 cm^{-1}, respectively. These peaks are similar to those found from other researchers (Orozco et al. 2009; L. Nikolic et al. 2010; Oliveira et al. 2013; C.-L. He et al. 2009).

The presence of hydroxyl groups (O-H) in the PVA molecule is revealed by a wide band at 3,293 cm^{-1}, while the bands corresponding to the ($-CH_2-$) asymmetric and the symmetric stretching are at 2,941 cm^{-1} and 2,901 cm^{-1}, respectively. The band at 1,425 cm^{-1} is attributed to O-H and C-H bending. Similar findings for PVA were also found by a number of authors (Labidi & Djebaili 2008; Fonseca et al. 2006; Shehap 2008; Parparita et al. 2012; Campos et al. 2011).

In order to verify the encapsulation of the drug in the nanofibrous samples, FTIR analysis was also performed for a sample of drug. The characteristics peak of lidocaine hydrochloride were observed at 1,654 cm^{-1} (C=O), 1,542 cm^{-1} (in-plane bending in the N-H mode), 1,472 cm^{-1} (hydrochloride), 1,271 (tertiary amine), 1,035, 716 and 604 cm^{-1} (aromatic ring). Additional bands between 2,600 and 2,300 cm^{-1}, and between 3,600 and 2,800 cm^{-1}, refer to the N-H vibrations and the amide bond (NH-CO), respectively (Rodrigues et al. 2013; Dubnika et al. 2012).

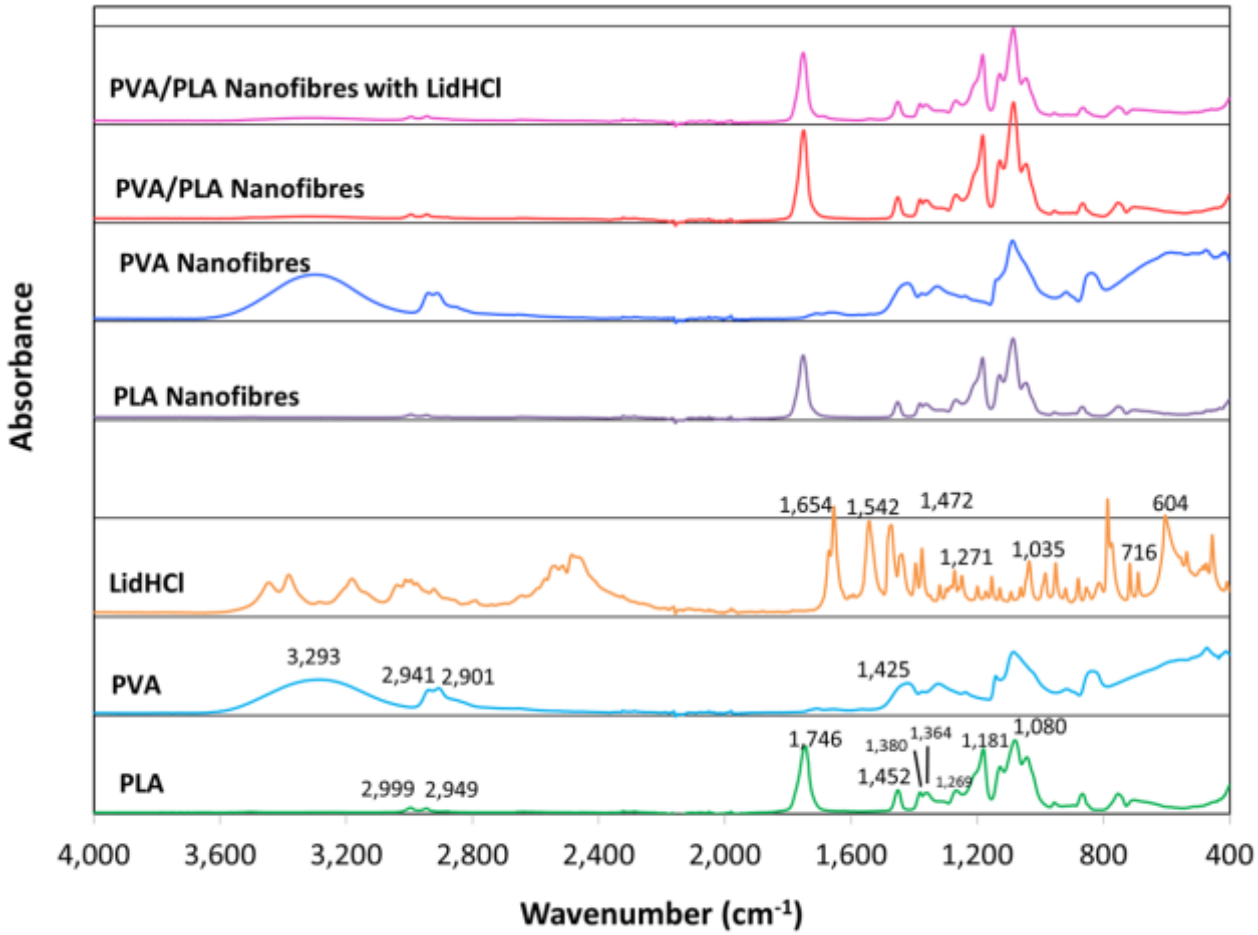

Figure 7.15 – FTIR spectra of bulk materials (PVA, PLA and LidHCl) and all electrospun nanofibrous samples, with and without drug.

By comparing raw materials (PLA and PVA) with electrospun nanofibrous samples produced with simple electrospinning, it has been found that there are no changes in the FTIR spectra regardless of whether it is a bulk material or in the nanofibre form. However, some differences were detected in the core-shell nanofibres with and without drugs as shown in Figure 7.16 and Figure 7.17, respectively. The peak at 1,746 cm^{-1} corresponding to the stretch of C=O is shifted to 1,750 cm^{-1} in the sample without drug (Figure 7.16 A). Additionally, the peaks related to asymmetric and symmetrical vibrations of C-O-C are shifted to 1,183 and 1,086 cm^{-1}, respectively. These slight shifts in absorption peaks position may be due to some physical interaction between PLA and PVA.

Similar observations were found for the core shell nanofibres loaded with drug. Moreover as shown in Figure 7.17 A, two peaks revealed the presence of LidHCl into the core shell nanofibres: the first one at 1,686 cm^{-1} corresponding to the carbonyl group (C=O) of the molecule, and the second one at 1,540 cm^{-1} which refers to the N-H bending. The intensity of these peaks is weaker most probably due to the small amount of drug in the sample resulting from the flow rate of the core solution much lower than that of the shell solution. The analysis was repeated five times and all spectra have shown these peaks confirming the presence of lidocaine in the nanofibrous samples.

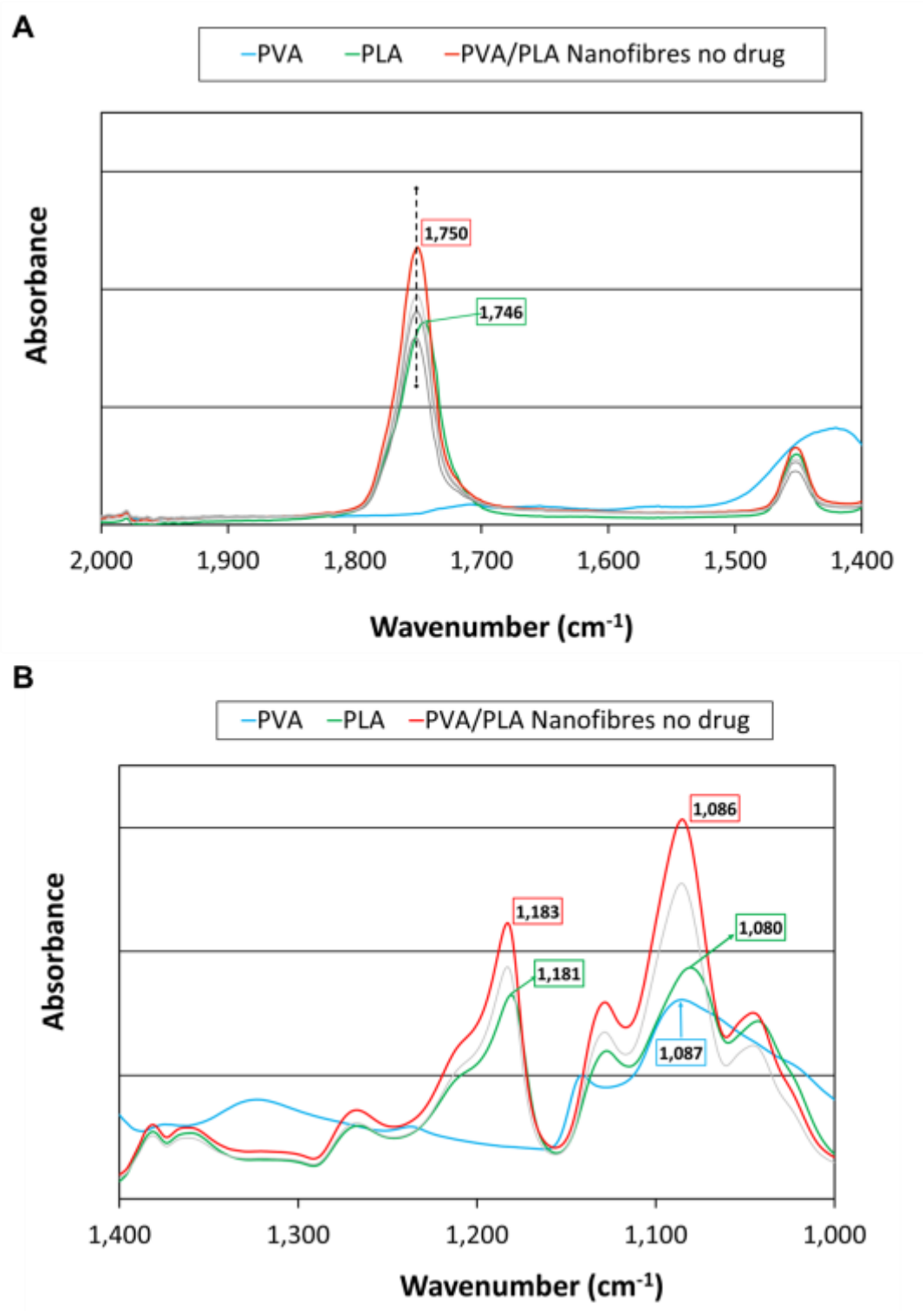

Figure 7.16 – FTIR spectra of bulk materials and core shell nanofibres without drug (A) 2,000 to 1,400 cm^{-1} (B) 1,400 to 1,000 cm^{-1}.

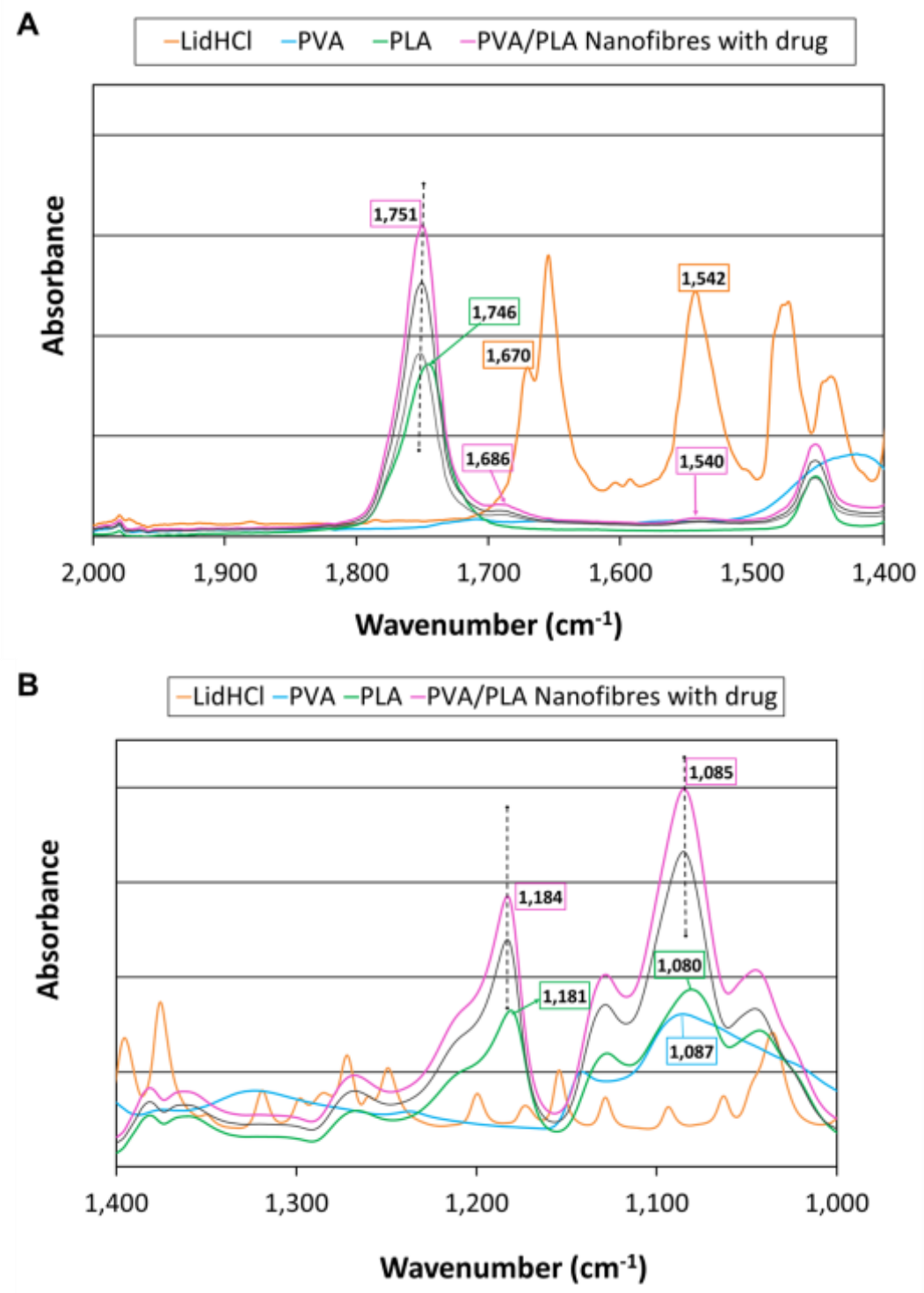

Figure 7.17 – FTIR spectra of bulk materials and core shell nanofibres with drug (A) 2,000 to 1,400 cm^{-1} (B) 1,400 to 1,000 cm^{-1}.

7.3.2.8 X-ray photoelectron spectroscopy (XPS) analysis

While FTIR and DSC analyses shows the presence of all materials, PLA, PVA and drug, in the electrospun nanofibrous mats, the composition of the fibre surface would be of great interest and importance to verify the core shell structure. XPS is an analysis method that could get the surface information of the elemental and average chemical composition of a material in 10 nm depth, by measuring the binding energy of electrons associated with atoms.

The XPS spectra of bulk materials, PLA, PVA and LidHCl, were initially obtained and the survey is reported in Figure 7.18. The molecular structures of PLA and PVA are composed of C and O elements, so as expected the XPS survey spectra indicated two peaks: C 1s and O 1s. The survey of LidHCl has shown two additional peaks corresponding to nitrogen and chlorine: N 1s and Cl2p (Figure 7.24 C). Figure 7.19 represents the high resolution XPS spectra of C 1s and O 1s of the bulk PLA, while the C 1s and O 1s spectra of PVA are shown in Figure 7.20. Three binding energies are related to C 1s of PLA and they correspond to the bonding C-C (285 eV), C-O (287 eV) and C=O (289 eV). Only two binding energies (C-C and C-O) are related to C 1s of PVA because there is no carboxylic bond (C=O) in its chemical structure The elemental composition of the sample was determined by the quantification of the spectrum as about 65% C and 35% O for PLA, whereas 68% C and 32% O for PVA.

Similarly, XPS high resolution scan of C 1s, O 1s and Cl 2p for LidHCl was performed (Figure 7.21). Three binding energies at 284 eV, 286 eV and 288 eV are related to the bonding C-C, C-N and C=O respectively, while there are two binding energies for Cl 2p at 197 eV (Cl 2p3) and 199 eV (Cl 2p1). The atomic percent of each element of LidHCl is shown in Table 7.4.

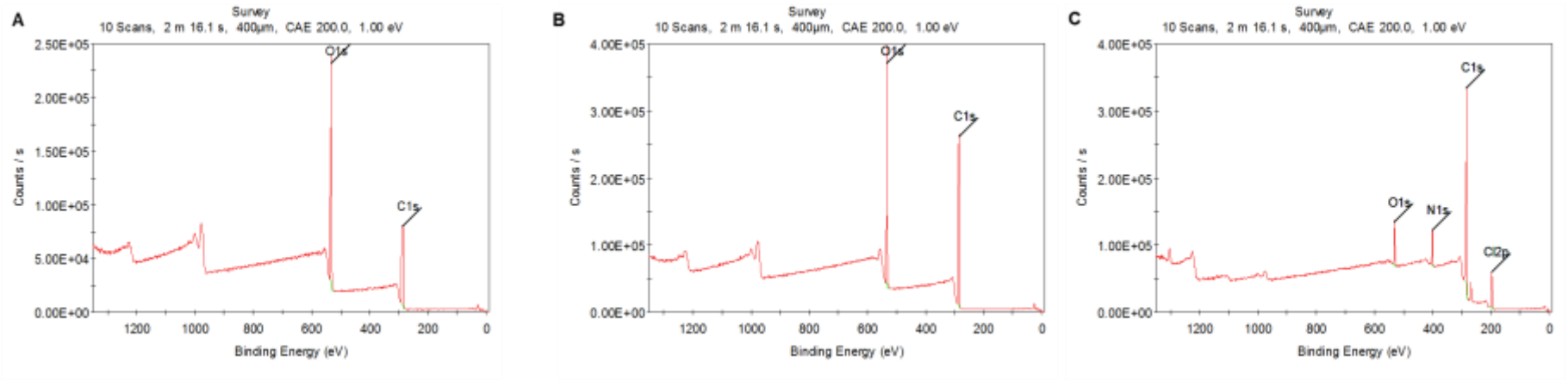

Figure 7.18 – Survey of neat materials (A) PLA pellet, (B) PVA powder, (C) LidHCl.

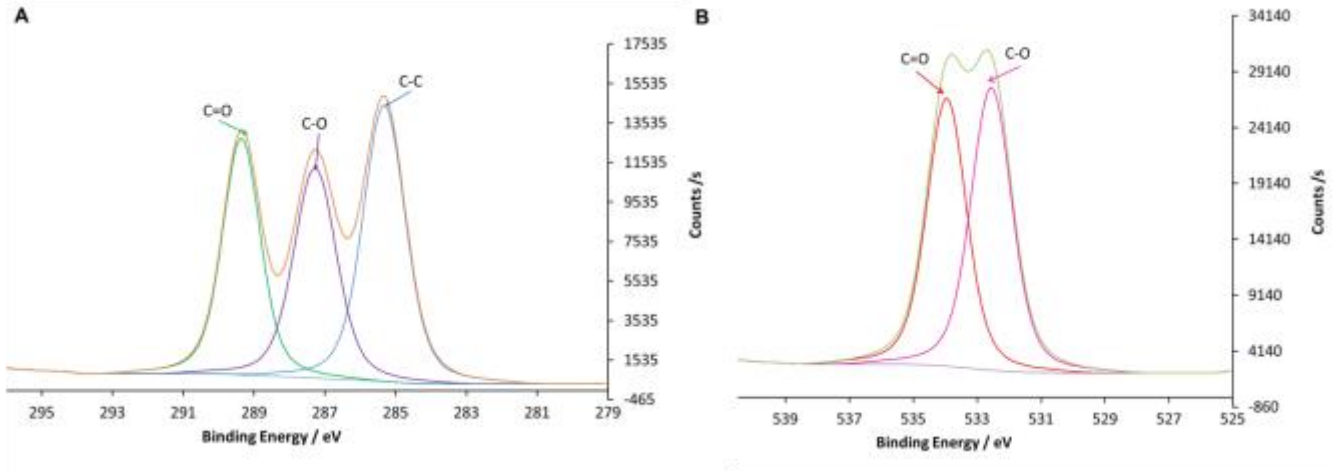

Figure 7.19 – High resolution XPS scan of PLA pellets (A) C 1s (B) O 1s.

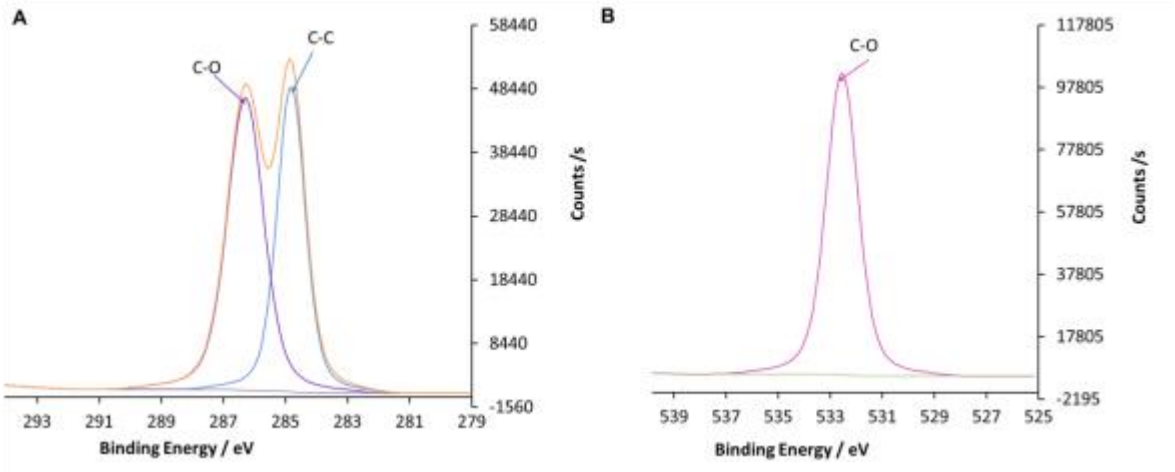

Figure 7.20 – High resolution XPS scan of PVA powder (A) C 1s (B) O 1s.

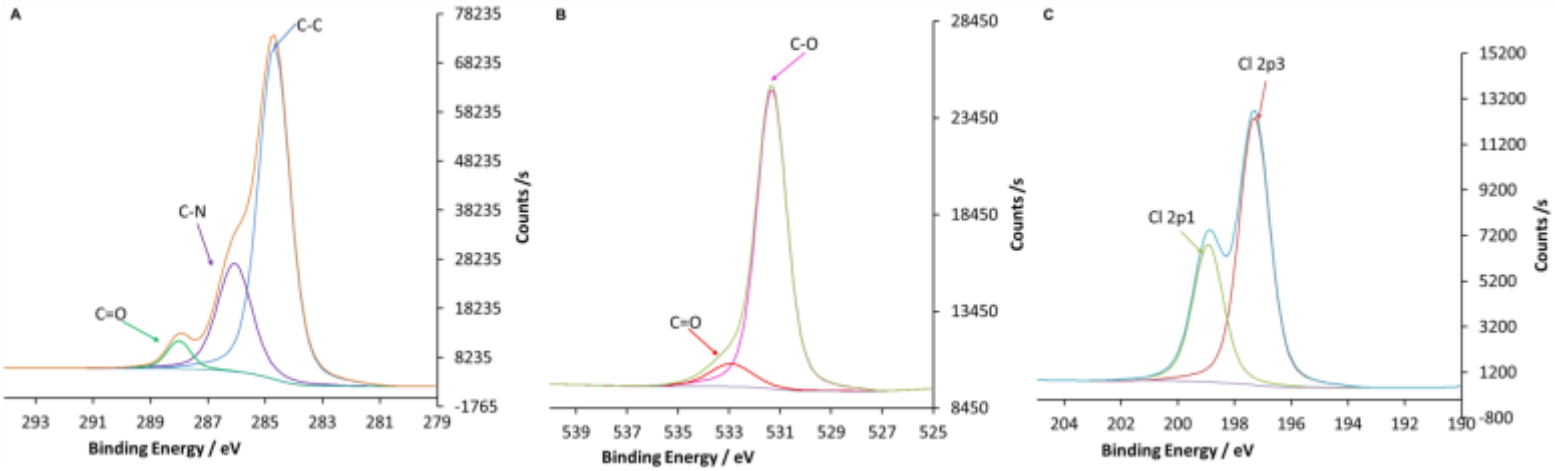

Figure 7.21 – High resolution XPS scan of LidHCl (A) C 1s (B) O 1s (C) Cl 2p.

Table 7.4 – Atomic percent of each element and amount (%) of each bonding in bulk materials.

Sample	C	O	N	Cl	C1s C=O	C1s C-C	C1s C-N	Cl2p3	O1s	O1s C=O
Point 1	78.12	5.29	10.41	6.17	4.13	62.22	20.67	6.17	5.93	0.58
Point 2	77.65	5.70	10.24	6.40	3.90	61.02	21.94	6.40	5.87	0.65

The next step involves the comparison between XPS spectra and binding energy of PLA and PVA bulk materials and nanofibres. Overlays were created for C 1s and O 1s for both materials and binding energy are reported in Table 7.5. Results have shown that the electrospinning process does not have an effect of the chemical composition of the material and similar binding energy values were obtained for both PLA and PVA nanofibres.

Table 7.5 – Binding energy for C1s and O1s for bulk materials and nanofibres.

	Binding energy eV				
	C1s			O1s	
	C=O	C-C	C-O	C=O	C-O
PLA pellet	289.34	285.28	287.24	533.94	532.55
PLA nanofibres	289.52	285.47	287.37	534.04	532.62
PVA powder	-	284.79	286.26	-	532.50
PVA nanofibres	-	284.79	286.27	-	532.53

The samples of core-shell PVA/PLA nanofibres with and without drug were then analysed. The samples without drug have shown the presence of carbon (about 61-63%) and oxygen (about 37-39%) and, as expected, no chlorine and nitrogen were detected. There is no significant difference in the atomic percent of the samples collected using different core solution flow rate (0.3, 0.5, 0.7 ml/h). On the other hand, the spectra of core shell nanofibres loaded with drug in some cases presented small peaks relative to Cl and N. This indicates the presence of the drug on the fibre surface. The percentage of each element is reported in Table 7.6, where the atomic percent of N is about 1% and that of Cl is between 0.2 and 0.3%. This may suggest that the drug in some cases is on the surface of the fibre or the shell may have broken in some places. However nitrogen and chlorine were not detected on the fibre surface in all points of scanning, which could also suggest that the drug is incorporated in the core shell nanofibres.

Table 7.6. Atomic percent of each element (C, O, N, Cl) and amount (%) of each bonding in core shell nanofibre samples with and without drug.

Sample	C	O	N	Cl	C1s C=O	C1s C-H	C1s C-O	Cl2p	N1s	O1s C=O	O1s C-O
No Drug											
2.1-0.3											
Point 1	62.67	37.33	-	-	22.84	18.83	21.00	-	-	26.28	11.05
Point 2	62.27	37.73	-	-	22.61	18.86	20.80	-	-	26.40	11.33
Point 3	61.42	38.59	-	-	21.34	19.26	20.82	-	-	25.98	12.61
2.1-0.5											
Point 1	61.97	38.03	-	-	21.48	19.24	21.25	-	-	24.69	13.34
Point 2	62.46	37.54	-	-	19.66	22.02	20.78	-	-	22.23	15.31
Point 3	62.61	37.39	-	-	20.27	21.51	20.83	-	-	22.69	14.7
2.1-0.7											
Point 1	62.82	37.19	-	-	20.23	21.60	20.99	-	-	22.18	15.01
Point 2	61.65	38.35	-	-	20.52	20.16	20.97	-	-	23.95	14.40
Point 3	62.75	37.25	-	-	20.13	21.79	20.83	-	-	22.50	14.75
With Drug											
2.1-0.3											
Point 1	62.78	36.07	0.88	0.28	20.46	21.21	21.11	0.28	0.88	24.81	11.26
Point 2	63.09	35.69	0.97	0.26	20.09	21.67	21.33	0.26	0.97	22.27	13.42
Point 3	62.75	37.26	-	-	19.99	21.1	21.66	-	-	22.16	15.10
Point 4	63.01	35.79	0.97	0.23	19.76	22.38	20.87	0.23	0.97	21.90	13.89
Point 5	62.81	35.74	1.10	0.35	19.34	23.15	20.32	0.35	1.10	19.85	15.89
2.1-0.5											
Point 1	63.38	36.62	-	-	20.61	20.82	21.95	-	-	22.58	14.04
Point 2	68.50	31.50	-	-	21.77	23.87	22.86	-	-	18.53	12.97
Point 3	63.01	37.00	-	-	20.98	21.02	21.01	-	-	22.96	14.04
Point 4	62.72	36.19	0.84	0.25	19.52	22.05	21.15	0.25	0.84	20.65	15.54
Point 5	63.36	35.62	0.84	0.18	18.98	23.29	21.09	0.18	0.84	20.19	15.43
2.1-0.7											
Point 1	62.74	36.09	0.90	0.27	19.70	21.75	21.29	0.27	0.90	21.50	14.59
Point 2	63.61	36.39	-	-	19.83	22.52	21.26	-	-	21.41	14.98
Point 3	63.33	36.67	-	-	19.91	23.02	20.40	-	-	21.15	15.52
Point 4	63.10	35.73	0.91	0.25	19.37	23.72	20.01	0.25	0.91	20.28	15.45
Point 5	63.13	35.75	0.92	0.19	18.97	23.41	20.75	0.19	0.92	19.87	15.88

7.3.2.9 Drug encapsulation efficiency and drug release

7.3.2.9.1 Efficiency of drug encapsulation

Initially two calibration curves in phosphate buffer solution at pH 7.4 and in the acetate buffer solution at pH 5.5 were prepared as shown in Figure 7.22. The next step focused on the determination of the apparent efficiency of lidocaine HCl encapsulation in the different nanofibrous mats, which is defined as the ratio of actual amount of drug loaded to the theoretical amount of drug loaded with the electrospinning process. The theoretical amount of drug was calculated considering the concentration of drug incorporated (50% weight by weight of the polymer PVA) and the core and shell solution flow rates. The actual amount of drug was determined after complete dissolution of the nanofibre sample in dimethyl sulfoxide (DMSO) followed by dilution with PBS and subsequently analysed using high performance liquid chromatography (HPLC) as mentioned in paragraph 3.9.4.1. The results are reported in Table 7.7.

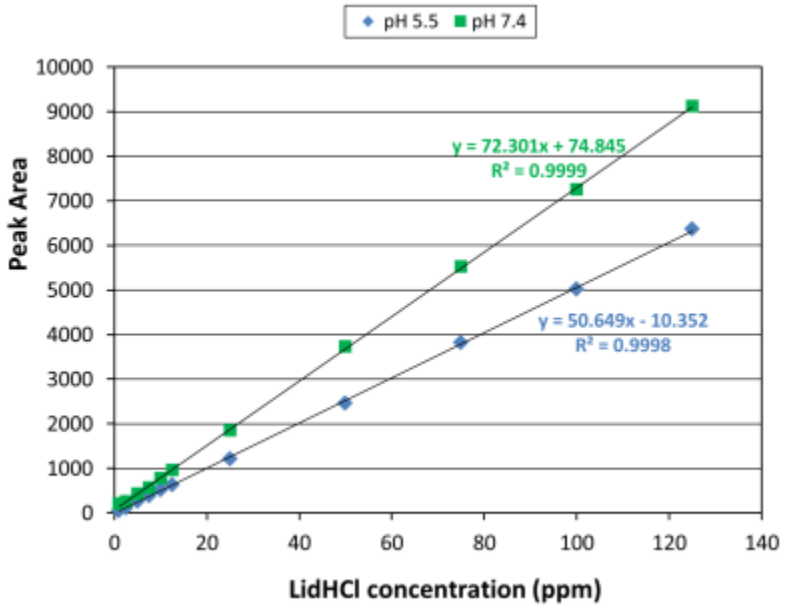

Figure 7.22 – Calibration curve of LidHCl in PBS solution at pH 7.4 and acetate buffer solution at pH 5.5.

Table 7.7 – Apparent efficiency of LidHCl encapsulation in the core shell nanofibrous samples.

Sample (shell-core solution flow rate, ml/h)	**2.1 - 0.3**	**2.1 - 0.5**	**2.1 - 0.7**
Nanofibre diameter (nm)	151±58	316±185	422±318
Theoretical % w. LidHCl/w. nanofibres	4.4	6.8	8.8
Efficiency drug encapsulation % w/w	88.6±9.5	89.2±7.7	87.3±3.4

The efficiency of encapsulation was approximately 89% for samples collected using a core solution flow rate of 0.3 and 0.5 ml/h, while an increase of core flow rate to 0.7 ml/h resulted in a slightly lower value, 87%. However a value of 100% would be logical, because the drug is mixed with the PVA solution and delivered through the inner part of the needle for electrospinning. A few discs of nanofibrous samples (about 5 or 6 for each condition) were dissolved in DMSO to extract the drug and then the apparent efficiency was determined (Table 7.7). Within the experimental uncertainty the recorded values show mean values between 87 and 89%. The message from these results is that the apparent efficiency is the same for all conditions used.

7.3.2.9.2 Drug release studies

The drug release properties of LidHCl loaded in PVA/PLA core-shell nanofibres in two different physiological conditions were investigated. The release study over 7 days was repeated three times for each sample. Figure 7.23 and Figure 7.24 show the release profile of the drug from the nanofibrous sample to the release medium at pH of 7.4 and at pH 5.5, respectively, and in each figure the inset is the enlarged section at a short incubation time of 4 hours. In the next paragraphs the different release profiles are compared and interpretations are given.

Overall a burst release of the drug in the medium at pH 7.4 was observed within 2 hours from all the nanofibrous samples (Figure 7.23). For the fibres collected using a core flow rate of 0.3 ml/h, 63±3% of the drug encapsulated was released out within 2 hours, while on increasing core solution flow rate higher drug release was detected, as shown in the inset of Figure 7.23. 80±7% of drug was released from the sample (2.1-0.5), while 74±6% from the

sample (2.1-0.7). This could indicate either that the drug was on the surface of the nanofibres or that the core of the nanofibres was exposed to the release medium through the sectioned edges of the nanofibres. More specifically, according to the method of performing the release studies, a sample disc of the nanofibre mat with diameter of 1 cm was sectioned and immersed into the release medium. Hence the fibre core was exposed to the release medium, which could solubilise the core through the edges of the disc. Dissolution and diffusion of the core polymer (PVA which was soluble to the release medium) to the release medium through the edges of the fibres would result in the burst release of the drug.

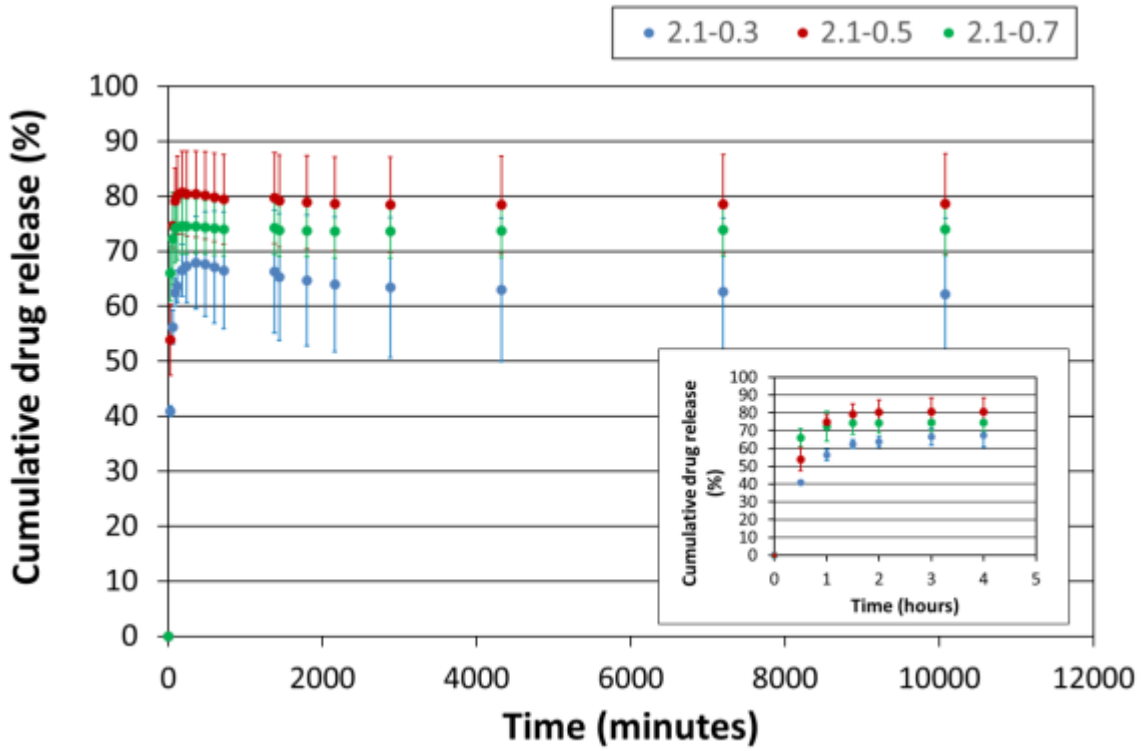

Figure 7.23 – LidHCl cumulative release from nanofibrous samples to the release medium at pH 7.4.

SEM images which did not show any crystals of drug on the surface of the electrospun mats (paragraph 7.3.2.1), the observed burst release may be attributed to the diffusion of the drug through the sectioned edges of the fibres. The nanofibrous mats are probably formed from both core shell and hollow nanofibres. The solvent from the shell solution (TFE) evaporates faster and forms a skin on the outer surface of the electrospun jet, while water will slowly evaporate from the inner core. As a result the skin solidifies earlier, while the core solution solidifies later and it continues to shrink due to the core solvent evaporation resulting in core shell fibres that are partly hollow. This partly hollow structure can facilitate the diffusion or circulation of the release medium within the fibres and the solubilisation and diffusion of the core polymer and drug to the release medium. A method to seal the sectioned edges of the fibres may be required to ensure that the release studies reflect the release rates through the fibres and not diffusion through the fibre edges.

An increase of core solution flow rate to 0.5 and 0.7 ml/h led to higher burst release percentage compared to that one for the sample produced at 0.3 ml/h. This may indicate that

if the drug is released by the diffusion mechanism, according to Fick's laws with decreasing diffusion path length the concentration gradients and mass transport rates, are expected to increase (J Siepmann et al. 2004). These observations may suggest that core-shell nanofibres with larger core are formed using flow rate of 0.5 and 0.7 ml/h compared to those collected at 0.3 ml/h.

The effect of core solution flow rate on the release rate was investigated and reported by few researchers (H. Jiang et al. 2005; Y Z Zhang et al. 2006; E. Yan et al. 2014; T. T. T. Nguyen et al. 2012; Joung et al. 2011). Jiang et al reported that an increase of the core solution (BSA-loaded PEG) flow rate leads to nanofibres with larger core and higher drug release. Similar observations were detected by Joung et al (Joung et al. 2011). The shell material was PLGA, whereas the core material was an aqueous solution of BSA and hyaluronic acid. With an increase in the flow rate of the core solution, there is an associated acceleration in BSA release. However no information was reported about the core diameter and the mechanism of the drug release.

The cumulative drug release percentage from the nanofibrous samples to the release medium at pH 5.5 is shown in Figure 7.24. Overall a more sustained release is observed compared to the drug release in the medium at pH 7.4. Approximately 60% of the drug is released within 4 hours. This may suggest that the dissolution or diffusion of the drug is pH-dependent. Local anaesthetics as lidocaine are weak bases but are usually injected in acidic solutions as hydrochloric salts (lidocaine hydrochloride). LidHCl has a pKa between approximately 7.2 and 7.8 (Sjberg et al. 1996). The pKa of a chemical compound represents the pH at which the concentrations of non-ionized (base form) and ionized forms are equal (Shicong et al. 2001). Therefore, this may explain the slower release of LidHCl at pH 5.5 compared to pH 7.4, as a result of the higher concentration of the non-ionized form at pH lower than its pKa. Nevertheless, unlikely the previous observations, there is no significant variation between the drug release profile for the samples collected using different core solution flow rates.

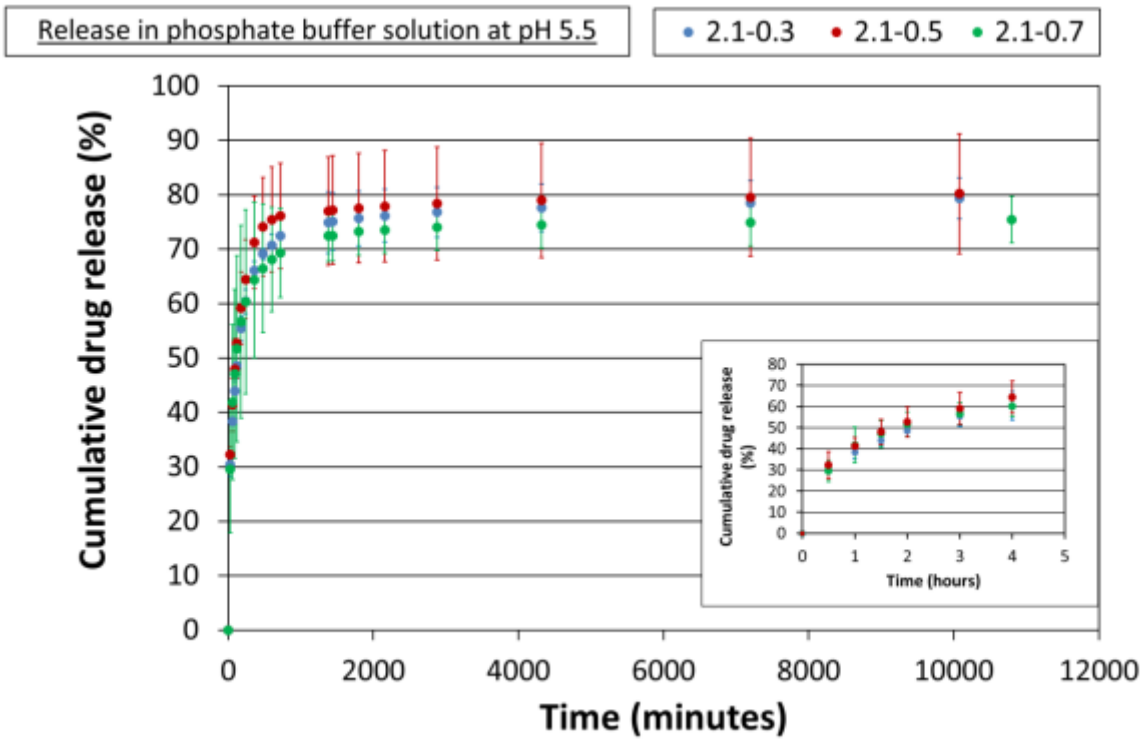

Figure 7.24. LidHCl cumulative release from nanofibrous samples to the release medium at pH 5.5.

The core-shell PVA/PLA nanofibrous samples belong to the reservoir-type release device, in which the drugs are encapsulated by a polymer hydrophobic shell. In order to find out the mechanism of the release of LidHCl from the PVA/PLA nanofibres samples, the first 60% drug release data were fitted in the Peppas model as suggested by Taepaiboon (H. Sciences 2010; P Taepaiboon et al. 2006; Pattama Taepaiboon et al. 2007).

$$\frac{M_t}{M_\infty} = kt^n$$

M_t is the cumulative amount of drug released at time t, M_∞ is the total mass loaded into the polymer matrix, k is the drug release rate reflecting the structural and geometric characteristics of the system, n is the release exponent suggesting the mechanism of release.

The data from the release of drug in the medium at pH 7.4 were not fitted because of the initial burst release. After one hour more than 60% of drug is already released, indicating therefore that most probably dissolution of the drug occurs through the non-sealed cutting ends of the nanofibrous samples. On the other hand, the release kinetic was studied for the

drug released in the acetate medium (pH 5.5) (Figure 7.25). R is close to 1 which indicates good fit of the data. The exponents n are calculated to be 0.32, 0.37 and 0.41 for the samples produced at core flow rate of 0.3, 0.5 and 0.7 ml/h, as shown in Table 7.8.

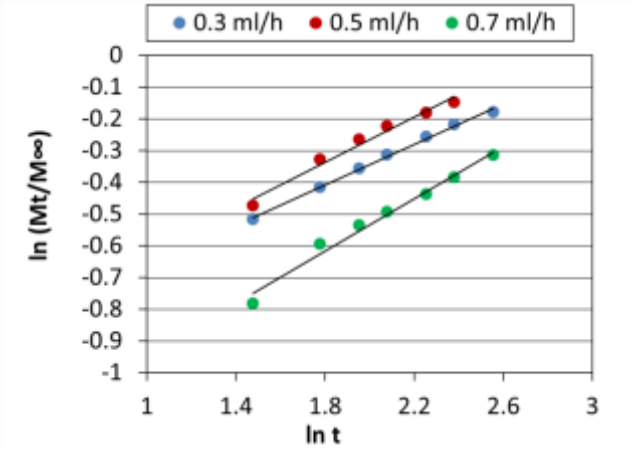

Figure 7.25 – Plot of ln(Mt/M∞) versus ln(t) for LidHCl release from core/shell nanofibres fabricated at a core feed rate of 0.3, 0.5 and 0.7 ml/h.

Table 7.8 – Data fit parameters of LidHCl release profiles.

Release medium pH 5.5	R			n		
Core solution flow rate (ml/h)	*0.3*	*0.5*	*0.7*	*0.3*	*0.5*	*0.7*
Up to 4 hours	0.99	0.98	0.97	0.32	0.37	0.41

For one-dimensional Fickian diffusion of drugs from mono-dispersed cylinders, n is 0.45 as reported in Table 2.6 (refer to paragraph 2.3.2). The exponent value found for PVA/PLA core-shell nanofibres is slightly lower than 0.45 for all samples. This may suggests that it is most probably a non-Fickian transport, or that both mechanism of diffusion and dissolution occurs. It is quite difficult at this stage to say which the mechanism is. The LidHCl loaded nanofibrous samples are composed of a fibrous mesh where nanofibres may have different core and shell thicknesses. Additionally the drug may be not homogeneously distributed in all core shell nanofibres and the electrospun mesh is highly porous most probably with wider pore size distribution that could affect the diffusion pathways of the drug.

There are limited investigations on the release mechanisms and kinetics of drug incorporated in the core-shell nanofibres (Sohrabi et al. 2013; Z. Li et al. 2014; Chi Wang et al. 2010). A

more sustained drug release was achieved most probably due to the homogenous distribution of the drug in the core-shell nanofibrous structures. But in this thesis, hollow nanofibres, core-shell nanofibres and fibres with discontinuous core were formed as shown by the morphological analysis (TEM, CLSM, FIB-SEM). Hence this could explain this type of release.

The SEM analysis was then utilised to observe the nanofibre morphology after the release process. Figure 7.26 shows that the nanofibrous samples overall maintained their structure and no pores on the fibre surface were observed. PLA is a hydrophobic polymer with degradation time longer than 7 days. Therefore this may support the previous hypothesis of drug release through the sectioned edges of the electrospun nanofibrous samples.

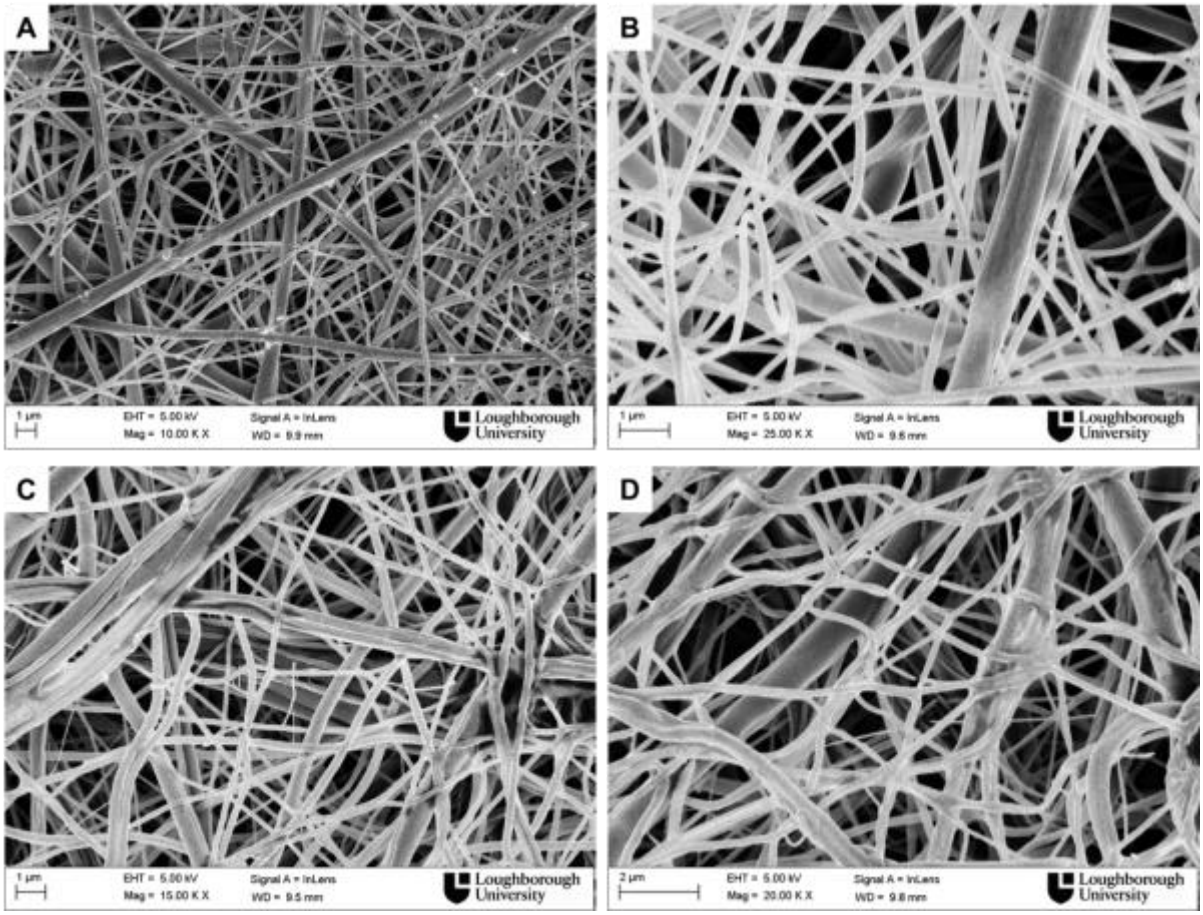

Figure 7.26 – SEM images of core shell nanofibrous discs after the drug release from the sample 2.1-0.3 (A, B) release medium at pH 7.4, (C, D) release medium at pH 5.5.

The results presented in this chapter provide a basis for further design and optimization of processing conditions to control the nanostructure of core-shell composite nanofibres in order to achieve highly sustainable and controllable drug release.

7.4 Conclusion

Many investigations using nanofibers for controlled release applications have demonstrated the weakness of the blend electrospinning method and highlighted the significant role of drug-polymer interaction in controlled releases. During preparation of the spinning solution for the blend electrospinning process, the long-time exposure of bioactive protein, growth factor or drug to harsh organic solvents would make it denatured to lose its activity. Hence coaxial electrospinning may provide an alternative and simple means to encapsulate these molecules.

In this thesis coaxial electrospinning was employed to produce nanofibres with a core shell structure. PLA was used as shell material, while PVA aqueous solution loaded with LidHCl was used a core material. Overall defect-free nanofibres with smooth surface were collected at all core solution flow rates, although some imperfections were observed as shown by SEM micrographs. This is most probably due to the jet instabilities especially at higher core flow rate. An increase in the shell diameter of the nanofibres was observed by increasing the core solution flow rate from 0.3 to 0.7 ml/h. In most scientific publications TEM analysis has been employed to verify the core shell structure. However only a short segment of the fibre has been shown and in some cases the boundaries are not clearly visible. In this thesis several techniques were employed to verify the core shell structure. The formation of core and shell layers was confirmed by means of TEM and CLSM analysis. The difference in electron transmission ability between the core and shell materials led to sharp boundaries in the TEM images indicating the core shell structure of the fibres. Nevertheless an increase of the solution core flow rate led sometimes to splitting of the jet. On the other hand, CLSM was challenging and different distributions of fluorescein in the core suggested that different morphologies co-existed: core shell fibres, hollow fibres and monolayer structures. In addition FIB-SEM suggested that a buckling effect most probably occurred during the electrospinning process, as a result of the immiscibility of core and shell solutions and slower

evaporation of the core solvent (water) compared to the shell solvent (TFE).

The surface wettability of the nanofibrous samples was investigated by measuring the water contact angle. The results have shown no significant difference between the water contact angle of pure PLA nanofibres and core/shell PVA/PLA nanofibres. This suggested that the core shell structure was formed and therefore successful incorporation of the hydrophilic PVA and LidHCl in the nanofibre shell was achieved. Differential scanning calorimetry and Fourier transform infrared spectroscopy analyses were used to identify any possible structural changes which might occur after electrospinning as well as interactions between PLA, PVA and LidHCl in the core/shell nanofibres. No significant changes were detected, although the presence of the drug in the samples was verify by two peaks at 1,686 and 1,540 cm^{-1} corresponding to the carbonyl group (C=O) and the N-H bending of the molecule, respectively.

The release studies were performed in release medium at pH of 7.4 and pH of 5.5. Burst release of the drug was overall observed from all samples to the medium at pH 7.4. This was probably due to the fact the fibre core was exposed to the release medium, which could solubilise the core, through the edges of the samples. More sustained release was instead achieved using release medium at pH 5.5, indicating that the drug is most probably pH dependent. The present study demonstrated that the incorporation of a hydrophilic drug may be achieved using coaxial electrospinning. However it is really important to measure the solution properties including viscosity, conductivity and surface tension, in order to understand the relationship between the stability of the electrospun jet, the final nanofibre morphology, the diameter of core and shell layers and hence the type of drug release.

8 CONCLUSION AND FUTURE WORK

This doctoral thesis has been overall focused to address some of the current challenges related to both single and coaxial electrospinning process.

8.1 Conclusions

In the first part of this work solution electrospinning was used to produce PLA nanofibres and the effect of solution properties on the morphology of the electrospun nanofibrous mats and mean nanofibre diameter was investigated. First, the effect of different single solvents on the morphology and mean diameter of amorphous PLA nanofibres was investigated. All solutions were electrospun using the polymer concentration of 10% w/v and same process parameters. SEM analysis was performed on the electrospun samples and the results have shown that between all single solvents only acetone was able to produce PLA nanofibres, although some defects were also detected. With the aim of producing defect-free nanofibres with narrow diameter distribution and for a better understanding of the solution properties on the PLA nanofibre morphology, the next step was the preparation of PLA solution in binary solvent systems using acetone and one of the other solvents. The thinnest defect-free nanofibres with narrow diameter distribution were produced using the solvent mixture acetone/dimethylformamide (AC/DMF) at ratio of 50/50 v/v. The mean diameter was 210 nm with standard deviation of 36 nm. On the other hand, larger nanofibres with wider diameter distribution and many defects within the nanofibrous web were collected using the other binary solvent systems. The production of uniform electrospun membranes is an important aspect for industrial applications as nanofibrous structures with reproducible properties including diameter, porosity and mechanical properties, are desired. AC is less toxic than the most common chlorinated and fluorinated solvents that have been mostly used for electrospinning of PLA. Solution properties, including solution viscosity, conductivity and surface tension were measured for all solutions. No relationship between each property and the electrospinning outcome was determined indicating therefore that the effect of these properties on the resultant nanofibre morphology and diameter cannot be studied separately. But, it was possible to correlate the boiling point (BP) of the second solvent of the binary mixture with the mean nanofibres diameter. An increase of BP resulted in the production of

the thinnest nanofibres and more homogenous defect-free mats. Next, the PLA concentration in the solvent mixture AC/DMF (50/50 v/v) was varied and the viscosity of each solution was measured. Both viscosity measurements and viscoelasticity measurements (G', G'') have shown that a clear relationship between the chain entanglement in solutions and the production of electrospun nanofibres exists. A sharp increase of shear viscosity and G', G'' on increasing the polymer concentration have shown to represent the transition between beads and beaded nanofibres known as entanglement concentration, C_e. Furthermore defect-free nanofibres were collected using a polymer concentration about 2 or 2.5 times higher than C_e.

Based on these results, new questions raised. How solvents should be selected for the production of homogeneous electrospinnable solution of specific polymer and hence successful production of electrospun defect-free nanofibres? Is it possible to use a simple procedure rather than the trial and error approaches in order to optimise the production of defect-free uniform nanofibrous webs? A three step systematic methodology was proposed in this work of thesis. More specifically, the three step methodology included 1) initial choice of solvent by solubility evaluation to meet thermodynamic criteria, 2) electrical properties i.e. conductivity and dielectric constant adjustment by using solvent mixtures to meet electrical property criteria, and 3) critical entanglement concentration (C_e) determination by viscosity measurements, supported by elastic and plastic moduli measurements, followed by concentration adjustment to meet rheological criteria. First, the solubility parameters of solvents and PLA were used to understand polymer-solvent interactions. Even though it was possible to dissolve PLA in all solvent systems and form homogeneous solutions, weak interactions were found between PLA and some solvents. Next, the addition of a solvent with high dielectric constant was found to enable the formation of thinner nanofibres. Moreover on increasing the polymer concentration shear viscosity and viscoelasticity measurements have shown a sharp increase at a value of entanglement concentration which corresponds to the transition between bead and beaded nanofibres. This methodology was proposed for PLA, but it can be applied for other polymers.

Even though the effect of process parameters has been investigated for some polymers, there are controversial results regarding the effect of some parameters on the morphology of the nanofibrous structures. This depends most probably on the types of polymer-solvent system. Furthermore the control over the diameter of electrospun nanofibres is still a bottleneck and

the derivation of one universal correlation between the nanofibre diameter and all parameters affecting the electrospinning process is a major challenge. A simple equation to predict the final nanofibre diameter by knowing both solution properties and process parameters has been proposed in the literature (Sergey V Fridrikh et al. 2003). Measurement of electric current of the electrospun jet is required, but this parameter is not generally measured in most of the experimental electrospinning studies. The work presented in this thesis has shown the effect of process parameters including voltage, flow rate and collection distance on the PLA nanofibre morphology and diameter. Morphological analysis has shown that the effect of voltage on the mean diameter depended on the value of flow rate. At the lowest flow rate, the thinnest nanofibres were collected in the middle range (10 and 15 kV), whereas at higher flow rate the thinnest nanofibres were collected at the highest voltage of 20 kV. These findings contribute to the clarification of the controversy encountered in the literature about the effect of the applied voltage on the diameter for various polymer-solvent systems under various electrospinning conditions. The electric current was recorded for all experiments in order to verify the validity of the equation proposed in the literature. The results have shown that the predicted nanofibre diameter was in good agreement with the measured nanofibre diameter for some experiments, while the stretching was over predicted for other experiments. It was shown that the equation should be modified to include solvent evaporation, solution viscosity and electrical conductivity.

The last part of this work focused on the production of core-shell PVA/PLA nanofibres loaded with a hydrophilic drug. The several morphological analyses have shown though that the nanofibrous samples are made of mixture of core shell structures, hollow fibres and monolayer structures. The incorporation of a hydrophilic drug was challenging most probably due to the higher conductivity of the core solution compared to the shell solution. This work emphasizes the importance of the electrodynamics of the coaxial electrospinning. Solution properties are not generally reported in most scientific publications on the production of core shell nanofibres by coaxial electrospinning. Nevertheless, there are several factors which are very critical for the production of core-shell nanofibres: the ratio of core and shell viscosities, the ratio of core and shell conductivities, the interfacial tension and miscibility of core and shell materials.

8.2 Framework for Testing and Designing Electrospun Nanofibres

A design strategy for investigating new polymer and solvent systems available to enable the production of defect free nanofibres, with the minimum number of experimental tests, is proposed in the flow diagram of Figure 8.1.

Hansen solubility parameters of the polymer (δ_P, δ_H, δ_D) are used to create the polymer solubility sphere. Then several solvents can be placed in the three dimensional graph. If a solvent point is located inside the solubility sphere, then the polymer can be dissolved by that solvent. On the other hand, if a solvent point is placed outside the solubility sphere, such solvent does not dissolve the polymer. The next step involves the measurement of the solution conductivity and if it is lower than 1 μS/cm, the addition polar solvents or salts, such as sodium chloride will help the production of nanofibres. The polymer concentration needed to collect defect free nanofibres is then determined by measurement of the elastic moduli (G') of the polymer solution. As the polymer concentration increases, rapid increase of G' indicates that sufficient chain entanglements are formed between the polymer chains in solution to form nanofibres. The polymer concentration at which this occurs is called entanglement concentration (C_e). Hence polymer concentration 2 or 2.5 times higher than C_e is ideal to collect defect free nanofibres. After solution parameters have been optimised, the electrospinning process is performed and a stable Taylor cone at the needle tip should be maintained during the experiments to enable the formation of defect free nanofibres. If an elongated cone is observed or droplets of polymeric solution are collected in front of the collector, then the process parameters, voltage, flow rate or collection distance, should be varied. An integrated current measurement system and a high speed camera are useful tools to test the stability of the electrospinning process with respect to time. Therefore the value of electric current recorded can be used to predict the final nanofibre diameter.

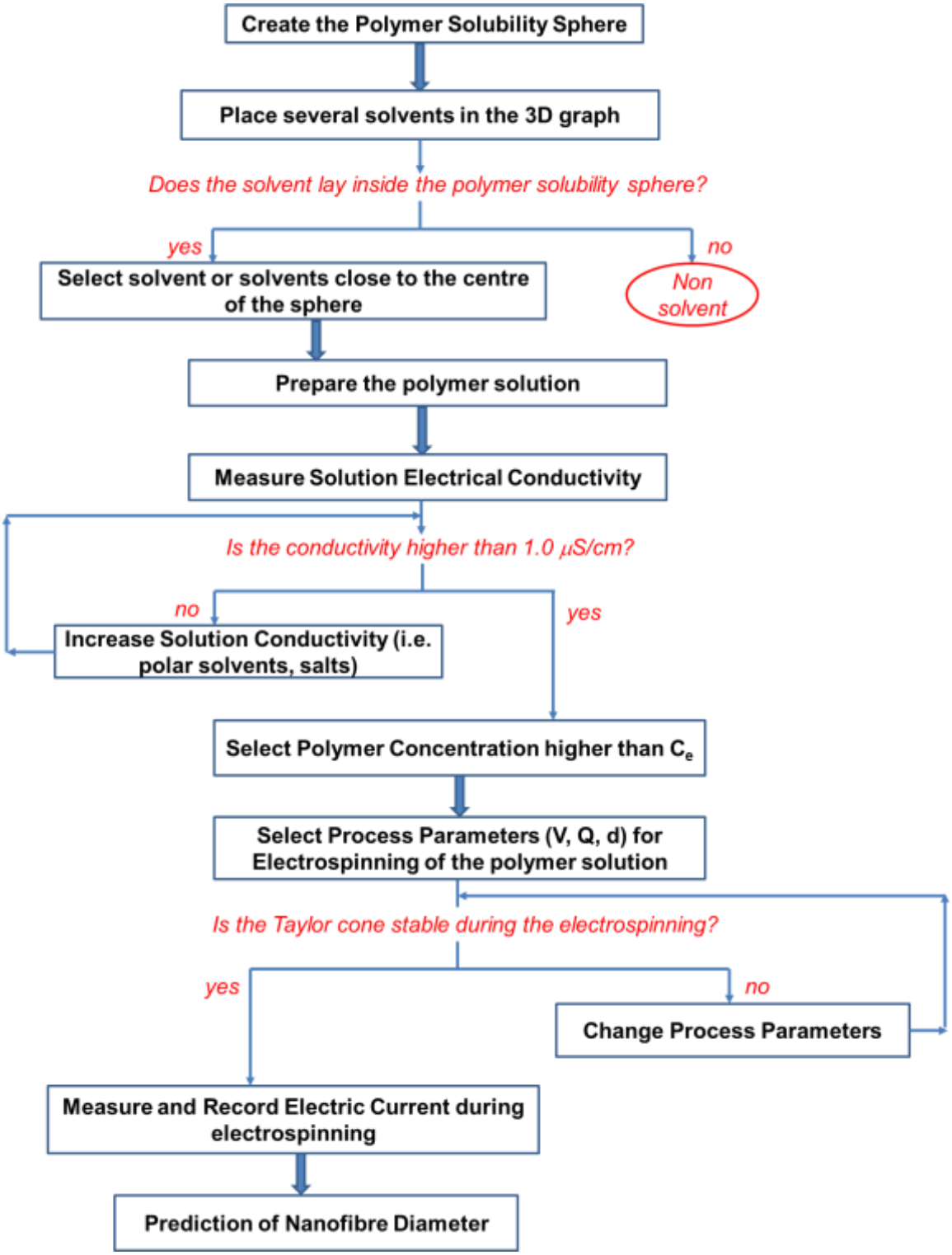

Figure 8.1 – Flow diagram for the production of defect free electrospun nanofibres.

8.3 Future work

In this section some recommendations for future work are given:

- The selection of greener solvents is still one of the main challenges for solution electrospinning. So far, synthetic polymers, including PLA, PCL and PLGA have been mostly dissolved in chlorinated and toxic solvents. The methodology proposed in this thesis can be used for the selection of less toxic solvent. Three key factors should be kept in mind: solution conductivity, solvent boiling point and solution viscosity. The use of less toxic solvent for solution electrospinning would be ideal especially for applications of the nanofibrous structures in the biomedical field. 2-Methyltetrahydrofuran (2-MeTHF) has been for example proposed as alternative to DCM and THF.
- The prediction of the mean nanofibre diameter would offer a great advantage because nanofibrous structures with reproducible properties including diameter, porosity and mechanical properties, are required in many applications. More systematic studies using solvent and mixture of solvents with different vapour pressure should be carried out in order to understand how the solvent evaporation may affect the charge transport during the electrospinning process and hence the electric current.
- The effect of solution properties of both core and shell solutions on the nanofibre morphology should be addressed in more details. In many scientific publications about electrospun nanofibres for biomedical applications, the incorporation of hydrophilic molecules required an aqueous solution to maintain the bioactivity. However water has a much higher dielectric constant than other organic solvents used for the shell solution. From the results achieved in this thesis, the solution conductivity of the PLA shell solution should be most probably higher than that of the PVA aqueous core solution. Different solvents and solvent mixtures for the shell solutions may be selected. Solvent miscible and immiscible with water and with different boiling points should be selected and a systematic investigation may be carried out to understand the diffusion rates.

- The fast release of the drug from the PVA/PLA nanofibres observed has been related to the sectioned edges of the electrospun samples. Hence a method to seal the nanofibrous sample could be explored in order to understand the type of release mechanisms.
- The pH of the release medium should be measured during the release studies and its composition analysed in order to understand the degradation rate of the material. Furthermore, after the release of the drug from the electrospun nanofibrous samples, measurements of weight loss and determination of the M_w of the samples should be carried out in order to understand the type of degradation.

REFERENCES

Abidian, M.R., Kim, D.-H. & Martin, D.C., 2006. Conducting-Polymer Nanotubes for Controlled Drug Release. *Advanced materials*, 18(4), pp.405–409.

Agrawal, A. et al., 2004. Constrained nonlinear optimization for solubility parameters of poly(lactic acid) and poly(glycolic acid)—validation and comparison. *Polymer*, 45(25), pp.8603–8612.

Agrawal, C.M., Niederauer, G.G. & Athanasiou, K.A., 1995. Fabrication and Characterization of PLA-PGA Orthopedic Implants. *Tissue engineering*, 1(3), pp.241–253.

Ahmed, J. & Varshney, S.K., 2011. Polylactides—Chemistry, Properties and Green Packaging Technology: A Review. *International Journal of Food Properties*, 14(1), pp.37–58.

Aluigi, A. et al., 2012. Study on the adsorption of chromium (VI) by hydrolyzed keratin/polyamide 6 blend nanofibres. *Journal of Nanoscience and Nanotechnology*, 12(9), pp.7250–7259.

Angammana, C.J. & Jayaram, S.H., 2011a. A Theoretical Understanding of the Physical Mechanisms of Electrospinning. *Proceedings ESA Annual Meeting on Electrstatics*, pp.1–9.

Angammana, C.J. & Jayaram, S.H., 2011b. Analysis of the Effects of Solution Conductivity on Electrospinning Process and Fiber Morphology. *IEEE Transactions on Industry applications*, 47(3), pp.1109–1117.

Angeles, M., Cheng, H. & Velankar, S.S., 2008. Emulsion electrospinning : Composite fibers from drop breakup during electrospinning. *Polymers for Advanced Technologies*, 19, pp.728–733.

Antoniou, E. & Alexandridis, P., 2010. Polymer conformation in mixed aqueous-polar organic solvents. *European Polymer Journal*, 46(2), pp.324–335.

Arinstein, A., Avrahami, R. & Zussman, E, 2009. Buckling behaviour of electrospun microtubes: a simple theoretical model and experimental observations. *Journal of Physics D: Applied Physics*, 42(1), p.015507.

Armentano, I. et al., 2010. Biodegradable polymer matrix nanocomposites for tissue engineering: A review. *Polymer Degradation and Stability*, 95(11), pp.2126–2146.

Ashammakhi, N. et al., 2008. Advancing tissue engineering by using electrospun nanofibers.

Regenerative medicine, 3(4), pp.547–74.

Auras, Rafael, Harte, B. & Selke, S., 2004. An overview of polylactides as packaging materials. *Macromolecular Bioscience*, 4(9), pp.835–864.

Aznar-Cervantes, S. et al., 2012. Fabrication of conductive electrospun silk fibroin scaffolds by coating with polypyrrole for biomedical applications. *Bioelectrochemistry*, 85, pp.36–43.

Badawi, M. a & El-Khordagui, L.K., 2014. A quality by design approach to optimization of emulsions for electrospinning using factorial and D-optimal designs. *European journal of pharmaceutical sciences*, 58, pp.44–54.

Barnes, C.P. et al., 2007. Nanofiber technology: designing the next generation of tissue engineering scaffolds. *Advanced drug delivery reviews*, 59(14), pp.1413–33.

Baumgarten, P.K., 1971. Electrostatic Spinning of Acrylic Microfibers. *Journal of Colloid and Interface Science*, 36(1), pp.71–79.

Benada, O. et al., 2012. Core/Shell Nanofibers with Embedded Liposomes as a Drug Delivery System. *Biomacromolecules*, 13, pp.952–962.

Bhardwaj, N. & Kundu, S.C., 2010. Electrospinning: A fascinating fiber fabrication technique. *Biotechnology Advances*, 28(3), pp.325–347.

Bianco, A. et al., 2011. Poly (L-lactic acid)/calcium-deficient nanohydroxyapatite electrospun mats for bone marrow stem cell cultures. *Journal of Bioactive and Compatible Polymers*, 26(3), pp.225–241.

Boateng, J.S. et al., 2008. Wound Healing Dressings and Drug Delivery Systems : A Review. *Journal of Pharmaceutical Sciences*, 97(8), pp.2892–2923.

Boland, E.D. et al., 2004. Utilizing acid pretreatment and electrospinning to improve biocompatibility of poly(glycolic acid) for tissue engineering. *Journal of biomedical materials research. Part B, Applied biomaterials*, 71(1), pp.144–52.

Bonino, C.A. et al., 2011. Electrospinning alginate-based nanofibers: From blends to crosslinked low molecular weight alginate-only systems. *Carbohydrate Polymers*, 85(1), pp.111–119.

Bosworth, L.A. & Downes, S., 2012. Acetone, a Sustainable Solvent for Electrospinning Poly(ε-Caprolactone) Fibres: Effect of Varying Parameters and Solution Concentrations on Fibre Diameter. *Journal of Polymers and the Environment*, 20(3), pp.879–886.

Briggs, T. & Arinzeh, T.L., 2014. Examining the formulation of emulsion electrospinning for improving the release of bioactive proteins from electrospun fibers. *Journal of Biomedical Materials Research - Part A*, 102, pp.674–684.

Buschle-Diller, G. et al., 2007. Release of antibiotics from electrospun bicomponent fibers.

Cellulose, 14(6), pp.553–562.

Campos, A. De, Marconato, J.C. & Martins-franchetti, S.M., 2011. Biodegradation of Blend Films PVA / PVC , PVA / PCL in Soil and Soil with Landfill Leachate. *Brazilian Archives Biology and Technology*, 54(December), pp.1367–1378.

Casper, C.L. et al., 2004. Controlling surface morphology of electrospun polystyrene fibers: Effect of humidity and molecular weight in the electrospinning process. *Macromolecules*, 37(2), pp.573–578.

Chen, J., Chu, Benjamin & Hsiao, Benjamin S, 2006. Mineralization of hydroxyapatite in electrospun nanofibrous poly (L-lactic acid) scaffolds. *Journal of Biomedical Materials Research Part A*, 79(2), pp.307–17.

Cheng, L. et al., 2014. NaF-loaded core-shell PAN-PMMA nanofibers as reinforcements for Bis-GMA/TEGDMA restorative resins. *Materials science & engineering. C, Materials for biological applications*, 34, pp.262–9.

Chisca, S. et al., 2012. Morphological and rheological insights on polyimide chain entanglements for electrospinning produced fibers. *The journal of physical chemistry. B*, 116(30), pp.9082–9088.

Choi, S. et al., 2011. Microstructural control and selective C2H5OH sensing properties of Zn2SnO4 nanofibers prepared by electrospinning. *The Royal society of Chemistry*.

Choktaweesap, N. et al., 2007. Electrospun Gelatin Fibers: Effect of Solvent System on Morphology and Fiber Diameters. *Polymer Journal*, 39(6), pp.622–631.

Chong, E.J. et al., 2007. Evaluation of electrospun PCL/gelatin nanofibrous scaffold for wound healing and layered dermal reconstitution. *Acta Biomaterialia*, 3, pp.321–330.

Chowdhury, M. & Stylios, G., 2010. Effect of experimental parameters on the morphology of electrospun Nylon 6 fibres. *International Journal of Basic & Applied Sciences*, 10(06), pp.116–131.

Chowdhury, M. & Stylios, G.K., 2012. Analysis of the effect of experimental parameters on the morphology of electrospun polyethylene oxide nanofibres and on their thermal properties. *Journal of the Textile Institute*, 103, pp.124–138.

Colby, R.H. et al., 1991. Effects of concentration and thermodynamic interaction on the viscoelastic properties of polymer solutions. *Macromolecules*, 24, pp.3873–3882.

Collins, G. et al., 2012. Charge generation, charge transport, and residual charge in the electrospinning of polymers: A review of issues and complications. *Journal of Applied Physics*, 111(4), pp.044701–1/18.

Conn, R.E., 1995. Safety assessment of polylactide (PLA) for use as a food-contact polymer. *Food and Chemical Toxicology*, 33(4), pp.273–283.

Cooley, J.F., 1902. Apparatus for electrically dispersing fluids. *US Patent 692,631*, (692).

Costa, L.M.M., 2010. Effect of Solution Concentration on the Electrospray/Electrospinning Transition and on the Crystalline Phase of PVDF. *Materials Sciences and Applications*, 01(04), pp.246–251.

Cui, W. et al., 2008. Degradation patterns and surface wettability of electrospun fibrous mats. *Polymer Degradation and Stability*, 93(3), pp.731–738.

Cui, W. et al., 2006. Investigation of drug release and matrix degradation of electrospun poly(DL-lactide) fibers with paracetanol inoculation. *Biomacromolecules*, 7, pp.1623–1629.

Cui, W., Zhou, Y. & Chang, J., 2010. Electrospun nanofibrous materials for tissue engineering and drug delivery. *Science and Technology of Advanced Materials*, 11, p.014108.

Dahlin, R.L. et al., 2011. Polymeric Nanofibers in Tissue Engineering. *Tissue engineering. Part B*, 17(5), pp.349–364.

Deitzel, J.M. et al., 2001. The effect of processing variables on the morphology of electrospun nanofibers and textiles. *Polymer*, 42(1), pp.261–272.

Demir, M.M. et al., 2002. Electrospinning of polyurethane fibers. *Polymer*, 43, pp.3303–3309.

Dhandayuthapani, B., Krishnan, U.M. & Sethuraman, S., 2010. Fabrication and characterization of chitosan-gelatin blend nanofibers for skin tissue engineering. *Journal of biomedical materials research. Part B, Applied biomaterials*, 94(1), pp.264–72.

Dhineshbabu, N.R., Karunakaran, G. & Suriyaprabha, R., 2014. Electrospun MgO/Nylon 6 Hybrid Nanofibers for Protective Clothing. *Nano-Micro Letters*, 6(1), pp.46–54.

Díaz, J.E. et al., 2006. Controlled encapsulation of hydrophobic liquids in hydrophilic polymer nanofibers by co-electrospinning. *Advanced Functional Materials*, 16, pp.2110–2116.

Ding, B. et al., 2009. Gas sensors based on electrospun nanofibers. *Sensors*, 9(3), pp.1609–24.

Ding, B. et al., 2002. Preparation and Characterization of Nanoscaled Poly (vinyl alcohol) Fibers via Electrospinning. , 3(2), pp.73–79.

Domb, A.J., Kumar, N. & Ezra, A. eds., *Biodegradable Polymers in Clinical Use and Clinical Development*, New York: John Wiley & Sons, Inc.

Dong, Y. et al., 2009. Degradation behaviors of electrospun resorbable polyester nanofibers. *Tissue engineering. Part B, Reviews*, 15(3), pp.333–51.

Dong, Y. et al., 2010. Distinctive degradation behaviors of electrospun polyglycolide, poly(DL-lactide-co-glycolide), and poly(L-lactide-co-caprolactone) nanofibers cultured

with/without porice smooth muscle cells. *Tissue engineering. Part A*, 16, pp.283–298.

Doshi, J. & Reneker, D.H., 1995. Electrospinning process and applications of electrospun fibers. *Journal of Electrostatics*, 35, pp.151–160.

Dow, A.C., 2004. The Sustainability of NatureWorks TM Polylactide Polymers and Ingeo TM Polylactide Fibers a : an Update of the Future Initiated by the 1 st International Conference on Bio-based Polymers. *Macromolecular Bioscience*, 4, pp.551–564.

Dror, Y. et al., 2007. One-step production of polymeric microtubes by co-electrospinning. *Small*, 3(6), pp.1064–73.

Drumright, R.E., Gruber, P.R. & Henton, D.E., 2000. Polylactic acid technology. *Advanced Materials*, 12(23), pp.1841–1846.

Dubnika, A., Loca, D. & Berzina-Cimdina, L., 2012. Functionalized hydroxyapatite scaffolds coated with sodium alginate and chitosan for controlled drug delivery. *Proceedings of the Estonian Academy of Sciences*, 61(3), p.193.

Eda, G., Liu, J. & Shivkumar, Satya, 2007. Solvent effects on jet evolution during electrospinning of semi-dilute polystyrene solutions. *European Polymer Journal*, 43, pp.1154–1167.

Elst, M. Van Der, Klein, C.P.A.T. & Blieck-hogervorst, J.M. De, 1999. Bone tissue response to biodegradable polymers used for intra medullary fracture fixation : A long-term in vivo study in sheep femora. *Biomaterials*, 20, pp.121–128.

Enomoto, K., Ajioka, M. & Yamaguchi, A., 1994. US 5,310,865-Polyhydroxycarboxylic acid and preparation process thereof.

Fallahi, D. et al., 2010. Effect of Applied Voltage on Surface and Volume Charge Density of the Jet in Electrospinning of Polyacrylonitrile Solutions. *Polymer Engineering and Science*, C(3), pp.0–4.

Fallahi, Delaram et al., 2008. Effect of applied voltage on jet electric current and flow rate in electrospinning of polyacrylonitrile solutions. *Polymer international*, 1368, pp.1363–1368.

Feng, J.J., 2003. Stretching of a straight electrically charged viscoelastic jet. *Journal of Non-Newtonian Fluid Mechanics*, 116, pp.55–70.

Feng, J.J., 2002. The stretching of an electrified non-Newtonian jet: A model for electrospinning. *Physics of Fluids*, 14(11), p.3912.

Ferdinand Rodriguez, 1996. *Principles of Polymer Systems* Fourth., Washington: Taylor and Francis.

Flory, P.J., 1953. *Principles of Polymer Chemistry*, Ithaca, NY: Cornell University Press.

Fong, H., Chun, I. & Reneker, D.H., 1999. Beaded nanofibers formed during electrospinning. *Polymer*, 40(16), pp.4585–4592.

Fonseca, E., Fábia, S. & Sander, H., 2006. Synthesis and Characterization of Poly(Vinyl Alcohol) Hydrogels and Hybrids for rMPB70 Protein Adsorption. *Materials Research*, 9(2), pp.185–191.

Formhals, A., 1934. Process and apparatus for preparing artificial threads, US Patent 1975504.

Fridrikh, Sergey V et al., 2003. Controlling the fiber diameter during electrospinning. *Physical review letters*, 90, pp.144502–1/4.

Friederike von Burkersroda, Luise Schedl, A.G., 2002. Why degradable polymers undergo surface erosion or bulk erosion. *Biomaterials*, 23, pp.4221–4231.

Garg, K. & Bowlin, G.L., 2011. Electrospinning jets and nanofibrous structures. *Biomicrofluidics*, 5(1), pp.013403–1/19.

Garlotta, D., 2002. A literature review of poly (lactic acid). *Journal of Polymers and the Environment*, 9(2), pp.63–84.

Gedde, U.W., 1995. *Polymer Physics* 1995th ed., London: Chapman & Hall.

De Gennes, P.-G., 1979. *Scaling Concepts in Polymer Physics*, London: Cornell University Press.

Gholipour Kanani, a. & Bahrami, S.H., 2011. Effect of Changing Solvents on Poly(Caprolactone) Nanofibrous Webs Morphology. *Journal of Nanomaterials*, 2011, pp.1–10.

Goddard, W.A. et al., 2003. *Handbook of Nanoscience and Technology*, CRC Press.

Greiner, A. et al., 2006. Biohybrid nanosystems with polymer nanofibers and nanotubes. *Applied microbiology and biotechnology*, 71(4), pp.387–93.

Grizzi, I. et al., 1995. Hydrolytic degradation of devices based on poly[m-lactic acid) size-dependence. *Biomaterials*, 16(4), pp.305–311.

Gruber, R.P. et al., 2001. US 6,326,458 B1 - Continuous process for the manufacture of lactid and lactide polymers.

Gu, S.-Y. & Ren, J., 2005. Process optimization and empirical modeling for electrospun poly(D,L-lactide) fibers using response surface methodology. *Macromolecular Materials and Engineering*, 290(11), pp.1097–1105.

Gu, X. et al., 2014. Electrospinning of poly(butylene-carbonate): effect of solvents on the properties of the nanofibers film. *International journal of electrochemical science*, 9,

pp.8045–8056.

Guarino, V. et al., 2011. Tuning size scale and crystallinity of PCL electrospun fibres via solvent permittivity to address hMSC response. *Macromolecular bioscience*, 11(12), pp.1694–705.

Guo, C., Zhou, L. & Lv, J., 2013. Fabrication and Characterization of Polyurethane Electrospun Nanofiber Membranes for Protective Clothing Applications. *Polymers and Polymer Composites*, 21(7), pp.449–456.

Gupta, B., Revagade, N. & Hilborn, J., 2007. Poly(lactic acid) fiber: An overview. *Progress in Polymer Science*, 32(4), pp.455–482.

Gupta, D. et al., 2009. Aligned and random nanofibrous substrate for the in vitro culture of Schwann cells for neural tissue engineering. *Acta biomaterialia*, 5(7), pp.2560–9.

Gupta, P. et al., 2005. Electrospinning of linear homopolymers of poly(methyl methacrylate): exploring relationships between fiber formation, viscosity, molecular weight and concentration in a good solvent. *Polymer*, 46(13), pp.4799–4810.

Hansen, C.M., 2007. *Hansen solubility paramaters: A User's Handbook*, CRC Press.

He, C. et al., 2006. Coaxial Electrospun Poly(L-Lactic Acid) Ultrafine Fibers for Sustained Drug Delivery. *Journal of Macromolecular Science, Part B*, 45(4), pp.515–524.

He, C.-L., Huang, Z.-M. & Han, X.-J., 2009. Fabrication of drug-loaded electrospun aligned fibrous threads for suture applications. *Journal of biomedical materials research. Part A*, 89(1), pp.80–95.

He, Ji Huan & Wan, Yu Qin, 2004. Allometric scaling for voltage and current in electrospinning. *Polymer*, 45(19), pp.6731–6734.

Heidei, L., Gupta, P. & Wilkes, G., 2004. Cooperative charging effects of fibers from electrospinning of electrically dissimilar polymers. *INJ Winter*, pp.39–45.

Hekmati, A.H. et al., 2013. Effect of needle length, electrospinning distance, and solution concentration on morphological properties of polyamide-6 electrospun nanowebs. *Textile Research Journal*, 83(14), pp.1452–1466.

Hohman, M.M. et al., 2001a. Electrospinning and electrically forced jets. I. Stability theory. *Physics of Fluids*, 13(8), p.2201.

Hohman, M.M. et al., 2001b. Electrospinning and electrically forced jets. II. Applications. *Physics of Fluids*, 13(8), p.2221.

Homayoni, H., Ravandi, S.A.H. & Valizadeh, M., 2009. Electrospinning of chitosan nanofibers: Processing optimization. *Carbohydrate Polymers*, 77(3), pp.656–661.

Hsu, C.M. & Shivkumar, S., 2004. Nano-sized beads and porous fiber constructs of Poly(ε-

caprolactone) produced by electrospinning. *Journal of Materials Science*, 39(9), pp.3003–3013.

Hsu, C.-M. & Shivkumar, Satya, 2004. N,N-Dimethylformamide additions to the solution for the electrospinning of poly(ε-caprolactone) nanofibers. *Macromolecular Materials and Engineering*, 289(4), pp.334–340.

Hu, Xiuli et al., 2014. Electrospinning of polymeric nanofibers for drug delivery applications. *Journal of controlled release : official journal of the Controlled Release Society*, 185, pp.12–21.

Huan, S. et al., 2015. Effect of Experimental Parameters on Morphological, Mechanical and Hydrophobic Properties of Electrospun Polystyrene Fibers. *Materials*, 8(5), pp.2718–2734.

Huang, L. et al., 2011. Controlling electrospun nanofiber morphology and mechanical properties using humidity. *Journal of Polymer Science, Part B: Polymer Physics*, 49(24), pp.1734–1744.

Huang, Z.M. et al., 2003. A review on polymer nanofibers by electrospinning and their applications in nanocomposites. *Composites Science and Technology*, 63(15), pp.2223–2253.

Huang, Z.M. et al., 2004. Electrospinning and mechanical characterization of gelatin nanofibers. *Polymer*, 45(15), pp.5361–5368.

Huang, Z.-M. et al., 2006. Encapsulating drugs in biodegradable ultrafine fibers through co-axial electrospinning. *Journal of biomedical materials research. Part A*, 77(1), pp.169–79.

Ishii, D. et al., 2009. In vivo tissue response and degradation behavior of PLLA and stereocomplexed PLA nanofibers. *Biomacromolecules*, 10(2), pp.237–42.

Jamnongkan, T. et al., 2013. Effect of ZnO nanoparticles on the electrospinning of poly(vinyl alcohol) from aqueous solution: Influence of particle size. *Polymer Engineering & Science*, p.n/a–n/a.

Jamshidian, M. et al., 2010. Poly-Lactic Acid: Production, applications, nanocomposites, and release studies. *Comprehensive Reviews in Food Science and Food Safety*, 9, pp.552–571.

Jannesari, M. et al., 2011. Composite poly(vinyl alcohol)/poly(vinyl acetate) electrospun nanofibrous mats as a novel wound dressing matrix for controlled release of drugs. *International journal of nanomedicine*, 6(19), pp.993–1003.

Jarusuwannapoom, T. et al., 2005. Effect of solvents on electro-spinnability of polystyrene solutions and morphological appearance of resulting electrospun polystyrene fibers. *European Polymer Journal*, 41(3), pp.409–421.

Jelinska, N. et al., 2010. Poly(vinyl alcohol)/poly(vinyl acetate) blend films. *Scientific Journal of Riga Technical University*, 21(1), pp.55–61.

Jeong, Sung In et al., 2008. Nanofibrous poly(lactic acid)/hydroxyapatite composite scaffolds for guided tissue regeneration. *Macromolecular Bioscience*, 8(4), pp.328–38.

Ji, W. et al., 2010. Fibrous scaffolds loaded with protein prepared by blend or coaxial electrospinning. *Acta biomaterialia*, 6(11), pp.4199–207.

Jia, L. & Qin, Xiao-hong, 2012. The effect of different surfactants on the electrospinning poly(vinyl alcohol) (PVA) nanofibers. *Journal of Thermal Analysis and Calorimetry*, 112(2), pp.595–605.

Jiang, H. et al., 2005. A facile technique to prepare biodegradable coaxial electrospun nanofibers for controlled release of bioactive agents. *Journal of Controlled Release*, 108, pp.237–243.

Jiang, H. et al., 2006. Modulation of protein release from biodegradable core – chell structured fibers prepared by coaxial electrospinning. *Journal of biomedical materials Research. Part B: Applied Biomaterials*, 79(2005), pp.50–57.

Jiang, Hongliang et al., 2004. Preparation and characterization of ibuprofen-loaded poly(lactide-co-glycolide)/poly(ethylene glycol)-g-chitosan electrospun membranes. *Journal of Biomaterials Science, Polymer Edition*, 15(3), pp.279–296.

Jin, G. et al., 2013. Controlled release of multiple epidermal induction factors through core-shell nanofibers for skin regeneration. *European Journal of Pharmaceutics and Biopharmaceutics*, 85(3), pp.689–698.

Jose, M.V. et al., 2009. Aligned PLGA/HA nanofibrous nanocomposite scaffolds for bone tissue engineering. *Acta biomaterialia*, 5(1), pp.305–15.

Joung, Y.K. et al., 2011. Controlled Release of Growth Factors from Core-Shell Structured PLGA Microfibers for Tissue Engineering. *Biomaterials Research*, 15(2), pp.78–84.

Jun, Z. et al., 2003. Poly-L-lactide nanofibers by electrospinning – Influence of solution viscosity and electrical conductivity on fiber diameter and fiber morphology. *E-Polymers*, 3(1), pp.102–110.

Kai, Dan et al., 2012. Mechanical properties and in vitro behavior of nanofiber-hydrogel composites for tissue engineering applications. *Nanotechnology*, 23(9), p.095705.

Kanani, A.G. & Bahrami, S.H., 2010. Review on electrospun nanofibers scaffold and biomedical applications. *Trends Biomaterial Artificial Organs*, 24(2), pp.93–115.

Kang, Y.O. et al., 2010. Chitosan-coated poly(vinyl alcohol) nanofibers for wound dressings. *Journal of biomedical materials research. Part B, Applied biomaterials*, 92(2), pp.568–76.

Kataria, K. et al., 2014. In vivo wound healing performance of drug loaded electrospun composite nanofibers transdermal patch. *International Journal of Pharmaceutics*, 469(1), pp.102–110.

Katti, D.S. et al., 2004. Bioresorbable nanofiber-based systems for wound healing and drug delivery: optimization of fabrication parameters. *Journal of biomedical materials research. Part B, Applied biomaterials*, 70, pp.286–296.

Kelloma, M. et al., 2000. Bioabsorbable scaffolds for guided bone regeneration and generation. *Biomaterials*, 21, pp.2495–2505.

Kenawy, E.R. et al., 2002. Release of tetracycline hydrochloride from electrospun poly(ethylene-co-vinylacetate), poly(lactic acid), and a blend. *Journal of Controlled Release*, 81, pp.57–64.

Kenawy, E.-R. et al., 2007. Controlled release of ketoprofen from electrospun poly(vinyl alcohol) nanofibers. *Materials Science and Engineering: A*, 459(1-2), pp.390–396.

Khan, N., 2012. Applications of electrospun nanofibers in the biomedical field. *Studies by Undergraduate Researchers at Guelph*, 5(2), pp.63–73.

Khil, M. et al., 2003. Electrospun nanofibrous polyurethane membrane as wound dressing. *Journal of biomedical materials research. Part B Applied Biomaterial*, 67(2), pp.675–679.

Ki, C.S. et al., 2005. Characterization of gelatin nanofiber prepared from gelatin–formic acid solution. *Polymer*, 46(14), pp.5094–5102.

Kijeńska, E. et al., 2014. Interaction of Schwann cells with laminin encapsulated PLCL core–shell nanofibers for nerve tissue engineering. *European Polymer Journal*, 50, pp.30–38.

Kim, B. et al., 2005. Poly(acrylic acid) nanofibers by electrospinning. *Materials Letters*, 59(7), pp.829–832.

Kim, E.S., Kim, Seong Hun & Lee, C.H., 2010. Electrospinning of polylactide fibers containing silver nanoparticles. *Macromolecular Research*, 18(3), pp.215–221.

Kim, G.H. et al., 2011. Wound Dressings for Wound Healing and Drug Delivery. *Tissue Engineering and Regeneartive Medicine*, 8(1), pp.1–7.

Kim, G.-M. et al., 2008. Electrospun PVA/HAp nanocomposite nanofibers: biomimetics of mineralized hard tissues at a lower level of complexity. *Bioinspiration & biomimetics*, 3(4), p.046003.

Kim, H.-W., Lee, H.-H. & Knowles, J.C., 2006. Electrospinning biomedical nanocomposite fibers of hydroxyapaite/poly(lactic acid) for bone regeneration. *Journal of Biomedical Materials Research Part A*, 79A, pp.643–649.

Kim, H.W., Yu, H.S. & Lee, H.H., 2008. Nanofibrous matrices of poly(lactic acid) and

gelatin polymeric blends for the improvement of cellular responses. *Journal of Biomedical Materials Research - Part A*, 87(1), pp.25–32.

Kim, K. et al., 2003. Control of degradation rate and hydrophilicity in electrospun non-woven poly(D,L-lactide) nanofiber scaffolds for biomedical applications. *Biomaterials*, 24, pp.4977–4985.

Kim, K. et al., 2004. Incorporation and controlled release of a hydrophilic antibiotic using poly(lactide-co-glycolide)-based electrospun nanofibrous scaffolds. *Journal of controlled release : official journal of the Controlled Release Society*, 98(1), pp.47–56.

Kim, K.H. et al., 2005. Biological efficacy of silk fibroin nanofiber membranes for guided bone regeneration. *Journal of biotechnology*, 120(3), pp.327–39.

Kim, S.E. et al., 2009. Electrospun gelatin / polyurethane blended nanofibers for wound healing. *Biomedical materials*, 4, pp.1–11.

Kim, S.J., Shin, K.M. & Kim, S.I., 2004. The effect of electric current on the processing of nanofibers formed from poly(2-acrylamido-2-methyl-1-propane sulfonic acid). *Scripta Materialia*, 51(1), pp.31–35.

Klaus Florey, 1985. *Analytical Profiles of Drug Substances*, Academic Press, INC.

Koenhen, D.M. & Smolders, C.A., 1975. The determination of solubility parameters of solvents and polymers by means of correlations with other physical quantities. *Journal of Applied Polymer Science*, 19(4), pp.1163–1179.

Koski, A., Yim, K. & Shivkumar, S., 2004. Effect of molecular weight on fibrous PVA produced by electrospinning. *Materials Letters*, 58(3-4), pp.493–497.

Krause, W.E., Bellomo, E.G. & Colby, R. H., 2001. Rheology of sodium hyaluronate under physiological conditions. *Biomacromolecules*, 2, pp.65–69.

Kriegel, C. et al., 2009. Influence of Surfactant Type and Concentration on Electrospinning of Chitosan–Poly(Ethylene Oxide) Blend Nanofibers. *Food Biophysics*, 4(3), pp.213–228.

Labidi, N.S. & Djebaili, a., 2008. Studies of The Mechanism of Polyvinyl Alcohol Adsorption on The Calcite/Water Interface in The Presence of Sodium Oleate. *Journal of Minerals & Materials Characterization & Engineering*, 7(2), pp.147 – 161.

Langer, R. & Vacanti, J.P., 1993. Tissue engineering. *Science*, 260, pp.920–925.

Lannutti, J. et al., 2007. Electrospinning for tissue engineering scaffolds. *Materials Science and Engineering: C*, 27(3), pp.504–509.

Larrondo, L. & Manley, R.S.J., 1981a. Electrostatic Fiber Spinning from Polymer Melts. I. Experimental Observations on Fiber Formation and Properties. *Journal of Polymer*

Science: Polymer Physics Edition, 19(6), pp.909–920.

Larrondo, L. & Manley, R.S.J., 1981b. Electrostatic Fiber Spinning from Polymer Melts. II. Examination of the Flow Field in an Electrically Driven Jet. *Journal of Polymer Science: Polymer Physics Edition*, 19, pp.921–932.

Larrondo, L. & Manley, R.S.J., 1981c. Electrostatic Fiber Spinning from Polymer Melts. III. Electrostatic Deformation of a Pendant Drop of Polymer melt. *Journal of Polymer Science: Polymer Physics Edition*, 19, pp.933–940.

Lasprilla, A.J.R. et al., 2012. Poly-lactic acid synthesis for application in biomedical devices - a review. *Biotechnology advances*, 30(1), pp.321–8.

Lee, J.S. et al., 2004. Role of molecular weight of atactic poly(vinyl alcohol) (PVA) in the structure and properties of PVA nanofabric prepared by electrospinning. *Journal of Applied Polymer Science*, 93(4), pp.1638–1646.

Lee, K.H. et al., 2003. Characterization of nano-structured poly(ε-caprolactone) nonwoven mats. *Polymer Journal*, 44, pp.1287–1294.

Lee, K.H. et al., 2002. Influence of a mixing solvent with tetrahydrofuran and N,N-dimethylformamide on electrospun poly(vinyl chloride) nonwoven mats. *Journal of Polymer Science Part B: Polymer Physics*, 40, pp.2259–2268.

Leung, V. et al., 2011. Bioactive Nanofibres for Wound Healing Applications. *Journal of Fiber Bioengineering and Informatics*, 4(1), pp.1–14.

Li, D. & Xia, Y., 2004. Direct Fabrication of Composite and Ceramic Hollow Nanofibers by Electrospinning. *Nano Letters*, 4(5), pp.933–938.

Li, L., Jiang, Z., et al., 2014. Predicting poly(vinyl pyrrolidone)'s solubility parameter and systematic investigation of the parameters of electrospinning with response surface methodology. *Journal of Applied Polymer Science*, 131(11), pp.40304–1/9.

Li, L., Li, R., et al., 2014. Theoretical selection of solvent for production of electrospun PMMA fibers with wrinkled surfaces. *RSC Advances*, 4(53), p.27914.

Li, Mengyan et al., 2005. Electrospun protein fibers as matrices for tissue engineering. *Biomaterials*, 26(30), pp.5999–6008.

Li, Xiaoqiang et al., 2010. Encapsulation of proteins in poly(L-lactide-co-caprolactone) fibers by emulsion electrospinning. *Colloids and surfaces. B, Biointerfaces*, 75(2), pp.418–24.

Li, Yajing et al., 2012. Electrospun poly(lactic acid)/chitosan core-shell structure nanofibers from homogeneous solution. *Carbohydrate polymers*, 90(4), pp.1445–51.

Li, Yan, Huang, Zhengming & Lǔ, Y., 2006. Electrospinning of nylon-6,66,1010 terpolymer. *European Polymer Journal*, 42(7), pp.1696–1704.

Li, Z. et al., 2014. Controlled release of liposome-encapsulated Naproxen from core-sheath electrospun nanofibers. *Carbohydrate Polymers*, 111, pp.18–24.

Liang, D., Hsiao, B.S. & Chu, B., 2007. Functional electrospun nanofibrous scaffolds for biomedical applications. *Advanced drug delivery reviews*, 59(14), pp.1392–412.

Liechty, W.B. et al., 2010. Polymers for Drug Delivery Systems. *Annual Rev Chem Biomol Eng*, 1, pp.149–173.

Lim, L.T., Auras, R. & Rubino, M., 2008. Processing technologies for poly(lactic acid). *Progress in Polymer Science*, 33(8), pp.820–852.

Lin, J. et al., 2010. Direct fabrication of highly nanoporous polystyrene fibers via electrospinning. *ACS Applied Materials and Interfaces*, 2(2), pp.521–528.

Lin, T. et al., 2005. Effects of Polymer Concentration and Cationic Surfactant on the Morphology of Electrospun Polyacrylonitrile Nanofibres. *Journal Material Science Technology*, 21, pp.1–4.

Lin, T. et al., 2004. The charge effect of cationic surfactants on the elimination of fibre beads in the electrospinning of polystyrene. *Nanotechnology*, 15(9), pp.1375–1381.

Liu, C., Xia, Z. & Czernuszka, J.T., 2007. Design and development of three-dimensional scaffolds for tissue engineering. *Chemical Engineering Research and Design*, 85(7), pp.1051–1064.

Liu, F. et al., 2009. Effect of Processing Variables on the Morphology of Electrospun Poly[(lactic acid)-co-(glycolic acid)] Nanofibers. *Macromolecular Materials and Engineering*, 294(10), pp.666–672.

Liu, Fujuan et al., 2009. Effect of processing variables on the morphology of electrospun poly[(lactic acid)-co-(glycolic acid)] nanofibers. *Macromolecular Materials and Engineering*, 294, pp.666–672.

Liu, H. & Hsieh, Y.L., 2002. Ultrafine fibrous cellulose membranes from electrospinning of cellulose acetate. *Journal of Polymer Science Part B: Polymer Physics*, 40(18), pp.2119–2129.

Liu, Wanjun, Huang, C. & Jin, X., 2015. Electrospinning of Grooved Polystyrene Fibers: Effect of Solvent Systems. *Nanoscale research letters*, 10(1), p.949. Available at: http://www.pubmedcentral.nih.gov/articlerender.fcgi?artid=4456588&tool=pmcentrez&rendertype=abstract [Accessed August 9, 2016].

Liu, Wenwen et al., 2013. Preparation of Multilayer Biodegradable Nanofibers by Triaxial Electrospinning. *ACS Macro Letters*, 2, pp.466–468.

Liu, Y. et al., 2008. Controlling numbers and sizes of beads in electrospun nanofibers. *Polymer International*, 636, pp.632–636.

Lou, C.-W. et al., 2008. Manufacturing and Properties of PLA Absorbable Surgical Suture. *Textile Research Journal*, 78(11), pp.958–965.

Lubasova, D. & Martinova, L., 2011. Controlled Morphology of Porous Polyvinyl Butyral Nanofibers. *Journal of Nanomaterials*, 2011, pp.1–6.

Ma, P.X. & Zhang, R., 1999. Synthetic nano-scale fibrous extracellular matrix. *Journal of Biomedical Materials Research*, 46(1), pp.60–72.

Maleki, M. et al., 2013. Electrospun Core – Shell Nanofibers for Drug Encapsulation and Sustained Release. *Polymer Engineering & Science*, pp.1771–1779.

Matthews, J.A. et al., 2002. Electrospinning of collagen nanofibers. *Biomacromolecules*, 3(2), pp.232–8.

Mazoochi, T. et al., 2012. Investigation on the morphological characteristics of nanofiberous membrane as electrospun in the different processing parameters. *International Journal of Industrial Chemistry*, 3, pp.1–8.

McCullen, S.D. et al., 2007. Development , Optimization , and Characterization of Electrospun Poly (lactic acid) Nanofibers Containing Multi-Walled Carbon Nanotubes. *Journal of Applied Polymer Science*, 105, pp.1668–1678.

McKee, M.G., Elkins, C.L. & Long, T.E., 2004. Influence of self-complementary hydrogen bonding on solution rheology/electrospinning relationships. *Polymer*, 45(26), pp.8705–8715.

McKee, Matthew G. et al., 2004. Correlations of solution rheology with electrospun fiber formation of linear and branched polyesters. *Macromolecules*, 37(5), pp.1760–1767.

Megelski, S. et al., 2002. Micro- and nanostructured surface morphology on electrospun polymer fibers. *Macromolecules*, 35(22), pp.8456–8466.

Meng, Y.H. et al., 2008. Fabrication and characterization of needle-like nano-HA and HA/MWNT composites. *Journal of materials science. Materials in medicine*, 19(1), pp.75–81.

Meng, Z.X. et al., 2010. Electrospinning of PLGA/gelatin randomly-oriented and aligned nanofibers as potential scaffold in tissue engineering. *Materials Science and Engineering: C*, 30(8), pp.1204–1210.

Merkle, V. et al., 2013. Gelatin shells strengthen polyvinyl alcohol core–shell nanofibers. *Polymer*, 54(21), pp.6003–6007.

Miller-Chou, B.A. & Koenig, J.L., 2003. A review of polymer dissolution. *Progress in Polymer Science*, 28(8), pp.1223–1270.

Min, B.M., Lee, G., et al., 2004. Electrospinning of silk fibroin nanofibers and its effect on the adhesion and spreading of normal human keratinocytes and fibroblasts in vitro.

Biomaterials, 25(7-8), pp.1289–97.

Min, B.M., Jeong, L., et al., 2004. Formation of silk fibroin matrices with different texture and its cellular response to normal human keratinocytes. *International journal of biological macromolecules*, 34(5), pp.281–8.

Mit-uppatham, C., Nithitanakul, M & Supaphol, P, 2004. Ultratine electrospun polyamide-6 fibers: Effect of solution conditions on morphology and average fiber diameter RID C-4353-2008. *Macromolecular Chemistry and Physics*, 205, pp.2327–2338.

Moghe, A.K. & Gupta, B.S., 2008. Coaxial Electrospinning for Nanofiber Structures: Preparation and Applications. *Polymer Reviews*, 48(2), pp.353–377.

Morelli, S., Holdich, R.G. & Dragosavac, M.M., 2016. Chitosan and Poly(Vinyl Alcohol) microparticles produced by membrane emulsification for encapsulation and pH controlled release. *Chemical Engineering Journal*, 288, pp.451–460.

Morota, K. et al., 2004. Poly(ethylene oxide) thin films produced by electrospray deposition: morphology control and additive effects of alcohols on nanostructure. *Journal of colloid and interface science*, 279(2), pp.484–92.

Morton, W.J., 1902. Method of dispersing fluid. *US Patent 705,691*.

Moutsatsou, P. et al., 2015. Conductive PANI fibers and determining factors for the electrospinning window. *Polymer (United Kingdom)*, 77, pp.143–151.

Muller, L. et al., 2009. Electrospinning and Characterization of Polyamide 66 Nanofibers With Different Molecular Weights. *Materials Research*, 12(2), pp.181–190.

Nageh, H. et al., 2014. Evaluation of Antibacterial Activity and Drug Release Behavior of Chitosan-Based Nanofibers (In Vitro Study). *UK Journal of Pharmaceutical and Biosciences*, 2(3), pp.1–5.

Nakano, A. et al., 2012. Solution parameters for the fabrication of thinner silicone fibers by electrospinning. *Physical review. E, Statistical, nonlinear, and soft matter physics*, 86, p.011801.

Nawalakhe, R. et al., 2013. Novel atmospheric plasma enhanced chitosan nanofiber/gauze composite wound dressings. *Journal of Applied Polymer Science*, 129(2), pp.916–923.

Nayak, R. et al., 2012. Recent advances in nanofibre fabrication techniques. *Textile Research Journal*, 82(2), pp.129–147.

Nezarati, R.M., 2013. Effects of Humidity and Solution Viscosity on Electrospun Fiber Morphology. *Tissue engineering: Part C*, 19(10), pp.1–10.

Nguyen, T.T.T. et al., 2013. Characteristics of curcumin-loaded poly (lactic acid) nanofibers for wound healing. *Journal of Materials Science*.

Nguyen, T.T.T. et al., 2012. Porous core/sheath composite nanofibers fabricated by coaxial electrospinning as a potential mat for drug release system. *International journal of pharmaceutics*, 439(1-2), pp.296–306.

Nguyen, T.T.T., Chung, O.H. & Park, J.S., 2011. Coaxial electrospun poly(lactic acid)/chitosan (core/shell) composite nanofibers and their antibacterial activity. *Carbohydrate Polymers*, 86(4), pp.1799–1806.

Nikolic, L. et al., 2010. Novel microwave-assisted synthesis of poly(D,L-lactide): The influence of monomer/initiator molar ratio on the product properties. *Sensors*, 10(5), pp.5063–5073.

Oliveira, J.E. et al., 2013. Structural and morphological characterization of micro and nanofibers produced by electrospinning and solution blow spinning: A comparative study. *Advances in Materials Science and Engineering*, 2013.

Ondarcuhu, T. & Joachim, C., 1998. Drawing a single nanofibre over hundreds of microns. *Europhysics Letters*, 42, pp.215–220.

Orozco, V.H. et al., 2009. Preparation and characterization of poly(Lactic Acid)- G-maleic anhydride + starch blends. *Macromolecular Symposia*, 277(1), pp.69–80.

Pai, C.L., Boyce, M.C. & Rutledge, Gregory C., 2009. Morphology of porous and wrinkled fibers of polystyrene electrospun from dimethylformamide. *Macromolecules*, 42(6), pp.2102–2114.

Pal, J. et al., 2014. Conducive 3D porous mesh of poly(ε-caprolactone) made via emulsion electrospinning. *Polymer*, 55(16), pp.3970–3979.

Parparita, E., Cheaburu, C.N. & Vasile, C., 2012. Morphological, thermal and rheological characterization of polyvinyl alcohol/chitosan blends. *Cellulose Chemistry and Technology*, 46, pp.571–581.

Pattamaprom, C. et al., 2006. The influence of solvent properties and functionality on the electrospinnability of polystyrene nanofibers. *Macromolecular Materials and Engineering*, 291(7), pp.840–847.

Pawar, R.P. et al., 2014. Biomedical Applications of Poly (Lactic Acid). *Recent patents on regenerative medicine*, pp.40–51.

Peesan, M., Rujiravanit, R. & Supaphol, Pitt, 2006. Electrospinning of hexanoyl chitosan/polylactide blends. *Journal of Biomaterials Science, Polymer Edition*, 17(5), pp.547–65.

Pham, Q.P., Sharma, U. & Mikos, A. G., 2006. Electrospun poly(caprolactone) microfiber and multilayer nanofiber/microfiber scaffolds: characterization of scaffolds and measurement of cellular infiltration. *Biomacromolecules*, 7(10), pp.2796–805.

Pham, Q.P., Sharma, U. & Mikos, A.G., 2006. Electrospinning of polymeric nanofibers for

tissue engineering applications: a review. *Tissue engineering*, 12(5), pp.1197–211.

Pillai, C. & Sharma, C., 2009. Electrospinning of chitin and chitosan nanofibres. *Trends in Biomaterials and Artificial Organs*, 22(3), pp.179–201.

Pillay, V. et al., 2013. A Review of the Effect of Processing Variables on the Fabrication of Electrospun Nanofibers for Drug Delivery Applications. *Journal of Nanomaterials*, 2013, pp.1–22.

Powers, J.G., Morton, L.M. & Phillips, T.J., 2013. Dressings for chronic wounds. *Dermatologic therapy*, 26(3), pp.197–206.

Prabhakaran, Molamma P, Venugopal, J. & Ramakrishna, S, 2009. Electrospun nanostructured scaffolds for bone tissue engineering. *Acta biomaterialia*, 5(8), pp.2884–93.

Prabhakaran, Molamma P. et al., 2011. Electrospun conducting polymer nanofibers and electrical stimulation of nerve stem cells. *Journal of Bioscience and Bioengineering*, 112(5), pp.501–507.

Puppi, D. et al., 2010. Polymeric materials for bone and cartilage repair. *Progress in Polymer Science*, 35(4), pp.403–440.

Qin, J. et al., 2013. Evaluation of drug release property and blood compatibility of aspirin-loaded electrospun PLA/RSF composite nanofibers. *Iranian Polymer Journal*, 22(10), pp.729–737.

Qin, X., Wang, H. & Wu, S., 2012. Investigation on structure and thermal properties of electrospun cellulose diacetate nanofibers. *Journal of Industrial Textiles*, 42(3), pp.244–255.

Qin, X.-H. et al., 2007. Effect of different salts on electrospinning of poly acrylonitrile (PAN) polymer solution. *Journal of Applied Polymer Science*, 103, pp.3865–3870.

Ranganath, S.H. & Wang, C.-H., 2008. Biodegradable microfiber implants delivering paclitaxel for post-surgical chemotherapy against malignant glioma. *Biomaterials*, 29(20), pp.2996–3003.

Rasool Hassan, B.A., 2012. Overview on Drug Delivery System. *Pharmaceutica Analytica Acta*, 03(10), p.4172.

Rathinamoorthy, R., Technology, F. & College, P.S.G., 2012. Nanofiber for drug delivery system –. , (February), pp.45–48.

Regev, O. et al., 2010. The role of interfacial viscoelasticity in the stabilization of an electrospun jet. *Polymer*, 51(12), pp.2611–2620.

Reneker, D.H. et al., 2000. Bending instability of electrically charged liquid jets of polymer

solutions in electrospinning. *Journal of Applied Physics*, 87(9), pp.4531–4547.

Reneker, D.H. et al., 2007. Electrospinning of nanofibers from polymer solutions and melts. *Advances in Applied Mechanics*, 41, pp.44–195.

Reneker, D.H. et al., 2002. Nanofiber garlands of polycaprolactone by electrospinning. *Polymer*, 43(25), pp.6785–94.

Reneker, D.H. & Chun, I., 1996. Nanometre diameter fibres of polymer, produced by electrospinning. *Nanotechnology*, 7(3), pp.216–23.

Reneker, D.H. & Yarin, A.L., 2008. Electrospinning jets and polymer nanofibers. *Polymer*, 49(10), pp.2387–2425.

Rho, K.S. et al., 2006. Electrospinning of collagen nanofibers: effects on the behavior of normal human keratinocytes and early-stage wound healing. *Biomaterials*, 27(8), pp.1452–61.

Ricci Júnior, E., Bentley, M.V.L.B. & Marchetti, J.M., 2002. HPLC assay of lidocaine in in vitro dissolution test of the Poloxamer 407 gels. *Revista Brasileira de Ciências Farmacêuticas*, 38, pp.107–111.

Rieger, K. a., Birch, N.P. & Schiffman, J.D., 2013. Designing electrospun nanofiber mats to promote wound healing – a review. *Journal of Materials Chemistry B*, 1(36), p.4531.

Riga, A.T., Golinar, M. & Alexande, K.S., 2007. Fast Scan Differential Scanning Calorimetry Distinguishes Melting, Melting-Degradation/Sublimation and Thermal Stability of Drugs. *Journal of ASTM International*, 4(3), pp.1–8.

Rodrigues, N.V.S. et al., 2013. Analysis of Seized Cocaine Samples by using Chemometric Methods and FTIR Spectroscopy. *Journal of the Brazilian Chemical Society*, 24(3), pp.507–517.

Rošic, R. et al., 2012. The role of rheology of polymer solutions in predicting nanofiber formation by electrospinning. *European Polymer Journal*, 48, pp.1374–1384.

Rošic, Romana et al., 2013. Nanofibers and their biomedical use. *Acta pharmaceutica (Zagreb, Croatia)*, 63(3), pp.295–304.

Rudeekit, Y. et al., 2008. Determining Biodegradability of Polylactic Acid under Different Environments. *Journal of metals, materials and minerals*, 18(2), pp.83–87.

Rujiravanit, R. et al., 2003. Preparation of Crosslinked Chitosan/Silk Fibroin Blend Films for Drug Delivery System. *Macromolecular Bioscience*, 3(10), pp.604–611.

Samatham, R. & Kim, K.J., 2006. Electric Current as a Control Variable in the Electrospinning Process. *Polymer Engineering and Science*, 46, pp.954–959.

Savioli Lopes, M., Jardini, a. L. & Maciel Filho, R., 2012. Poly (lactic acid) production for

tissue engineering applications. *Procedia Engineering*, 42(August), pp.1402–1413.

Scampicchio, M. et al., 2012. Electrospun nonwoven nanofibrous membranes for sensors and biosensors. *Electroanalysis*, 24(4), pp.719–725.

Van der Schueren, L. et al., 2011. An alternative solvent system for the steady state electrospinning of polycaprolactone. *European Polymer Journal*, 47(6), pp.1256–63.

Sciences, H., 2010. Kinetic modeling on drug release from controlled drug delivery systems. *Acta Poloniae Pharmaceutica-Drug Research*, 67(3), pp.217–223.

Sell, S. a et al., 2009. Electrospinning of collagen/biopolymers for regenerative medicine and cardiovascular tissue engineering. *Advanced drug delivery reviews*, 61(12), pp.1007–19.

Shao, S. et al., 2011. Osteoblast function on electrically conductive electrospun PLA/MWCNTs nanofibers. *Biomaterials*, 32(11), pp.2821–2833.

Shehap, A., 2008. Thermal and spectroscopic studies of polyvinyl alcohol/sodium carboxy methyl cellulose blends. *Egypt. J. Solids*, 31(1), pp.75–91.

Shicong, J. et al., 2001. The Effect of pH on the Permeation of Lidocaine Hydrochloride across excised rat skin. *Journal of Chinese Pharmaceutical science*, 10(3), pp.133–135.

Shin, Y.M. et al., 2001. Electrospinning: A whipping fluid jet generates submicron polymer fibers. *Applied Physics Letters*, 78(8), p.1149.

Siepmann, J et al., 2004. Effect of the size of biodegradable microparticles on drug release: experiment and theory. *Journal of controlled release : official journal of the Controlled Release Society*, 96(1), pp.123–34.

Siepmann, J. & Peppas, N.A., 2012. Modeling of drug release from delivery systems based on hydroxypropyl methylcellulose (HPMC). *Advanced Drug Delivery Reviews*, 64, pp.163–174.

Siepmann, Juergen, Siegel, R.A. & Siepmann, F., 2011. Overview of Controlled Release Mechanisms. In *Fundamentals and Appliactions of Controlled Releease Drug Delivery*. pp. 19–43.

Sill, T.J. & Von Recum, H.A., 2008. Electrospinning: applications in drug delivery and tissue engineering. *Biomaterials*, 29(13), pp.1989–2006.

Sjberg, H., Karami, K. & Beronius, P., 1996. Ionization conditions for iontophoretic drug delivery . A revised pKa of lidocaine hydrochloride in aqueous solution at 25 ° C established by precision conductometry. *International Journal of Pharmaceutics*, 141, pp.63–70.

Smallwood, I.M., 1996. *Handbook of organic solvent properties*, London: Halsted Press.

Södergård, A. & Stolt, M., 2002. Properties of lactic acid based polymers and their

correlation with composition. *Progress in Polymer Science*, 27(6), pp.1123–1163.

Sohrabi, A. et al., 2013. Sustained drug release and antibacterial activity of ampicillin incorporated poly(methyl methacrylate)–nylon6 core/shell nanofibers. *Polymer*, 54(11), pp.2699–2705.

Soliman, S. et al., 2010. Multiscale three-dimensional scaffolds for soft tissue engineering via multimodal electrospinning. *Acta biomaterialia*, 6(4), pp.1227–37.

Son, W.K. et al., 2004. The effects of solution properties and polyelectrolyte on electrospinning of ultrafine poly(ethylene oxide) fibers. *Polymer*, 45(9), pp.2959–2966.

Son, Y.J., Kim, W.J. & Yoo, H.S., 2014. Therapeutic applications of electrospun nanofibers for drug delivery systems. *Archives of Pharmacal Research*, 37(1), pp.69–78.

Song, W. et al., 2013. Coaxial PCL/PVA electrospun nanofibers: osseointegration enhancer and controlled drug release device. *Biofabrication*, 5(3), p.035006.

Spivak, A.F., 1998. Asymptotic decay of radius of a weakly conductive viscous jet. *Applied Physics*, 73(21), pp.3067–3069.

Srinivasarao, M. et al., 2001. Three-dimensionally ordered array of air bubbles in a polymer film. *Science (New York, N.Y.)*, 292(5514), pp.79–83.

Srouji, S., Kizhner, T. & Livne, E., 2006. 3D scaffolds for bone marrow stem cell support in bone repair. *Regenerative medicine*, 1(4), pp.519–28.

Su, Y. et al., 2012. Dual-Drug Encapsulation and Release from Core–Shell Nanofibers. *Journal of Biomaterials Science, Polymer Edition*, 23, pp.861–871.

Subbiah, T. et al., 2005. Electrospinning of nanofibers. *Journal of Applied Polymer Science*, 96(2), pp.557–569.

Sui, G. et al., 2007. Poly-L-lactic acid/hydroxyapatite hybrid membrane for bone tissue regeneration. *Journal of Biomedical Materials Research Part A*, 82(2), pp.445–454.

Sun, Z. et al., 2003. Compound core–shell polymer nanofibers by co-electrospinning. *Advanced Materials*, 15(22), pp.1929–1932.

Sundarrajan, S. et al., 2014. Electrospun Nanofibers for Air Filtration Applications. *Procedia Engineering*, 75, pp.159–163.

Supaphol, P., Mit-uppatham, C. & Nithitanakul, M., 2005. Ultrafine electrospun polyamide-6 fibers: effects of solvent system and emitting electrode polarity on morphology and average fiber diameter. *Macromolecular Materials and Engineering*, 290(9), pp.933–942.

Taepaiboon, P, Rungsardthong, U & Supaphol, P, 2006. Drug-loaded electrospun mats of poly(vinyl alcohol) fibres and their release characteristics of four model drugs.

Nanotechnology, 17(9), pp.2317–2329.

Taepaiboon, Pattama, Rungsardthong, Uracha & Supaphol, Pitt, 2007. Vitamin-loaded electrospun cellulose acetate nanofiber mats as transdermal and dermal therapeutic agents of vitamin A acid and vitamin E. *European journal of pharmaceutics and biopharmaceutics*, 67(2), pp.387–97.

Tan, S.H. et al., 2005. Systematic parameter study for ultra-fine fiber fabrication via electrospinning process. *Polymer*, 46(16), pp.6128–6134.

Tanford Charles, 1961. *Physical Chemistry of Macromolecules*, London: John Wiley & Sons, Inc., New York.

Tang, C. et al., 2010. In situ cross-linking of electrospun poly(vinyl alcohol) nanofibers. *Macromolecules*, 43(2), pp.630–637.

Taylor, G., 1964. Disintegration of water drops in an electric field. *Proceedings of thr Royal Society of London. Series A, Mathematical and Physical Sciences*, 280(1382), pp.383–97.

Taylor, G., 1969. Electrically Driven Jets. *Proceedings of the Royal Society of London. Series A. Mathematical and Physical Sciences*, 313(1515), pp.453–75.

Tchemtchoua, V.T. et al., 2011. Development of a Chitosan Nanofibrillar Scaffold for Skin Repair and Regeneration. *Biomacromolecules*, 12, pp.3194–3204.

Tehrani, N.S. et al., 2012. Burn-dressing materials with antibacterial activity from electrospun Chitosan nanofiber mats containing Silver sulfadiazine. In *4th International conference on nanostructures (ICNS4)*. pp. 820–822.

Teo, W.E. & Ramakrishna, S., 2006. A review on electrospinning design and nanofibre assemblies. *Nanotechnology*, 17(14), pp.R89–R106.

Theron, S.A., Zussman, E. & Yarin, A.L., 2004. Experimental investigation of the governing parameters in the electrospinning of polymer solutions. *Polymer*, 45(6), pp.2017–2030.

Thompson, C.J. et al., 2007. Effects of parameters on nanofiber diameter determined from electrospinning model. *Polymer*, 48(23), pp.6913–6922.

Thorvaldsson, A. et al., 2008. Electrospinning of highly porous scaffolds for cartilage regeneration. *Biomacromolecules*, 9(3), pp.1044–9.

Tiwari, S.K. & Venkatraman, S., 2012. Electrospinning pure protein solutions in core–shell fibers. *Polymer International*, 61, pp.1549–1555.

Tripatanasuwan, S., Zhong, Z. & Reneker, Darrell H., 2007. Effect of evaporation and solidification of the charged jet in electrospinning of poly(ethylene oxide) aqueous solution. *Polymer*, 48(19), pp.5742–5746.

Tsung, J. & Burgess, D.J., 2012. *Fundamentals and Applications of Controlled Release Drug Delivery*,

Tucker, N., Stanger, J.J. & Staiger, M.P., 2012. The History of the Science and Technology of Electrospinning from 1600 to 1995. *Journal of Engineered Fibers and Fabrics*, pp.63–73.

Ueda, H. & Tabata, Y., 2003. Polyhydroxyalkanonate derivatives in current clinical applications and trials. *Advanced drug delivery reviews*, 55, pp.501–518.

Ulery, B.D., Nair, L.S. & Laurecin, C.T., 2012. Biomedical applications of biodegradable polymers. *Journal of Polymer science part B: Polymer Physics*, 49, pp.832–864.

Uppal, R. et al., 2011. Hyaluronic acid nanofiber wound dressing--production, characterization, and in vivo behavior. *Journal of biomedical materials research. Part B, Applied biomaterials*, 97(1), pp.20–9.

Uyar, T. & Besenbacher, F., 2008. Electrospinning of uniform polystyrene fibers: The effect of solvent conductivity. *Polymer*, 49(24), pp.5336–5343.

Venugopal, J. et al., 2005. In vitro study of smooth muscle cells on polycaprolactone and collagen nanofibrous matrices. *Cell biology international*, 29(10), pp.861–7.

Verreck, G. et al., 2003. Incorporation of drugs in an amorphous state into electrospun nanofibers composed of a water-insoluble, nonbiodegradable polymer. *Journal of Controlled Release*, 92(3), pp.349–360.

Vink, E.T.H. et al., 2003. Applications of life cycle assessment to NatureWorks™ polylactide (PLA) production. *Polymer Degradation and Stability*, 80(3), pp.403–419.

Vowden, K. & Vowden, P., 2014. Wound dressings: principles and practice. *Surgery*, 32(9), pp.462–467.

De Vrieze, S. et al., 2009. The effect of temperature and humidity on electrospinning. *Journal of Materials Science*, 44(5), pp.1357–1362.

Wan, Y.Q. et al., 2007. Electrospinning of high-molecule PEO solution. *Journal of Applied Polymer Science*, 103(6), pp.3840–3843.

Wang, C. et al., 2007. Electrospinning of polyacrylonitrile solutions at elevated temperatures. *Macromolecules*, 40, pp.7973–7983.

Wang, Chi et al., 2010. Biodegradable Core/Shell Fibers by Coaxial Electrospinning: Processing, Fiber Characterization, and Its Application in Sustained Drug Release. *Macromolecules*, 43(15), pp.6389–6397.

Wang, Chong et al., 2011. Conventional Electrospinning vs. Emulsion Electrospinning: A Comparative Study on the Development of Nanofibrous Drug/Biomolecule Delivery

Vehicles. *Advanced Materials Research*, 410, pp.118–121.

Wang, H.S., Fu, G.D. & Li, X.S., 2009. Functional polymeric nanofibers from electrospinning. *Recent Patents on Nanotechnology*, 3(1), pp.21–31.

Wang, X. et al., 2005. Formation of water-resistant hyaluronic acid nanofibers by blowing-assisted electro-spinning and non-toxic post treatments. *Polymer*, 46(13), pp.4853–4867.

Wang, Yazhou et al., 2010. A Novel Controlled Release Drug Delivery System for Multiple Drugs Based on Electrospun Nanofibers Containing Nanoparticles. *Journal of Pharmaceutical Sciences*, 99(12), pp.4805–4811.

Wannatong, L., Sirivat, A. & Supaphol, Pitt, 2004. Effects of solvents on electrospun polymeric fibers: preliminary study on polystyrene. *Polymer International*, 53(11), pp.1851–1859.

Wei, Y. et al., 2015. Masking the bitter taste of injectable lidocaine HCl formulation for dental procedures. *AAPS PharmSciTech*, 16(2), pp.455–65.

Weir, N. a et al., 2004. Degradation of poly-L-lactide. Part 1: in vitro and in vivo physiological temperature degradation. *Proceedings of the Institution of Mechanical Engineers. Part H, Journal of engineering in medicine*, 218, pp.307–319.

Whitesides, G.M. & Grzybowski, B., 2002. Self-Assembly at All Scales. *Supramolecular chemistry and self-assembly*, 295, pp.2418–2421.

Williamson, M.R., Black, R. & Kielty, C., 2006. PCL-PU composite vascular scaffold production for vascular tissue engineering: attachment, proliferation and bioactivity of human vascular endothelial cells. *Biomaterials*, 27(19), pp.3608–16.

Van de Witte, P. et al., 1996. Phase separation processes in polymer solutions in relation to membrane formation. *Journal of Membrane Science*, 117(1-2), pp.1–31.

Wu, X.F., Salkovskiy, Y. & Dzenis, Y. a., 2011. Modeling of solvent evaporation from polymer jets in electrospinning. *Applied Physics Letters*, 98(22), pp.2009–2012.

Xie, J. & Wang, C.-H., 2006. Electrospun micro- and nanofibers for sustained delivery of paclitaxel to treat C6 glioma in vitro. *Pharmaceutical research*, 23(8), pp.1817–26.

Xie, Zhiwei et al., 2013. Dual growth factor releasing multi-functional nanofibers for wound healing. *Acta Biomaterialia*, 9(12), pp.9351–9359.

Xu, Jia et al., 2009. Preparation of chitosan/PLA blend micro/nanofibers by electrospinning. *Materials Letters*, 63(8), pp.658–660.

Xu, Xiuling et al., 2006. Preparation of Core-Sheath Composite Nanofibers by Emulsion Electrospinning. *Macromolecular Rapid Communications*, 27(19), pp.1637–1642.

Xu, Xiuling et al., 2005. Ultrafine medicated fibers electrospun from W/O emulsions.

Journal of Controlled Release, 108, pp.33–42.

Yan, E. et al., 2014. Biocompatible core-shell electrospun nanofibers as potential application for chemotherapy against ovary cancer. *Materials Science and Engineering C*, 41, pp.217–223.

Yan, S. et al., 2009. Poly(l-lactide-co-ε-caprolactone) electrospun nanofibers for encapsulating and sustained releasing proteins. *Polymer*, 50(17), pp.4212–4219.

Yang, F et al., 2004. Characterization of neural stem cells on electrospun poly(L-lactic acid) nanofibrous scaffold. *Journal of biomaterials science. Polymer edition*, 15(12), pp.1483–1497.

Yang, F. et al., 2005. Electrospinning of nano/micro scale poly(L-lactic acid) aligned fibers and their potential in neural tissue engineering. *Biomaterials*, 26(15), pp.2603–10.

Yang, Ying et al., 2006. Experimental investigation of the governing parameters in the electrospinning of polyethylene oxide solution. *IEEE Transactions on Dielectrics and Electrical Insulation*, 13(3), pp.580–585.

Yarin, A.L., Koombhongse, S. & Reneker, D.H., 2001a. Bending instability in electrospinning of nanofibers. *Journal of Applied Physics*, 89(5), p.3018.

Yarin, A.L., Koombhongse, S. & Reneker, D.H., 2001b. Taylor cone and jetting from liquid droplets in electrospinning of nanofibers. *Journal of Applied Physics*, 90(9), pp.4836–46.

Yener, F. & Yalcinkaya, B., 2013. Electrospinning of polyvinyl butyral in different solvents. *E-Polymers*, 021, pp.1–13.

Yeo, L.Y. & Friend, J.R., 2006. Electrospinning carbon nanotube polymer composite nanofibers. *Journal of Experimental Nanoscience*, 1(2), pp.177–209.

You, Y. et al., 2006. Effect of solution properties on nanofibrous structure of electrospun poly(lactic-co-glycolic acid). *Journal of Applied Polymer Science*, 99(3), pp.1214–1221.

Yu, D.-G., Williams, G.R., et al., 2013. Dual drug release nanocomposites prepared using a combination of electrospraying and electrospinning. *RSC Advances*, 3(14), p.4652.

Yu, D.-G., 2009. Electrospun nanofiber-based drug delivery systems. *Health*, 01(02), pp.67–75.

Yu, D.-G., Chian, W., et al., 2013. Linear drug release membrane prepared by a modified coaxial electrospinning process. *Journal of Membrane Science*, 428, pp.150–156.

Yu, J. H., Fridrikh, S. V. & Rutledge, G. C., 2004. Production of Submicrometer Diameter Fibers by Two-Fluid Electrospinning. *Advanced Materials*, 16(17), pp.1562–1566.

Yu, J. H., Fridrikh, S. V. & Rutledge, G. C., 2006. The role of elasticity in the formation of

electrospun fibers. *Polymer*, 47(13), pp.4789–4797.

Yu, Q., Dai, Z.W. & Lan, P., 2011. Fabrication of high conductivity dual multi-porous poly (l-lactic acid)/polypyrrole composite micro/nanofiber film. *Materials Science and Engineering: B*, 176(12), pp.913–920.

Yuan, X.Y. et al., 2004. Morphology of ultrafine polysulfone fibers prepared by electrospinning. *Polymer International*, 53(11), pp.1704–1710.

Zahedi, P. et al., 2009. A review on wound dressings with an emphasis on electrospun nanofibrous polymeric bandages. *Polymers for Advanced Technologies*, 21, pp.77–95.

Zamani, M., Prabhakaran, Molamma P & Ramakrishna, Seeram, 2013. Advances in drug delivery via electrospun and electrosprayed nanomaterials. *International journal of nanomedicine*, 8, pp.2997–3017.

Zargham, S. et al., 2012. The Effect of Flow Rate on Morphology and Deposition Area of Electrospun Nylon 6 Nanofiber. *Journal of Engineered*, 7(4), pp.42–49.

Zeng, J. et al., 2003. Biodegradable electrospun fibers for drug delivery. *Journal of Controlled Release*, 92(3), pp.227–231.

Zeng, J. et al., 2005. Influence of the drug compatibility with polymer solution on the release kinetics of electrospun fiber formulation. *Journal of controlled release : official journal of the Controlled Release Society*, 105(1-2), pp.43–51.

Zhang, C. et al., 2005. Study on morphology of electrospun poly(vinyl alcohol) mats. *European Polymer Journal*, 41(3), pp.423–432.

Zhang, Hong et al., 2010. Electrospinning of ultrafine core/shell fibers for biomedical applications. *Science China Chemistry*, 53(6), pp.1246–1254.

Zhang, Y Z et al., 2006. Coaxial electrospinning of (fluorescein isothiocyanate-conjugated bovine serum albumin)-encapsulated poly(epsilon-caprolactone) nanofibers for sustained release. *Biomacromolecules*, 7(4), pp.1049–57.

Zheng, J. et al., 2012. Construction of hierarchical structures by electrospinning or electrospraying. *Polymer*, 53(2), pp.546–554.

Zheng, Jian-yi et al., 2014. The Effect of Surfactants on the Diameter and Morphology of Electrospun Ultrafine Nanofiber. *Journal of Nanomaterials*, 2014, pp.1–9.

Ziani, K. et al., 2011. Effect of nonionic surfactant and acidity on chitosan nanofibers with different molecular weights. *Carbohydrate Polymers*, 83(2), pp.470–476.

Zong, X. et al., 2002. Structure and process relationship of electrospun bioabsorbable nanofiber membranes. *Polymer*, 43(16), pp.4403–4412.

Zuo, W. et al., 2005. Experimental study on relationship between jet instability and formation

of beaded fibers during electrospinning. *Polymer Engineering & Science*, 45(5), pp.704–709.

Zussman, E. et al., 2006. Electrospun Polyacrylonitrile/Poly(methyl methacrylate)-Derived Turbostratic Carbon Micro-/Nanotubes. *Advanced Materials*, 18(3), pp.348–353.

Zussman, E., Yarin, A.L. & Weihs, D., 2002. A micro-aerodynamic decelerator based on permeable surfaces of nanofiber mats. *Experiments in Fluids*, 33(2), pp.315–320.

APPENDIX

Differential scanning calorimetry was used to check thermal characteristics of the electrospun nanofibres after electrospinning in order to compare them with the pure polymers. Figure A.1 shows the thermogram of PLA bulk and nanofibres. As described on paragraph 7.3.2.6 (page 202), the electrospinning process does not change the polymer structure. The analysis was repeated three times for both samples, and a mean value was calculated as shown in Table A.1. The value of glass transition temperature, T_g, is about 59°C for both samples.

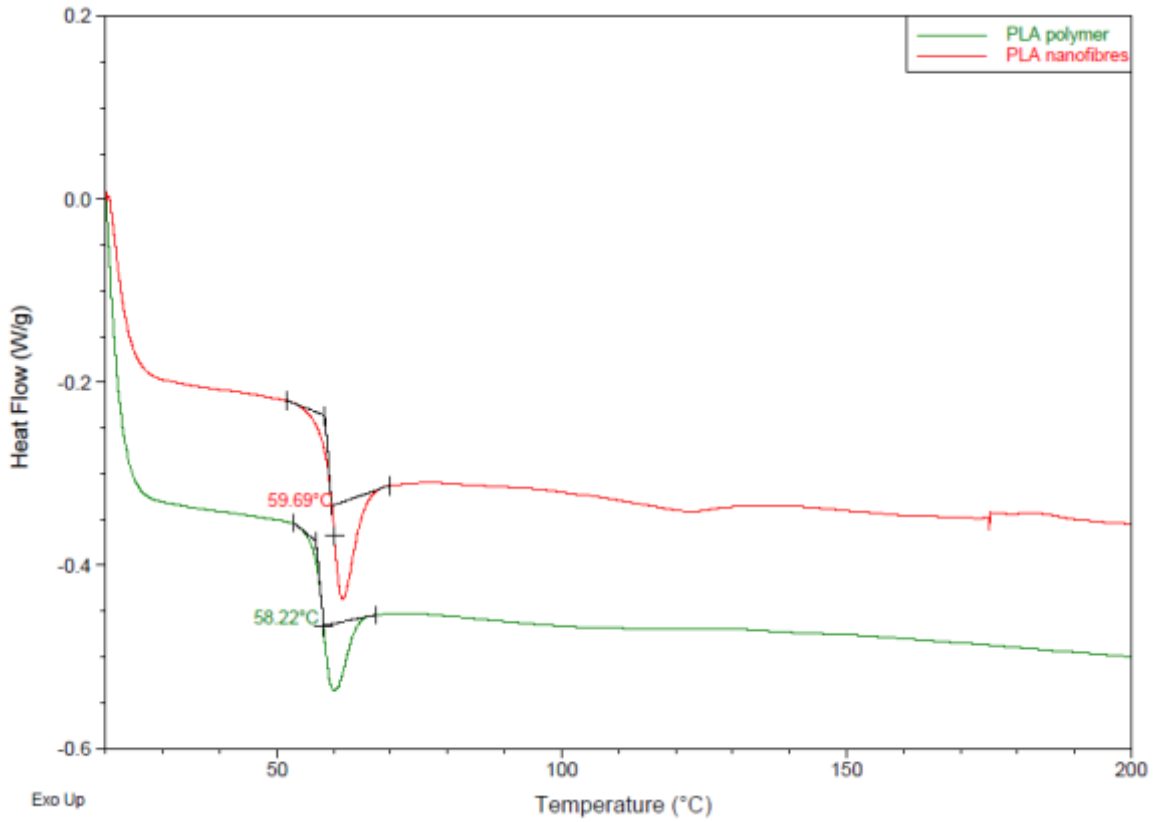

Figure A.1 – Differential scanning calorimetry thermogram of bulk PLA (green curve) and PLA nanofibres (red curve).

Table A.1 – Glass transition temperature of PLAs.

Sample	T_g (°C) (mean ± standard deviation)
PLA powder	59.5 ± 1.6
PLA nanofibres	59.4 ± 0.6

Similarly, DSC thermogram for PVA powder and PVA nanofibres were obtained as shown in Figure A.2. PVA nanofibres presented a different thermogram to that of PVA powder. As described on page 202, two features differentiate the samples. The heating cycle of PLA nanofibres (red curve) presents a slight reduction of heat flow (from 50°C to 150°C) which denotes moisture lost from the sample, and a double peak, which denotes the melting of the sample between 227°C and 233°C, is a result of imperfect crystal formation.

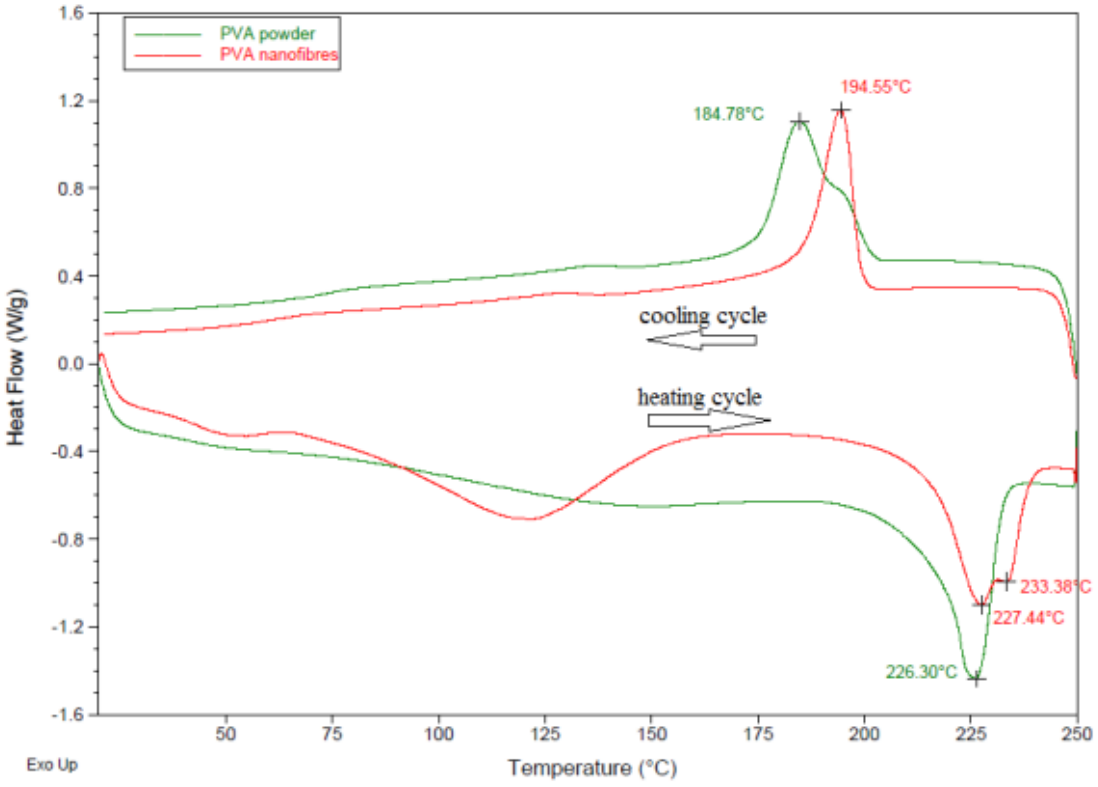

Figure A.2 – Differential scanning calorimetry curve of neat PVA and PVA nanofibres.

Table A.2 – Melting point (T_m), heat of fusion (ΔH_m), crystallization temperature (T_c) and heat of crystallization (ΔH_c) of PVAs.

Sample	T_{m1} (°C)	T_{m2} (°C)	ΔH_m (J/g)	T_c (°C)	ΔH_c (J/g)
PVA powder	226.7±0.5	/	73.5±1.3	184.3±1.4	59.8±1.0
PVA nanofibres	225.8±1.5	232.4±1.0	61.1±3.2	194.4±0.4	43.4±1.5